Bancza

Acta Morphologica Hungarica

VOLUME 37, NUMBER 1–2, 1989

EDITOR-IN-CHIEF
K. LAPIS

COPY-EDITOR
ERZSÉBET L. JUHÁSZ

EDITORIAL BOARD
I. TÖRŐ (Chairman), E. BEREGI, B. CSILLIK, P. ENDES, B. HALÁSZ, H. JELLINEK, GY. RAPPAY, GY. ROMHÁNYI, P. RÖHLICH, E. SOMOGYI, J. SUGÁR, GY. SZÉKELY, J. SZENTÁGOTHAI, I. TARISKA

Akadémiai Kiadó, Budapest
ACTA MORPH. HUNG. HU ISSN 0236—5391

ACTA MORPHOLOGICA
HUNGARICA

A QUARTERLY OF THE HUNGARIAN ACADEMY OF SCIENCES

Acta Morphologica publishes original papers on experimental morphology and pathology in English.

Acta Morphologica is published in yearly volumes of four issues by

AKADÉMIAI KIADÓ
Publishing House of the Hungarian Academy of Sciences
H-1117 Budapest, Prielle K. u. 19—35.

Manuscripts and editorial correspondence should be addressed to

Acta Morphologica
Ist Institute of Pathology and Experimental Cancer Research, Semmelweis Medical University,
1085 Budapest, Üllői út 26, Hungary

Subscription information

Orders should be addressed to

KULTURA Foreign Trading Company
H-1389 Budapest P.O. Box 149

or to its representatives abroad

Acta Morphologica Hungarica is abstracted/indexed in Biological Abstracts, Chemical Abstracts, Chemie-Information, Current Contents–Life Sciences, Excerpta Medica, database (EMBASE), Gerontological Abstracts, Index Medicus

---

© *Akadémiai Kiadó, Budapest*

Acta Morphologica

Hungarica

Editorial Board

I. Törő, E. Beregi, B. Csillik, P. Endes, B. Halász,
H. Jellinek, Gy. Rappay, Gy. Romhányi, P. Röhlich,
E. Somogyi, J. Sugár, Gy. Székely, J. Szentágothai, I. Tariska

Copy-Editor

Erzsébet L. Juhász

Editor-in-Chief

K. Lapis

INDEX

Volume 37

Akadémiai Kiadó, Budapest
1989

ACTA MORPHOLOGICA HUNGARICA

VOLUME 37 NUMBERS 1—4

CONTENTS

Dendritic changes in the hippocampus of aged rats. *Ivanka Lolova* 3

Three-dimensional reconstruction and synaptic architecture of cerebellar glomeruli in the rat. *R. L. Jakab* 10

Comparison of the effects of NaF and CaF_2 on rat gastric mucosa. A light-, scanning- and transmission electron microscopic study. *Pálma Kertész, T. Kerényi, Janina Kulka, Jolán Bánóczy* 21

Dendritic cells of the lymphoepithelial organs. *I. Törő, I. Oláh* 29

Immunohistological demonstration of lymph node reticulum cells in the acquired immunodeficiency syndrome related complex. *Gy. Szekeres, J. Audouin, J. Diebold* 47

In situ hybridization of peptide mRNA-s on vibratome sections. *M. Réthelyi, Carol B. Metz, T. J. Görcs, P. Kay Lund* 55

Relative growth of the human temporal bone in the prenatal period. *C. A. Mandarim-de-Lacerda* 65

Myenteric plexus of frog large intestine; a light- and electron microscopy of fiber system and neurons. *R. Gábriel, I. Benedeczky, Mária Csoknya* 71

Comparative study of glial fibrillary acidic protein (GFAP)-immunreactivity in the rat and monkey cerebellum. *I. Kótai, F. Hajós, L. Seress* 85

Experimentally induced acute changes in veins studied by scanning microscopy. *U. Fuchs, H. Jellinek, Anna Kádár* 93

Immune complex nephropathies in patients with malignant tumours. *L. Kun, Judit Nagy, M. Schmelczer, C. Trinn, T. Burger* 101

Chronomorphology of the duodenum in man. *A. Markiewicz, Anna Lelek, Barbara Panz, J. Wagiel, H. Boldys, M. Hartleb, M. Kaminski* 111

S-100 protein immunreactivity in human islets of Langerhans. *Z. Lászik, T. Krenács, E. Dobó* 117

Endocervical cytology: characterization of the cells by image analyser. *Veronika Tóth, M. Bodó, Gy. Lehoczky, B. Molnár, J. Sugár* 125

Alterations of the submandibular glands of female mice during pregnancy and lactation. A histological, histometrical and histochemic study. *J. A. Rossi, L. C. Bruschi* ... 135

GAP junction between T-colony cells. *T. Neumark, D. C. Huynh* 147

Analyses of the tidemark on human femoral heads. I. Histochemical, ultrastructural and microanalytic characterization of the normal structure of the intercartilaginous junction. *R. Oettmeier, K. Abendroth, Sabine Oettmeier* 155

Analyses of the tidemark on human femoral heads. II. Tidemark changes in osteoarthrosis. A histological and histomorphometric study in non-decalcified preparations. *R. Oettmeier, K. Abendroth, Sabine Oettmeier* 169

Morphology of supravital brain slices pre-incubated in a physiological solution prior to fixation. *F. Hajós, J. Garthwaite, G. Garthwaite, A. Csillag* 181

Cadmium influence on the liver. *M. Vojtišek, D. Hulínská, D. Bitternová, M. Cikrt, V. Hulínský* 201
Ultrastructure of the Ito cells in liver disease associated with fibrosis. *I. Bartók, Sz. Virágh, Cs. Hegedűs, Katalin Bartók* 219
Renal complications in multiple myeloma. *B. Iványi* 235
Antifreeze (ethylene glycol) intoxications in Baltimore. Report of six cases. *F. Introna, J. A. Smialek* 245
Haemophagocytic sinus histiocytosis with massive lymphadenopathy: Early lesions, progression and involution. *G. Kelényi, L. Olasz* 265

AUTHOR INDEX

B

Bartók I.—Virágh Sz.—Hegedűs Cs.—Hegedűs Katalin: 219

F

Fuchs U.—Jellinek H.—Kádár Anna: 93

G

Gábriel R.—Benedeczky I.—Csoknya Mária: 71

H

Hajós F.—Garthwaite J.—Garthwaite G.—Csillag A.: 181

I

Iványi B.: 235
Introna F.—Smialek J. A.: 245

J

Jakab R. L.: 10

K

Kertész Pálma—Kerényi T.—Kulka Janina—Bánóczy Jolán: 21
Kótai I.—Hajós F.—Seres L.: 85
Kun L.—Nagy Judit—Schmelczer M.—Trinn C.—Burger T.: 101
Kelényi G.—Olasz L.: 265

L

Lolova Ivanka: 3
Lászik Z.—Krenács T.—Dobó E.: 117

M

Mandarim-de-Lacerda C. A.: 65
Markiewicz A.—Lelek Anna—Panz Barbara—Wagiel J.—Boldys H.—Hartleb M.—Kaminski M.: 111

N

Neumark T.—Huynh D. C.: 147

O

Oettmeier R.—Abendroth K.—Oettmeier Sabine: 155
Oettmeier R.—Abendroth K.—Oettmeier Sabine: 169

R

Réthelyi M.—Metz B. Carol—Görcs T. J.—Lund P. Kay: 55
Rossi J. A.—Bruschi L. C.: 135

S

Szekerts Gy.—Audouin J.—Diebold J.: 47

T

Törő I.—Oláh I.: 29
Tóth Veronika—M. Bodó—Lehoczky Gy.—Molnár B.—Sugár J.: 125

V

Vojtišek M.—Hulinská D.—Bitternová D.—Cikrt M.—Hulínský V.: 201

CONTENTS

Normal and experimental morphology

Dendritic changes in the hippocampus of aged rats. *Ivanka Loiova* 3

Three-dimensional reconstruction and synaptic architecture of cerebellar glomeruli in the rat. *R. L. Jakab* 11

Comparison of the effects of NaF and CaF_2 on rat gastric mucosa. A light-, scanning- and transmission electron microscopic study. *Pálma Kertész, T. Kerényi, Janina Kulka, Jolán Bánóczy* 21

Dendritic cells of the lymphoepithelial organs. *I. Törő, I. Oláh* 29

Immunohistological demonstration of lymph node reticulum cells in the acquired immunodeficiency syndrome related complex. *Gy. Szekeres, J. Audouin, J. Diebold* 47

In situ hybridization of peptide mRNAs on vibratome sections. *M. Réthelyi, Carol B. Metz, T. J. Görcs, P. Kay Lund* 55

Relative growth of the human temporal bone in the prenatal period. *C. A. Mandarim-de-Lacerda* 65

Myenteric plexus of frog large intestine; light- and electron microscopy of fiber system and neurons. *R. Gábriel, I. Benedeczky, Mária Csoknya* 71

Comparative study of glial fibrillary acidic protein (GFAP)-immunoreactivity in the rat and monkey cerebellum. *I. Kótai, F. Hajós, L. Seress* 85

Pathology

Experimentally induced acute changes in veins studied by scanning microscopy. *U. Fuchs, H. Jellinek, Anna Kádár* 93

Immune complex nephropathies in patients with malignant tumours. *L. Kun, Judit Nagy, M. Schmelczer, C. Trinn, T. Burger* 101

Chronomorphology of the duodenum in man. *A. Markiewicz, Anna Lelek, Barbara Panz, J. Wagiel, H. Boldys, M. Hartleb, M. Kamiński* 111

S-100 protein immunoreactivity in human islets of Langerhans. *Z. Lászik, T. Krenács, E. Dobó* 117

Acta Morphologica Hungarica 37 (1—2), pp. 3—9 (1989)

DENDRITIC CHANGES IN THE HIPPOCAMPUS OF AGED RATS

Ivanka LOLOVA

INSTITUTE OF PHYSIOLOGY, BULGARIAN ACADEMY OF SCIENCES, SOFIA, BULGARIA

(Received 24 May 1988)

Age-related changes in dendritic branches in stratum lacunosum-moleculare of the CA1 hippocampal field were examined using quantitative ultrastructural methods. A decrease by 38% was demonstrated in the number of dendritic branch profiles per tissue square area in the group of aged (24-month-old) rats as compared to that in the group of young adult (3-month-old) rats. The total volume fraction and total surface of dendrites per volume neuropil were decreased by 23% and 35%, respectively in aged rats. The percentage area of neuropil occupied by dendritic branch profiles was smaller in aged rats (by 22%) than that in young adult rats. The width of the layers including the apical dendrites of the CA1 hippocampal pyramidal cells was unchanged in the group of aged rats. The degree of the changes in different parameters examined suggests that the atrophy and loss of dendrites in aging hippocampus affect preferentially terminal branches.

Keywords: Hippocampus, dendrites, ultrastructural quantification, aging

Introduction

It is postulated that a close correlation exists between the deterioration of the brain functions and the changes of the postsynaptic surface in aging [17]. Considering the important role of the hippocampal formation in learning and memory the great interest to the age-related alterations of the dendritic tree of this structure is quite conceivable. Progressive changes in the dendrites of the aged human and animal hippocampal formations have been demonstrated in qualitative and quantitative Golgi studies [6, 10, 13, 16, 18]. It has also been found that the vulnerability of the dendrites under experimental conditions increases with advancing age [15]. However, the quantitative ultrastructural data on age-dependent dendritic changes in the hippocampal formation concern rat dentate gyrus [8] and ultrastructural data on the hippocampus are not available.

The objective of this ultrastructural study was to quantify the dendritic branches in stratum lacunosum-moleculare (str. L-M) of CA1 hippocampal field in young adult and aged rats. The CA1 hippocampal field was chosen for examination because recent ultrastructural and immunocytochemical studies

Send offprint requests to: Dr. I. Lolova, Institute of Physiology, Bulgarian Academy of Sciences, Akad. G. Bonchev Str., Bldg. 23, 1113 Sofia, Bulgaria

have demonstrated that the nerve cells in the outer layers of the lateral entorhinal cortex and pyramidal cells in CA1 hippocampal field in humans are early and strongly affected with advancing age [1, 23]. The str. L-M was chosen for the quantitative analysis because quantitative Golgi studies have revealed early impairement of the terminal branches of both apical and basal dendrites in the neocortex of aged animals [2, 20]. The terminal branches of the apical dendrites of the hippocampal pyramidal cells are localized in str. L-M.

Materials and methods

Seven young adult (3-month-old) and seven aged (24-month-old) Wistar rats were used. The animals were perfused transcardially with 3% glutaraldehyde in 0.1 M phosphate buffer, pH 7.4, for 20 min. Coronal 2—3 mm thick slices were cut from the rostral portion of the dorsal hippocampal formation, fixed in the same fixative for 40 min and postfixed in 1% OsO_4 for 90 min. Following dehydratation the tissue blocks were embedded in Durcupan.

Three blocks from each animal were examined. The localization of the CA1 hippocampal field was determined in semithin sections stained with toluidine blue. Two sets of 3—4 semithin sections were obtained from each block at intervals of 200 μm. The width of the str. radiatum and str. L—M from the apical edge of the CA1 pyramidal cell bodies to the hippocampal fissure was estimated using a Zeiss light microscope. This width was measured at medial, central and lateral parts of one section from each set.

Ultrathin sections (silver-gold) were stained with uranyl acetate and lead citrate and examined in an Opton 10 C electron microscope. The micrographs were taken through the str. L—M using only one section from each block in order to obtain a random sample of the dendritic branches at a magnification of $\times$12 500 and printed at a magnification of $\times$2.32. The micrographs did not contain non-pyramidal nerve and glial cell bodies or blood vessels. At least 30 micrographs from each animal were used for the quantitative analysis. The following parameters were calculated: number of dendritic branch profiles per square area of a micrograph (24 sq.μm), total volume fraction and total surface area of these profiles per unit tissue volume and percentage area of neuropil occupied by dendritic branch profiles. These dendritic parameters were determined using a stereological pointcounting and intersection-counting procedures [3, 22]. Mean values for each animal were derived from analysis of all micrographs from the animal. Mean values per the two age groups were derived from analysis of all micrographs taken from the animals in the respective group. The results were analyzed statistically by Student's-*t*-test. The individual differences in each group were evaluated by the coefficient of variance-V = SD/M. 100. Standard deviation (SD) and mean (M) were the values perage group calculated from the individual mean values in the group.

Results

The structure of the neuropil of the str. L-M in the CA1 hippocampal field in aged rats was similar to that in young adult rats. However, the dendritic and axon profiles in the neuropil of aged rats were surrounded by more and

——→

Fig. 1. The dendritic and axon profiles in 24-month-old rats were surrounded by enlarged glial processes rich in lipofuscin granules and fibrilles (arrows)

Fig. 2. Two bulbous dilatations (A) along dendrite in CA1 hippocampal field of 24-month-old rats

Fig. 3. Middle-sized dendrite containing lipofuscin and lipid granules (arrows) in the neuropil of 24-month-old rats

Fig. 4. A dendrite containing dense bodies (arrow) in the neuropil of 24-month-old rats

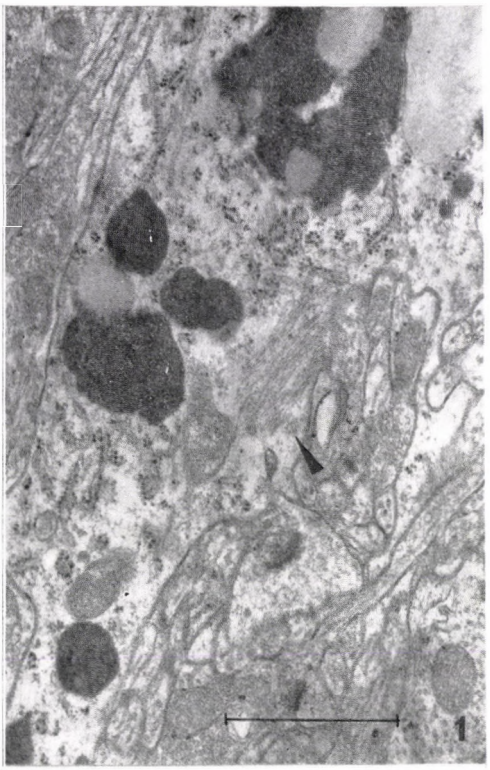
1

A
A
2

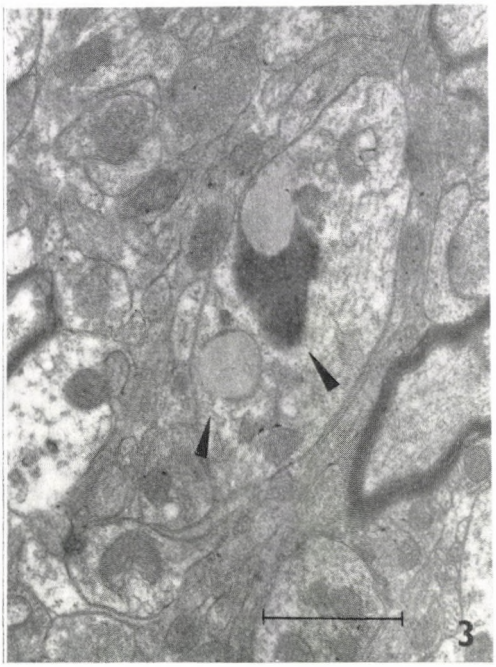
3

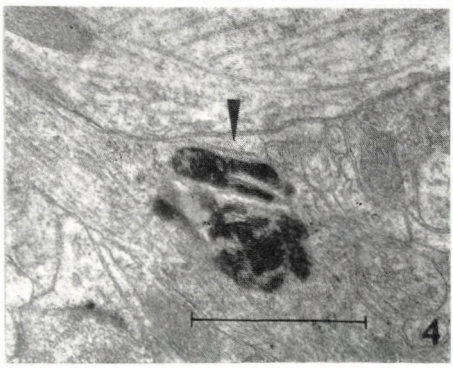
4

larger glial processes (Fig. 1). Large bulbous dilatations along dendrites occasionally occurred in aged rats (Fig. 2). These dilatations contained microtubules, mitochondria and cisterns of the smooth endoplasmatic reticulum. Many unchanged presynaptic terminals ended on the dilatations. Middle-sized dendrites containing lipofuscin granules, lipid globules and dense bodies were found in the neuropil of aged rats (Fig. 3). No dendritic profiles exhibiting dark or light type of degeneration described in aged humans and dogs [17, 21] were found in aged rats examined.

The quantitative ultrastructural analysis showed a high decrease in the mean number of dendritic branch profiles per tissue square area (by 38%) in the group of aged rats as compared to that in the group of young adult rats (Table I). All individual mean values in the group of aged rats were lower (1.20 to 1.93 times) than those in the young adult group. The total volume fraction of dendritic branches per volume neuropil was also decreased (by 23%) in the group of aged rats as compared to that in the group of young adult rats (Table I). The individual mean values in the group of aged rats were lower (1.14 to 1.65 times) than those in the young adult group. The total surface area of dendritic branch profiles per volume neuropil was diminished (by 35%) in the group of aged rats as compared to that in the group of young adult rats (Table II). No overlapping of individual mean values of the animals from the two age groups was observed. The percentage area of neuropil occupied by

Table I

Number and total volume fraction of dendritic branches in str. L-M of the CA1 hippocampal field in young adult and aged rats

	Number of profiles		Volume fraction of profiles	
	3 months	24 months	3 months	24 months
Mean ± S.E.M. per animal	9.29±0.40	5.78±0.34	0.258±0.015	0.197±0.013
	9.66±0.48	5.74±0.29	0.262±0.011	0.208±0.012
	10.50±0.56	6.85±0.55	0.281±0.015	0.224±0.015
	10.09±0.44	6.63±0.38	0.321±0.014	0.241±0.016
	9.71±0.52	6.19±0.44	0.264±0.015	0.196±0.011
	11.07±0.70	7.60±0.45	0.243±0.007	0.194±0.012
	13.17±0.90	6.86±0.48	0.304±0.016	0.227±0.011
Mean ± S.E.M. per group	10.50±0.57	6.52±0.42	0.276±0.013	0.212±0.013
Per cent of 3-month-old group		62.00		76.81
P		< 0.001		< 0.001
V	11.62%	9.47%	9.27%	8.03%

P significant level. V coefficient of variance.

Number of counted micrographs in this and next tables was 224 in the group of young adult rats and 230 in the group of aged rats

dendritic branch profiles in the group of aged rats was significantly decreased (by 22%) as compared to that in the group of young adult rats (Table II). However, two individual mean values in the young adult group were almost equal to two individual mean values in the aged group. The individual mean values for the remaining five young adult rats were higher (1.1 to 1.65 times) than those for aged rats.

Table II

Total surface area of dendritic branches and percentage area of neuropil occupied by dendritic branches in str. L-M of the CA1 hippocampal field in young adult and aged rats

	Surface area of profiles		Percentage area of neuropil	
	3 months	24 months	3 months	24 months
Mean ± S.E.M. per animal	0.249±0.008	0.180±0.010	22.51±1.28	16.69±1.28
	0.254±0.012	0.161±0.008	26.24±1.15	20.97±1.11
	0.282±0.017	0.188±0.015	28.20±1.52	22.36±1.55
	0.344±0.018	0.212±0.012	32.09±1.38	24.07±1.56
	0.237±0.009	0.172±0.010	26.38±1.53	19.35±1.23
	0.265±0.014	0.191±0.010	24.39±0.71	19.36±1.19
	0.365±0.023	0.188±0.007	30.67±1.63	22.10±0.98
Mean ± S.E.M. per group	0.285±0.014	0.185±0.010	27.10±0.55	21.12±0.51
Per cent of 3-month-old group		64.90		78.00
P		< 0.001		< 0.001
V	16.16%	16.22%	11.50%	9.70%

P significant level. V coefficient of variance.

Table III

Width of str. radiatum and str. L-M of the CA1 hippocampal field in young adult and aged rats

	3 months	24 months
Mean ± S.E.M. per animal	440± 8.00	481± 6.80
	429±14.10	423±18.16
	462± 9.44	422±11.68
	463± 8.80	481±11.60
	453±10.10	484± 8.32
	445± 8.24	455± 8.88
	422±12.72	417±11.00
Mean ± S.E.M. per group	446±4.50	451±5.52
P		> 0.05
V	3.28%	6.30%

P significant level. V coefficient of variance.

Number of counted slices was 39 for the group of young adult rats and 41 for the group of aged rats

The coefficients of variance of the individual mean values in the two age groups were considerably lower as compared to the age-related differences for all parameters examined.

No significant differences in the width of the layers including the apical dendrites of the CA1 pyramidal cells in the two age groups were found (Table III).

Discussion

The present quantitative ultrastructural data showing a marked age-dependent decrease in the number of the dendritic branch profiles in the hippocampus confirm the qualitative and quantitative data of Golgi studies on a dendritic loss in various regions of aged human and animal brain: the neocortex [2, 4, 5, 14, 17, 19, 20], dentate gyrus [6, 16, 18], cerebellum [13], brain stem and spinal cord [11], hypothalamus [12] and olfactory bulb [9]. The decrease in the number of dendritic branches observed in the present study (by 38%) is considerably higher than the decrease in the number of dendritic shafts found by Geinisman et al. [8] in the dentate gyrus of aged rats (by 24%). This difference may be due to the study of different parts of the hippocampal formation. Of even greater significance with respect to the different results is the study of different zones of the molecular layer in these two parts. In the supragranular zone of the dentate molecular layer main dendritic shafts are predominantly localized, whereas in the str. L-M of the CA1 hippocampal field terminal dendritic branches are localized. Such an interpretation is in good agreement with the quantitative Golgi data on a preferential loss of terminal dendritic branches in aging [2, 20]. The disproportion between the great decrease in the dendritic number and relatively small decrease in the dendritic volume fraction observed in the present studies is consistent with the finding of Geinisman et al. [8] on the aged dentate gyrus and shows that the age-related changes affect the peripheral portions rather than the main shafts of dendrites.

Thinning of the dendrites in aging has been described in Golgi observations [5, 14, 17, 18, 20]. The great decrease in the total surface of dendritic profiles as well as in the percentage area of neuropil occupied by these profiles observed in the present study indicate an atrophy of the existing dendritic branches in the str. L-M of CA1 hippocampal field in aged rats.

The mechanism underlying the deterioration of dendritic branches in aging is not yet clear. Based on the neuropathological changes in aged humans Scheibel et al. [17, 18] have suggested that accumulation of neurofibrillary tangles at the base of dendrites disrupts the normal cytoplasmatic transport along dendrites and causes their disappearance. No accumulation of neurofibrillary tangles has been established in any animal species [2]. Some

authors have supposed that the atrophy and loss of dendrites in aging may be due to a partial deafferentation [5, 9, 20]. As supportive evidence for this suggestion Geinisman et al. [8] have pointed out a loss of synapses on the dendritic shafts [7].

Notwithstanding the loss and atrophy of the dendritic branches, we failed to find significant difference in the width of the layers including the apical dendrites of the CA1 pyramidal cells in the two age groups. Nor has difference been observed in the width of the dentate molecular layer of mature and aged rats [8]. Most probably the dendritic atrophy and loss are compensated by hypertrophy of astrocyte processes.

REFERENCES

1. Braak H, Braak E: On areas of transition between entorhinal allocortex and temporal isocortex in the human brain. Normal morphology and lamina-specific pathology in Alzheimer's disease. Acta Neuropathol (Berl) 68: 325, 1985
2. Cupp CJ, Uemura E: Age-related changes in prefrontal cortex of *Macaca mulatta:* quantitative analysis of denderitic branching patterns. Exp Neurol 69: 143, 1980
3. Elias H, Henning H, Schwartz DE: Stereology: Applications to biomedical research. Physiol Rev 51: 158, 1971
4. Feldman ML: Dendritic changes in aging rat brain: pyramidal cell dendrite length and ultrastructure. In: Nandy K., Sherwin I. (eds). The Aging Brain and Senile Dementia. Advances in Behavioral Biology. Vol. 23: Plenum New York 1977 p. 323
5. Feldman ML, Dowd C: Loss of dendritic spines in aging cerebral cortex. Anat Embryol 148: 279, 1975
6. Flood DG, Buel SJ, Horwitz GJ, Coleman PD: Dendritic extent in human dentate gyrus granule cells in normal aging and senile dementia. Brain Res 402: 205, 1987
7. Geinisman Y, Bondareff W, Dodge JT: Partial deafferentation of neurons in the dentate gyrus of the senescent rat. Brain Res 134: 541, 1977
8. Geinisman Y, Bondareff W, Dodge JT: Dendritic atrophy in the dentate gyrus of the senescent rat. Am J Anat 152: 321, 1978
9. Hinds JW, McNelly NA: Aging of the rat olfactory bulb: growth and atrophy of constituent layers and changes in size and number of mitral cells. J Comp Neurol 171: 345, 1977
10. Machado-Salas J, Scheibel AB: Limbic system of the aged mouse. Exp Neurol 63: 347, 1979
11. Machado-Salas, J, Scheibel ME, Scheibel A: Neuronal changes in the aging mouse: spinal cord and lower brain stem. Exp Neurol 54: 504, 1977a
12. Machado-Salas J, Scheibel ME, Scheibel A: Morphological changes in the hypothalamus of the old mouse. Exp Neurol 57: 102, 1977b
13. Mehraein P, Yamada M, Tarnowska-Dziduszko E: Quantitative study on dendrites and dendritic spines in Alzheimer's disease and senile dementia. In: Kreutzberg GW (ed.) Advances in Neurology, Vol 12. Physiology and Pathology of Dendrites Raven Press 1975 p. 453,
14. Mervis R: Structural alterations in neurons of aged canine neocortex: A Golgi study. Exp Neurol 62: 417, 1978
15. Pentney RJ: Quantitative analysis of ethanol effects on Purkinje cell dendritic tree. Brain Res 249: 397, 1982
16. Ruiter De JF, Uylings HBM: Morphometric and dendritic analysis of fascia dentata granule cells in human aging and senile dementia. Brain Res 402: 217, 1987
17. Scheibel ME, Lindsay RD, Tomiyasu U, Scheibel AB: Progressive dendritic changes in aging human cortex. Exp Neurol 47: 392, 1975
18. Scheibel ME, Lindsay RD, Tomiyasu U, Scheibel AB: Progressive dendritic changes in the aging human limbic system. Exp Neurol 53: 420, 1976
19. Scheibel ME, Tomiyasu U, Scheibel AB: The aging human Betz cell. Exp Neurol 56: 598, 1977

20. Vaughan DW: Age-related deterioration of pyramidal cell basal dendrites in rat auditory cortex. J Comp Neurol 171: 501, 1977
21. Verbitskaya LB, Vorobyova TY, Semenchenko II, Pavlovskaya VI: Age-dependent changes in dendrite ultrastructure. Bul Exp Biol Med 10: 474, 1986 (in Russian)
22. Weibel ER: Stereological principles for morphometry in electron microscopic cytology. Int Rev Cytol 26: 235, 1969
23. Yamaguchi H, Morimatsu M, Hirai S, Takahasi K: Alzheimer's neurofibrillary tangles are penetrated by astroglial processes and appear eosinophilic in their final stages. Acta Neuropathol (Berl) 72: 214, 1987

Acta Morphologica Hungarica 37 (1—2), pp. 11—20 (1989)

THREE-DIMENSIONAL RECONSTRUCTION AND SYNAPTIC ARCHITECTURE OF CEREBELLAR GLOMERULI IN THE RAT

R. L. JAKAB

NEUROBIOLOGY RESEARCH LABORATORY OF THE HUNGARIAN ACADEMY OF SCIENCES AND SEMMELWEIS UNIVERSITY MEDICAL SCHOOL, BUDAPEST, HUNGARY

(Received 20 April 1988)

Cerebellar glomeruli of simple type were studied by quantitative morphological and stereological methods. It has been found that in one glomerulus the centrally located mossy terminal forms synaptic contacts with about 50 granule cell dendrites, all deriving from distinct granule cells. The three-dimensional reconstruction of the glomeruli revealed that the terminal portion of the dendrites, the so called digits, are elongated, thin processes. Synaptic contacts by mossy terminals are established exclusively on the dendritic digits. Although these digits are the main postsynaptic targets for the Golgi axon terminals as well, these inhibitory endings might also synapse with the proximal portion of the granule cell dendrites.

Introduction

The cerebellar cortex receives its major input via mossy fibers from almost all parts of the body. These impulses are relayed to the cortex through the intercalated complex synapses, the cerebellar glomeruli. The cerebellar glomeruli are complex assembles of granule cell dendrites closely grouped around the excitatory mossy fiber swellings. The granule cell dendrites are contacted also at the periphery of the glomerulus by numerous varicosisties of the inhibitory Golgi axons [2, 14]. Another postsynaptic element, the dendrite of Golgi cell is occasionally present, participating in about 9% of all glomeruli [6]. Previous studies have analyzed the organization of the cerebellar glomeruli of different species in detail [3—5, 7, 9—13, 15]. More recently direct measurement of glomerular potentials has been made by Taylor et al. [18]. Furthermore, Chauvet [1], using theoretical arguments, suggested that the presumed modifiability of synapses between mossy fibers and granule cell dendrites would have a crucial role in cerebellar learning. Although the general principles of the glomerular organization became a "textbook data", relevant and realistic quantitative and stereological information about the distribution and location of synapses, an important prerequisite for any functional model of this structure, is still in need. Accordingly, the purpose of this study was to obtain further information on the ultrastructural organization of cerebellar glomeruli as investigated by three-dimensional reconstruction of serial thin sections.

Send offprint requests to: R. L. Jakab, Neurobiology Res. Lab. of the Hungarian Academy of Sciences and Semmelweis University Medical School, Budapest, Tűzoltó Str. 58, H-1094, Hungary

Materials and methods

Adult female albino rats were anaesthetized with chloralhydrate (350 mg/kg i.p.) and perfused transcardially first with a saline solution (2—3 min) and then with a fixative containing 1% paraformaldehyde and 1% glutaraldehyde in 0.1 M phosphate buffer at pH 7.4. The brains were then removed, small blocks from the cerebellar hemispheres were excised and refrigerated overnight in the same fixative solution. The specimens were then osmificated, dehydrated, and embedded in Durcupan ACM resin (Fluka). Serial thin sections were cut with an LKB V. ultratome. Section thickness was about 80 nm as judged by their interference colour [16]. Ribbons of 120—200 successive sections were placed on Formvar-coated single-slot grids (eight to ten sections per grid) that were kept in serial order so that neuronal processes could be reconstructed throughout the series. All sections were stained with lead citrate [17] and uranyl acetate. The sections were viewed and photographed under a JEOL 100B electron microscope. The final magnification of the micrographs to be analyzed was ×27 000.

Altogether five cerebellar glomeruli were analyzed and reconstructed in their full extent .The transected profiles of neural elements of the glomeruli were identified one by one and traced throughout the whole series. When possible, dendrites of granule cells were traced to their parent cell bodies. The following number of consecutive sections covered the five fully reconstructed glomeruli:

glomerulus 1 — 131 sections
glomerulus 2 — 123 sections
glomerulus 3 — 159 sections
glomerulus 4 — 170 sections
glomerulus 5 — 113 sections.

In order to obtain and compare the sizes of the glomerular components, cross-sectional area of all axonal and dendritic profiles, the perimeter and area of mossy terminals, as well as the length of postsynaptic membrane specializations facing the mossy swellings were measured with a planimeter. The (partial) three-dimensional (3D) reconstruction of cerebellar glomeruli was made with the aid of a computer system consisting of: a PDP 11/34 minicomputer,Quantimet 720 image analyzer, Macroviewer table and Canon camera for image input, and a Hawlett—Packard 7221B 4-colour plotter as graphic output device. The system was controlled by computer programs AP1 and AP3 [19]. The contours of processes selected for reconstruction were traced onto acetate sheets by using internal reference points such as axons or blood vessels cut in cross section. Then the outlines were digitized and fed into the computer. Thus, the 3D models were built from a series of 2D outlines. In the visualization phase the reconstructed objects were investigated from different viewpoints with their hidden lines removed. Due to the limited capacity of the computer program, the 3D reconstruction was restricted to a few representative glomerular elements using every third or fourth section in the series. The precise location of synaptic contacts on the postsynaptic granule cell dendrites from mossy and Golgi axon terminals were indicated on the computer drawings. The volume and surface of the reconstructed objects were computed by the computer program AP3 and checked by planimetric measurements.

The Golgi-impregnation of small blocks (3×4 mm) from cerebellar cortex has been performed, following fixation and osmification as described before. The blocks were placed in 3.5% potassium dichromate overnight, followed by a treatment with silver nitrate (0.7%) for 6—7 h. Thereafter the blocks were covered with agar (8% solution) and cut into μm thick sections using a Sorvall TC-2 tissue chopper. The sections were then mounted on slides in a drop of glycerol, and examined under the light microscope. Sections containing well-impregnated neurons were dehydrated and embedded.

Results

Since the maximum of 200 serial sections obtained did not allow to analyze and reconstruct large, so called "complex" glomeruli (glomeruli with more than one mossy terminal) in their full extent, five glomeruli of the "simple type" were examined in this study.

The electron micrographs showed that one mossy fiber rosette, containing large, spheroid synaptic vesicles, is the central component of each five glomeruli (Fig. 1). The mossy fiber swelling is not necessarily an ending, the fiber may leave the glomerulus and form further rosettes. Nevertheless, in accordance with the accepted terminology, all five of them will be called mossy terminals (MT in abbreviations) in this study. As seen in Fig. 1, the multilobulate contour

Fig. 1. Electron micrograph of a cross-section from rat's cerebellar glomerulus (glom. 4). The digits (d), processes of granule cell dendrites (Grd), form synapses both with the central mossy terminal (MT), which contain large, spheroid synaptic vesicles, and the peripherally located Golgi axon varicosities (Ga) containing small, flattened vesicles. The "excitatory" MT-synapses (of asymmetric type) are indicated by arrows, while the "inhibitory" Ga-synapses (of symmetric type) by open arrow. Arrowheads refer to symmetric attachment plagues, which are desmosome-like membrane specializations formed between dendrites and/or dendritic digits

of the mossy terminal is covered by numerous postsynaptic profiles of granule cell dendrites (Grd), which establish with the MT asymmetric synaptic contacts. The processes of Grd-s are also postsynaptic to the axonal varicosities of Golgi cells which contain small, pleomorphic synaptic vesicles, and give rise to symmetrical synaptic junctions. The Golgi axon varicosities (Ga) contact the granule cell dendrites at the periphery of the glomeruli. None of the five cerebellar glomeruli were found to contain Golgi cell dendrite.

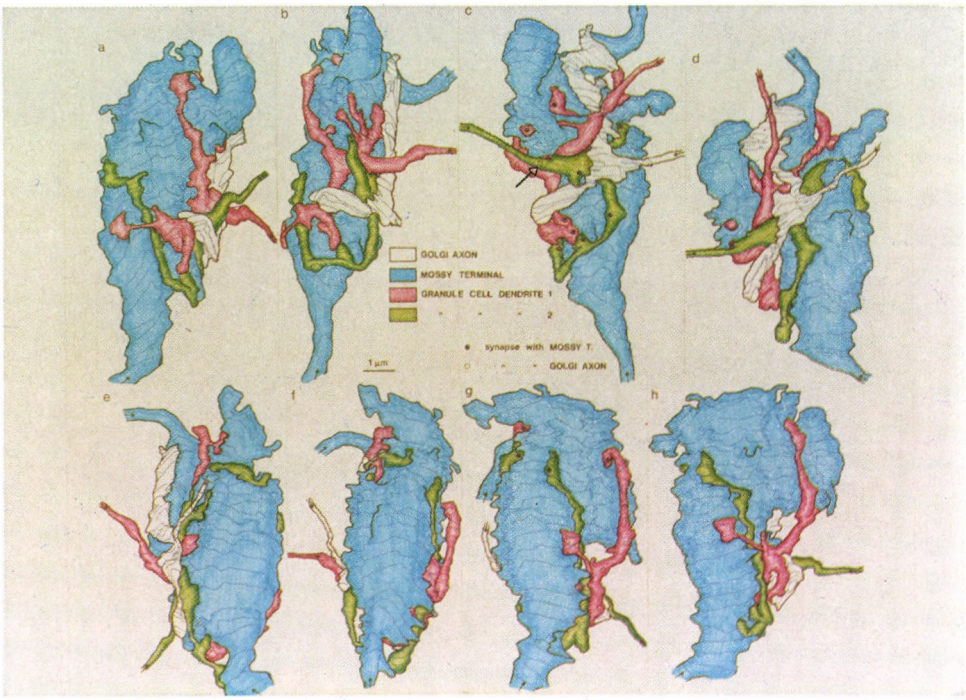

Fig. 2. Computer-assisted reconstruction of representative elements from cerebellar glomerulus of "en passant" type (glom. 4). The drawings, being rotated by 45°, can be seen from different viewpoints. The locations of synapses are illustrated on the processes of granule cell dendrites curving around the mossy fiber swelling (c and g). The MT- and Ga-synapses are indicated by closed and opened circles, respectively. On Fig. c. the open arrow shows a Golgi axon synaptic site at the proximal part of granule cell dendrite 2 (see also Fig. 5b). On these and subsequent drawings the reconstructed structures are of equal magnification and angle of inclination from the plain of sectioning (40°), which permit to compare their sizes

Tracing the granule cell dendrites throughout the whole series to their parent cell bodies revealed that no granule cell send more than one dendrite to the same glomerulus. Furthermore, all dendrites terminated in the glomerulus they entered. Finally, none of the dendrites were seen to bifurcate or to give side-branches before entering the glomerulus. These features indicate that each

dendrite of a glomerulus derives from different granule cells. Within the glomerulus, however, the Grd-s provide rich branching patterns, curving around the mossy terminal, and giving off shorter or longer side-branches called "dendritic digits" (Figs 2—4). All Grd-s were seen to make synaptic contacts with mossy terminal, moreover, each dendritic digit formed synaptic junction either with MT, or with Ga, or both (Fig. 5a). Electron microscopic analysis of the serial sections also revealed that mossy terminals give rise to synaptic contacts

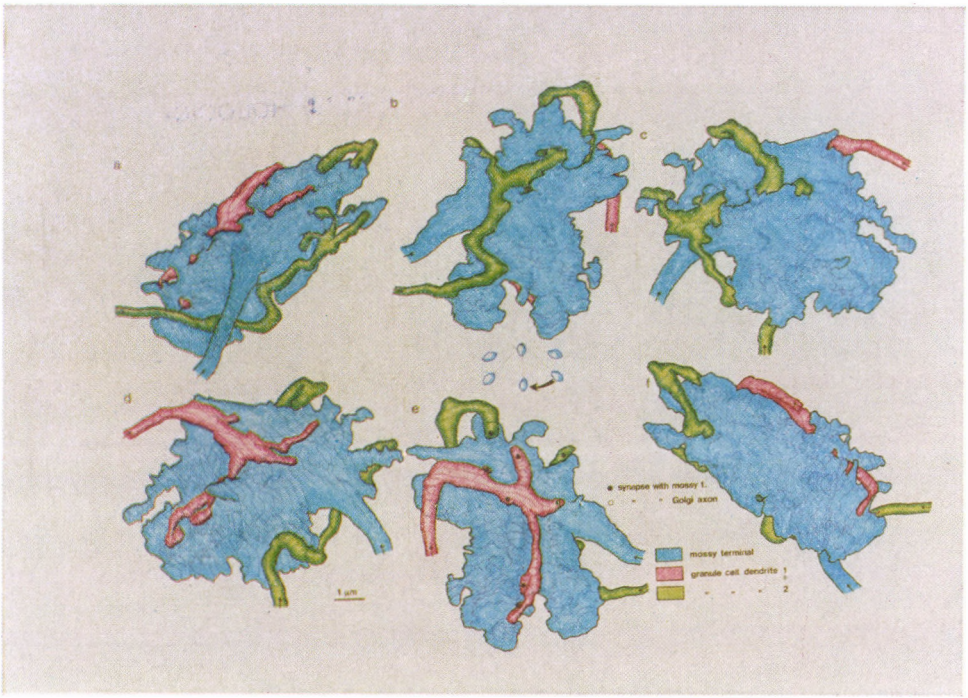

Fig. 3. Reconstruction of some components from cerebellar glomerulus of "terminal" type (glom. 1). The reconstructed structure (inclined to 40°) is rotated around by 60°. The locations of synapses are illustrated on Fig. b and e; symbols as in Fig. 2. The granule cell dendrite 1, without synaptic contacts from Golgi axons, demonstrates, as an example, that not all dendrites establish synapses with Golgi axons

exclusively with the dendritic digits of Grd-s, and avoid the proximal, "neck portion" of the dendrites. This feature is illustrated on the computer-assisted drawings by indicating the precise location and distribution of synaptic membrane specializations on the processes of Grd-s (Figs 2—4). The figures 2 and 4 demonstrate that the thin, varicose Golgi axons make synaptic contacts also predominantly with the dendritic digits. In some rare cases, however, synaptic contacts may be established with the "neck" of a dendrite (Fig. 5b).

The mossy fiber rosettes may be divided according to their position into *en passant* (Figs 2 and 4) and *terminal* (Fig. 3) types. The mossy fiber left the glomerulus (belonging to *en passant* type) in three cases, while in two glomeruli they terminated *(terminal* type). As clearly seen on the 3D reconstruction drawings, the *terminal* rosette is of more irregular shape than those of *en passant* type, which are roughly spindle-shaped.

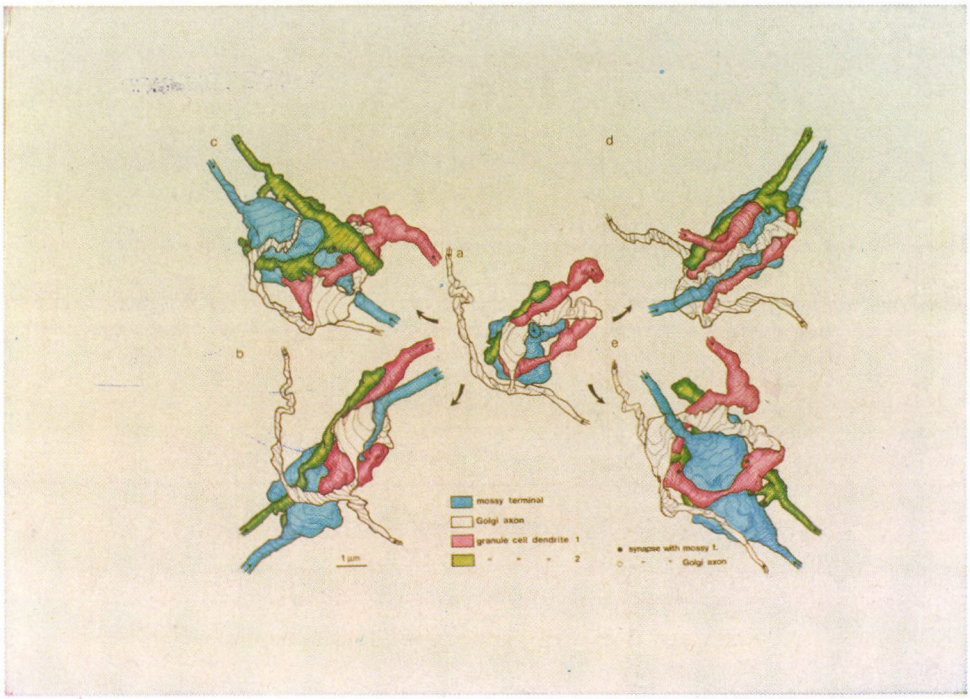

Fig. 4. Reconstruction of a few representative components from the "mini" cerebellar glomerulus (glom. 5). Fig. a. Upper view of the reconstructed structure concerning the plain of sectioning. The four subsequent drawings (b, c, d, e; inclined to 40°) show different sides of the glomerular structure being rotated by 90°. The location of synapses are illustrated in Fig. c and e; symbols as in Fig. 2. As seen on the drawings in this "mini" glomerulus, there is a greater proportion of Ga-synapses to MT-synapses than in the rest, "normal" glomeruli

While data of four glomeruli (1, 2, 3, and 4) were fairly similar to each other as described in detail in a previous paper [8], interestingly, *glomerulus* 5 seemed to differ from the four other both quantitatively and qualitatively. The data demonstrated in Table I indicate that there are significant differences in almost all attributes: including the small size, small number of neural components and of synapses. Due to these features, the *glomerulus* 5 was named "*mini*" *glomerulus*. Beside its *mini* character, which is evident, as compared its 3D reconstruction drawing (Fig. 4) with the other "normal" glomeruli (Figs

2 and 3), however, more additional features distinguish the *mini* glomerulus from the other four glomeruli. 1) The volume distribution of its neural components is different, having much greater proportion of Golgi axon varicosities than the other glomeruli. As a consequence, more dendritic digits form synapses with Golgi axons than in the other four "normal" glomeruli. 2) The synaptic perimeter (i.e. per cent of mossy terminal surface occupied by synaptic junctions) is much smaller (4.3%) than in the other glomeruli (5.4 to 5.5%). 3) In contrast to the four glomeruli, within the *mini* glomerulus *all* dendrites, without excep-

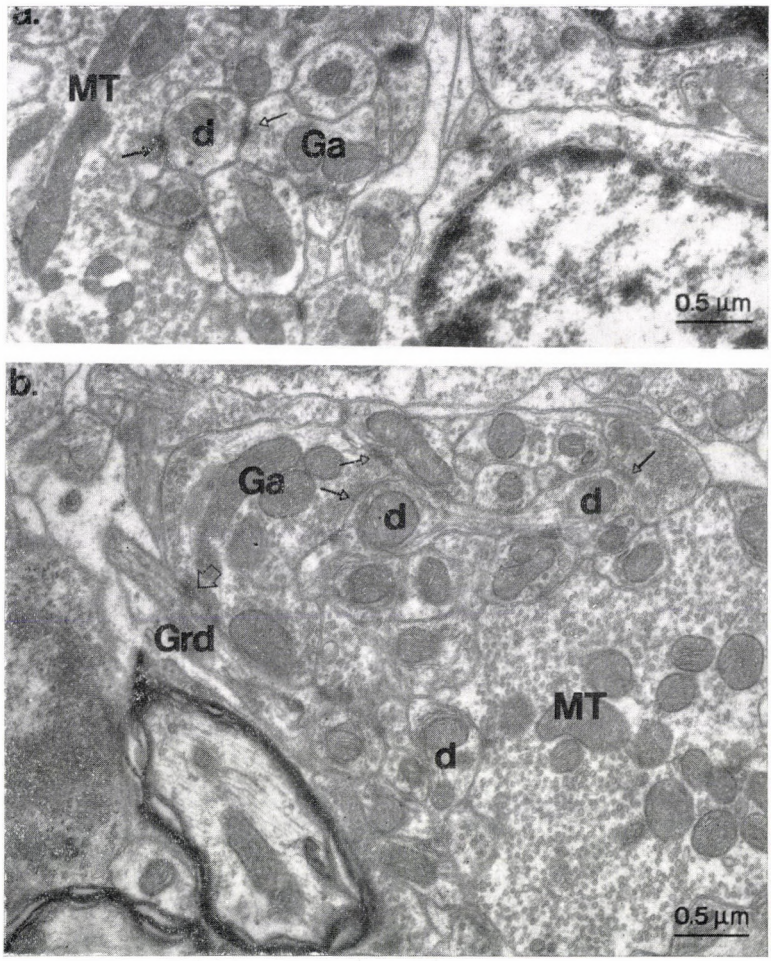

Fig. 5. a. A dendritic digit (d) establishes synaptic contacts both with a mossy terminal (MT, arrow) and Golgi axon (Ga, open arrow). b. Although dendritic digits (d) are the main targets for Ga-synapses (indicated by small open arrows), in some rare cases the proximal, "neck" portion of a granule cell dendrite (Grd) forms also synapses with Golgi axon (big open arrow). The same synapse is indicated also in Fig. 2c

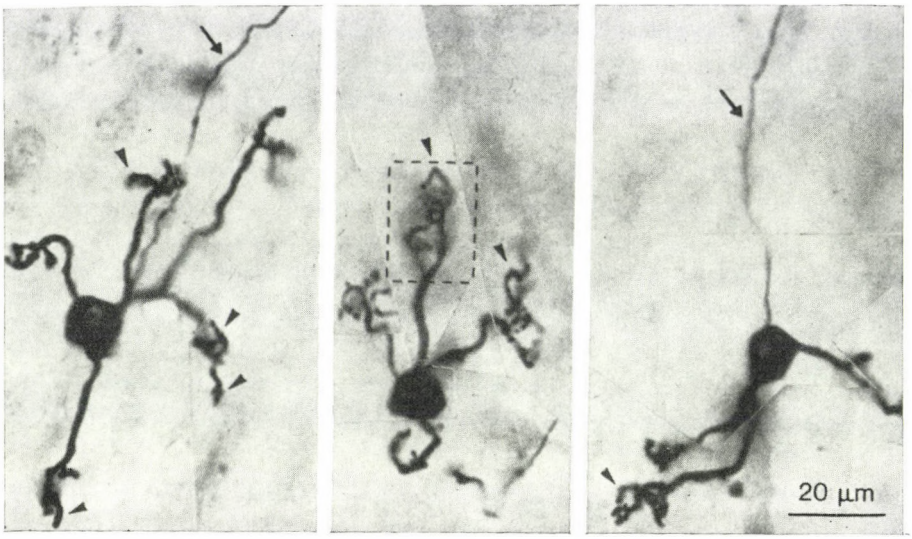

Fig. 6. Light micrographs of Golgi-impregnated granule cells from the granular layer of rat cerebellar cortex. The processes at the distal part of the granule cell dendrites are elongated and digitiform side-branches (arrowheads), which are incorporated into the characteristic glomerular organization (one is indicated by square), surrounding the mossy fiber swellings (not stained and invisible here). Arrows indicate the axons of granule cells

tion, establish synaptic contacts not only with mossy terminals but also with Golgi axons (see also Table I).

Table I

Quantitative data of the "mini" glomerulus and the four "normal" glomeruli

		"Normal" glomeruli	"Mini" glomerulus
Glomerular volume		114— 193 μm^3	41.58 μm^3
MT-volume		39.4—60.8 μm^3	9.78 μm^3
MT-surface		168— 266 μm^2	40.55 μm^2
	MT%	33.9%	23.5%
Volume distribution	Grd%	52.8%	52.3%
	Ga%	13.3%	24.2%
Number of Grd-s		53 (47—57)	10
Number of digits		208 (150—285)	75
Number of digits/Grd		3.9 (3.1—5.0)	5.8
Number of MT-synapses		113—176	31
Number of Ga-synapses		43—145	57
Number of Ga-varicosities		12— 28	13
% of Grd-s synapsing with Ga		60.4% (53.7%—73.7%)	100%
% of digit synapsing with	MT	67% (63.6%—73.7%)	38%
	Ga	25% (21.5%—26.6%)	50%
	MT + Ga	8% (5.5%— 9.8%)	12%
Synaptic perimeter (%)		5.45% (5.4%— 5.5%)	4.3%

MT = mossy terminal, Grd = granule cell dendrite, Ga = Golgi axon

Discussion

All five glomeruli studied belonged to the "simple" type, i.e. those having only one mossy terminal. More complex type glomeruli, the so called cerebellar "protoplasmic islets" [14], which incorporate two or more individual mossy terminals, could not be investigated by the methods used in this study. Nevertheless, a few general conclusions on the structural organization of this complex synaptic arrangement can be drawn on the basis of studying the simple type glomeruli.

1) The reconstruction of cerebellar glomeruli revealed that the dendritic digits, the terminal processes of Grd-s, are not short, claw-like elements, as it was previously described by Szentágothai for the cat [2], but, in the rat cerebellum they appear as long side-branches not thicker than the primary dendrites. This finding is in accordance with our light microscopic observations from Golgi-stained material, in which elongated, digitiform side-branches of granule cell dendrites, curve around the mossy terminal (Fig. 6). The computer-assisted drawings suggest that the articulation between the granule cell dendrites and the mossy fiber rosettes, being similar to the fingers of a hand grasping into a soft object, appears to be an advantageous morphological substrate for fast transmission of excitation. Indeed, single glomerular potentials have recently been described and the synaptic delay of mossy terminal-granule cell dendrite junction was calculated to be 0.17 ms, which is at the lower limit reported for chemical synapses [18].

2) The finding that each dendrite of a glomerulus originates from separate granule cells, implies that there is a huge divergence from mossy fibers to the granule cells (see also [8]).

3) The dendritic digits are the exclusive locations for all (excitatory) mossy fiber synapses, and for the most (inhibitory) Golgi axon synapses as well, however, a small per cent of the Golgi axonal synapses are also located at the proximal granule cell dendrites. This difference in location of the "inhibitory" synapses may also have functional consequences, as an inhibition provided at the proximal part of a dendrite may block the impulse-propagation of the dendrite while that at the dendritic digits seems to have less influence on the activation of a granule cell, as a whole.

4) The *mini* glomerulus, one of the five glomeruli, appears to differ significantly from the others with respect to the size, number of components, and of synapses. It is of particular interest that in this glomerulus the proportion of inhibitory axon terminals is higher than in "normal" simple glomeruli, with the consequence that in the *mini* glomerulus all granule cell dendrites receive synaptic contact from Golgi axons. Obviously, more *mini* glomeruli are needed to be studied, before assuming that this type would represent a separate class of cerebellar glomeruli.

REFERENCES

1. Chauvet J: Habituation rules for a theory of the cerebellar cortex. Biol Cybern 55: 201, 1986
2. Eccles J, Ito M, Szentágothai J: The Cerebellum as a Neuronal Machine. Springer, Berlin, Heidelberg New York, 1967
3. Fox CA, Hillman DE, Siegesmund KA, Dutta CR: The primate cerebellar cortex: a Golgi and electron microscopic study. In: Fox CA, Snider RS, (eds)The Cerebellum. Progress in Brain Research Vol. 25. 1967, p. 174
4. Gray EG: The granule cells, mossy synapses and Purkinje spine synapses of the cerebellum: light and electron microscope observations. J Anat (Lond) 95: 345, 1961
5. Hámori J.: Identification in the cerebellar isles of Golgi II axon endings by aid of experimental degeneration. In: Titlbach M. (ed.) Electron Microscopy 1964. Proceedings of the Third European Regional Conference held in Prague, Vol B, Czechoslovak Academy of Sciences, Prague, 1964, p. 291
6. Hámori J, Somogyi J: Formation of new synaptic contacts by Purkinje axon collaterals in the granular layer of deafferented cerebellar cortex of adult rat. Acta Biol Hung 34: 163, 1983
7. Hámori J., Szentágothai J: Participation of Golgi neuron processes in the cerebellar glomeruli: An electron microscopic study. Exp Brain Res 2: 35, 1966
8. Jakab R. L., Hámori J: Quantitative morphology and synaptology of cerebellar glomeruli in the rat. Anat Embryol 179: 81, 1988
9. Larramendi LMH: Morphological characteristics of extrinsic and intrinsic nerve terminals and their synapses in the cerebellar cortex of the mouse. In: Fields WS, Willis WD (eds) The Cerebellum in Health and Disease. WHM Green Inc, St Louis, 1969a, p. 63
10. Larramendi LMH: Analysis of synaptogenesis in the cerebellum of the mouse. In: Llinas R (ed.) Neurobiology of Cerebellar Evolution and Development. AMA-ERF Institute for Biomedical Research, Chicago, 1969b, p. 803
11. Llinas R, Hillman DE: Physiological and morphological organization of the cerebellar circuits in various vertebrates. In: Llinas R (ed.) Neurobiology of Cerebellar Evolution and Development, AMA-ERF Institute for Biomedical Research, Chicago, 1969, p. 43
12. Mugnaini E: The histology and cytology of the cerebellar cortex. In: Larsell O, Jansen J (eds) The Comparative Anatomy and Histology of the Cerebellum: The Human Cerebellum, Cerebellar Connections and Cerebellar Cortex. University of Minnesota Press, Minneapolis, 1972, p. 201
13. Palay SL: The electron microscopy of glomeruli cerebellosi. In: Cytology of Nervous Tissue, Proceedings of Anatomical Society of Great Britain and Ireland, Taylor and Francis, London, 1961, p. 82
14. Palay SL, Chan-Palay V: Cerebellar Cortex. Springer, Berlin, Heidelberg, New York, 1974
15. Palkovits M, Magyar P, Szentágothai J: Quantitative histological analysis of the cerebellar cortex in the cat. IV. Mossy fiber-Purkinje cell numerical transfer. Brain Res 45: 15, 1972
16. Peachey LD: Thin sections: 1. A study of section thickness and physical distortion produced during microtomy. J Biophys Biochem Cytol 4: 233, 1958
17. Reynolds ES: The use of lead citrate at high pH as an electron opaque stain in electron microscopy. J Cell Biol 17: 208, 1963
18. Taylor A, Elias SA, Somjen G: Focal synaptic potentials due to discrete mossy-fibre arrival volleys in the cerebellar cortex. Proc R Soc Lond B 231: 217, 1987
19. Zsuppán F: A computer reconstruction system for biological macro- and microstructures traced from serial sections . Acta Morph Hung 33: 33, 1985

Acta Morphologica Hungarica 37 (1—2), pp. 21—28 (1989)

COMPARISON OF THE EFFECTS OF NaF AND CaF_2 ON RAT GASTRIC MUCOSA A LIGHT-, SCANNING- AND TRANSMISSION ELECTRON MICROSCOPIC STUDY*

Pálma KERTÉSZ[1], T. KERÉNYI[2], Janina KULKA[2], Jolán BÁNÓCZY[1]

[1]DEPARTMENT OF CONSERVATIVE DENTISTRY AND [2]SECOND DEPARTMENT OF PATHOLOGY, SEMMELWEIS UNIVERSITY MEDICAL SCHOOL, BUDAPEST, HUNGARY

(Received 21 June 1988)

Rat stomachs were studied after intragastrically administered, repeated doses of 0.1 N HCl, 100 mmol/l NaF, 50 mmol/l CaF_2 in 0.1 N HCl, respectively. NaF produced extensive desquamation and cell injury, while CaF_2 caused some desquamation and a slight decrease in secretory activity as revealed by light microscopic, SEM and TEM examinations.

Keywords: Rat gastric mucosa, NaF, CaF_2

Introduction

Topical application of fluoridated gels is today a routine dental treatment, aiming at increasing the resistance of dental enamel. The fluoride concentration of these gels is 1—2% (562—1052 mmol/l), and they are applied in preventive dentistry, generally 1—4 times a year. The gel or paste (approx. one gramme) which passes into the stomach during treatment or afterwards is diluted 50—100 times with saliva or gastric juice, and its final concentration is still 5—20 mmol/l.

Another area of local fluoride application is the follow-up to radiotherapy treatment affecting the maxillo-facial region performed 3—7 times a week for several (3—4) months. One treatment may cause around 5—40 mg fluoride load for the patients [5, 6, 7, 8]. These quantities do not influence considerably the fluoride balance of the human organism, but should be taken into consideration when systemic fluoride supplementation is precalled to prevent dental caries. As a side effect of fluoride intake nausea, vomitus and abdominal pain [2] may arise. No data were found in the literature concerning the effect on the human gastric mucosa of fluoride swallowed together with the saliva during and after the topical application of fluoridated preparations. On rat gastric mucosa however, after a single dose of 10 mmol/l NaF, light- and electron microscopic lesions and permeability changes for small molecules could

* This work was supported by the Borrow Dental Milk Foundation

Send offprint requests to: P. Kertész, Dept. of Conservative Dentistry, Budapest, Mikszáth sq. 5., 1088-Hungary

be observed [3, 4, 10]. Occurrence of similar changes on the human gastric mucosa as a result of the use of agents with high fluoride content, cannot be excluded. Nor were reports in the literature on the effect of CaF_2, which is one of the deposit forms of fluoride in the oral cavity [9]. CaF_2 has a considerably smaller absorption rate from the stomach than NaF [1, 11].

The aim of our study was to investigate the possible effect of CaF_2 on the rat gastric mucosa, and to compare it with that of NaF.

Materials and methods

18 female rats, from inbred laboratory strain weighing 220—400 g were assigned to three groups, (control, NaF and CaF_2) six animals to each group. The animals were treated with intragastrically administered solution of 0.1 N HCl, 100 mmol/l NaF or 50 mmol/l CaF_2, both dissolved in 0.1 N HCl, one ml/100 g body weight. Sufficient amount of mannitol was

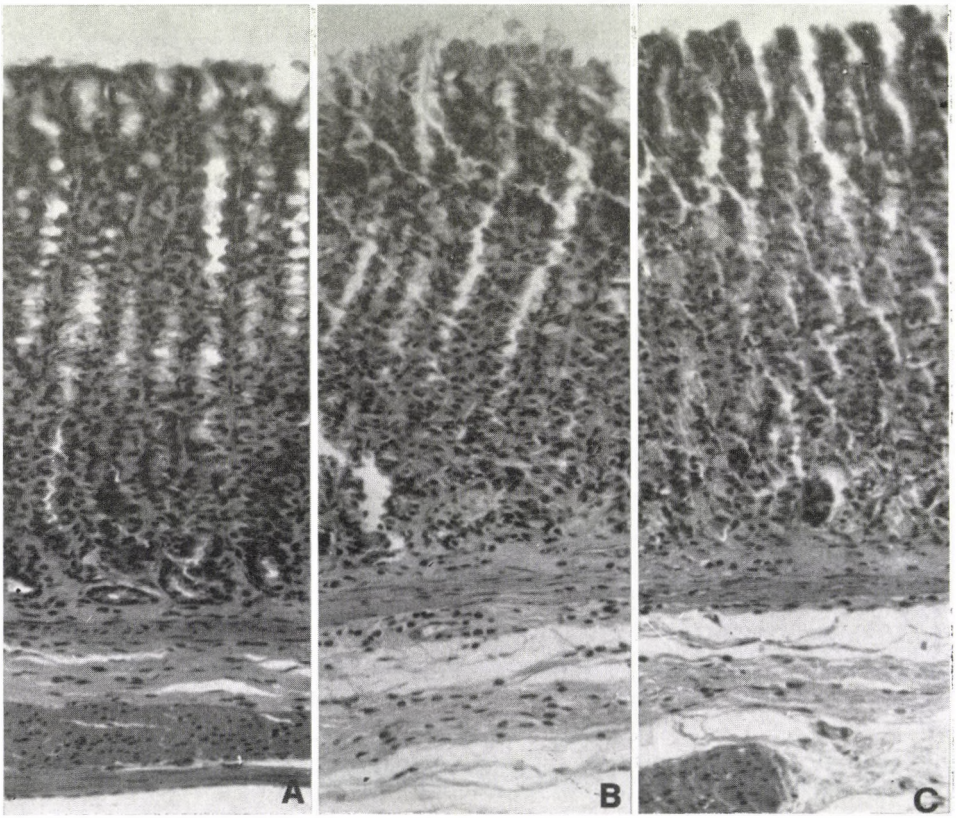

Fig. 1. Histological examination of gastric mucosa, HE staining ×250. A. Control animal exposed to 0.1 N HCl: foveolae are lined with mucous epithelial cells B. NaF treated animal exposed to 100 mmol/l NaF in 0.1 N HCl: gross appearance of the mucosa seems normal but the foveolar cells contain less mucosal substances. The layer of luminal cells is continuous and covered with some cell debris. C. CaF_2 treated animal exposed to 50 mmol/l CaF_2 in 0.1 N HCl: normal foveolae and intact mucosa

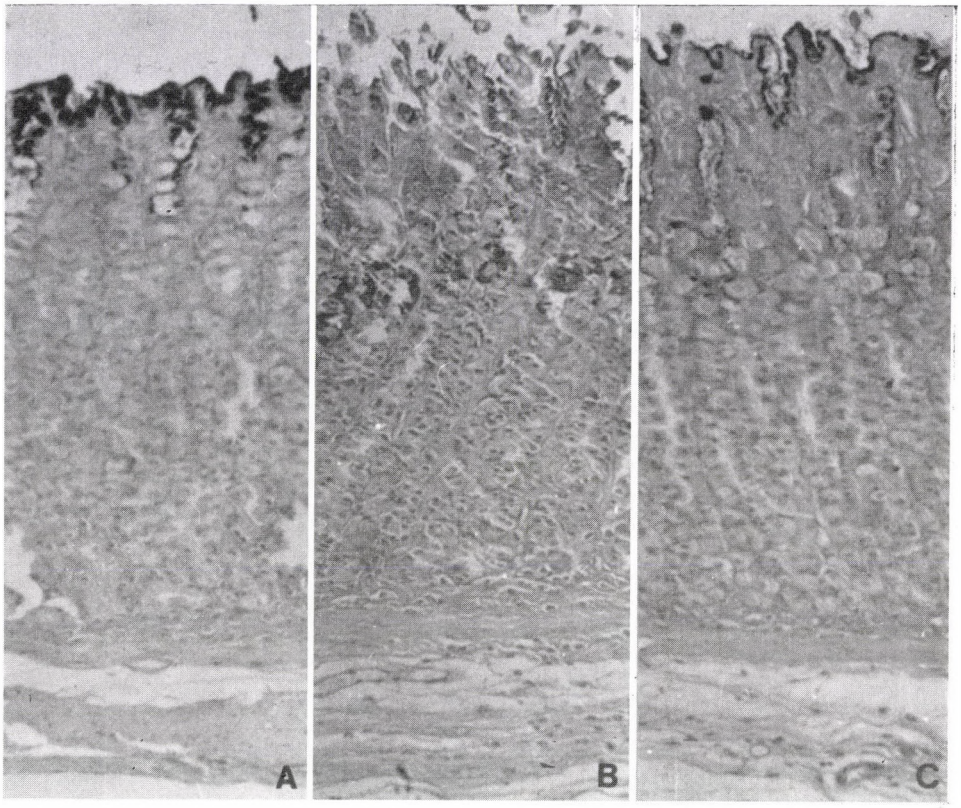

Fig. 2. Histochemical examination of gastric mucosa, Alcian-blue-PAS staining ×250. A. Control animal exposed to 0.1 N HCl: normal mucoid material in the cells of superficial mucosa B. NaF trated animal exposed to 100 mmol/ NaF in 0.1 N HCl: intensive desquamation on the surface accompanied with uneven loss of mucous material from the superficial layers of mucosa C. CaF_2 treated animal exposed to 50 mmol/l CaF_2 in 0.1 N HCl: partial loss of mucous substances from the superficial layers of mucosa

added to the solutions to be isotonic to rat plasma, and to avoid any osmotic damage of the mucosa. The animals received the test solutions three times, every second day.

One hour after the third treatment, stomachs were filled in situ with 4% glutaraldehyde with the help of an oesophagial sonde, under ether anaesthesia. Following the ligation of the oesophagus and duodenum, the stomach was removed and immersion fixed with the same glutaraldehyde solution. In this way fixation differences due to the concentration and inappropriate penetration of the fixative could be avoided. After 1 h of immersion fixation 1×4 mm specimens were cut and fixed for another hour again, than dehydrated and embedded in Durcupan-ACM (Fluka). Following the dehydration some specimens were critical point dryed, coated with gold for scanning electron microscopic investigation.

One micron sections from the resin embedded specimens were stained with methylene blue and selected for electron microscopic investigation. Ultrathin sections were made by a Reichert OmU-2 ultramicrothome, contrasted with uranyl acetate and lead citrate.

The rest of the stomach was fixed in 8% formaldehyde for 24—48 h, and embedded in paraffin. Sections of paraffin embedded specimens were stained with haematoxyline eosin, alcian blue and periodic acid-Schiff (PAS) reactions.

Transmission and scanning electron microscopic specimens were examined with a JEOL 100 B electron microscope equipped with a scanning adapter.

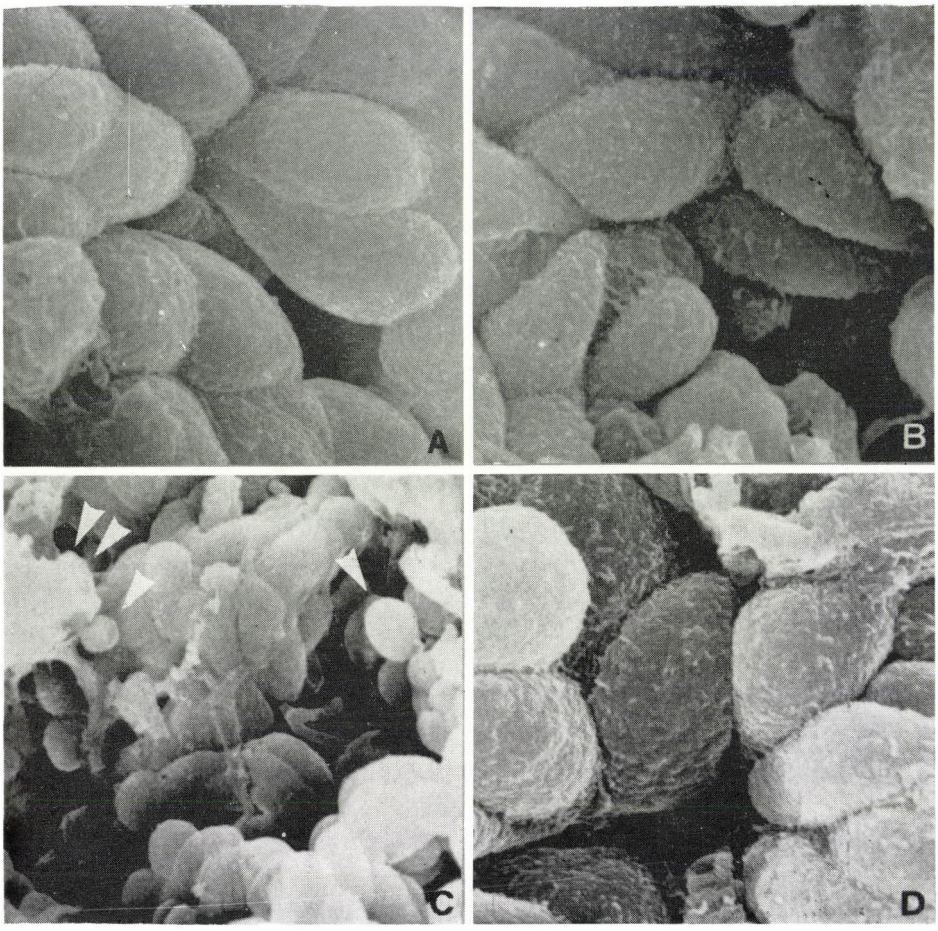

Fig. 3. Surface structure of the gastric mucosa following the different treatments. Scanning electron micrograph reveals fine villous superficial epithelial cells surrounding the openings of the gastric glands. A. Control animals exposed to 0.1 N HCl, ×4500 B. NaF treated animal exposed to 100 mmol/l NaF in 0.1 N HCl, ×4500. C. NaF treated animal exposed to 100 mmol/l NaF in 0.1 N HCl: mucosal surface covered with desquamated cells (↓), and amorphous material (↓↓), ×2500 D. CaF_2 treated animal exposed to 50 mmol/l CaF_2 in 0.1 N HCl, ×4500

The thickness of the gastric mucosa was measured microscopically with a PZO Warsawa K-15, ocular micrometer. 1 ml blood samples were obtained from each animal, by cardial punction just before the preparation of the stomach. The blood sample was centrifuged with 500 *g*, and the supernatant (the plasma) was diluted twice with TISAB buffer. Then the fluoride concentration was measured with a fluoride sensitive electrode (OP 4771, Radelkis, Budapest). NaF standards and TISAB buffer were obtained from Radelkis, Budapest, NaF from REANAL, Budapest, and CaF_2 from Riedel-deHaen, Seelze-Hannover.

The statistical evaluation was made by calculating the means, standard deviation, and the Student's unpaired *t*-test was used.

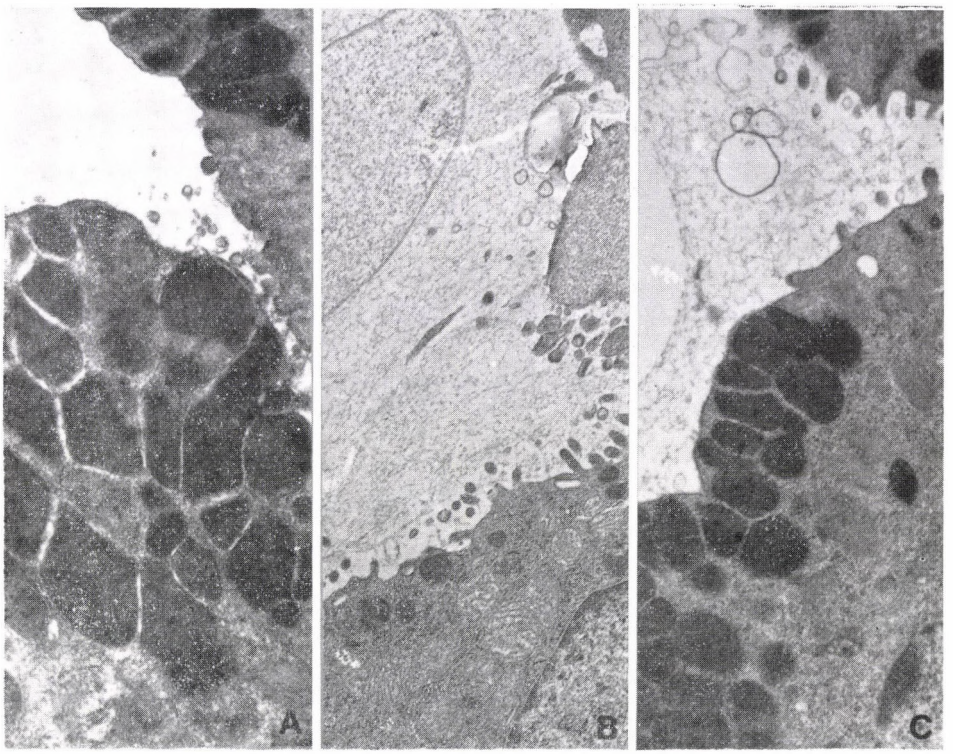

Fig. 4. Transmission electron micrographs of the superficial epithelium of gastric mucosa. A. Control animal exposed to 0.1 N HCl: secretation granules and intact organelles of the gastric mucosa, ×14 400 B. NaF treated animal exposed to 100 mmol/l NaF in 0.1 N HCl: decreased number of secretory granules in the cells and necrobiotic cell debris in the lumen, ×9000 C. CaF_2 treated animal exposed to 50 mmol/l CaF_2 in 0.1 N HCl: intact structure and signs of normal secretion activity, ×14 400

Results

The epithelial thickness of the gastric mucosa did not show significant differences in the control, NaF, and CaF_2 groups (Fig. 1A, B, C).

In the group treated with NaF (Fig. 2B) the amount of acidic mucopolysaccharides in the gastric mucosa was less than in the other two groups (Fig. 2A, C). On the mucosal surface of the NaF treated group the large number of desquamating cells was striking (Figs 2B; 3B, D; 4B), fewer desquamating cells were found in the CaF_2 treated group (Fig. 2C) and none in the control animals (Fig. 2A). The villosity of the superficial cells, though changing from cell to cell did not show any consistent difference between the three groups (Fig. 3A, B, C).

The secretory activity of the gastric mucosa, as seen in the ultrathin sections, was well preserved in the CaF_2 and control groups (Fig. 4A, C) but

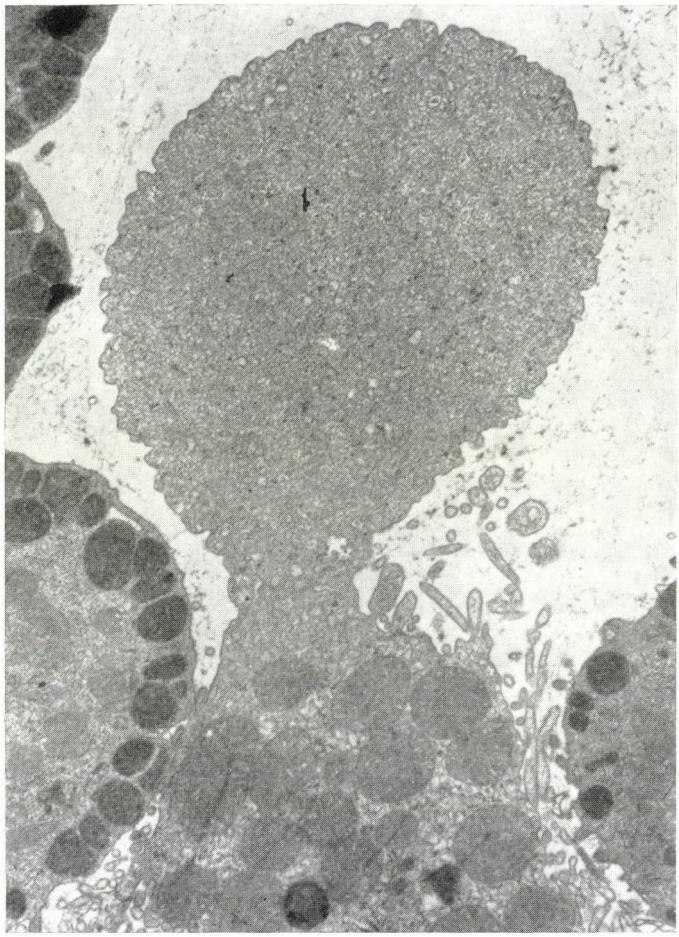

Fig. 5. Transmission electron micrographs from NaF treated animal exposed to 100 mmol/l NaF in 0.1 N HCl. Protrusion of the surface of a damaged cell between normal secreting ones, ×9600

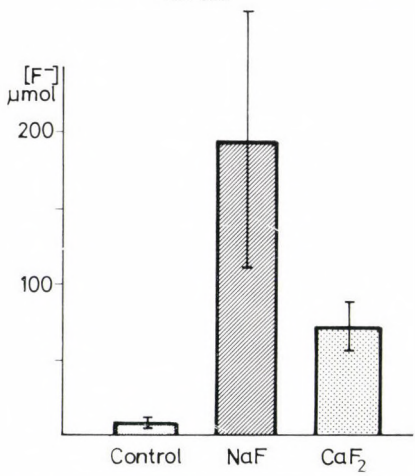

Fig. 6. The plasma fluoride concentrations of the groups one hour after the different treatments

decreased moderately in the NaF group (Fig. 4B). In the latter group oedematous protrusions could be observed on the cell surface (Fig. 5). Membrane-coated cell debris without cell organelles could be also seen in the lumen.

Differences between the plasma fluoride concentration of the three groups, measured one hour after the last treatment, were significant (NaC/C: $p < 0.001$, CaF_2/C: $p < 0.001$, NaF/CaF_2: $p < 0.01$). The plasma fluoride concentration in the NaF treated group was nearly three times higher than in the CaF_2 treated group (Fig. 6).

Discussion

The light- and scanning electron microscopic alterations of rat gastric mucosa described after a single dose of fluoride [3, 4, 10] were found in our experiments to be diminished after three subsequent doses of 100 mmol/l NaF. The observed cell desquamation seen in our study has been described by Easmann et al. [3] after a single 10 mmol/l NaF treatment. The plasma fluoride concentration in the NaF treated group is in good accordance with the data of the above mentioned team [12]. This shows that the NaF contacted the gastric musosa after the treatment and has been absorbed. The milder character of the gastric mucosal changes observed by us, may be explained by the use of a laboratory inbred rat strain, a bred close to, but not exactly identical with the Wistar strain.

Considerble changes in the thickness of gastric mucosa may be expected only after longer test period.

The villosity of the mucosal surface, — which is a sensible indicator of surface damage — did not show significant changes, however, the protrusions observed in the NaF treated group, point to focal damage of the superficial membrane and of the cells. The continuity of the epithelium on the scanning micrographs may be explained by the fact that after dequamation of the superficial cells, the lower regenerated cells are seen. The increased ratio of desquamating cells in the groups treated with fluoride is an observation made one hour after the last treatment. Although we did not examine the dynamics of the desquamation and regeneration, the decreased secretory activity accompanying desquamation, and the fact that the control group showed no signs of desquamation, points to the topical effect of fluoride.

Comparing the degree of desquamation and the plasma fluoride concentration in the two fluoride groups, the CaF_2 group showed less desquamation with lower plasma fluoride concentration, and the NaF group represented more pronounced desquamation with significantly higher plasma fluoride concentration. Although animals in both groups received stoechiometrically

just the same quantity of fluoride, CaF_2 caused less damage to gastric mucosa. This might be the consequence of a lower absorption rate for CaF_2 through the gastric mucosa, than for NaF [1, 11].

On the basis of our results it seems that the potential risk of side effects on the gastric mucosa is smaller after the use of CaF_2, than in the case of NaF.

Acknowledgements

The authors wish to thank Mrs. M. Purucki and Mrs. H. Deák for their technical assistance and Mrs. J. Kováts for the preparation of photographs.

REFERENCES

1. Afseth, J, Ekstrand J, Hagelid P: The dissolution of calciumfluoride tablets in vitro and bioavailability in man. Scand J Dent Res 95: 191, 1987
2. Beal J.F, Rock WP: Fluoride gels. A laboratory and clinical investigation. Br Dent J 140: 307, 1976
3. Easmann RP, Steflik DE, Pashley DH, McKinney RV, Whitford GM: Surface changes in rat gastric mucosa induced by sodium fluoride: A scanning electron microscopic study. J Oral Path 13: 255, 1984
4. Easmann RP, Pashley DH, Birdsong NL, McKinney Jr. RV, Whitford GM: Recovery of rat gastric mucosa following single fluoride dosing. J Oral Path. 14: 779, 1985
5. Ekstrand J, Koch G, Petersson LG: Plasmafluoride concentration and urinary fluoride excretion in children following application of the fluoride-containing varnish Duraphat. Caries Res 14: 185, 1980
6. Ekstrand J, Koch G, Lindgreen LE, Petersson LG: Pharmacokinetics of fluoride gels in children and adults. Caries Res 15: 213, 1985
7. Einwag J: Bioverfügbarkeit von Fluorid nach lokaler Anwendung. Dtsch zahnarztl Z 38: 54, 1983
8. Einwag J: Fluorid-konzentrationen im Serum nach Löffelapplikation von Gelees mit unterschiedlichem Gehalt an Aminfluorid. Dtsch zahnarztl Z 38: 650, 1983
9. Grön P: Chemistry of topical fluorides. Caries Res (11. Suppl) 1: 172, 1977
10. Pashley DH, Allison BN, Easmann RP, McKinney RV, Horner JA, Whitford GM: The effects of fluoride on gastric mucosa of the rat. J Oral Path 13: 535, 1984
11. Trautner K, Einwag J: Factors influencing the bioavailability of fluoride from calcium-rich, health-food products and CaF_2 in man. Archs Oral Biol 32: 401, 1987
12. Whitford GM, Birdsong-Whitford NL, Lowe BR: Fluoride pharmacokinetics: Effect of light exercise in rats. Caries Res 22: 106, 1988

Acta Morphologica Hungarica 37 (1—2), pp. 29—46 (1989)

DENDRITIC CELLS OF THE LYMPHOEPITHELIAL ORGANS

I. Törő, I. Oláh

2ND DEPARTMENT OF ANATOMY, SEMMELWEIS MEDICAL UNIVERSITY, BUDAPEST, HUNGARY

(Received 11 July 1988)

Introduction

At the oral and anal openings of the developing alimentary canal lymphoepithelial rings are located which suggest their essential role [7, 33]. The palatine tonsil is formed in the second branchial pouch. The thymic anlage develops from the epithelium of the ventral parts of the third and fourth pouches. During ontogenesis the thymus detaches of the branchial pouch losing its connection with the body surface (Fig. 1), while the tonsils establish a permanent connection with the surface. The anatomical situation of these organs is reflected in their role; namely the thymus and the tonsils function in antigen poor and antigen rich environment, respectively.

Among the lymphoepithelial organs the avian bursa of Fabricius seems to represent a unique situation. In the early fifties this organ has come into the focus of interest which resulted in an explosion-like development in modern immunology. The discovery of the bursa's function was a major contribution to the establishment of the basic two-cell dogma (T and B) in immunology. The bursal lumen is connected with the cloaca but its lymphoepithelial compartment is isolated from the surface.

In vertebrates the function of lymphoepithelial tissues and organs is enigmatic. The term lymphoepithelial reflects their common histological feature namely that the epithelial anlage of entodermal origin is infiltrated by mesodermal mobile cells.

In addition to the lymphoepithelial organs (thymus, tonsils and bursa of Fabricius) lymphoepithelial tissues are also formed by lymphoid cells entering the intestinal, bronchial and skin epithelium [2, 3, 5, 7, 29, 31]. These

Abbreviations: (1) B, Bursa of Fabricius; (2) BM, Basement membrane; (3) C, Capsule; (4) Co, Cortex; (5) Ep, Ectoplasm; (6) FAE, Follicule-associated epithelium; (7) FDC, Follicular dendritic cell; (8) IDC, Interdigitating dendritic cell; (9) IFE, Interfollicular epithelium; (10) L, Lymphocyte; (11) LE, Lymphoepithelial; (12) Ma, Macrophage; (13) M, Medulla; (14) Th, Thymus; (15) To, Tonsils

Send offprint requests to: I. Törő, 2nd Dept. of Anatomy, Semmelweis Medical University, Budapest, Tűzoltó Str. 58, H-1094, Hungary

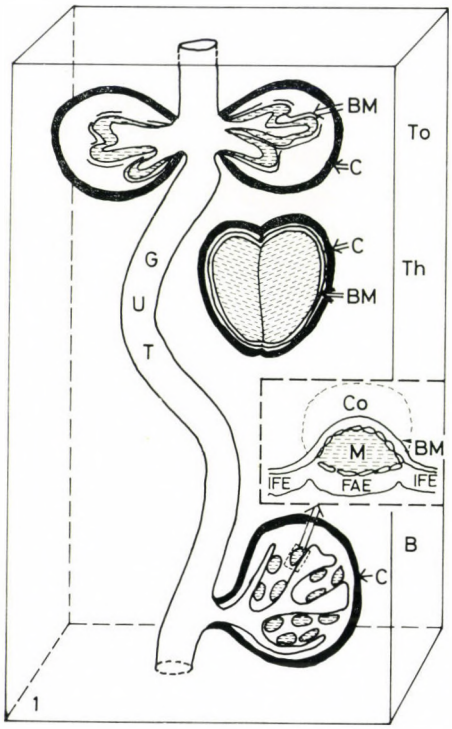

Fig. 1. The LE organs are associated with the digestive tube. The striped areas represent the LE substance of the tonsils thymus and bursa of Fabricius [8]. The Th is completely (anatomically and histologically) separated from the surface. In the bursa the FAE separates (histologically) the LE compartment from the bursal lumen. The tonsillar LE tissue forms the surface epithelium (neither anatomical nor histological separation)

lymphoepithelial structures are built into other non-lymphoid organs forming gut (GALT), bronchus (BALT) and skin (SALT) associated lymphoid tissues. They cannot be removed surgically.

Meckel's diverticulum which is a remnant of the omphaloenteric duct turns to be also lymphoepithelial in the chicken at the beginning of the life (between 2—7 weeks of age) [20]. This period remarkably correlates with the formation of lymphopineal tissue where the lymphoid cells are in intimate topographical relationship with the pinealocytes [19]. In the case of the Meckel's diverticulum and pineal body, it has not been proved that the lymphoid invasion would be a manifestation of a rapid burst of lymphoid proliferation around day 10—14 or, it would represent some special differentiational or functional significance at the end of maturation of lymphoid systems. The appearance of lymphopineal tissue may reflect a distinct immunmodulatory relationship between neuroendocrine and lymphoid organs.

Thymus

The thymus is the largest lymphoepithelial organ which is lobulated like the glands. During the past century the thymus was always in the focus of investigations. In spite of this intensive and wide interest of histologists, embryologists, endocrinologists and — finally — immunologists, its function is still unclear. There were several booms of the study of thymus which are worth to mention in a brief historical survey. The first one was around the turn of the century, when the histologists and embryologists studied the structure and development of the thymus. Our basic knowledge concerning the histology and embryology of this organ originated from that time. This period of investigation proved that the thymic epithelial reticulum is of entodermal origin, the network of which is filled with lymphocytes. The question was raised whether lymphocytes are of blood borne or intrinsic, intrathymic origin, namely they are transformed epithelial cells. Currently the latter claim is only of historical interest and it is convincingly proved that the lymphocyte precursors in the lymphoepithelial organs and tissues, are blood borne [11]. It is worth to mention, that the term thymocyte was originally used for the cell population generated by transformation of thymic epithelial cells.

During the forties and early fifties when endocrinology developed rapidly a new era started in the investigation of the thymus. Very early, it was realized, that the thymus is sensitive for corticosteron which suggested the existence of a negative feedback mechanism between the adrenal cortex and thymus. Further studies revealed that actually the cortical thymocytes were sensitive to cortisone. Similar results were obtained by X-ray examinations. These examinations established that the cortical and medullary lymphocytes are different concerning their cortison and radiation sensitivity. The interactions between the thymus and other endocrine organs, such as thyroid, gonads and pituitary were also intensively studied but it did not bring any essential theoretical and/or practical results.

However, this era brought one of the most crucial discoveries of modern immunology which is related to the bursa of Fabricius. The bursa of Fabricius was thought to be an endocrine organ, therefore bursectomy might cause some endocrine deficiency. A fortunate accident revealed that birds, bursectomized at hatch failed to produce antigen specific IgG antibodies against Salmonella bacteria suggesting the essential role of the bursa in the antibody response [6]. Right after this discovery the thymectomy in newborn mice has thrown some light on the function of the thymus. Thymectomy in newborn animals caused wasting disease and lymphocyte depletion in the T dependent areas of the peripheral lymphoid organs. The major functional deficiency manifested in the impaired cellular immunity. [13]. The clinical immunology of the Di George syndrome supports the experimental observations.

Fig. 2. Thymic dendritic (special) cell. The bean-shaped nucleus is situated eccentrically in the cytoplasm. The cell granules accumulate in the endoplasm around the centriole. The ectoplasm is markedly dendritic surrounding the lymphocytes

The function of the thymus in the T cell differentiation is essential but the mechanism is still obscure. It is generally believed, that the epithelial reticulum of entodermal origin plays a significant role in the T cell differentiation by producing some humoral factors and/or by direct cellular contact. A few years ago Wekerle and his co-workers [31] isolated a cell cluster from the thy-

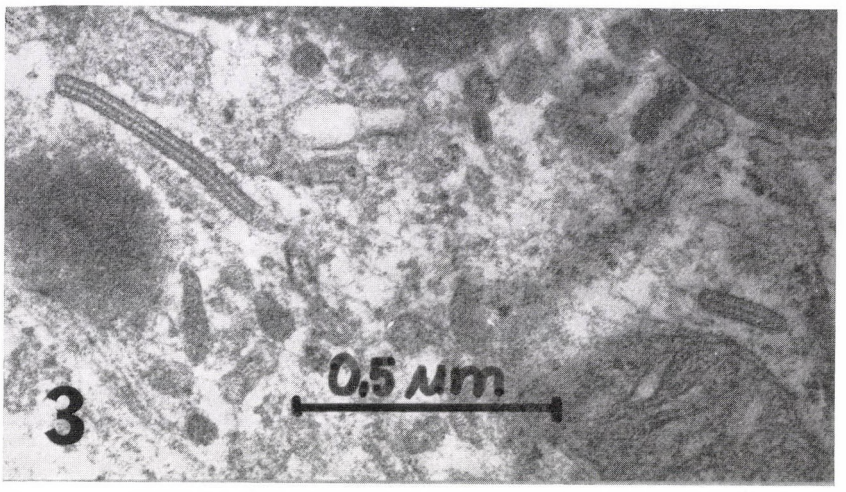

Fig. 3. Bierbeck granules in a thymic dendritic cell

mus which consisted of many thymocytes engulfed by epithelial cell. This epithelial cell was called "nurse cell" which "feeds" the thymocytes for a while. This type of emperipolesis is quite unusual in vertebrate tissues, and its presence was postulated only on the basis of in vitro experiments. The in situ electron microscopic studies never verified clearly this cytoplasmic "bath" [10]. However, the existence of a nurse cell could be justified by the special environmental requirements of cytogenic tissues.

Twenty years ago we discovered a new cell type in the rat's thymus what we called the special cell [14]. This cell type locates at the cortico-medulla border, possesses a well developed Golgi region with secretory granules and occasionally Bierbeck granules (Figs 2, 3). The cell surface is highly interdigitated and covered by an electron dense substance. Thymocytes during their intrathymic differentiation migrate from the cortex to the medulla. Before they become functionally mature, they have to come into contact with the special cells at the cortico-medullary border (Fig. 2). On the basis of their cytoplasmic structure and distinct location we suggested that this cell may be responsible for producing thymic humoral factor(s).

A few years later during the early seventies, the dendritic cell as an accessory or antigen presenting cell of the immune response has been described. The histological and immunological experiments concerning the accessory cells proved that this cell population is heterogeneous, Ia surface antigen positive, and is present not only in the lymphoid but also in the non-lymphoid organs. The discovery of the function of the skin's Langerhans cells directed the attention of the researchers towards the thymic special cell. Now, there is evidence that the special cell is identical with the thymic dendritic cell contribut-

ing the thymic microenvironment. Besides the thymic epithelium the special cell or in other words, the interdigitating dendritic cell is participating in the thymocyte's differentiation. Recently, it has been published that in different thymomas the altered thymic epithelium is not followed by functionally and immunhistochemically impaired thymocyte differentiation [30]. Therefore, the role of the dendritic cells in the thymocyte maturation has been upgraded. In the future, the research concerning the thymus has to pay more attention to the dendritic cells and its ontogenetic, cell cooperational (functional) involutional and pharmaco-toxicological aspects.

Bursa of Fabricius

The bursa of Fabricius is responsible for B cell differentiation and immunoglobulin class switch. The surface epithelium consists of two different areas (Fig. 4). 1) Interfollicular epithelium (IFE) which covers about 90% of the whole bursal surface and it produces mucoid substances. 2) Follicular associated epithelium (FAE) is 10% of the surface and immunologically oriented [16], capable of bidirectional transport [4, 28]. However, careful examinations made questionable the transport from the follicle toward the bursal lumen [12]. Neither IFE nor FAE are of lymphoepithelial nature but in starling's bursa the FAE revealed a few mobile cells resembling to "abortive" secretory cells [8].

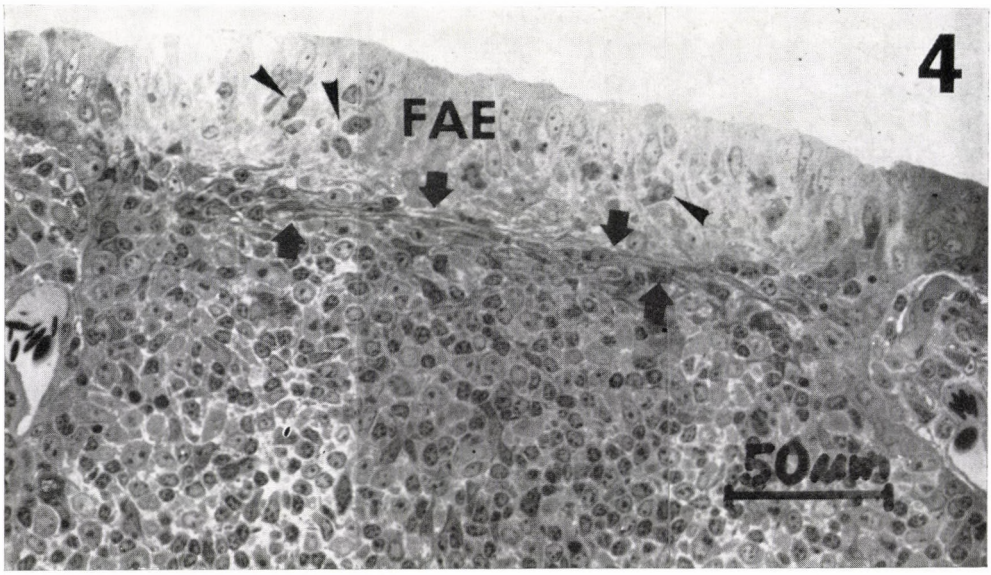

Fig. 4. Underneath the FAE there is an epithelial network running parallel with the surface (arrow). No lymphoid cells are in the FAE, but abortive secretory (dendritic) cells (arrowhead) are present

The real lymphoepithelial tissue of the bursa of Fabricius is the medulla which is isolated from both the vascularized follicular cortex by a basal lamina and from the bursal lumen by FAE. Underneath the FAE there is an epithelial network which is of 2—4 cell thickness oriented parallel with the surface (Fig. 4). This epithelial network "prevents" the lymphoid cells to enter the FAE. This distinct histological feature provides for the bursal lymphoepithelial tissue an isolated condition. The existence of the FAE which is capable of antigen uptake (Fig. 5) and the isolated condition of the lymphoeptihelial tissue well correlate with the double bursal functions i.e. central and peripheral [28].

The medulla of the bursal follicles develops from the entoderm during the early embryonic life while the cortex is of mesenchymal origin and develops mainly after hatch. Therefore, the medulla can be regarded as a central lymphoid organ, and the cortex as a peripheral lymphoid one. The luminal ends of the FAE cells contain coated and flattened vesicles as well as tubular structures (Fig. 6). These structures resemble that of the M cells of the tonsillar epithelium [24, 25], function of which may be related to antigen uptake from the bursal lumen.

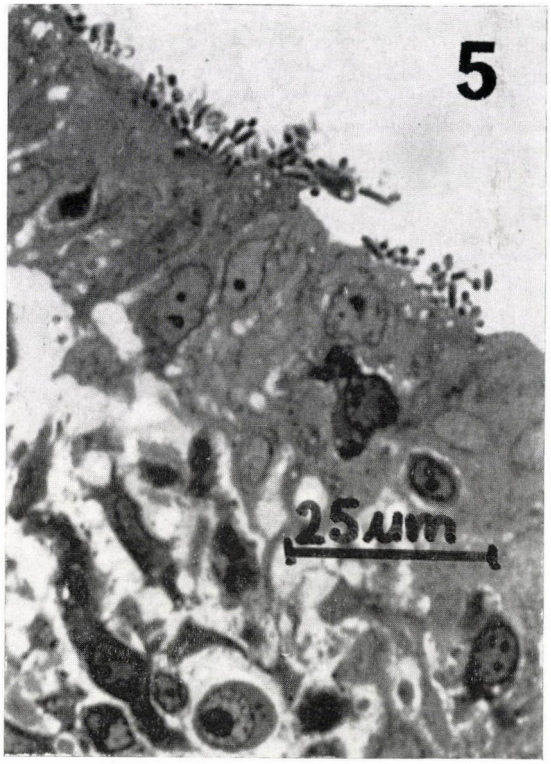

Fig. 5. Bacteria are attached and invaded in the FAE showing that these epithelial cells are capable of antigen uptake

It is well established, that the function of the thymic interdigitating dendritic cell is engaged in the T cell education. It was reasonable to assume, that a dendritic-like cell should also exist in the bursa contributing to the B cell maturation by soluble substances and/or cell contact. The secretory cell (Figs 7, 8) which we have identified in the lymphoepithelial compartment of the bursa of Fabricius forms about 0.5% of bursal cell content [17, 21]. This percentage of secretory cell well correlates with the number of lymphoid dendritic cells in the mouse lymphoid organs. Our detailed morphological studies proved that the secretory cell is the only cell type which may be a candidate for the bursal dendritic cell.

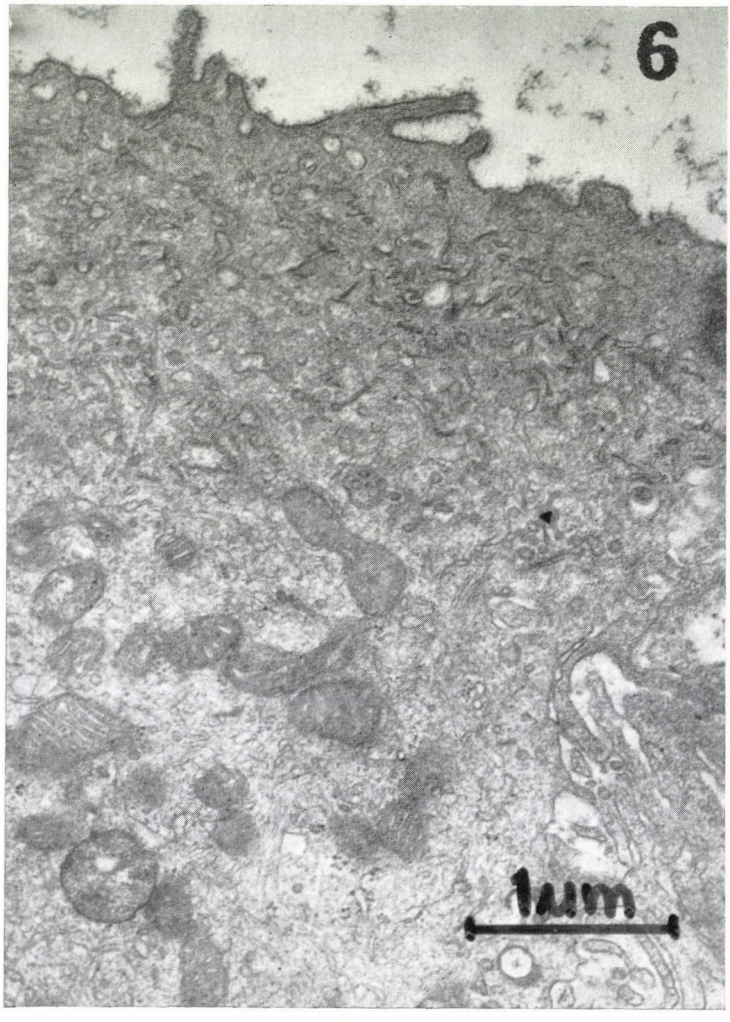

Fig. 6. The cells of the FAE, like the tonsillar M cells, produce pinocytotic vesicles and flattened vacuolar structures at the apical surface

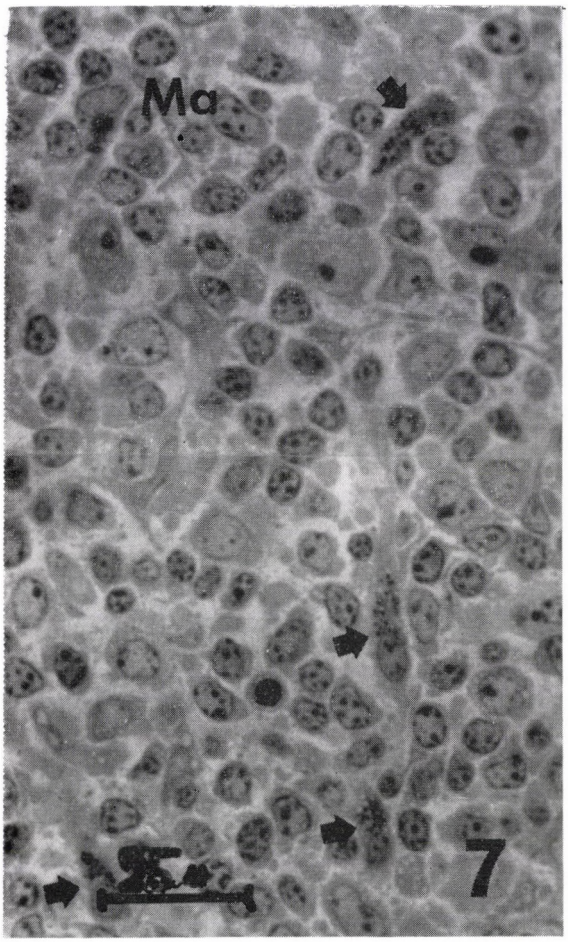

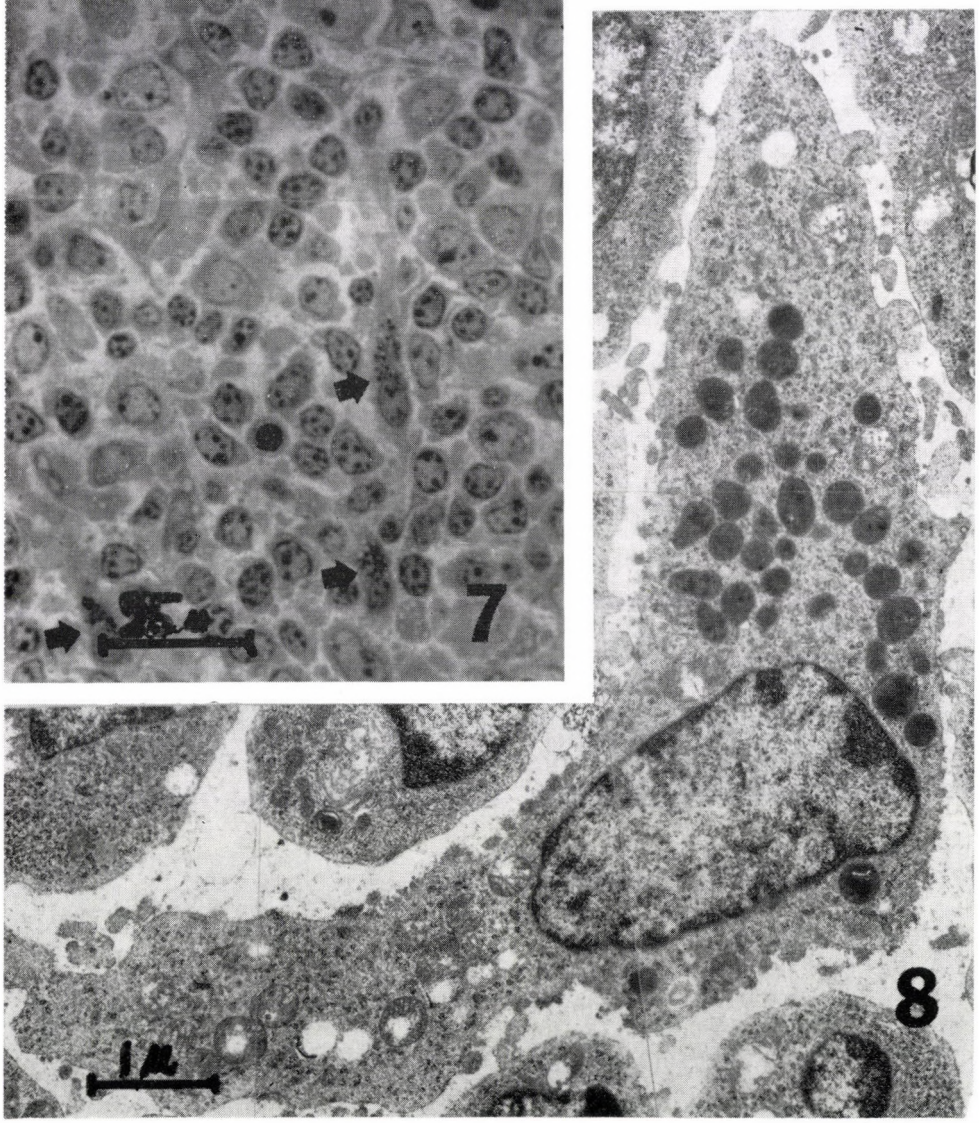

Fig. 7. Bursal dendritic (secretory) cells have elongated cytoplasm. The secretory granules locate on one side of the nucleus (arrow)

Fig. 8. The transmission electron micrograph shows that the surface membrane of the secretory cell is covered by spotted electron dense substance around the nuclear area

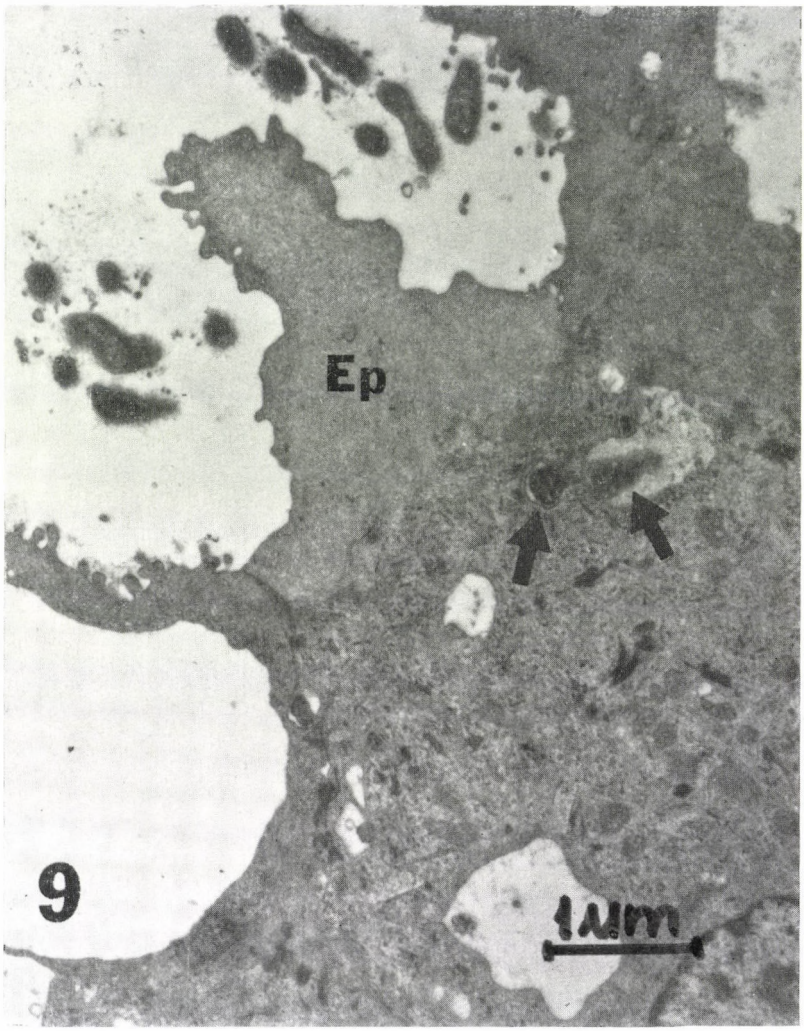

Fig. 9. Tonsillar M cell is exposed by bacteria. Two bacteria are in the cell (arrow). Under the ectoplasmic area the cytoplasm is loaded with flattened vacuolar structures

The bursal dendritic cell is modified for secretory function contributing to the bursal microenvironment in loco, and influences the formation and function of the antigen presenting cells in the spleen [9, 19].

The periellipsoidal white pulp (PWP) is B dependent area of the spleen. After surgical bursectomy [22] the differentiation of the PWP's cells to ellipsoid associated cells (EAC) — which are precursors of interdigitating dendritic cells — is impaired. The EAC are capable of antigen uptake which triggers their migration to the T dependent areas where they may function as interdigitating dendritic cells (IDC), activating T cells. This sequential transformation

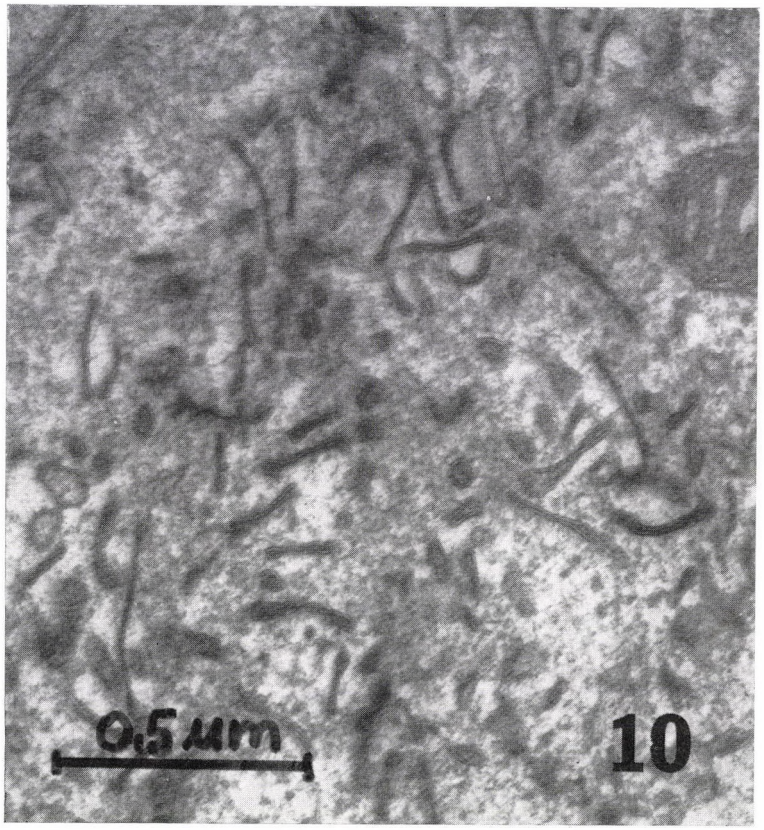

Fig. 10. Vacuoles and flattened vacuolar structures in the tonsillar M cell

and maturation of PWP-cells (PWP cells → EAC → IDC → FDC (follicular dendritic cell) are influenced by the product of bursal secretory cell [18, 22]. In the absence of the bursa i.e. bursal secretory cells, this sequence of events is impaired which results in a greatly reduced number of germinal centers and the lack of switch from antigen specific IgM to IgG.

The precursors of bursal secretory cells differentiate from the bursal mesenchyme during embryonic days 9—11 [23]. They migrate into the surface epithelium inducing bud formation which is the primordium of follicular medulla. The differentiation of the secretory cell's precursor is testosteron (TP) sensitive i.e. testosteron treatment prevents the mesenchymal cells to transform secretory cell's precursor [23]. In consequence of the TP treatment there is no bud formation and as a result of chemical bursectomy the epithelial anlage of the bursa rapidly regresses after 12—14 day of embryonic life. This experimental observation suggests that the bursal development — actually the B cell system — depends upon the differentiation of precursor of secretory cells

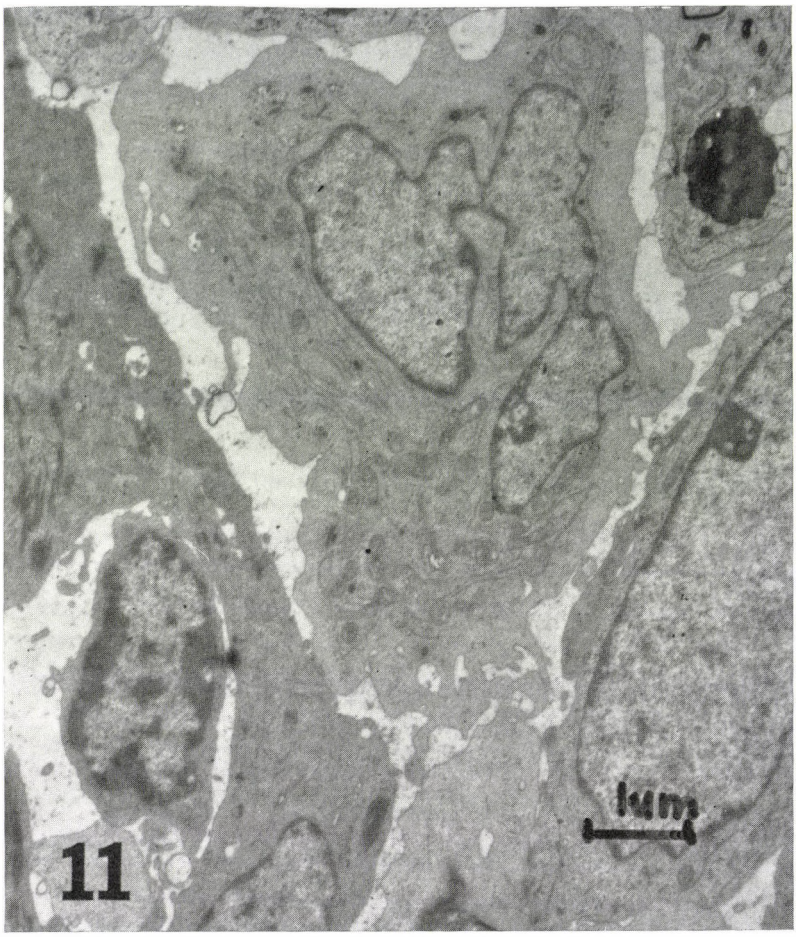

Fig. 11. "Veiled cell" with irregular nucleus in the intraepithelial passage of the tonsil

from the bursal mesenchyme. It may be assumed that the mammalian bursa equivalent organ is not an organ but actually a cell of mesenchymal origin which is functionally identical with the bursal secretory cell. This may be supported by the finding of Audhya et al. [1] who stated that the tripeptide bursin is served during the evolution and functions not only in birds but also "in the mammalian system including human".

GALT and tonsils

These lymphoepithelial structures consist of two parts both in mammals and birds. The surface epithelium which is lymphoepithelial in nature and the subjacent dense lymphoid tissue. The latter can be separated further for follicles (B dependent area) and interfollicular substance (T dependent area).

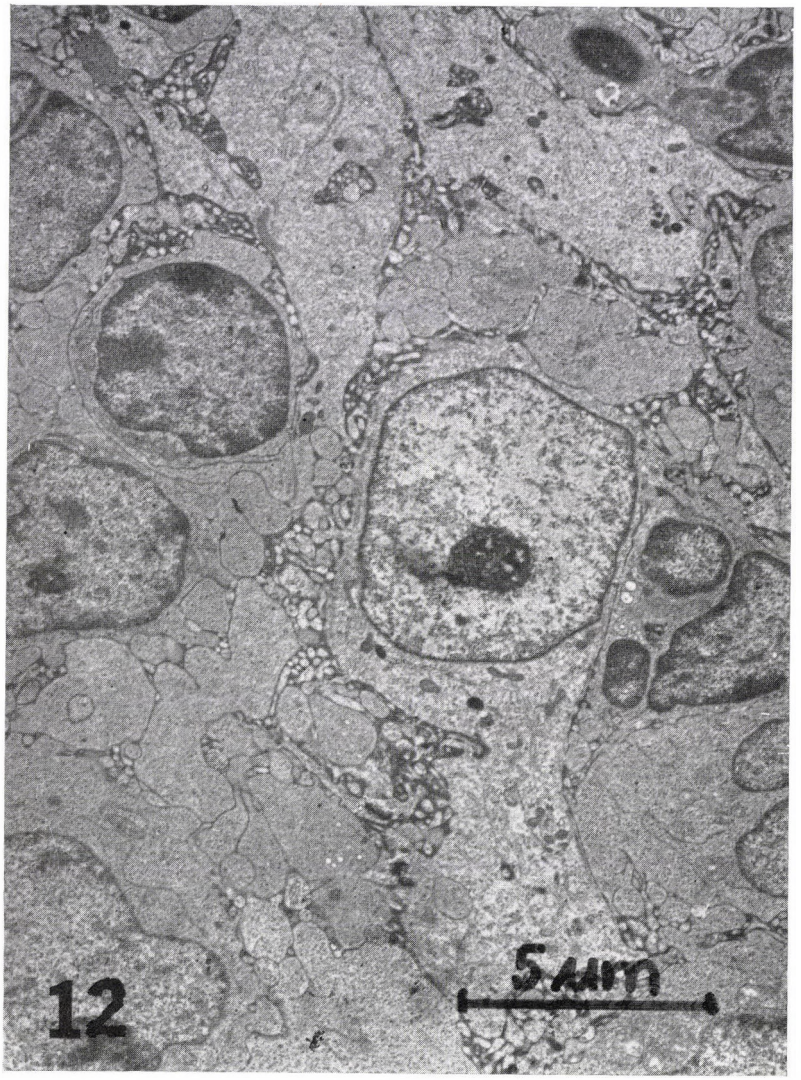

Fig. 12. Follicular dendritic cell in monkey tonsillar follicle. Around the dendritic processes electron-dense substance is deposited

Among the surface epithelial cells the M cells (microfold) are capable of antigen uptake [15]. The tonsillar M cells (Figs 9, 10) elaborate cytoplasmic tubular structures which are very similar to that of the bursal FAE (Fig. 6). The M cells were first described by Owen [26] in Peyer's patches.

In addition to epithelial antigen uptake by M cells, the intraepithelial passages of the tonsils contain many macrophages and dendritic-like cells (Fig. 11) which are also capable of antigen uptake. These cells migrate freely in the intraepithelial passages to take up the antigen and carry it to the deep

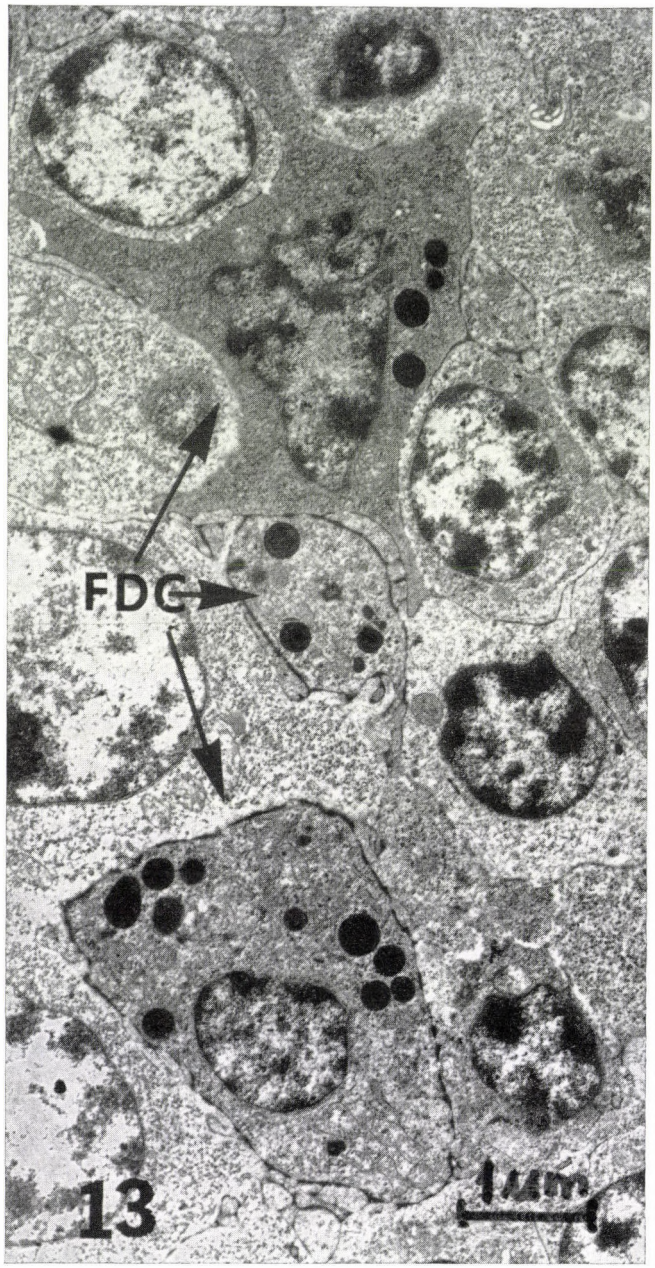

Fig. 13. FDC in a follicle of chicken's caecal tonsil. These FDC reveal less developed dendritic processes but the cytoplasmic granules are more prominent than in the mammalian FDC. The appearance of the electron-dense surface substance seems to be identical with that of the mammals

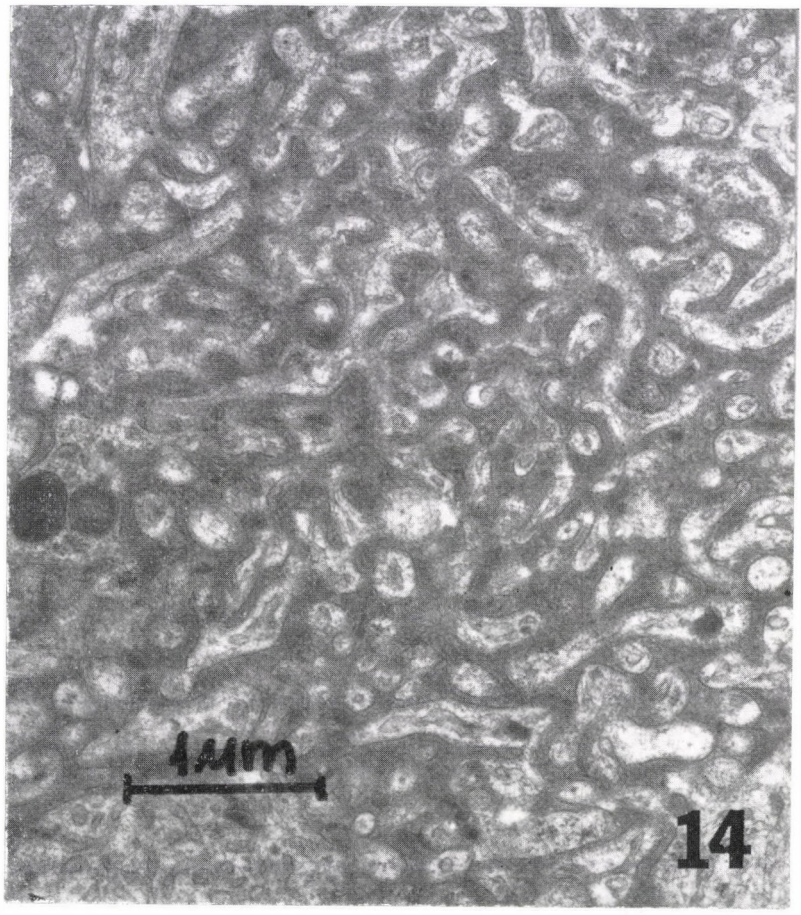

Fig. 14. Higher magnification of the intricate dendritic processes and the electron-dense surface material of human tonsilar FDC

tonsillar substance. These mobile dendritic-like cells appear in the blood and lymph circulation where they are called "veiled-cells" [27]. The M cells together with the macrophages and dendritic-like cells of the intraepithelial passages supply the immune system with continuous antigen information which is necessary for keeping the lymphoid system alert.

The B dependent areas i.e. the follicles reveal an other dendritic type cell so-called follicular dendritic cell (Figs 12, 13). The most characteristic cytological feature of these cells is the intricate membrane invaginations that are filled with electron dense substance (Fig. 14). These cells bind immune complexes on their surface and stimulate the centroblasts. They probably have some role in the formation of B memory cells. Table I summarizes the basic characteristics of the lymphoepithelial organs.

Table I

Comparison of lymphoepithelial compartments of the thymus, tonsils and bursa of Fabricius

	Thymus	Tonsils and GALT	Bursa of Fabricius
Surface epithelium	no	yes	yes
LE location	isolated from surface and vascular bed	not isolated	isolated from surface and vascular bed
Antigen uptake by epithelial M cells or by analogue cells from the environment	no	yes	yes
Development of LE	early intraembryonic life	around birth	early intraembryonic life
Dentritic cells	*special cell* at the cortico-medullary border contributes to the T differentiation	*IDC* T-dependent area T cell stimulant *FDC* B dependent area germinal center antigen trapping Ia + dendritic like cell in the LE passages, i.e. *veiled cell*	*secretory cell* in the medulla of the follicles contributes to the B cell differentiation

Conclusion

The lymphoepithelial organs consists of at least three major cell types. *The epithelial cells* are of endodermal origin and form a supporting network for the other cell types and provide an isolated environment for the differentiation of *T and B cells. The dendritic cells* are of mesenchymal origin and serve the maturation of T and B cells. The thymic dendritic cells (special cell) locate at the corticomedullary border, therefore the immature T cells migrating from the cortex to medulla should be in contact with these cells before entering the medulla. The secretory cell of the bursa of Fabricius is a modified dendritic cell. In embryos the secretory cell is responsible for the development of the LE compartment — and after hatching — produces some secretory substance which contributes to the B cell maturation. The FAE can be regarded both structurally and functionally as M cells which are capable for antigen uptake. The LE compartment of the tonsils and the GALT, but not of the bursa, produces intraepithelial passages in which "veiled cells" freely migrate. The follicles of the tonsils and GALT contain FDC, specialized for immune complex trapping, while the IDC cooperates with the T cells at the interfollicular area.

REFERENCES

1. Audhya T, Kroon D, Heavner G, Viamontes G, Goldstein G: Tripeptide structure of bursin a selective B-cell differentiating hormone of the bursa of Fabricius. Science, 231: 997—999 1986
2. Bienenstock J, Johnston N, Perey DYE: Bronchial lymphoid tissue. I. Morphologic characteristics. Lab Invest 28: 686—692 1973
3. Bienenstock J, Johnston N, Perey DYE: Bronchial lymphoid tissue. II. Functional characteristics. Lab Invest 28: 693—698 1973
4. Bockman DE Stevens W: Gut-associated lymphoepithelial tissue. Bidirectional transport of tracer by specialized epithelial cells associated with lymphoid follicles. J Reticuloendothel Soc 21: 245—254 1977
5. Bos JD Kapsenberg ML: The skin immune system. Its cellular constituents and their interactions. Immunology Today, 7: 235—240 1986
6. Glick B: The bursa of Fabricius: A central issue, Bioscience 20: 602—604 1970
7. Glick B, Oláh I: Gut-associated lymphoid tissue of the chicken. Scanning Electron Microscopy Vol. III. 1981 99—108
8. Glick B, Oláh I: The morphology of the Starling (Sturnus vulgaris) bursa of Fabricius: A scanning and light microscope study. Anat Rec 204: 341—348 1982
9. Glick B and Oláh I: A continuum of cells leading to an in vivo humoral response. Immunology Today 5: 162—165 1984
10. Kyewski BA Kaplan HS: Lymphoepithelial interactions in the mouse thymus: phenotypic and kinetic studies on thymic nurse cells. J Immunol 128: 2287—2294 1982
11. LeDouarin NM, FV Jotereau: The ontogeny of the thymus. In: MD Kendall, (ed.), The Thymus Gland. Academic Press, London, New York, Toronto, Sidney, San Francisco 981, pp 37—62
12. Lupetti M Dolfi A: Concerning bidirectional transport by the lymphoid follicle-associated epithelial cells. Cell Mol Biol 26: 609—613 1980
13. Miller JFAP: Effect of thymic ablation and replacement. In: BA Good, AE Gabrielsen (eds), The Thymus Immunobiology. Harper and Row, New York, Evanston, London 1964, pp 436—460
14. Oláh I, Dunay Csilla, Röhlich P, Törő I: A special type of cells in the medulla of the rat thymus. Acta Biol Acad Sci Hung 19: 97—113 1968

15. Oláh I, Everett NB: Surface epithelium of the rabbit palatine tonsil: Scanning and transmission electron microscopic study. J Reticuloendothel Soc 18: 53—62 1975
16. Oláh I, Glick B: The number and size of the follicular epithelium (FE) and follicles in the bursa of Fabricius. Poultry Sci 57: 1445—1450 1978
17. Oláh I, Glick B: Secretory cell in the medulla of the bursa of Fabricius. Experientia 34: 1642—1643 1978
18. Oláh I, Glick B: Splenic white pulp and associated vascular channels in chicken spleen. Amer J Anat 165: 445—480 1982
19. Oláh I, Glick B: Lymphopineal tissue in the chicken. Dev Comp Immunol 8: 855—862 1984
20. Oláh I, Glick B: Meckel's diverticulum. II. A novel lymphoepithelial organ in the chicken. Anat Rec 208: 253—263 1984
21. Oláh I, Glick B: Effect of carrageenan on the histology of the bursa of Fabricius and the humoral immune response to Salmonella O antigen. Anat Rec 214: 398—404 1986
22. Oláh I, Glick B, Taylor Jr RL: Effect of surgical bursectomy on the ellipsoid, ellipsoid-associated cells, and periellipsoid region of the chicken's spleen. J Leuk Biol 38: 459—469 1985
23. Oláh I, Glick B, Törő I: Bursal development in normal and testosteron-treated chick embryos. Poultry Sci 65: 574—588 1986
24. Oláh I, Röhlich P, Törő I: Ultrastructure of lymphoid organs. An electron-microscopic atlas. JB Lippincott Co., Philadelphia and Toronto. 1975
25. Oláh I, Surján Jr. L, Törő I: Electron microscopic observations on the antigen reception in the tonsillar tissue. Acta Biol Acad Sci Hung 23: 61—73 1972
26. Owen RL: Sequential uptake of horseradish peroxidase by lymphoid follicle epithelium of Peyer's patches in the normal unobstructed mouse intestine: an ultrastructural study. Gastroenterology 72: 440—451 1977
27. Sorvári R, Sorvári TE: Bursa Fabricii as a peripheral lymphoid organ. Transport of various materials from the anal lips to the bursal lymphoid follicles with reference to its immunological importance. Immunology 32: 499—505 1977
28. Streilein JW: Lymphocyte traffic T-cell malignancies and the skin. J Invest Dermatol 71: 167—171 1978
29. Takács L, Savino W, Monostori Éva, Ando I, Bach JF, Dardenne Mireille: Cortical thymocyte differentiation in thymomas: an immunohistologic analysis of the pathologic microenvironment. J Immunol 138: 687—698 1987
30. Törő I, Oláh I, Kittner Zsuzsa: Functional structure in lymphoepithelial cooperation. Acta Morph Acad Sci Hung 28: 375—391 1980
31. Wekerle H, Ketelsen UP, Ernst M: Thymic nurse cells. Lymphoepithelial cell complexes in murine thymuses: morphological characterization. J Exp Med 151: 925—944 1980
32. Hellman T: Der lymphatische Rachenring/Der Waldeyersche Schludring. Die Tonsillen. Der lymphoepithelische Schlundring. In: Handbuch der mikroskopische Anatomie des Menschen. Vol. V/1 Springer, Berlin 1927

Acta Morphologica Hungarica 37 (1—2), pp. 47—53 (1989)

IMMUNOHISTOLOGICAL DEMONSTRATION OF LYMPH NODE RETICULUM CELLS IN THE ACQUIRED IMMUNODEFICIENCY SYNDROME RELATED COMPLEX A STUDY IN BOUIN-FIXED TISSUES

Gy. Szekeres[1], J. Audouin[2], J. Diebold[2]

[1]DEPARTMENT OF PATHOLOGY, UNIVERSITY MEDICAL SCHOOL, PÉCS, HUNGARY AND
[2]LABORATORY OF PATHOLOGY, HÔTEL-DIEU, PARIS, FRANCE

(Received 29 July 1988)

The results of an immunohistochemical study on paraffin sections of the lymph nodes from 5 patients with the acquired immunodeficiency syndrome (AIDS) related complex (ARC) are presented. The distribution and frequency of follicular dendritic cells (FDC) and of interdigitating cells (IDC) were examined with the monoclonal antibodies J3D3 (directed against the C3b complement receptor, CD 35) and IOB1a (specific for the C3D, CD21) as well as with the polyclonal anti-S-100 protein antiserum in Bouin-fixed, paraffin-embedded sections using a Streptavidin-biotin-peroxidase technique. Disruption of the follicular FDC network was demonstrated. No major alteration of the IDC was noted. The immunomorphological patterns observed in this study were comparable with the previously reported lymph node alterations studied in frozen section.

Keywords: AIDS-related complex

Introduction

The acquired immunodeficiency syndrome- or AIDS-related complex (ARC) is defined by the association of at least 2 clinical symptoms (lymphadenopathy in at least 2 extrainguinal sites, loss of at least 7 kg or 10% body weight, intermittent or continuous fever at 38 °C or higher, diarrhoea, asthenia, and night sweats) and 2 biological signs (reduction in the number of helper cells in the peripheral blood, a decrease in the helper/suppressor ratio, anaemia, leukopenia, thrombopenia, lymphopenia, polyclonal serum hypergammopathy, reduced blastogen response of the lymphocytes to mitogens, cutaneous anergy, circulating immune complexes) which must exist for at least 3 months [6, 7].

On the basis of previous histological, immunological and ultrastructural studies [1, 4, 5, 6, 7, 10, 11, 16] several types of lymph node lesions may be distinguished in the lymphadenopathy of patients with ARC: predominant follicular hyperplasia with a disruption of the network of follicular dendritic cells (FDC) and an increase in number of cytotoxic/suppressor cells or type IA

Send offprint requests to: Gy. Szekeres, Dept. of Pathology, University Medical School, Pécs, 12 Szigeti Str., H-7624 Hungary

in our classification, multicentric hypervascular, Castleman-like lymphadenopathy (type IB) [6, 11]; angio-immunoblastic lymphadenopathy-like lymphadenitis (AIL-like) with the disappearance of follicles, disruption of the FDC network and markedly reduced number of the helper/inducer (CD4) cells (type II); extensive lymphoid depletion (type III); Kaposi's sarcoma (type IVA or B).

Additional features favouring the diagnosis of ARC can be obtained by further immunomorphological tests or by electron microscopy (immunohistochemical demonstration of the structural proteins of the human immunodeficiency virus (HIV), the presence of viral particles at the ultrastructural level) [4, 6, 10, 11, 13].

To distinguish T and B lymphocytes and their subsets by immunohistochemistry, frozen sections are needed. However, FDC can be selectively demonstrated in Bouin-fixed and paraffin-embedded sections with the monoclonal antibodies J3D3 (directed against the C3b complement receptor, CD35) and IOB1a (directed against the C3d complement receptor, CD21) [14]. The immune-accessory cell of T-zone, the interdigitating reticulum cell (IDC) is characterized by a positivity with antibodies directed against the S-100 protein [15].

With these antibodies we have attempted to demonstrate the 2 types of immune accessory cells in the lymph nodes of 5 patients with ARC in Bouin-fixed and paraffin-embedded sections using a Streptavidin-biotin-peroxidase technique. The immunomorphological features were compared with the previously reported results obtained with frozen section immunohistochemistry [1, 7].

Materials and methods

Lymph node biopsies were obtained from 5 patients with ARC of the Paris area in 1985 [6] The samples were fixed in Bouin's solution and embedded in paraffin. The staining procedure was described previously [14]. Monoclonal antibody J3D3 was kindly provided by Dr. Claude Boucheix (INSERM U268, Hôpital Paul-Brousse, Villejuif). Two other antibodies were used: the monoclonal IOB1a (Immunotech, Marseille) and the polyclonal anti-S-100 protein (DAKOPATTS, Copenhagen). Labeling reagents were: biotin-conjugated rabbit anti-mouse IgG (Vepex, Budapest), goat anti-rabbit IgG (Biolyon, Lyon), the Streptavidin-biotin-peroxidase complex (Vepex, Budapest), as well as peroxidase rabbit anti-peroxidase, PAP complex (Biolyon, Lyon).

Results

In the lymph node of the case with type IA lesion the FDC network showed a "moth-eaten" appearance at its periphery, with mantle zone effacement (Fig. 1). The number of S-100 protein positive IDC of the paracortex was within normal limits. They were large cells with cytoplasmic extensions and intense staining.

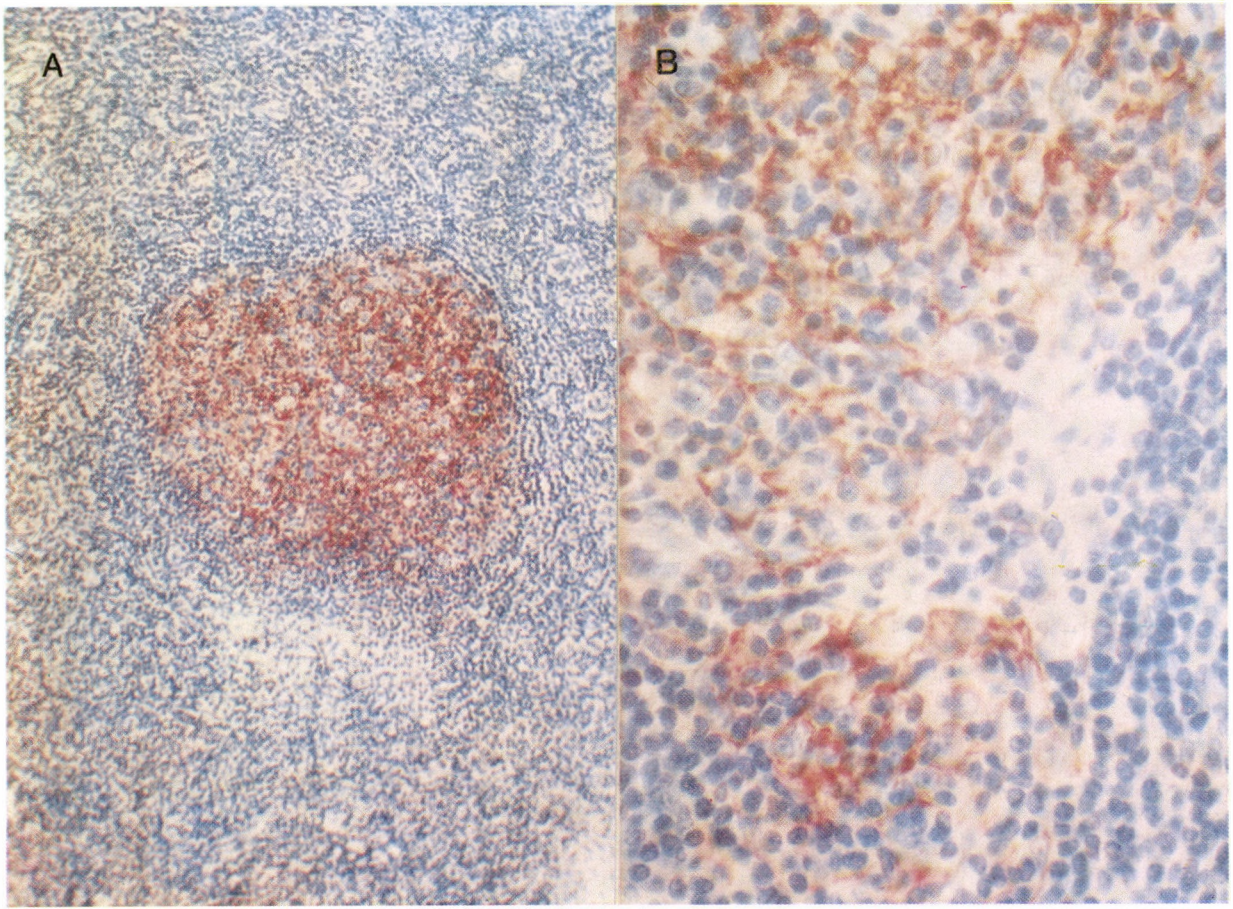

Fig. 1. ARC type IA. A: Follicular hyperplasia with irregular FDC network, decreased thickness of the mantle zone. B: The network of FDC shows some negative areas. (Bouin-paraffin, antibody J3D3, CD35, hematoxylin counterstain, A: ×100, B: ×300)

The Castlemen's disease-like pattern (type IB) was observed in an other case. In the germinal centers small vessels within the irregular concentric pattern of FDC network ("onion bulb" aspect) were seen (Fig. 2). Numerous plasma cells and S-100 positive IDC populated the extrafollicular lymphoid tissues. Some IDC were seen within the follicles (Fig. 2).

There were 2 cases showing features of type II. Several follicles in these cases exhibited various degrees of involution characterized by partial destruction of the FDC network, only its remnants being present (Fig. 3). In one case follicular hyperplasia and AIL-like pattern were seen in the same lymph node. The distribution of S-100 protein positive IDC was normal.

In the case with extensive lymphoid depletion (type III) no germinal centers were observed, however a case of follicular lesion with a typical mycobacteriosis was found. The immunohistological staining was negative for both FDC and IDC.

Discussion

On the basis of the present observations obtained with immunomorphological techniques in Bouin-fixed, paraffin-embedded lymph nodes which were previously studied in frozen sections [1, 6, 7], as well as of the reviewed literature data, our findings may be summarized as follows:

1) Predominant follicular hyperplasia (type IA), seen in one case, is histologically and immunomorphologically not specific for ARC, other etiologies, in particular viral infections should be considered [2, 6, 9]. The disruption of the FDC network is the only immunohistochemical feature suggesting the diagnosis of ARC [8, 12].

2) The particular form (type IB) simulating Castlemen's disease is rare. In our only case a marked increase in blood vessels and numerous plasma cells, as well as a S-100 positive IDC hyperplasia in the extrafollicular lymphoid tissue were considered as an unusual coexistence. Some IDC were seen also within the hypervascular follicles [3].

3) The type II of the ARC lymph node modification has an aspect more or less close to that of an AIL. The follicular remnants are more numerous than in AIL, and more conspicious when the monoclonal antibodies J3D3 and IOB1a are used. In one case an AIL-like pattern and follicular hyperplasia were seen in the same lymph node suggesting a possible transformation of type IA to II [6].

Immunohistology in Bouin-fixed and paraffin-embedded sections using the monoclonal antibodies J3D3 (CD35) and IOB1a (CD21) and the polyclonal anti-S-100 protein antibody are useful in the typing of lymph node lesions in ARC. By their use it is possible at least to suspect the diagnosis of ARC. The findings in fixed-embedded tissues and frozen sections were similar [1, 2, 6, 7,

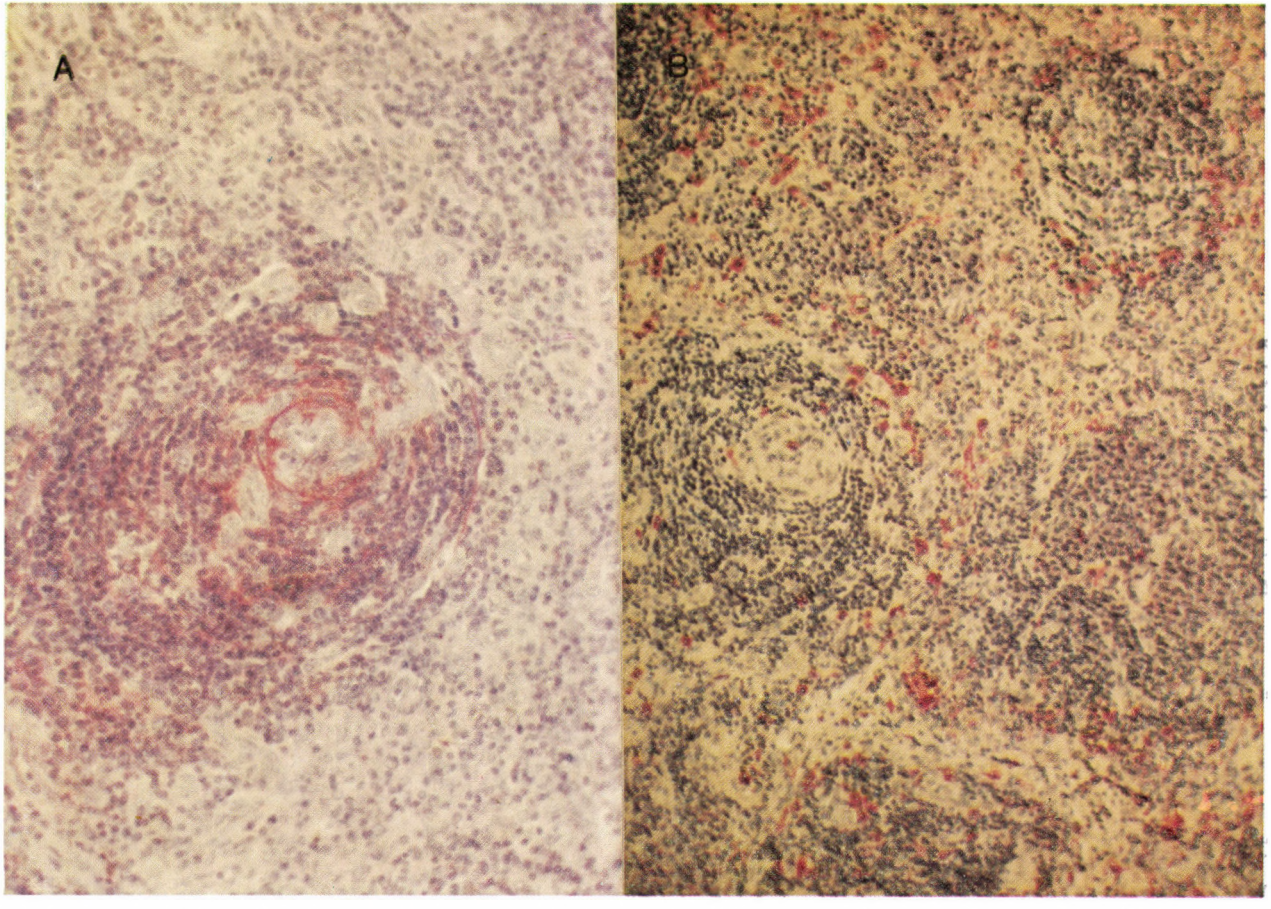

Fig. 2. ARC type IB. A: Germinal center with onion-like aspect, perifollicular vascular hyperplasia. Irregular FDC network with concentric appearance. B: S-100 protein positive IDC in the interfollicular areas and some IDC in the follicles. (A: Bouin-paraffin, antibody J3D3, CD35, hematoxylin counterstain, ×150, B: anti-S-100 protein antibody, hematoxylin counterstain, ×100)

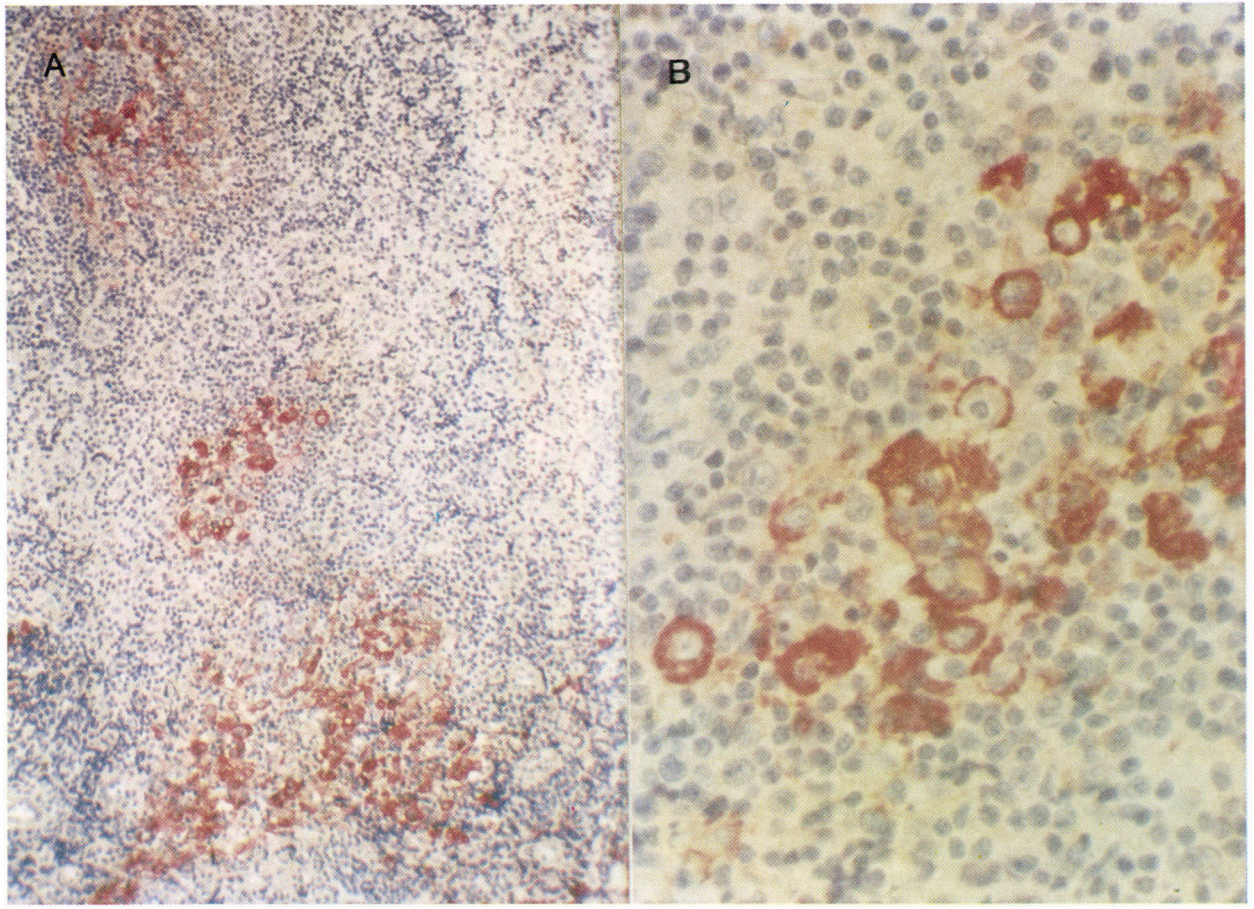

Fig. 3. ARC type II. Effacement of the normal lymph node structure. Some follicle recognizable with involution. Destruction of the FDC network, many round FDC without dendritic processes. (Bouin-paraffin, antibody J3D3, CD35, hematoxylin counterstain, A: ×100, B: ×450)

11]. Additional data supporting the diagnosis can be obtained by ultrastructural studies and by the demonstration of the structural proteins of HIV with immunohistochemistry, as well as by the identification of the virus genom with in situ hybridization technique [6, 10].

Acknowledgements

We are indepted to Mr. Serge Bain for skillful technical assistance. The colour reproductions were made possible by the generous support of VEPEX (Budapest, Hungary).

REFERENCES

1. Audouin J, Le Tourneau A, Marche C, Diebold J: Etude immunopathologique des adénopathies persistantes liées ā l'infection LAV-HTLV III. Ann Pathol 6: 271, 1986
2. Audouin J, Diebold J: Modifications histologiques des ganglions lymphatiques au cours des réactions de stimulation immunitaire. Ann Pathol 6: 85, 1986
3. Baroni CD, Pezzella F, Stoppacciaro A, Mirolo M, Pescarmona E, Vitolo D, Cassano AM, Barsotti P, Nicoletti L, Ruco LP, Uccini S: Systemic lymphadenopathy (LAS) in intravenous drug abusers. Histopathology 9: 1275, 1985
4. Biberfeld P, Ost A, Porwit A, Sandstedt B, Pallesen G, Bottiger B, Morfelt-Mansson L, Biberfeld G: Histopathology and immunohistology of HTLV-III/LAV related lymphadenopathy and AIDS. Acta Pathol Microbiol Immunol Scand Sect A 95: 47, 1987
5. Boylston AW, Cook HT, Francis ND, Goldin RD: Biopsy pathology of acquired immune deficiency syndrome (AIDS)? J Clin Pathol 40: 1, 1987
6. Diebold J, Marche C, Audouin J, Aubert JP, Le Tourneau A, Bouton C, Reynes M, Wizniak J, Capron F, Tricottet V: Lymph node modification in patients with the AIDS or with ARC. Path Res Pract 180: 590, 1985
7. Diebold J, Audouin J, Marche C, Le Tourneau A: Aspects histopathologiques des adénopathies dans le syndrome des adénopathies persistantes (LAS) et les syndromes associés au SIDA (ARC). Ann Pathol 6: 266, 1986
8. Domingo J, Chin NW: Lymphadenopathy in a heterogeneous population at risk for the AIDS. Am J Clin Pathol 80: 649, 1983
9. Guettier C, Gatter KC, Heryet A, Mason DY: Dendritic reticulum cells in reactive lymph nodes and tonsils: an immunohistological study. Histopathology 10: 15, 1986
10. Le Tourneau A, Audouin J, Diebold J: Etude ultrastructurale des ganglions, chez le sujet ā risque pour le SIDA. Ann Pathol 6: 275, 1986
11. Rácz P, Tenner-Rácz K, Kahl C, Feller AC, Dietrich M: Spectrum of morphological changes of lymph nodes from patients with AIDS or ARC. Progr Allergy 37: 81, 1986
12. Schuurman HJ, Kluin PM, Meijling FHJG, van Unnik JAM, Kater L: Lymphocyte status of lymph node and blood in AIDS and ARC disease. J Pathol 147: 269, 1985
13. Scott GB, Buck BE, Leterman JG, Bloom FL, Parks WP: AIDS in infants. N Engl J Med 310: 76, 1984
14. Szekeres G, Audouin J: Reactive cells and immune accessory cells in non-Hodgkin's malignant lymphomas. Zentralbl allg Pathol pathol Anat 132: 153, 1986
15. van den Oord JJ, de Wolf-Peeters C, de Vos R, Desmet VJ: The paracortical area in dermatopathic lymphadenitis and other reactive conditions of the lymph node. Virchows Arch (Cell Pathol) 45: 289. 1984
16. Stanley MV, Frizzera G: Diagnostic specificity of histologic features in lymph node biopsy specimens from patients at risk for the acquired immunodeficiency syndrome. Hum Pathol 17: 1231, 1986.

Acta Morphologica Hungarica 37 (1—2), pp. 55—63 (1989)

IN SITU HIBRIDIZATION OF PEPTIDE mRNAs ON VIBRATOME SECTIONS*

M. RÉTHELYI[1]**, CAROL B. METZ[1], T. J. GÖRCS[2]***, P. KAY LUND[1]

[1]DEPARTMENT OF PHYSIOLOGY, UNIVERSITY OF NORTH CAROLINA AT CHAPEL HILL, CHAPEL HILL, NC 27514, [2]U. S.-JAPAN BIOMEDICAL RESEARCH LABORATORIES, LMNED, TULANE UNIVERSITY, HERBERT RESEARCH CENTER, BELLE CHASSE, LA 70037

(Received 9 August 1988)

In situ hybridization procedures that have been used successfully for the localization of somatostatin and cholecystokinin mRNAs in neurons on cryostat sections of rat brain, were tested for applicability to vibratome sections of rat and guinea pig brain. Somatostatin and cholecystokinin mRNAs were localized to neurons in 30 μm thick vibratome sections of brain from both species by use of ^{32}P labelled oligodeoxyribonucleotide (oligomer) probes. Somatostatin mRNAs was localized to neurons in the periventricular region of the preoptic area of rat, and guinea pig brain. Cholecystokinin mRNAs were localized to neurons of rat hippocampus. Hybridization signal, background and resolution achieved with vibratome sections were comparable to those obtained with the more commonly used cryostat sections.

Keywords: *In situ* hybridization — somatostatin — cholecystokinin — vibratome sections

Introduction

In situ hybridization (ISH) is now widely used to detect cells that contain specific mRNAs. Paraffin embedded or cryostat sections have been most commonly used for ISH [for reviews see Ref. 3, 5, 8]. Vibratome sections have potential advantages for mapping of the regional distribution of neurons that express a particular mRNA because of the greater tissue mass in each section. In the present study we describe methods that allowed successful cellular localization of somatostatin and cholecystokinin (CCK) mRNAs on vibratome sections prepared from brain of rats and guinea pigs.

* This work was supported by NIH grant No. NS23804 (P.K.L.). M. R.'s stay was sponsored by a collaborative arrangement between NIH, NINCDS (grant No. NS10321) and Ministry of Health, Budapest, Hungary. T. G. received support from NIH (grant No. DK09094-21).

** Visiting professor on leave from 2nd Department of Anatomy, Semmelweis University Medical School, Budapest, Hungary.

*** Present address: 1st Department of Anatomy, Semmelweis University Medical School, Budapest, Hungary

Send offprint requests to: Dr. M. Réthelyi, 2nd Dept. of Anatomy, Semmelweis University Medical School, Tűzoltó u. 58. 1094 Budapest, Hungary

Materials and methods

Probe preparation and labelling

Oligodeoxyribonucleotide (oligomer) probes complementary to portions of the mRNAs encoding pro-somatostatin and pro-CCK were synthesized on an Applied Biosystems DNS synthesizer. The specificity of these probes for the localization of pro-somatostatin and pro-CCK mRNAs on cryostat sections of rat and guinea pig tissues has been described previously [9, 13]. 50 pMol aliquots of each probes were 5'-end labelled with ^{32}P using T4 polynucleotide kinase and 100 pMol gamma ^{32}P ATP (ICN Radiochemicals, CA, 7000 Ci/mMol) followed by purification on 15% polyacrylamide gels containing 7M urea [10]. After autoradiography of gels on X-ray film (Kodak XAR-5), polyacrylamide slices 2×0.2 cm containing probe were excised. Probe was eluted from polyacrylamide by incubation in 1 ml 10 mM Tris-HCl pH 7.0 overnight at 37 °C. Polyacrylamide was separated from eluted probe by centrifugation for 5 min at room temperature in a microfuge. Aliquots of probe were liophylized and resuspended in 2X hybridization buffer for direct use in ISH. Probe specific activities were routinely $0.5-1 \times 10^6$ cpm/pMol.

Tissue preparation

Intact, untreated rats (150—300 g, Sprague—Dawley strain) and guinea pigs (150—300 g, Hartley strain) were anaesthetized by intraperitoneal injection of Nembutal (60 mg/kg for rats and 50 mg/kg for guinea pigs) and perfused through the heart with a solution containing 4% paraformaldehyde and 0.2% glutaraldehyde in 0.1 M phosphate buffer (pH = 7.4). The aldehyde perfusion was preceded with a brief vascular rinse. The brain was dissected, and kept in the fixative for 24 to 72 h after perfusion at 4 °C. Thirty μm thick coronal sections were prepared using a Vibratome (Oxford). Sections were colleted in ice cold phosphate buffered saline (PBS), mounted onto chrome alum subbed slides from water/gelatin, dried overnight at 37 °C and kept at 4 °C for several days (up to 2 weeks). For comparison, tissue blocks were cryoprotected in 0.1 M posphate buffer containing 30% sucrose then ten μm thick frozen cryostat sections were prepared, mounted onto chrome alum subbed slides and stored at 4 °C for several days (up to 2 weeks).

Prehybridization and hybridization

Sections were washed in PBS containing Triton-X 100 (0.2%) for 60 min. A mixture of 50 μl of 2X hybridization buffer [6] and 50 μl of 60% deionized formamide was spread on to each slide. The buffer was boiled for 2 min and chilled on crushed ice before mixing it with the formamide. The sections were covered with Parafilm [14] and kept at 37 °C for 1.5 to 2 h in humid chambers. At the end of the prehybridization period, sections were dehydrated in ethanol containing 0.33 M ammonium acetate, air dried for 10 min and then 100 μl of a mixture of 2X hybridization buffer containing the labelled probe and equal volume of 60% deionized formamide was spread on the slide. The 2X hybridization buffer containing labelled probe was boiled for 2 min and quickly chilled on crushed ice before mixing with the formamide. Probe concentrations used were identical for cryostat and vibratome sections. The 41 base somatostatin probe as well as both the 30 base and 26 base CCK oligomers were used at a concentration of 3×10^6 cpm in a volume of 100 μl applied to each slide. Up to 6 brain cross sections were processed on each slide. During the hybridization period (48 to 72 h) the sections were covered with coverslips and the slides were kept at 37 °C in moist chamber. Following hybridization, the coverslips were removed by immersion of the glass slides in 4X SSC (20X SSC = 3 M NaCl, 0.3 M Nacitrate, pH = 7.0). Sections were then washed in decreasing concentrations of salt solutions (4X, 2X and 0.1X SSC) for 2 to 3 h at room temperature, dehydrated through ascending ethanol series containing 0.33 M ammonium acetate and air dried for 5—10 min. Slides were exposed to X-ray film (Kodak XAR-5) for 24 h at room temperature.

Inclusion of 1.0% Triton-X 100 and 0.1% saponin, respectively in the PBS wash solution was compared with inclusion of 0.2% Triton-X 100 for effects on hybridization signal intensity.

Autoradiography

Sections were dipped in Kodak NTB-3 photoemulsion diluted in 0.33 M ammonium acetate (2 : 1, v : v, emulsion to 1 M ammonium acetate). Slides were dried for 1.5 to 2 h at 28 °C and 80% relative humidity. After drying, slides were exposed at 4 °C in light tight plastic boxes for 1 to 3 weeks. Sections were developed in Kodak D-19 developer diluted 1 : 1 with distilled water, fixed in Kodafix and coverslipped without counterstaining.

Microscopical examination

Low power dark field microscope (Leitz Dialux 22) was used to scan sections and locate groups of silver grains that are indicative of labelled neuronal perikarya. Those areas were photographed. After photography, the coverslips were removed and the sections were stained with 0.5% thionin and recoversliped. Areas of potential interest as assessed during the dark field examination were reexamined and the topographical relationship between groups of silver grains and perikarya was verified.

Immunohistochemistry

Vibratome sections adjacent to those used for ISH were treated with ethanol [7]. Free floating sections were incubated with somatostatin antiserum TG-SOM-R85/722-11-8 at a dilution of 1 : 5000 for 24 h at 4 °C. Immunostaining was detected using a modification of the peroxidase-antiperoxidase (PAP) method of Sternberger et al. [15] as described by Merchenthaler et al. [11]. The somatostatin antiserum was prepared by immunization of New Zealand white rabbits with somatostatin 1—14 (Peninsula Laboratories) conjugated to bovine thyroglobulin (Sigma) using the glutaraldehyde method [2]. Titer and specificity of the antiserum was tested by enzyme linked immunoassay (ELISA) as described by Görcs et al. [4]. No cross-reactivity was detected with peptides tested in ELISA. Immunostaining controls included elimination of immunostaining of somatostatinergic neurons by pre-absorption with 15 μg (0.9 nMol) of somatostatin 1—14 and no diminution of immunostaining by preabsorption with up to 50 μg of a wide variety of other peptides including alpha-melanocyte stimulating hormone, growth hormone releasing hormone (rat), secretin, adrenocorticotropic hormone 1—24, and 22—39, dynorphin 1—17, cholecystokonin sulfated octapeptide, luteinizing hormone-releasing hormone, vasoactive intestinal polypeptide, leucin-enkephalin, substance-P, corticotropin releasing hormone (rat), PHI, neuropeptide-Y, diazepam binding inhibitor, neurotensin, thyrotropin releasing hormone, and arginin-vasopressin.

Results

Somatostatin mRNA was localized to individual neurons in the periventricular region of rat preoptic area (Fig. 1). Autoradiograms prepared either by exposure of the sections to an X-ray film or photoemulsion revealed hybridization signals with the characteristic symmetrical distribution of somatostatinergic neurons along the walls of the third ventricle (Fig 1A). Somatostatin immunoreactive neurons on adjacent vibratome section showed a similar distribution (Fig. 1B). With vibratome and cryostat sections, the background hybridization (defined as silver grain density in non-cellular regions) was comparable. There was no evidence that use of 30 μm thick vibratome sections impeded probe penetration as hybridization signal intensity and resolution were comparable in vibratome and cryostat sections (Fig. 1A and C).

In the guinea pig, somatostatin mRNA was localized to cells of dimensions 8—10 μm by 16—20 μm that were distributed in several colums around

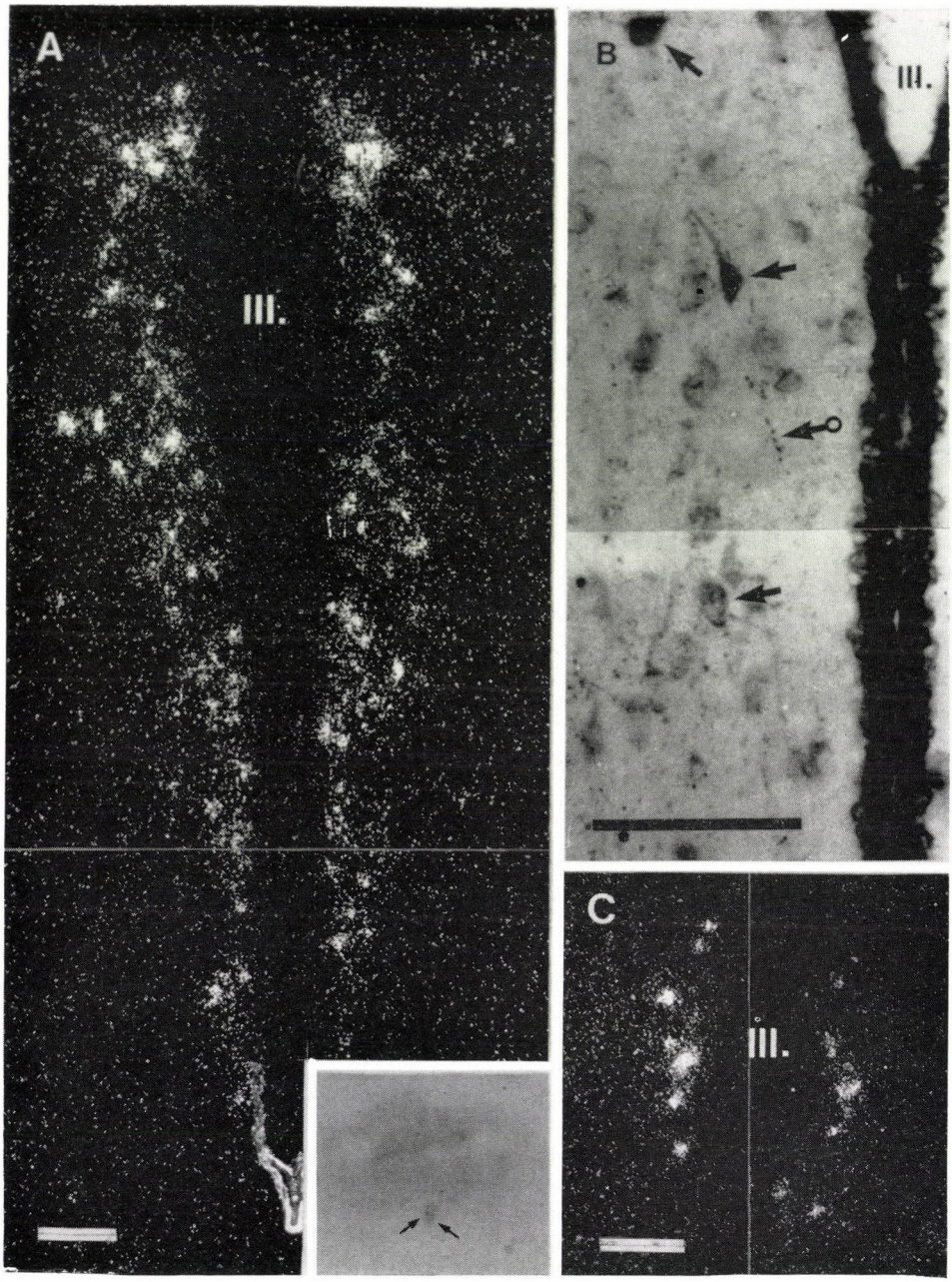

Fig. 1. Localization of somatostatin mRNA and immunoreactivity in neurons of the periventricular region of rat preoptic area. *A:* Low power photograph taken with dark field illumination, of hybridization of the ^{32}P labelled somatostatin oligomer to neurons in a vibratome section. Insert (bottom) shows that hybridization of the somatostatin probe (between arrows) on the same vibratome section is evident on an autoradiogram prepared by exposure of the section to X-ray film for 24 h at room temperature. In the example shown, probe penetration was facilitated by 1.0% Triton-X 100, but hybridization signal and background were indistinguishable from those on adjacent sections treated with 0.2% Triton-X 100 (data not shown). *B:* Immunostaining of neurons (arrows) in vibratome section with somatostatin antiserum. Immunostaining of fine varicose fibers is also observed (ringed arrow). *C:* Low power photograph taken with dark field illumination of somatostatin mRNA containing anterior periventricular neurons on a cryostat section. III. = third ventricle. Scales: 100 μm for A and C, 50 μm for B

the third ventricle (Fig. 2A) and that were surrounded by a dense population of non-labelled neurons (Fig. 2B).

Using vibratome sections, CCK mRNA was localized to individual neurons in all layers of the CA_1 region of rat hippocampus (Fig. 3). Occasionally, with both the CCK and somatostatin oligomers the density of silver grains observed over distinct brain regions was higher than background hybridization (Fig. 3 shows an example for CCK oligomer and the pyramidal cell layer of the hippocampus). Such regional hybridization is not characteristic of vibratome sections as it occurs also with cryostat sections and with a wide range of oligomers that are complementary to mRNAs other than CCK and somatostatin. Clusters of silver grains over individual neurons can still be detected easily, however, within these areas (Fig. 3, neuron 2).

Photographs taken with bright field illumination (Figs 2 and 3) show that with vibratome sections of brain, tissue preservation is comparable if not superior to cryostat sections. Increasing the concentration of Triton-X 100 in the PBS wash solution or substitution with another detergent, saponin resulted in no obvious differences in hybridization signal intensity.

Discussion

In the present study somatostatin mRNA was localized to neurons of the periventricular region of rat and guinea pig preoptic area by use of a 41 base ^{32}P labelled oligomer as probe on vibratome sections. Hybridization signals and background observed in neurons on vibratome sections of the rat periventricular region using either X-ray film autoradiography or photoemulsion, were comparable to those reported previously on cryostat sections [1, 9, 12, 16].

CCK mRNA was localized to individual neurons of the CA_1 region of rat hippocampus by use of a ^{32}P labelled oligomer on vibratome sections. Siegel and Young [14] reported a similar localization of CCK mRNA in hippocampal neurons using an ^{35}S labelled cRNA probe on cryostat sections. As in our study, they also found a diffuse regional accumulation of silver grains over the pyramidal cell layer of the hppocampus. It seems unlikely that this represents specific hybridization to CCK mRNA in all cells in the pyramidal layer, because in contrast to the hybridization signals localized to individual neuronal perikarya, the diffuse accumulations of silver grains were not eliminated by pretreatment of sections with ribonuclease prior to hybridization (data not shown) and occur with a wide range of oligomer probes complementary to mRNAs other than CCK (e.g. oligomers to somatostatin, glucagon, and substance K mRNAs). Further studies are required to establish the origin of such regional and probably non-specific hybridization.

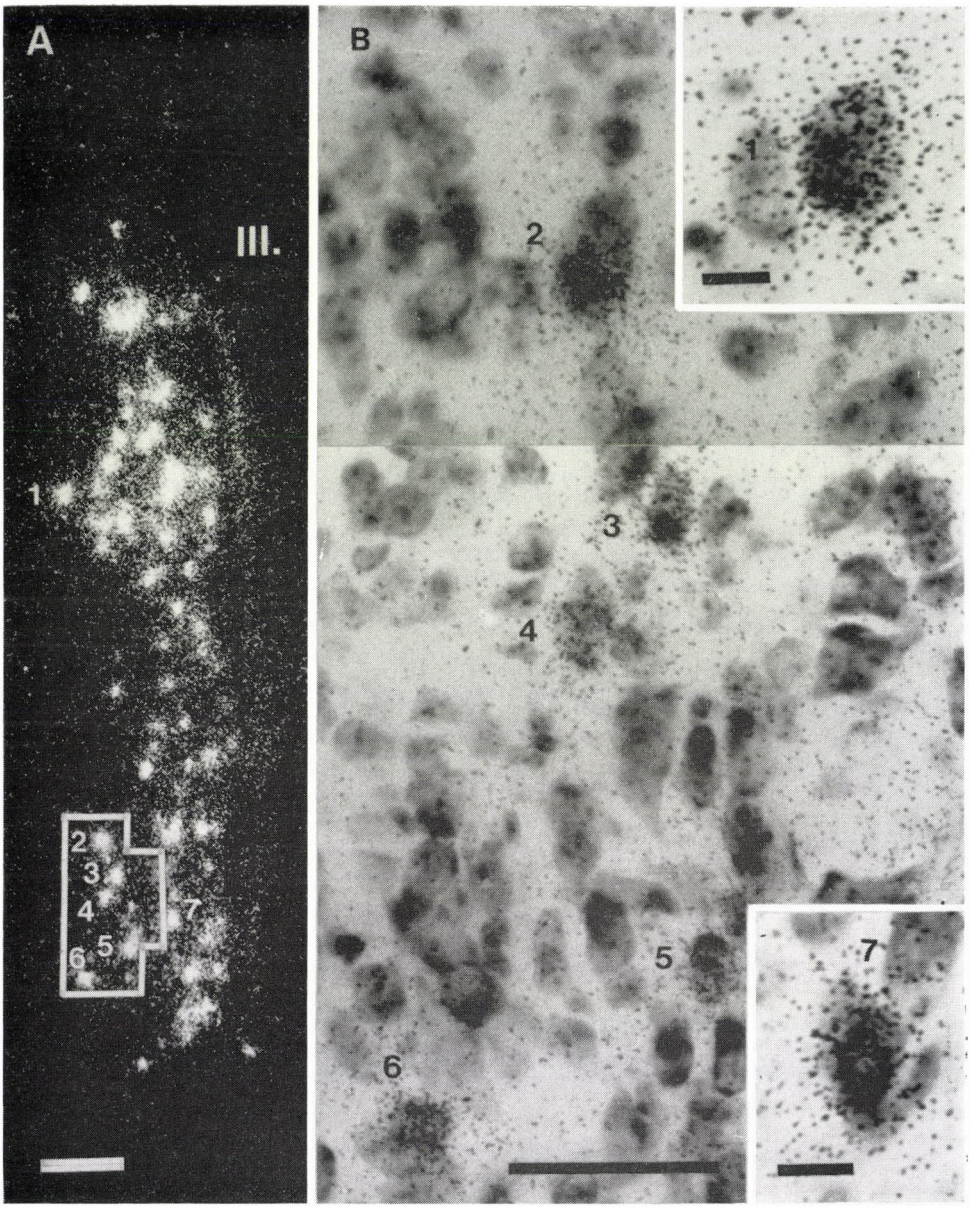

Fig. 2. Localization of somatostatin mRNA to neurons in the periventricular region of guinea pig preoptic area. *A:* Low power dark field photomontage of hybridization to neurons in a vibratome section. *B:* High power bright field photomontage of the rectangle outlined in A to show that clusters of silver grains overly individual neurons (cells numbered 1—7 in A and B + inserts). III. = third ventricle. Scales: 100 μm for A, 50 μm for B and 10 μm for the two inserts

Fig. 3. Localization of CCK mRNA to neurons in the rat hippocampus (CA_1 region). Top panel: Low power dark field photograph of hybridization of the CCK oligomer to neuronal perikarya in a vibratome section. Numbered arrows 1—7 point to clusters of silver grains.

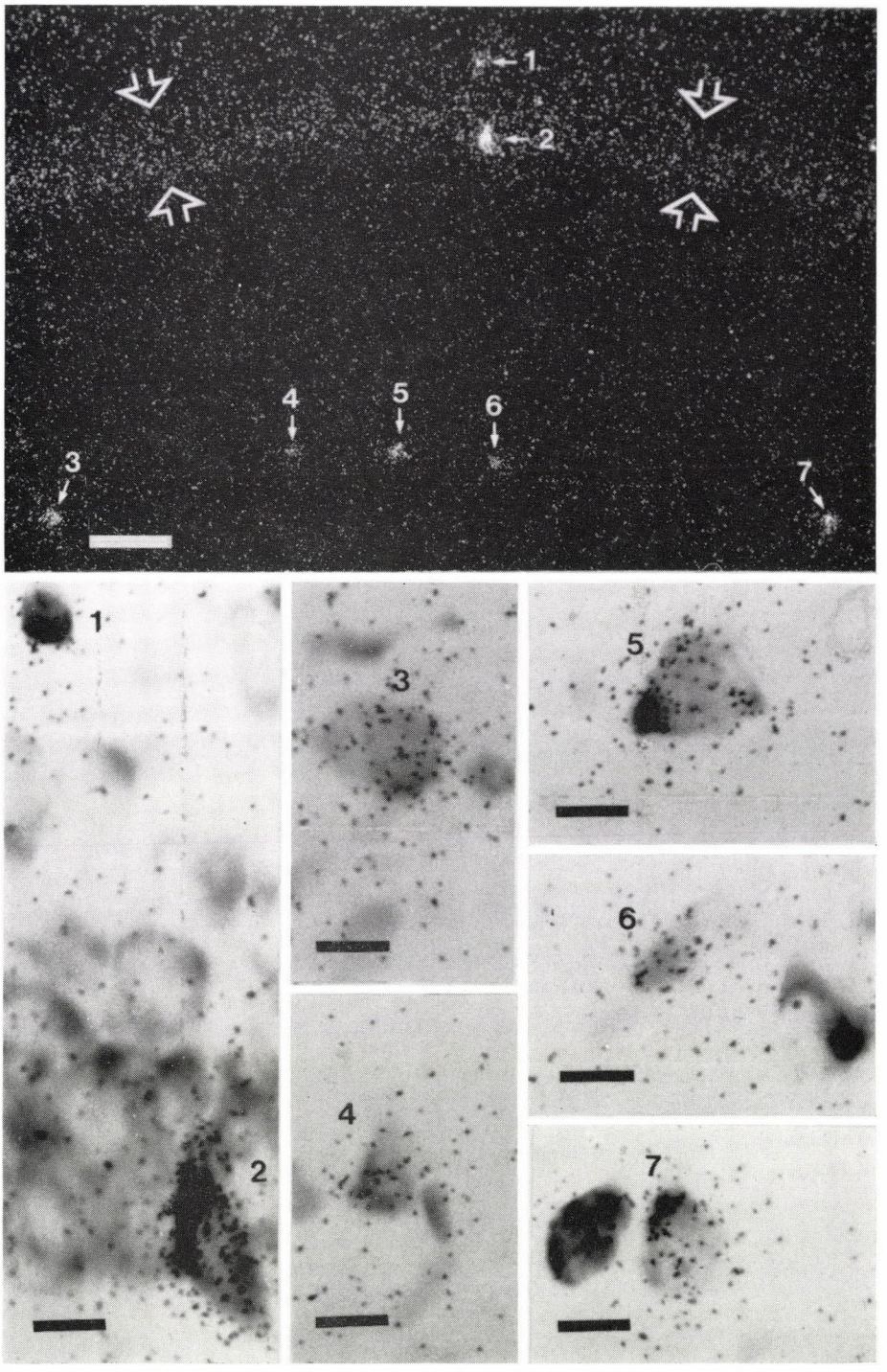

The same areas are shown in numbered high power, bright field photographs in the bottom panels. Neuron 1 is in the stratum oriens, neuron 2 in the stratum pyramidale whereas neurons 3—7 are in stratum radiatum and lacunosum-moleculare. A band of silver grains (between contour arrows) follows the neurons of the stratum pyramidale. Scales: 100 μm for top panel and 10 μm for others

Our localization of somatostatin and CCK mRNAs to individual neurons on vibratome sections of rat and guinea pig brain suggests that for ISH in the central nervous system (CNS), vibratome sections are a valid alternative to the more commonly used cryostat and paraffin sections. Comparable hybridization signals with vibratome and cryostat sections suggest no losses of mRNA during preparation of vibratome sections and floating of the sections in PBS. Conventional procedures to facilitate probe penetration as described previously for cryostat sections [6, 12] are sufficient to allow probe penetration into the thicker vibratome sections. Vibratome sections had no greater tendency to dissociate from the glass slides than cryostat sections. The known advantages of vibratome sections over cryostat sections for histological analyses of the CNS include more easily attained preservation of cellular structure and clearer boundaries for defined nuclei and histological structures. These advantages, together with our success in localization of CCK and somatostatin mRNAs on vibratome sections by ISH, suggest that combined ISH and immunohistochemistry on vibratome sections will be of value in mapping and analyses of the expression of specific genes encoding neuropeptides.

Acknowledgements

The authors are thankful to D. McGehee for the labelling of the oligomer probes, to Drs P. Petrusz and I. Merchenthaler for their help in the immunohistochemical procedure and to Dr. E. R. Perl for his support.

REFERENCES

1. Arentzen R, Baldino F Jr, Davis LG, Higgins GA, Lin Y, Manning RW, Wolfson B: In situ hybridization of putative somatostatin mRNA within hypothalamus of the rat using synthetic oligonucleotide probes. J Cell Bioch 27: 415—422, 1985
2. Arimura A, Sato H, Coy DH, Schally AV: Radioimmunoassay for GH-release inhibiting hormone. Proc Soc Exp Biol Med 148: 784—789, 1985
3. Gee CE, Roberts JL: In situ hybridization histochemistry: a technique for the study of gene expression in single cells. DNA 2: 157—163, 1983
4. Görcs TJ, Gottschall PE, Coy DH, Arimura A: Possible recognition of the GnRH receptor by an antiserum against a peptide encoded by nucleotide sequence complementary to mRNA of a GnRH precursor peptide. Peptides 7: 1137—1145, 1986
5. Griffin WST, Morrison MR: In-situ hybridization — visualization and quantitation of genetic expression in mammalian brain. Peptides 6; (Suppl 2) 89—96, 1985
6. Han VKM, Hynes MA, Jin C, Towle AC, Lauder JM, Lund PK: Cellular localization of proglucagon/glucagon-like peptide I messenger RNAs in rat brain. J Neurosc Res 16: 97—107, 1986
7. Honda CN, Réthelyi M, Petrusz P: Preferential immunohistochemical localization of vasoactive intestinal polypeptide (VIP) in the sacral spinal cord of the cat: light and electron microscopic observations. J Neuroscience 3: 2183—2196, 1983
8. Lewis ME, Sherman TG, Watson SJ: In situ hybridization histochemistry with synthetic oligonucleotides: strategies and methods. Peptides 6; (Suppl 2) 75—87, 1985
9. Lund PK, Perl ER, Priestley JV: Localization of somatostatin mRNA in rat brain by *in situ* hybridization. J Physiol (Lond) 372: 18P 1986

10. Maxam A, Gilbert W: A new method for sequencing DNA. Proc Natl Acad Sci USA 74: 560—564, 1977
11. Merchenthaler I, Vigh S, Petrusz P, Schally AV: Immunocytochemical localization of corticotropin-releasing factor (CRF) in the rat brain. Amer J Anat 165: 385—396, 1982
12. Priestley JV, Hynes MA, Han VKM, Réthelyi M, Perl ER, Lund PK: *In situ* hybridization using ^{32}P labeled oligodeoxyribonucleotides for the cellular localization of mRNA in neuronal and endocrine tissue. Histochemistry 89: 467—479, 1988
13. Réthelyi M, McGehee D, Lund PK: Neuronal Localization of Cholecystokinin mRNA in Rat and Guinea Pig Brain. Soc Neurosc Abstr Vol 12 Part 2 p 1041, 1986
14. Siegel RE, Young WS III: Detection of preprocholecystokinin and preproenkephalin A mRNA in rat brain by hybridization histochemistry using complementary RNA probes. Neuropeptides 6: 573—580, 1985
15. Sternberger LA, Hardy PH Jr, Cuculis JJ, Meyer HG: The unlabeled antibody enzyme method of immunohistochemistry. Preparation and properties of soluble antigen-antibody complex (horseradish peroxidase-antiperoxidase) and its use in identification of spirochetes. J Histochem Cytochem 18: 315—333, 1970
16. Uhl GR, Sasek CA: Somatostatin mRNA: regional variation in hybridization densities in individual neurons. J Neuroscience 6: 3258—3254, 1986

Acta Morphologica Hungarica 37 (1—2), pp. 65—69 (1989)

RELATIVE GROWTH OF THE HUMAN TEMPORAL BONE IN THE PRENATAL PERIOD

CARLOS A. MANDARIM-DE-LACERDA

DEPARTMENT OF ANATOMY, STATE UNIVERSITY OF RIO DE JANEIRO (UERJ),
AV. PROF. MANUEL DE ABREU 48 — BR 20550 — RIO DE JANEIRO, RJ — BRAZIL

(Received 19 September 1988)

Thirty right temporal bones of Brazilian fetuses (ranging from 14th to 36th weeks) were studied by the allometric method in order to define the pattern of the whole temporal bone weight growth and the weight growth of the temporal bone portions: squamous, petrous and tympanic. These data were compared to fetal weight. The increase of the data of the temporal bone shows a positive allometry except for the tympanic portion (isometry). The squamous portion shows the highest allometric coefficient. These data are important to the knowledge of the human skull growth.

Keywords: Temporal bone growth, allometry, anatomy

Introduction

The fetal temporal bone has three major portions with origin in several structures. Multiple centers of ossification in the cartilage of the otic capsule produce a composite, bony shell around the inner ear, the petrous portion of the temporal bone. The other portions of this bone, the squamous and tympanic portions, are of intramembranous origin [1]. A definite mastoid process first develops after birth by an outward bulging of the petrous portion, while the styloid process originates from the dorsal end of the second branchial arch [14].

Endochondral bone is three-dimensional in its growth pattern, ossifying from one or more deeply situated and slowly expanding centers. Membraneous bone is two-dimensional and is laid down in broad sheets with extreme speed, especially over rapidly growing areas [19].

Morphological aspects on growth and modelling of the human temporal bone as a component of the basicranium have been subject of many previous studies [2, 4, 5, 6, 8, 12, 14, 15 and 25]. Moreover, quantitative determinations on growth of the temporal bone during human fetal life are scarce in the literature. These determinations may be useful to appreciate the normal growth of

Send offprint requests to: C. A. Mandarim-de-Lacerda, MD, State Univ. of Rio De Janeiro, Av. Prof. Manuel de Abreu 48, 20550 Rio De Janeiro, Brasil

the human basicranium as well as its anomalies in fetal life. Thus, numerical approach of the relative growth of the temporal bone would be an accessory index for classification of cephalic anomalies.

Individual bones can show considerable variations from the overall rate of growth. These variations are only examples of the differential growth that has been found to exist between various parts of the developing organism [17].

The aim of the present study is to consider the growth of the temporal bone in human fetal period by means of the allometric method.

Materials and methods

The subjects were 30 normal human Brazilian fetuses ranging in age from weeks 14 to 36 from the collection of the Department of Anatomy, at the State University of Rio de Janeiro (Table I). They had been preserved in a 10% formalin solution for at least one month. Right temporal bones were carefully dissected under a low power stereomicroscope. Auditory ossicles and all tissues were removed. Weights of the dryed bones were recorded from whole temporal bone, petrous portion, squamous portion and tympanic portion. Male and female bones were combined into one group.

The data were analyzed by the allometric method [9 and 10] considering the logarithmic from

$$[\log y = k(\log x) + \log b]$$

for bivariate normal cases [20].

In the equation k is the allometric coefficient and $\log b$ is the initial growth coefficient [10].

The data were fitted according to model II regression (because both variables are subject to error measurement) [18], by the reduced major axis method [7, 16 and 21]. For the analyses of the relative growth of the temporal bone, weights of temporal bone is the ordinate (y) while weights of fetuses is the abscissa (x).

Table I

Distribution of the fetuses according to the age

Fetal age (weeks)	Number	%
14—20	9	30.0
21—26	11	36.7
27—32	7	23.3
33—36	3	10.0
Total	30	100.0

Results and discussion

Results are shown in Table II and Graph I. Sex differences were not considered in the analysis of the data because they are not statistically significant [22 and 24].

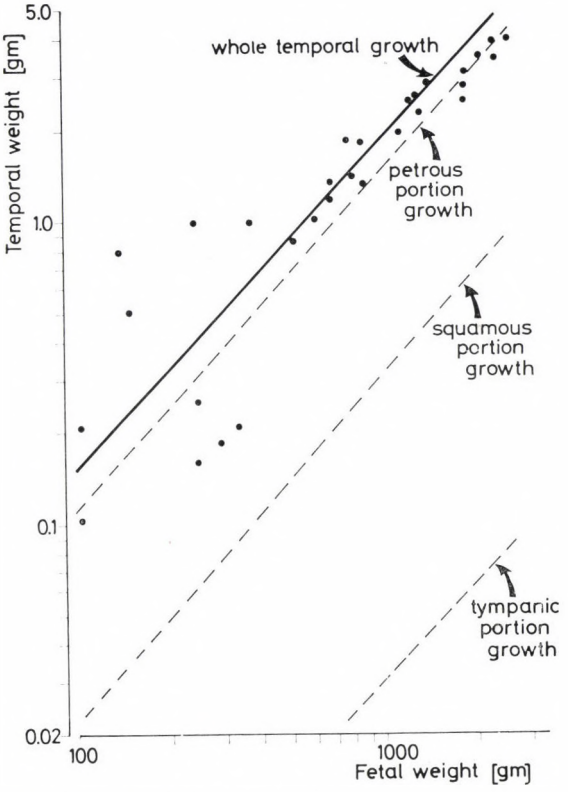

Fig. 1. Schematic drawing of the temporal bone and its three portions at birth

Table II

Regressions of temporal bone weight against fetal weight [$\log y = k(\log x) + \log b$]

Log (x)	Log (y)	Log (b)	k	95% CI(k)[a]	r	Prob(r)[b]
Bodys' weight	Temporal weight	−3.03	1.10	0.89−1.30	0.88	0.01
	Squamous weight	−3.99	1.16	1.00−1.31	0.94	0.01
	Petrous weight	−3.22	1.13	0.89−1.36	0.85	0.01
	Tympanic weight	−4.53	1.01	0.78−1.24	0.81	0.01

[a] 95% confidence interval for the slope estimate k.
[b] Prob(r) is the probability that r is different from zero

During fetal period the average of the relative growth shows, except for tympanic portion of the temporal bone which grows isometrically ($k \simeq 1$), that squamous and petrous portions of the temporal bone present positive allometry ($k > 1$). The average of the relative growth of the whole temporal bone is allometrically positive.

These determinations agree with morphological evidence on development of the temporal bone. Before birth the bone consists of three portions the tympanic portion being in the form of a ring (Figure 1). At birth the tympanic ring has united with the squamous portion and subsequently grows in depth to become the tympanic part which forms the anterior wall and the floor of the external auditory meatus [11].

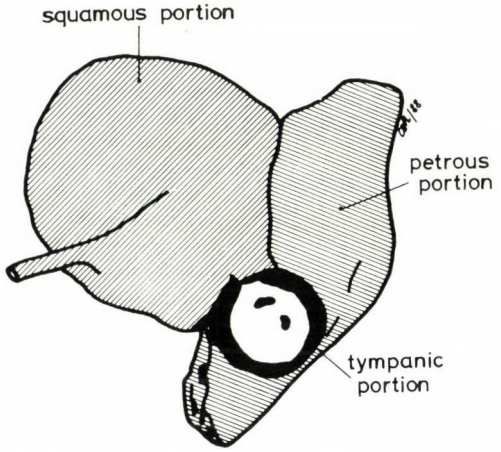

Graph. I. Regression of temporal bone weight against fetal weight according to the data indicated in Table II. The lines were fitted by reduced major axis method. Plots are individual data from fetuses to whole temporal bone weight

The present findings are similar to those of metacarpals' and metatarsals' weights versus fetal body weight that present a positive allometry [3 and 23]. Studying the growth of the skeleton in human fetuses Trotter and Hixon (22) also found positive allometry for the weight increase.

Calculations of the mean growth patterns for large populations establish standards with which an individual child might be compared, and offers an opportunity to statistically predict the growth pattern that a child might follow [13].

This work studies the growth of temporal bones in South-American fetuses (Brazil) for the first time.

Acknowledgements

The author is grateful to Mr. C. J. Santos Matos for his technical assistance. This work was supported by Grant CNPq no. 30.09.04/87.8 (Brazil).

REFERENCES

1. Arey LB: Developmental anatomy. A Textbook and Laboratory Manual of Embryology. Saunders, Philadelphia 1974
2. Bardeen CR: The development of the skull, the hyoid bone, and the larynx. In: Keibel F, Mall FP (eds) Manual of Human Embryology, Vol. 1 Lippincott, Philadelphia 1910, pp. 398—453
3. Barros RSM, Mandarim-de-Lacerda CA: Relative growth of the human metacarpals in the prenatal period: anatomical basis to preventive surgery for congenital deformities of the hand. Surg Radiol Anat 11: 49, 1989
4. Bosma JF: Symposium on Development of the Basicranium. U.S. Department of Health, Bethesda 1976
5. De Beer GR: The Development of the Vertebrate Skull. Clarendon Press, Oxford 1937
6. Fawcett E: Some observations on the roof of the primordial human cranium. J Anat 57: 245, 1923
7. Gould SJ: Allometry and size in ontogeny and phylogeny. Biol Rev 41: 587, 1966
8. Grube D, Reinbach W: Das Cranium eines menschlichen Embryo von 80 mm Sch.-St.-Länge. Anat Embryol 149: 183, 1976
9. Huxley JS: Relative growth and form transformation. Proc Roy Soc Biol (London) 137: 465, 1950
10. Huxley JS, Tessier G: Terminology of relative growth. Nature 137: 780, 1936
11. Joseph J: Locomotor system. In: Hamilton WJ (ed) Textbook of Human Anatomy, Mosby, Saint Louis 1976, pp. 72—75
12. Macklin CC: The skull of a human fetus of 40 mm. Am J Anat 16: 317, 1914
13. McKeown M: The allometric growth of the skull. Am J Orthod 76: 412, 1975
14. Müller F, O'Rahilly R: The human chondrocranium at the end of the embryonic period, proper, with particular reference to the nervous system. Am J Anat 159: 33, 1980
15. Pierce RH, Mainen MW, Bosma JF: The Cranium of the Newborn Infant. An Atlas of Tomography and Anatomical Sections. U.S. Department of Health, Bethesda 1978
16. Ricker WE: Linear regressions in fishery research. J Fish Res Board Can 30: 409, 1973
17. Sissons HA: The growth of bone. In: Bourne GH (ed.) The Biochemistry and Physiology of Bone. Academic Press, New York 1956, pp. 443—471
18. Sokal RR, Rohlf FJ: Biometry. The Principles and Practice of Statistics in Biological Research. Freeman, New York 1981
19. Sperber GH: Craniofacial embryology. Wright and Sons, Chicago 1976
20. Sprent P: Linear relationships in growth and size studies. Biometrics 24: 639 1968
21. Tessier G: La relation d'allométrie, sa signification statistique et biologique· Biometrics 4: 14, 1948
22. Trotter M, Hixon BB: Sequencial changes in weight, density, and percentage ash weight of human skeletons from an early fetal period through old age. Anat Rec 179: 1, 1974
23. Vasconcellos HA, Mandarim-de-Lacerda CA: Human metatarsal growth: an allometrical analysis in prenatal period. Arch Ital Anat Emb 93: 155, 1989
24. Wakasa K: The studies on the fetal extremities. Kanazawa Daigaku Igakubu Kaibogaku Kyoshitsu Gyoseki 48: 51, 1953
25. Youssef EH: The development of the skull in a 34 mm human embryo. Acta Anat 57: 72, 1964

Acta Morphologica Hungarica 37 (1—2), pp. 71—84 (1989)

MYENTERIC PLEXUS OF FROG LARGE INTESTINE: LIGHT AND ELECTRON MICROSCOPY OF FIBER SYSTEM AND NEURONS

R. GÁBRIEL[1], I. BENEDECZKY[1], MÁRIA CSOKNYA[2]

[1]DEPARTMENT OF ZOOLOGY, JÓZSEF ATTILA UNIVERSITY, SZEGED, HUNGARY
[2]DEPARTMENT OF ZOOLOGY, JANUS PANNONIUS UNIVERSITY, PÉCS, HUNGARY

(Received 28 November 1988)

The myenteric plexus of the frog large intestine was studied by means of silver impregnation, NADH-diaphorase histochemistry and electron microscopy. The main fiber bundles of the myenteric plexus are situated between the longitudinal and circular smooth muscle layers. Most of the branches of this main plexus could be followed into the circular muscle layer. The diameter of the large nerve bundles was demonstrated by impregnation to be 7—8 μm. NADH-diaphorase histochemistry revealed a random distribution of the nerve cells; the nerve cells did not form ganglia. The maximal profile of these mostly multipolar cells was 75—100 μm^2. The packing density of nerve cells was 710 $\pm$ 23 per cm^2. At the electron microscopic level, the plexus consisted of a number of unmyelinated nerve profiles, a few myelinated axons, Schwann cells and neurons. The proportion of myelinated fibers did not exceed 1%. The nerve profiles contained vesicles, small agranular vesicles or mixed vesicle populations. Synapses were extremely rare in the neuropil. The possibility and importance of non-synaptic transmitter release and presumed transmitter substances are discussed.

Keywords: Frog, large intestine, myenteric plexus, silver impregnation, NADHd, ultrastructure

Introduction

The large intestine of the frog is different in anatomy from that of mammals. It is relatively short, but has a huge diameter compared with that of the small intestine, and can be localized in the lower part of the body cavity. Only a few studies have been performed on its innervation [8, 39, 41, 47, 54, 55]. Gunn described the gut plexuses and their cell types in the frog [41]. She pointed out that the small and large intestines contain Dogiel type II and III cells, which are probably interconnected with each other. Nerve fibers presumably containing catecholamines were identified by means of fluorescence in whole mounts of the toad gut; they were numerous in the circular muscle layer of the large intestine [62, 63]. Neither perikarya nor pericellular baskets were seen [76], but the innervation proper of the smooth muscle seemed to be richer than in mammals. Other data on the organization of the large intestine plexuses are not available in the literature; the lack of studies on the size and number of neurons and on the ultrastructure of neural elements of the myenteric plexus is

Send offprint requests to: R. Gábriel, Department of Zoology, József Attila University, Szeged, Hungary H-6722 P.O.B. 659

conspicuous. Our aim was to obtain these missing data by means of light- and electron microscopic methods.

Materials and methods

Adult specimens of frog (males and females: a total of 17) were used for the experiments.

Silver impregnation was carried out on 15—30 μm thick frozen sections with the Bielschowsky—Gros—Cauna method [19].

NADH-diaphorase histochemistry followed the procedure of Gabella [31]. Briefly, the appropriate segment of the gut was removed, immersed into Krebs solution, distended with it and incubated (for 30—50 min) in a medium containing 2.5 mg nitroblue tetrazolium (NBT) and 10 mg nicotinamide adenine dinucleotide (reduced from; NADH) in 20 ml 0.1 M phosphate buffer, then fixed in 10% neutral formalin. "Whole mounts" were prepared by cutting 1 cm wide rings of large intestine, from which the mucosal and submucosal layers were removed. Specimens were then stretched on slides, mounted with glycerine and covered with glass cover slips. Photographs were taken in a Zeiss light microscope .

The packing density of labeled cells was counted directly from the whole mounts and the standard deviation was calculated. Approximately 120 cells were measured on the photographs for calculation of the maximal profiles according to Gabella [32].

For electron microscopic examinations, animals were perfused transcardially first with frog Ringer solution, followed by a fixative contained 2% paraformaldehyde (freshly prepared) and 2% glutaraldehyde in 0.1 M phosphate buffer (pH 7.4). Small tissue blocks were then cut from the muscular layer and kept in the same fixative for 4 h. After a short rinse in phosphate buffer, blocks were postfixed in phosphate-buffered 2% OsO_4 and dehydrated in ascending series of ethanol. Samples were stained "en bloc" in 75% ethanol saturated with uranyl acetate. After embedding in Durcupan ACM resin, ultrathin sections were made on a Reichert OM U2 ultramicrotome, stained with lead citrate [64], viewed and photographed in a JEOL 100B or Tesla BS 540 electron microscope.

For quantitative analysis of the vesicle population of the axon profiles, 165 of them were chosen (all were larger than 4 μm^2) randomly from 15 different areas of the plexus.

Results

a) Light microscopy

The wall of the large intestine, similarly to that in mammals consisted of 4 layers, as was revealed in a cross-section stained with hematoxylin-eosin (Fig. 1a). The mucosal and submucosal layers were relatively thin, and the muscular layer was built up from a well-developed inner circular and an outer longitudinal muscle coat. Between the muscle layers, neurons and nerve bundles were revealed by means of silver impregnation (Fig. 1b). These bundles were relatively thin: 7—8 μm in diameter. Nerve cells could hardly be recognized in these preparations. The distribution of the fibers in the longitudinal direction was observed in the sections of muscle coat directed tangentially in the gut wall. A loose network of relatively thin nerve bundles (Fig. 1c) was seen; neurons were observed only in low numbers.

→

Fig. 1a. Cross-section of the large intestine of frog, stained with hematoxylin-eosin. The main histological layers are similar to those of mammals. muc: tunica mucosa, sm: tela submucosa, tm: tunica muscularis, ser: tunica serosa. Original magnification: ×100 *1b.* The same sectioning plane as in a. Frozen section stained by silver impregnation. Nerve bundles (open arrow) and the sections of nerve cells (arrows) are visible. sm: tela submucosa; tml: tunica muscularis longitudinal layer, tmc: tunica muscularis circular layer, subs: connective tissue of subserosa, bv: blood vessel. Original magnification: ×100 *1c:* Tangential frozen section of the muscular

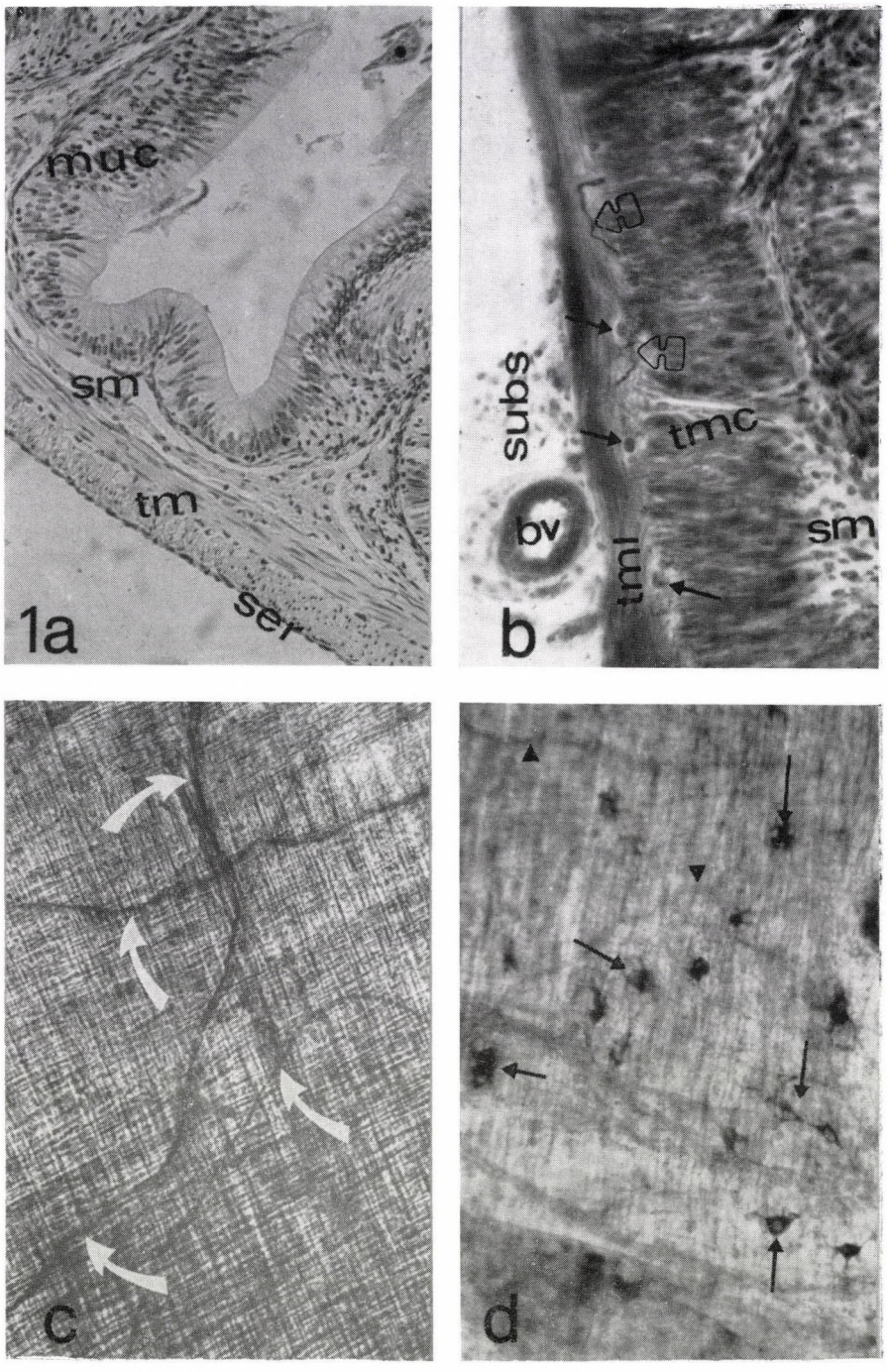

layer, stained with silver. Relatively thin nerve bundles (arrows) of myenteric plexus are located mostly between the circular and longitudinal muscle cells. Original magnification: ×100 *1d:* Myenteric neurons (arrows) stained with formazan, the end-product of the NADH-diaphorase reaction. These cells are multipolar, with short dendrites. Note the nerve bundles (arrow-heads) which are slightly labelled by this technique. Original magnification: ×100

Nerve cells were also demonstrated with the NADH-diaphorase method (Fig. 1d). The neurons did not form ganglia in this portion of the gut, but rather had a solitary arrangement. These cells were multipolar, generally with short dendrites. The maximal profile of the nerve cells was 75—100 μm^2. The density of the neurons reached 710 $\pm$ 23 cells/cm^2 in this region of the alimentary canal.

b) Electron microscopy

The general view of the myenteric plexus at the electron microscopic level was characteristic, because of the presence of large granulated vesicles (LGVs) in many profiles. Schwann cells were embedded in the plexus. The main strands of the plexus were covered with a glial sheath and were situated between the circular and longitudinal muscle layers. Small branches consisting of 10—15 fibers ran to the muscle cells (Fig. 2a). Occasionally, myelinated axons were also revealed. Neurons were not contained by the main bundles of the plexus. A low number of unmyelinated axons could be seen in close proximity to the nerve cells (Fig. 2b). Schwann sheaths were sometimes inserted between the axon profiles and the nerve cells. These profiles contained mainly small agranular vesicles (AGVs) and/or LGVs. Synaptic contacts between the abovementioned elements were not observed. The perikaryon of these cells always contained a small number of neurosecretory granules (Figs 2b, 3a). Generally, the proximal segments of dendrites could also be seen (Fig. 3a). The processes of the Schwann cells covered only a part of the perikarya; other details of them were free of both Schwann sheath and axon profiles (Fig. 3a).

Myelinated fibers were situated between Schwann cells and were surrounded by a narrow connective tissue layer which separated them from the unmyelinated profiles (Fig. 3b). The proportion of myelinated axons did not exceed 1%. Four or five myelinated fibers ran occasionally in groups, while in other cases they had a solitary course.

Synaptic contacts between the neural elements were extremely rare (Fig. 4a). Most of these contacts were established between an axon terminal and the initial segment of another axon in the myenteric neuropil. The synapsing profile (Fig. 4a) contained a mixed vesicle population of AGVs and LGVs. Synapses between the axons and the perikarya have not been observed so far, and synapses were also lacking in the nerve bundles running between the muscles (Fig. 4b). As regards the vesicle population of the myenteric axons, 165 of them were examined; all were larger than 4 μm^2. 65 of them contained LGVs. Another 12 contained AGVs only. The remaining 88 had mixed profiles; 18 of them consisted of flattened vesicles (FVs) and LGVs or dense-core vesicles (DCVs), while 44 contained DCVs and FVs or AGVs. FVs were present in the mixed profiles only. The most frequent mixed profiles were AGVs + LGVs [44]; a few AGVs + DCVs [12] were also observed. These axons were some-

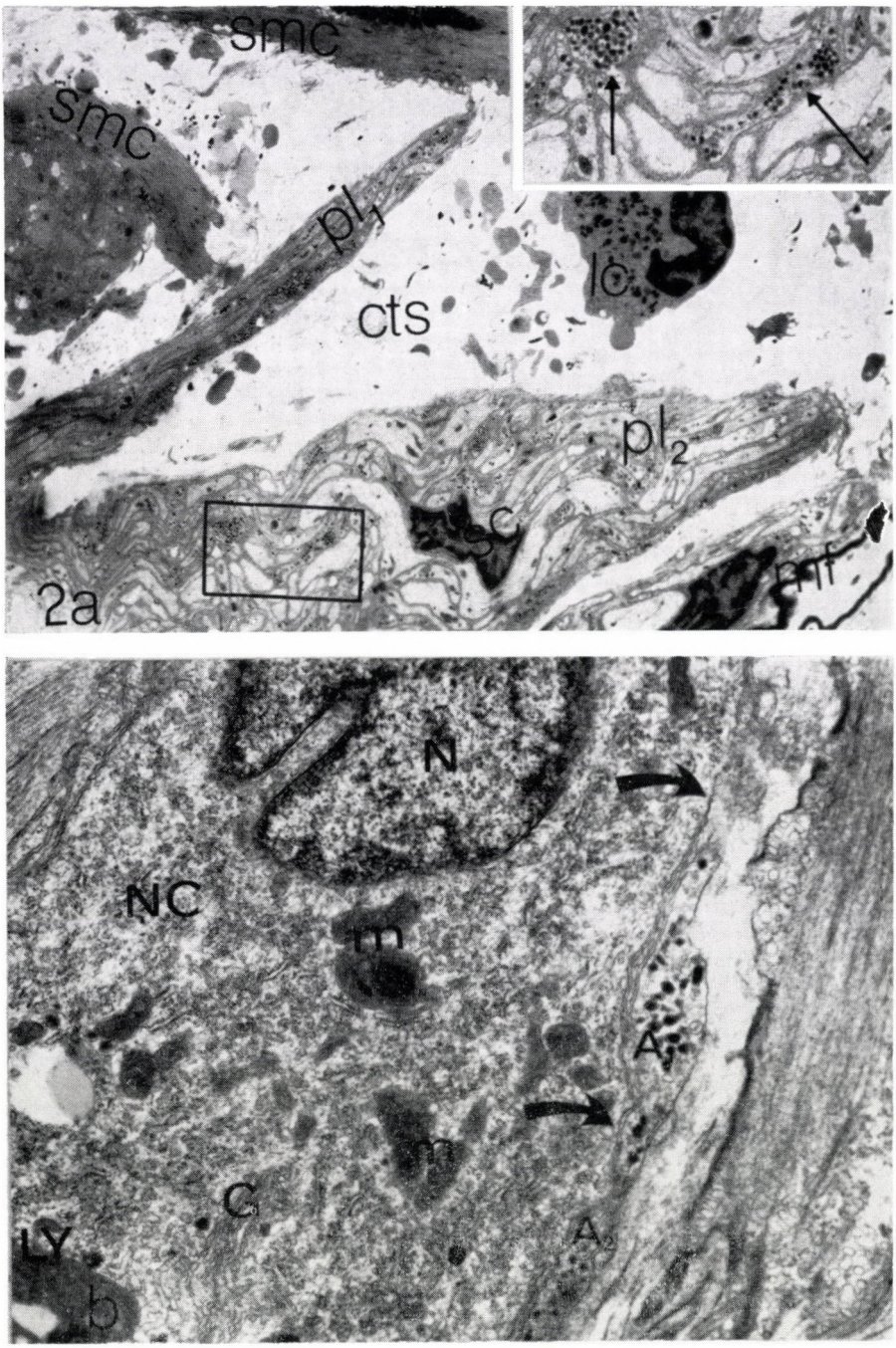

Fig. 2a. Branching nerve bundle in the myenteric plexus. Note the large amount of LGV profiles (arrows, insert). SC: Schwann cell, lc: leukocyte, smc: smooth muscle cell, cts: connective tissue sheath, mf: myelinated fiber, pl_1 and pl_2: branches of the plexus. Original magnification: ×5000. In frame: the same as in insert. *2b.* Nerve cell (NC) from the plexus adjacent to the smooth muscle. The nucleus (N) of the cell is poor in chromatin; organelles (m: mitochondrion, G: Golgi apparatus; LY: lysosome) can be recognized in the cytoplasm. Axon profiles (A_1 and A_2) are situated in close proximity to the neuron. The Schwann sheath cannot be seen everywhere between the axons and the perikaryon (arrows). Original magnification: ×12 000

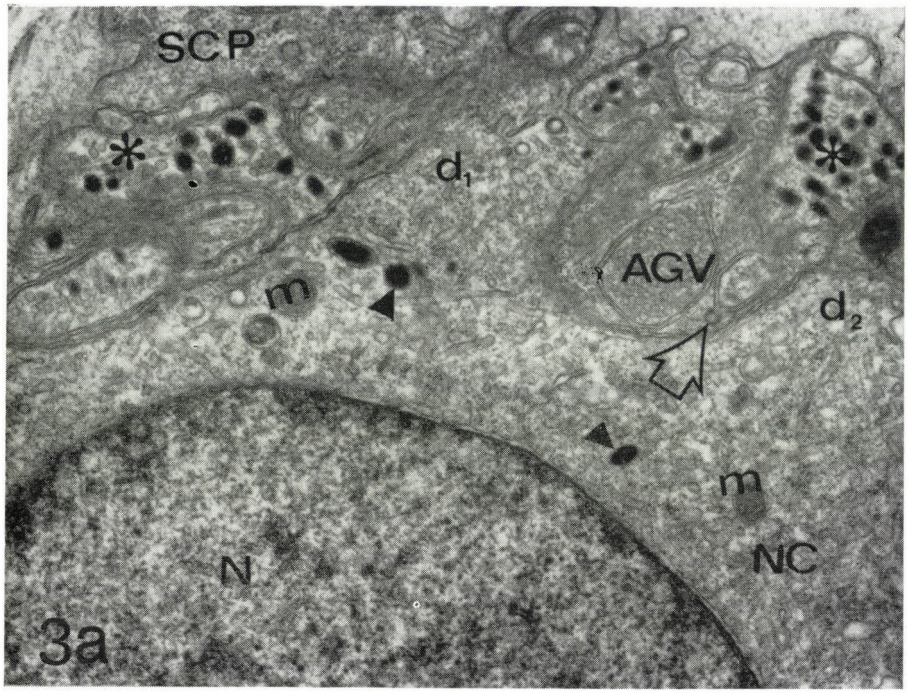

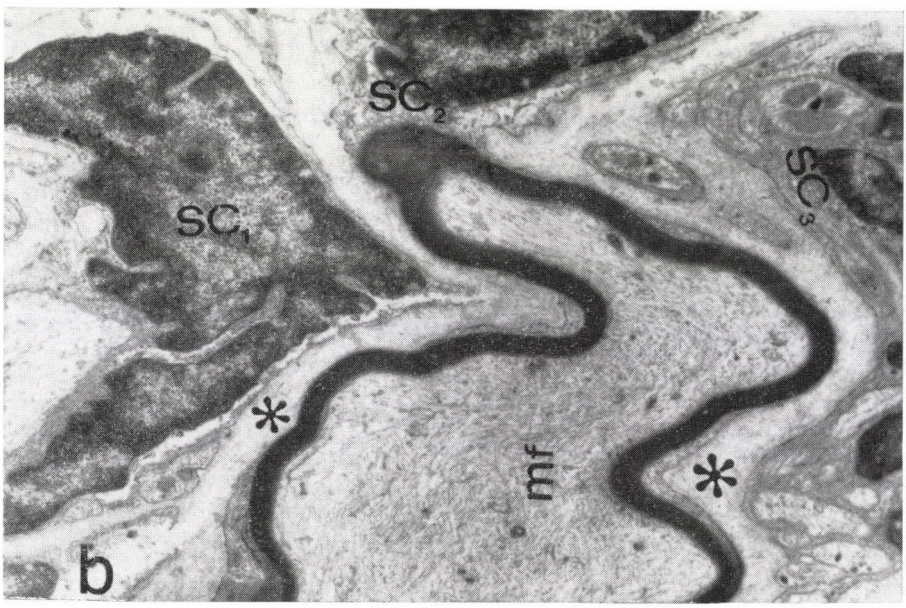

Fig. 3a. Myenteric neuron (NC) surrounded by axon profiles. Initial portion of its dendrites (d_1 and d_2) are covered by axons or glial sheath. m: mitochondrion, N: nucleus, arrow-heads: neurosecretory granules; open arrow: coated vesicle, LGV: profile with LGVs, asterisks: axons with mixed vesicle population, SCP: Schwann cell process. Original magnification: ×17 000. *3b.* Myelinated fiber (mf) surrounded by a connective tissue sheath (asterisks) and Schwann cells (SC_1, SC_2 and SC_3). Note that SC_2 gives the sheath of this axon in this sectioning plane. Original magnification: ×12 000

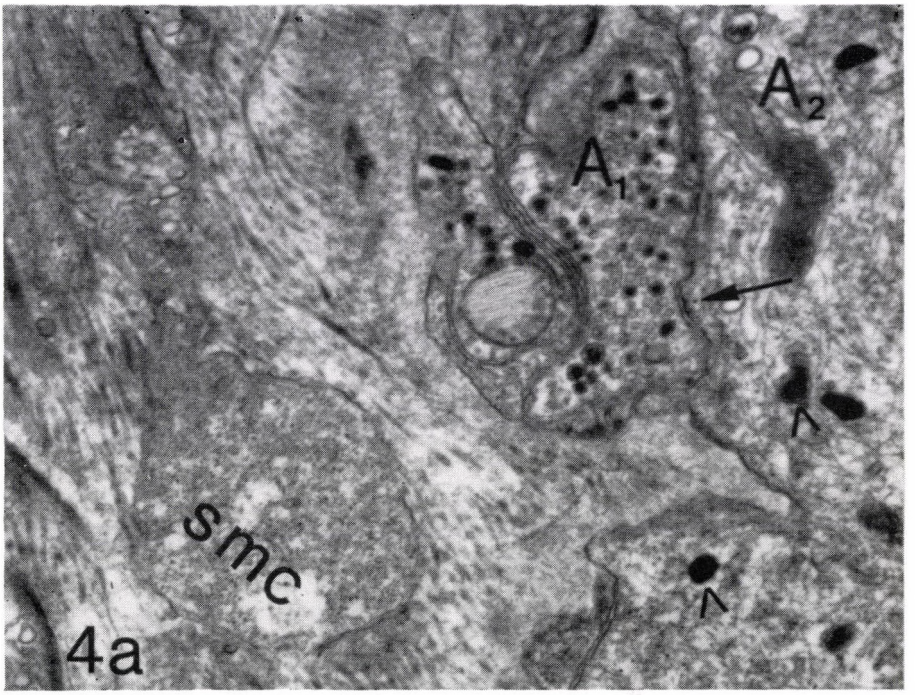

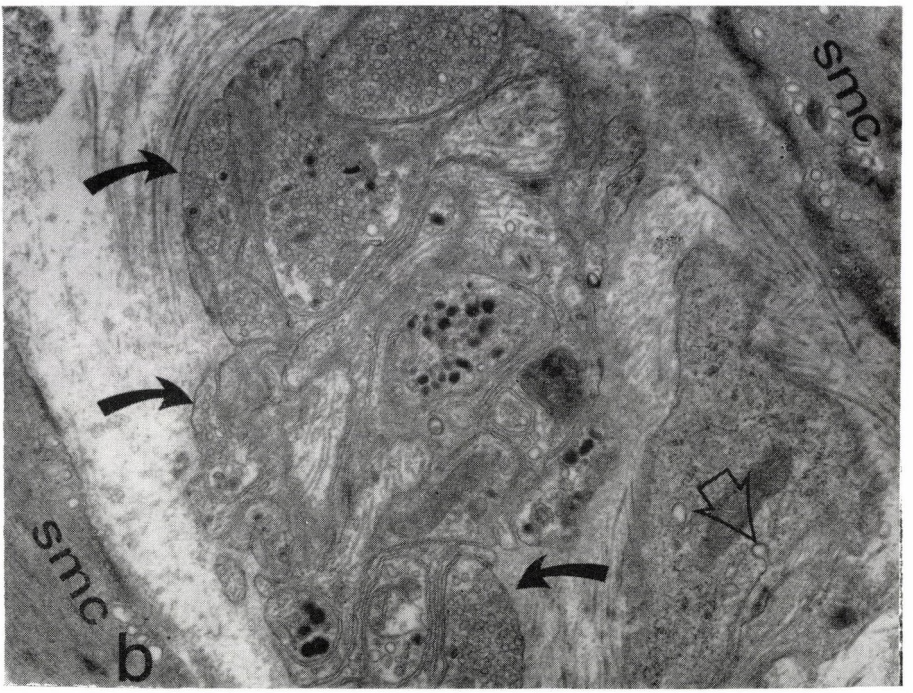

Fig. 4a. Synaptic contact in the neurophil between two axons (A_1 and A_2). arrow: postsynaptic thickening, arrowhead: neurosecretory granules in the postsynaptic axon, smc: smooth muscle process. Original magnification: $\times 7000$ *4b.* Nerve bundle between smooth muscle cells (smc). Arrows indicate uncovered fibers. Open arrow shows a coated vesicle. Original magnification: $\times 15\ 000$

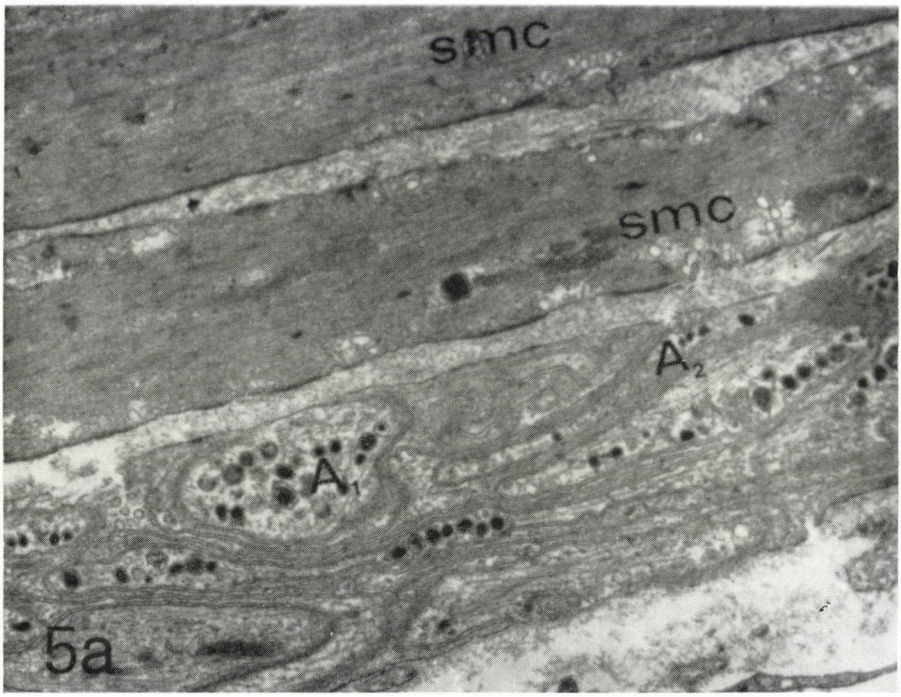

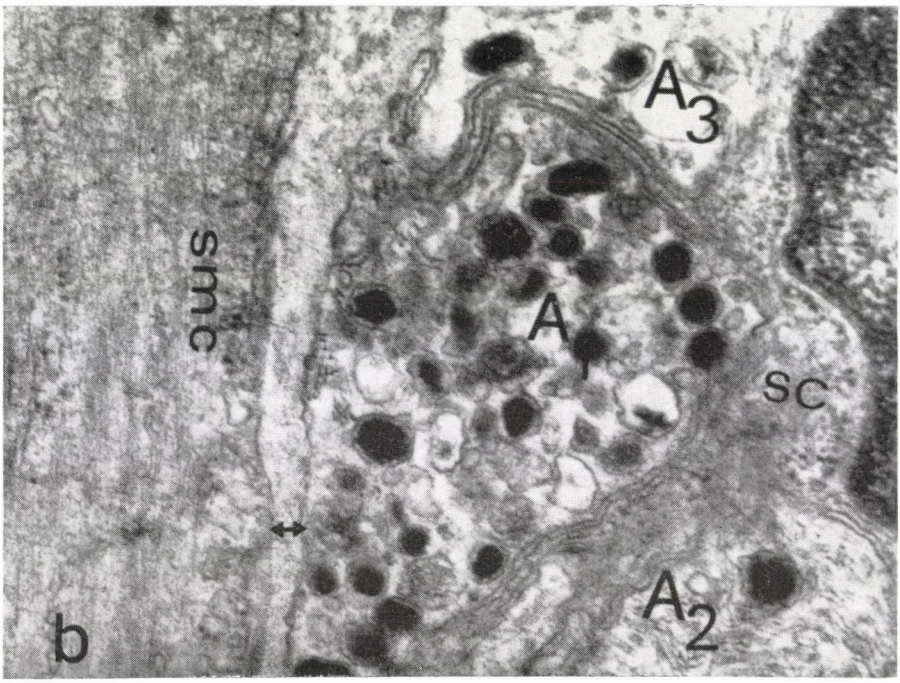

Fig. 5a. Axon profiles (A_1 and A_2) opposed to the smooth muscle cells (smc). They contain mainly LGVs and are free of glial cover (arrows). Original magnification: ×17 000 *5b.* Schwann cell covers 3 axons (A_1, A_2 and A_3) in the neighbourhood of a smooth muscle cell (smc). Profile A_1 contains LGVs and approaches the muscle cell to 80—100 nm at the site of the double arrow. Original magnification: ×40 000

times free of glial sheath (Fig. 4b). Small branches of axons ran to the muscle cells. The distance between them and the muscle cells was usually less than 500 nm (Fig. 5a). Some of these profiles were free of glial sheath and contained mainly LGVs, or rarely they had a mixed AGV + LGV vesicle population. These axons (without glial cover) occasionally ran as close as 80—100 nm to the muscle cells (Fig. 5b).

Discussion

The myenteric plexus of the frog large intestine, in contrast with that of the stomach, is located in a connective tissue layer between the circular and longitudinal smooth muscles. Silver impregnation was used to map the nerve bundles, and the NADH-diaphorase reaction to observe the site, size and quantity of neurons.

As reported formerly, the location of the plexus changes throughout the length of the alimentary canal [36]. The plexus of the stomach is situated outside the muscular layers, in the connective tissue of subserosa. This kind of localization of the myenteric plexus is also known in the case of the avian gizzard [35, 51]. In further parts of the frog alimentary canal, the myenteric plexus is localized in between the longitudinal muscle cells or, as in the case of the large intestine, between the circular and longitudinal muscle layers.

The nerve cells of the plexus have a random, solitary arrangement in this part of the gut plexus. Gunn described that the myenteric neurons of the frog small and large intestines did not form ganglia [41], in contrast with the foregut region, which has a ganglionated arrangement [18, 21, 26]. The reason for this difference may be the different origin of the myenteric neurons. Andrew reported (4) that the possible sources of the enteric neurons are the colony of the vagus in the medulla or the ventral half of the neural tube in the region of the trunk. Strong evidence [3, 38, 61, 76] indicates that the neurochemical natures of the frog foregut and mid/hindgut neurons are very different in connection with the different morphology of the myenteric plexus. The myenteric neurons situated in the different parts of the alimentary canal may be different in origin: foregut nerve cells from the vagus colony and mid/hindgut nerve cells from the neural tube.

The number of myenteric nerve cells per cm^2 in the different parts of the gut of different species varied from 1100 (monkey foregut (58)) to 20 000 (guinea-pig small intestine (50)). In lower vertebrates, Burnstock described [10] the neuron density of the trout gut: he found nearly 2000 neurons/cm^2. All the previously mentioned data were obtained via methylene blue staining. A comparative study was performed on some invertebrate and vertebrate species [37], where the average neuronal packing density of the lower ver-

tebrate alimentary canal was found with the NADH-diaphorase technique to range between 500 and 1200/cm^2. The packing density of nerve cells throughout the length of the frog alimentary canal was earlier observed [36] to vary from the stomach cardia (619 $\pm$ 80) to the distal part of the small intestine (1004 $\pm$ 55). The neuronal packing density found in the large intestine in the present study (710 $\pm$ 23) was nearly the same as described previously [36] in the duodenum (772 $\pm$ 105). This relatively high neuronal packing density might be connected with the large inner volume of this organ.

Only multipolar neurons were seen in the large intestine. This description corresponds to the classification of Gunn, who characterized these nerve cells as Dogiel type II and III neurons [41]. Type II and III cells are not present in the foregut and are rare in the proximal part of the duodenum, but become predominant in the rest of the intestine [36, 40, 73]. Type I neurons are predominant in the foregut [41], but rare in the midgut [36] and, as described in the present paper, absent from the large intestine. These large neurons are probably connected with vagus fibers, which is why they are not present in the hindgut.

Nerve cells were not built into the main strands of the plexus, as is usual in the case of ganglionated myenteric systems [2, 6, 24, 28, 33, 34, 42, 56, 65, 66]. Only a few individual fibers ran to the neurons. Synapses on the somata and dendrites of nerve cells have not been observed so far, while synaptic contacts have been seen occasionally on fish gut silitary neurons [45]. The reason for this difference is unknown at present.

The presence of myelinated axons is characteristic in the oesophagus and large intestine only in the frog gut. These fibers might be largely extrinsic in origin [20, 57]. This suggestion is supported by the fact that a narrow connective tissue sheath surrounds the myelinated axons. In the different regions of the cat colon, 2.71% to 4.41% of the axons were myelinated [20]. In the case of the frog, the proportion of myelinated axons did not exceed 1%. As concerns this difference, two possibilities should be discussed:

i) The extrinsic innervation of the frog large intestine is not so well developed as that in mammals. At the same time, the sacral plexus of the frog has been described to have a very strong influence on the frog viscera in the lower part of the body cavity through spinal nerves VIII—IX—X. [8, 11, 71, 73].

ii) The great predominance of unmyelinated fibers over myelinated ones suggests that the composition of the extrinsic nerves to the large intestine of the frog is not similar to that of mammals.

In the neuropil region, synapses were observed very rarely; in other vertebrate species, synaptic contacts are rather numerous [22, 28, 33, 34, 35, 40, 53, 65, 66, 68].

Morphological evidence has been found [7, 9, 74, 77] that non-synaptic release may play an important role in the integrative processes of certain peri-

pheral and central nervous system structures (PNS and CNS). The sources of the non-synaptically released transmitters are the LGVs and DCVs. Because of the large number of LGVs and the extremely low number of synapses in the frog large intestine, the possibility of this mode of transmitter release cannot be excluded.

The main vesicle type of the plexus is the LGVs. The LGVs are known to contain peptides and/or purines [11, 14, 15, 16, 22, 28, 33, 43, 46, 68]. In the frog, there is no evidence so far of the presence of peptidergic innervation, whereas the existence of purinergic nerves has been demonstrated [11, 71].

The other important vesicle type is the AGVs. The AGVs may contain acetylcholine (ACh) [17], which has been shown to collocalize with different peptides in the profiles with a mixed vesicle population [28, 30, 34, 75]. Nothing is known of the possible peptides collocalizing with ACh in the frog gut.

DCVs and FVs occurred in mixed profiles only. Profiles with a mixed vesicle content suggest cotransmission [12, 13, 48, 49, 59, 69]. DCVs usually contaning monoamines, are present in the toad large intestine [62, 63]. The collocalization of monoamines with different peptides has been proved in the case of mammals [23, 27, 48, 49, 69]. Since the first detection of γ-aminobutyric acid (GABA) in the vertebrate CNS [67] it has been suspected that the FVs may contain GABA in the Gray type II inhibitory synapses [25, 60]. Jessen et al. [52] provided the first evidence of the presence of this substance in the PNS of mammals. As concerns the lower vertebrates, a paper has been published on GABA in the avian enteric nervous system (ENS), [5]. Our study on the occurrence of GABA in the frog appeared recently [36a]. It can be concluded that the FVs in the frog large intestine may contain GABA. Because of the mixed FV profiles, peptide cotransmitters are presumably to be found in these axon terminals, as revealed in the mammalian CNS [70]. GABA is probably not involved directly in the regulation of smooth muscle movement, but rather through its action on the release of other transmitter substances [72].

Neuromuscular junctions are similar to those described in the gut of other vertebrate species [22, 28, 29, 33, 34, 44, 46, 65, 66, 68]. A large number of LGV profiles in close proximity to smooth muscle cells is also characteristic for the toad large intestine [8, 68] and the neuromuscular junctions of the snail alimentary canal [1, 7, 46]. Thus the main transmitter substances in the neuromuscular contacts in these species may be peptides and/or purines.

REFERENCES

1. Ábrahám A: Ultrastructural studies on the gastrointestinal nervous system of *Helix normatia*. Acta Biol Szeged 29: 129, 1983
2. Ali H, McLelland J: Avian enteric nerve plexuses. A histochemical study. Cell Tissue Res 189: 537, 1978
3. Anderson C, Campbell G: Evidence for 5-HT neurones in the gut of the toad. *Bufo marinus*. Cell Tissue Res 238: 313, 1984
4. Andrew A: The origin of intramural ganglia. J Anat 108: 169, 1971
5. Baetge G, Gershon MD: GABA in the PNS: Demonstration in enteric neurons. Brain Res Bull 16: 421, 1986
6. Baumgarten HG, Holstein AF, Owman CH: Auerbach's plexus of mammals and man: electron microscopic identification of three different types of neuronal processes in the myenteric ganglia of the large intestine of rhesus monkeys guinea-pigs and man. Z Zellforsch mikr Anat 106: 376, 1970
7. Benedeczky I, Halasy K: Visualization of non-synaptic release sites in the myenteric plexus of snail. Neuroscience 25: 163, 1988
8. Boyd H, Burnstock G, Rogers D: Innervation of the large intestine of the toad *(Bufo marinus)*. Brit J Pharmacol 23: 151, 1964
9. Buma P, Roubos EW, Buijs RM: Ultrastructural demonstration of exocytosis of neural neuroendocrine and endocrine secretions with an in vitro tannic acid (TARI) method. Histochemistry 80: 247, 1984
10. Burnstock G: The innervation of the gut of the brown trout *(Salmo trutta)*. Q J Micr Sci 100: 199, 1959
11. Burnstock G: Purinergic nerves. Pharmacol Rev 24: 509, 1972
12. Burnstock G: Do some nerve cells release more then one neurotransmitter? Neuroscience 1: 239, 1976
13. Burnstock G: Do some sympathetic neurons release both adrenalin and acetilcholine? Prog Neurobiol 11: 205, 1978
14. Burnstock G: The changing face of autonomic neurotransmission. Acta Physiol Scand 126: 67, 1986
15. Burnstock G: Present status of purinergic neurotransmission-implications for vascular control. In: Nobin A, Owman C, Arneklo-Nobin B (eds). Neuronal Messengers in Vascular Function Elsevier Publishers (Biomedical Division), New York, 1987, p 327
16. Burnstock G, Satchell DG, Smythe A: A comparison of the excitatory and inhibitory effects of non-adrenergic, non-chonlinergic nerve stimulation and exogenously applied ATP on a variety of smooth muscle preparations from different vertebrate species. Brit J Pharmacol 46: 234, 1972
17. Burt A, Silver A: Histochemistry of choline-acetyltransferase: A critical analysis. Brain Res 62: 509, 1973
18. Cajal SRy: Nota sobre el plexo de Auerbach de la Rana. Trab Lab Histol Fac Med (Barcelona) 2: 23, 1902
19 Cauna N: The mode of termination of the sensory nerves and its significance. J Comp Neurol 113: 169, 1959
20. Christensen J, Rick GA: Distribution of myelinated nerves in ascending nerves and myenteric plexus of cat colon. Am J Anat 178: 250, 1987
21. Cole EC: Notes on the extension and organization of the myenteric plexus of frog. J Comp Neurol 41: 311, 1926
22. Cook RD, Burnstock G: The ultrastructure of Auerbach's plexus in guinea-pig. I. Neuronal elements. J Neurocytol 5: 171, 1976
23. Costa M, Furness JB: Somatostatin is present in the subpopulation of noradrenergic nerve fibres supplying the intestine. Neuroscience 13: 911, 1984
24. Csoknya M, Benedeczky I: Cell types of the enteric nerve plexuses in the chicken. Acta Biol Szeged 32: 93, 1986
25. Curtis DR, Johnston GAR: Amino acid transmitters in the mammalian central nervous system. Rev Physiol Biochem Exp Pharmacol 69: 97, 1974
26. Dixon WE: The innervation of frog stomach. J Physiol (London) 28: 57, 1902
27. Ekblad E, Hakanson R, Sundler F: VIP and PHI coexist with an NP-like peptide in intramural neurons of the small intestine. Regulatory Peptides 9: 297, 1984
28. Furness JB, Costa M: Types of nerves in the enteric nervous system. Neuroscience 5: 1, 1980
29. Furness JB, Costa M: The Enteric Nervous System. Churchill Livingstone, Edinburgh 1987

30. Furness JB, Costa M, Keast JR: Choline-acetyltransferase and peptide immunoreactivity of submucous neurons in the small intestine of guinea-pig. Cell Tissue Res 237: 328, 1984
31. Gabella G: Detection of nerve cells by a histochemical technique. Experientia 25: 218, 1969
32. Gabella G: Neuron size and number in the myenteric plexus of the newborn and adult rat. J Anat 109: 81, 1971
33. Gabella G: Fine structure of the myenteric plexus in the guinea-pig ileum. J Anat 111: 69, 1972
34. Gabella G: Innervation of the gastrointestinal tract. Int Rev Cytol 59: 129, 1979
35. Gabella G, Halasy K: On the nerve plexus of chicken gizzard. Anat Embyol 177: 97, 1987
36. Gábriel R, Halasy K, Csoknya M: Cytochemical detection of NADH-disphorase positive nerve cells in the intestinal canal of frog. Acta Biol Szeged 33: 85, 1987
36a. Gábriel R, Eckert M: Demonstration of GABA- like immunoreactivity in myenteric plexus of frog Stomach. Histochem 91: 523, 1989
37. Gábriel R, Halasy K, Csoknya M: Visualization of neurons by NADH-diaphorase staining in the myenteric plexus of some invertebrate and vertebrate species. Z mikr- anat Forsch 102: 769, 1988
38. Gábriel R, Fekete É, Halasy K: Consecutive diaphorase-acetylcholinesterase study on the myenteric plexus of frog stomach. Acta Histochem 85: 135, 1989
39. Gaupp E: Ecker's and Wiedersheim's Anatomie des Froschen. F Vieweg Braunschweig 1899, 214
40. Gordon-Weeks PR: Neuroscience properties of nerve endings with small agranular vesicles in the distal colon and rectum of the guinea-pig. Neuroscience 6: 1, 1981
41. Gunn M: A study of the enteric plexus in some amphibians. Q Jl micr. Sci 92: 55, 1951
42. Gunn M: Histological, histochemical observations on the myenteric and submucous plexuses of mammals. J Anat 95: 160, 1968
43. Halasy K, Benedeczky I: Electron microscopic study on the innervation of the gut musculature in the carp. Acta Biol Szeged 31: 27, 1985
44. Halasy K, Benedeczky I, Ábrahám A: Fine structure of the neuromuscular junction in the small intestine of a teleostean fish: tench *(Tinca tinca* L.) Acta Morph Hung 34: 73, 1986
45. Halasy K, Fekete É, Csoknya M, Gábriel R, Benedeczky I: Fine structure and cytochemical features of enteric neuromuscular junctions in lower vertebrates. Neuroscience 22(S): 344, 1987
46. Halasy K, Benedeczky I, Fekete É, Tóth L, Gábriel R: Enteric neuromuscular junctions: comparison of ultrastructural features in different phylogenetic groups. Neuroscience 25: 147, 1988
47. Hirt A: Die vergleichende Anatomie des sympathischen Nervensystem. In: Boln L, Göppert E, Kallius E, Lubosch WL (eds). Handbuch der vergleichenden Anatomie der Wirbeltiere. Vol. II: Urban and Schwarzenberg Berlin—Wien 1934, 709
48. Hökfelt T, Elfvin LG, Elde R, Schultzberg M, Goldstein M, Luft R: Occurrence of somatostatin-like immunoreactivity in some periferal sympathetic noradrenergic nerves. PNAS 74: 3587, 1977
49. Hökfelt T, Lundberg JM, Skirboll L, Johansson O, Schultzberg M, Vincent SR: Coexistence of classical transmitters and peptides in neurones. In: Cuello AC (ed.) Co-transmission. MacMillen Press London 1982, 77
50. Irwin DA: The anatomy of Auerbach's plexus. Am J Anat 49: 141, 1931
51. Iwanow IF: Die sympatische Innervation des Verdauungstraktes einiger Vogelarten. Z mikr- anat Forsch 22: 469, 1930
52. Jessen KR, Mirsky R, Dennison ME, Burnstock G: GABA may be a neutrotransmitter in the vertebrate peripheral nervous system. Nature 281: 71, 1979
53. Komuro T, Baluk P, Burnstock G: An ultrastructural study of nerve profiles in the myenteric plexus of the rabbit colon. Neuroscience 7: 295, 1982
54. Langley JN, Orbeli LA: Observation on the sympathetic and sacral autonomic system of the frog. J Physiol (London) 41: 450, 1910
55. Langley JN, Orbeli LA: Some observations on the degeneration in the sympathetic and sacral autonomic nervous system of Amphibia. J Physiol (London) 42: 113, 1911
56. Leaming DB, Cauna N: A qualitative and quantitative study of the myenteric plexus in the small intestine of the cat. J Anat 95: 160, 1961
57. Lee IM: The distribution of myelinated nerves in the colon of the dog. Arch Jap Surg 25: 263, 1956
58. Ohkubo K: Studien über das intramurale Nervensystem des Verdauungskanals III. Affe und Mensch. Jap J med Sci Anat 6: 219, 1936b

59. Osborne NN: Do snail neurones contain more than one neurotransmitter? Nature (Lond.) 270: 622, 1977
60. Peters A, Palay SL, Webster HF: The fine structure of the nervous system. Saunders, Philadelphia 1976
61. Rashid S: The nature of the parasympathetic nerve fibers of the stomach of *Rana temporaria*. Arch Int Pharmacodyn 195: 247, 1972
62. Read JB, Burnstock G: Comparative histochemical studies of adrenergic nerves in the enteric plexuses of vertebrate large intestine. Comp Biochem Physiol 27: 505, 1968
63. Read JB, Burnstock G: Adrenergic innervation of the gut musculature in vertebrates. Histochemie 17: 263, 1969
64. Reynolds ES: The use of lead citrate as an electron dense stain in electron microscopy. J Cell Biol 17: 208, 1963
65. Richardson KC: Electron microscopic observation on Auerbach's plexus in the rabbit with special reference to the problem of smooth muscle innervation. Amer J Anat 103: 99, 1958
66. Richardson KC: Electron microscopic identification of autonomic nerve endings. Nature 210: 756, 1966
67. Roberts E, Frankel S: Y-aminobutiric acid in brain. Fed Proc 9: 219, 1950
68. Rogers DC, Burnstock G: Multiaxonical autonomic junctions in intestinal smooth muscle of the toad *(Bufo marinus)* J Comp Neurol 126: 255, 1966
69. Schultzberg M, Hökfelt T, Nilsson G, Terenius L, Rehfeld JF, Brown M, Elde R, Goldstein M, Said S: Distribution of peptide and catecholamine-containing neurons in the gastrointestinal tract of rat and guinea-pig: immunohistochemical studies with antisera to substance P, vasoactive intestinal polipeptide, encephalin, somatostatin, gastrin/cholecystokinin, neurotensin and dopamine B-hydroxylase. Neuroscience 5: 689, 1980
70. Somogyi P, Hodgson AJ, Smith AD, Nunzi MG, Gorio A, Wu JY: Different population of GABAergic neurons in the visual cortex and hippocampus of cat contain somatostatin or cholecystokinin-immunoreactive material. J Neurosci 4: 2590, 1984
71. Sneddon JD, Smithe A, Satchell D, Burnstock G: An investigation of the identity of the transmitter substance released by non-adrenergic, non-cholinergic excitatory nerves supplying the small intestine of some lower vertebrates. Comp Gen Pharmacol 4: 53, 1973
72. Taniyama K, Kusunoki M, Saito N, Tanaka C: GABA evoked ACh release from isolated guinea-pig ileum. Life Sci 32: 2349, 1983
73. Taxi J: Morphology of the autonomic nervous system. In: Frog Neurobiology, Elsevier, New York 1982
74. Thureson-Klein A: Exocytosis from large and small densecored vesicles in noradrenergic nerve terminals. Neuroscience 10: 245, 1983
75. Willard AL, Nishi R: Neuropeptides mark functionally distinguishable cholinergic enteric neurones. Brain Res 422: 163, 1987
76. Wong WC, Sit KH, Ngu KKF, Chin KN: A cholinesterase study of the enteric plexuses in the toad *(Bufo melanosticus)*. Acta Anat (Basel) 80: 82, 1971
77. Zhu PC, Thureson-Klein RL: Exocytosis from large dense-cored vesicles outside the active synaptic zones of terminals within the trigeminal subnucleus caudalis: A possible mechanism for neuropeptide release. Neuroscience 19: 43, 1986

Acta Morphologica Hungarica 37 (1–2), pp. 85–92 (1989)

COMPARATIVE STUDY OF GLIAL FIBRILLARY ACIDIC PROTEIN (GFAP)–IMMUNOREACTIVITY IN THE RAT AND MONKEY CEREBELLUM*

I. Kótai[1], F. Hajós[1], L. Seress[2]

[1]DEPARTMENT OF ANATOMY AND HISTOLOGY, UNIVERSITY OF VETERINARY SCIENCE,
[2]DEPARTMENT OF PHYSIOLOGY, UNIVERSITY MEDICAL SCHOOL, PÉCS, HUNGARY

(Received 28 November 1988)

Vibratome sections of perfusion-fixed rat and monkey cerebella were incubated with an antiserum to glial fibrillary acidic protein (GFAP). Immunolabelled elements showed in both species a principally similar distribution but the presence of long, transverse branches of Bergmann fibres was found to be characteristic to the monkey cerebellum. It is concluded that current methods enable fine interspecies differences of GFAP-localization to be demonstrated. This bears a relevance to the use of GFAP-immunostaining as a diagnostic tool in neuropathology.

Keywords: Glia, GFAP, cerebellum

Introduction

The immunohistochemical demonstration of glial fibrillary acidic protein (GFAP), an integral protein of glial intermediate filaments, shed new light on glial cell populations of the central nervous system [7]. Antibodies to GFAP were shown to decorate, in addition to classical astroglia [2, 4], cell types such as hypothalamic tanycytes, retinal Müller cells, embryonic radial glia and its derivatives, etc. [1, 3, 5, 12]. In view of these findings a broader class of cells has been proposed to be regarded as astroglial having in common GFAP-immunoreactivity as a marker.

Cerebellar Bergmann fibres were among the first described to show GFAP-immunoreactivity [2]. There is ample evidence for regarding this localization of immunostaining as one of the most consistent features of the mammalian cerebellum. Accordingly, many of its aspects have extensively been investigated [6, 10, 15]. Comparative studies are, however, scarce in spite of the fact that recent advance in immunohistochemical methodology enables both qualitative and quantitative analyses to be performed at a finer microscopic resolution than with earlier techniques.

* Supported by the OTKA Foundation (grant No. 1221) of the Hungarian Academy of Sciences

Send offprint request to: I. Kótai, Dept. of Anatomy and Histology, University of Veterinary Science, Budapest POB 2, H-1400, Hungary

In this work we took the advantage of an up-to-date method to demonstrate GFAP-immunoreactivity and to compare its localization in the rat and monkey cerebellum with special regard to the diagnostic value of this staining in neuropathology [9].

Materials and methods

Adult albino rats of either sex and a Rhesus monkey *Macaca mulatta* weighing 5 kg were used in this study.

Animals were transcardially perfused under Nembutal anaesthesia with 4% paraformaldehyde solution in 0.1 M phosphate buffer (PB, Ph 7.4). Cerebella were removed from the skull, and after an overnight fixation in the same fixative and a subsequent 24 h wash in several changes of PB, they were transferred to a vibratome (Campden Instruments). From the upper vermis 50 μm sections were cut and processed for immunohistochemistry.

As a first step of the immunohistochemical procedure, sections were treated with 3% H_2O_2 for 5 min to exhaust endogenous peroxidase activity. Immunostaining was carried out with antiserum to GFAP kindly provided by Dr. Rebecca Pruss (Laboratory of Cell Biology, NIMH Bethesda) and was used in a dilution of 1 : 1500. As second antibody biotinylated anti-rabbit IgG and peroxidase-conjugated avidin-biotin complex (Vectastain) were used. The immune-complex molecule was visualized by the DAB-reaction.

For control, the procedure was performed with preabsorbed antiserum and with the omission of the primary antiserum.

Some immunostained sections were counterstained with haematoxylin to give an orientation of cellular architecture.

Results

In the rat cerebellum, GFAP-immunoreactive Bergmann fibres were seen to span vertically the molecular layer (Fig. 1). Immunostained fibres were arranged in arrays with roughly equally wide territories interposed between the arrays. This regular arrangement resulted in a radially striped overall pattern of the rat molecular layer if looked at with lower magnification. Under the pial surface immunostained fibres had a brush-like terminal portion with secondary branches ending with end-feet under the pia (Fig. 2). Individual fibres had a straight course and apart from their terminal tufts, no major side-branches were encountered (Fig. 3). The number of immunoreactive Bergmann fibres was approximately the same at the convex and concave portions of cerebellar folia.

The cell bodies from where Bergmann fibres originate (Golgi epithelial cells) remained unstained. The surrounding of Purkinje cells was enmeshed by short GFAP-immunoreactive processes (Fig. 3).

In the granular layer (Figs 1, 4), astrocytes showed a marked GFAP-reaction. They appeared to be stellate with several processes and were evenly distributed. Their processes were running without further branching to form a network throughout the granular layer. The white matter of the folia contained irregularly distributed GFAP-stained astrocytes. Many of them were elongated parallel to the course of neighbouring fibre tracts.

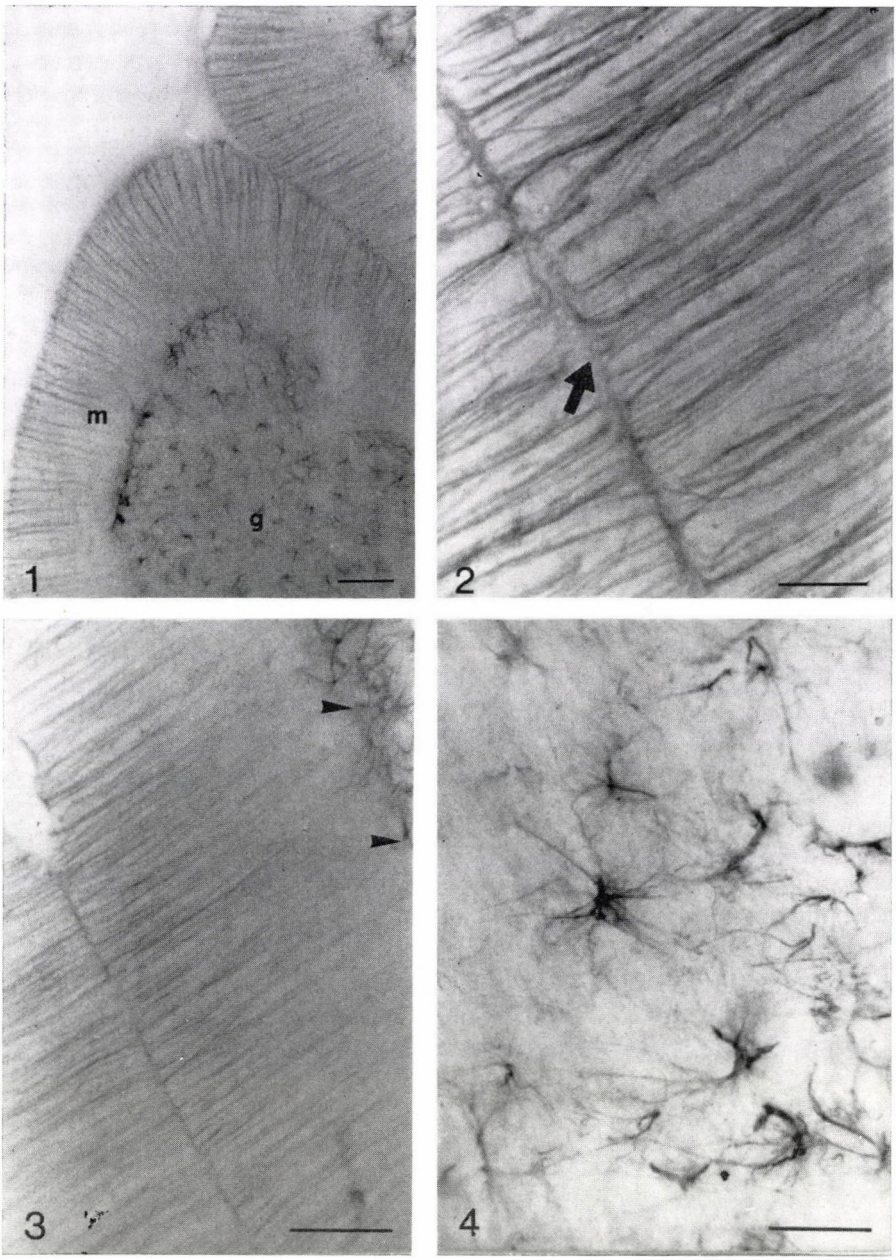

Fig. 1. GFAP-staining of the rat cerebellum. Note the radially striped pattern of immunoreactive Bergmann-fibres of the molecular layer (m) and the evenly scattered astrocytes of the granular layer (g). Bar scale = 100 μm

Fig. 2. Immunostained terminal tufts of Bergmann-fibres of the pial surfaces (arrow) of two neighbouring cerebellar folia. Bar scale = 20 μm

Fig. 3. Pericellular net (arrowhead) around the unstained Purkinje-cell bodies. Bar scale = 100 μm

Fig. 4. Stellate astrocytes in the granular layer. Fine GFAP-positive fibres form a loose network. Bar scale = 50 μm

Evenly distributed stellate astrocytes were seen with the GFAP-reaction in the deep cerebellar nuclei.

The molecular layer of the monkey cerebellum (Fig. 5) showed a less regular GFAP-pattern than that of the rat cerebellum. This was mainly due to the increased and uneven distances between immunoreactive Bergmann fibres running individually and not in arrays. A remarkable feature of the monkey cerebellum was the abundant branching of Bergmann fibres in the lower and middle zone of the molecular layer (Fig. 6). Side branches originated often in a right angle from the main fibre and were running transversely within the layer for considerable distances. Tertiary branches were not observed. The course of the main Bergmann fibres was radial and particularly at the end-portions slightly undulated. Terminal tufts were similar to those observed in the rat molecular layer. It is also noteworthy that some Bergmann fibres did not run up to the pial surface but bended to transverse at various depths of the molecular layer (Fig. 7). The number and packing density of Bergmann fibres was found unaltered when apical and basal portions of folia were compared. Cells of origin of Bergmann fibres were unstained.

The GFAP-positive fibre-meshwork around Purkinje cells was pronounced (Fig. 8). Astrocytes of the monkey granular layer were moderately immunoreactive. Cells appeared to be stellate but having only a few processes. The glial fibre network of the granular layer was less abundant than in the rat.

GFAP-staining in the white matter did not differ from that observed in the rat.

Deep cerebellar nuclei were not included in the tissue sample of the monkey cerebellum we could get hold of.

Sections counterstained with haematoxylin (Figs 9, 10) revealed the relationship of immunostained elements to cell types and layers. From this respect the transverse branches of Bergmann glia were particularly thoroughly studied. Some were seen to be related to blood vessels, while most of them had no special association with cellular elements. They appeared to form club-shaped terminals ending freely in the neuropil of the molecular layer.

Neither the rat nor the monkey cerebellar sections showed any GFAP-staining if incubated with pre-absorbed antiserum or with peroxidase conjugates alone.

Discussion

Studies of GFAP-distribution in the mammalian CNS [11] have shown regional differences not accounted for by the distribution of astrocytes. This implies a selective expression of GFAP immunoreactivity by certain astroglial populations. As GFAP may be present in glial cells both in soluble and filament-bound forms [14] the localization of immunoprecipitate does not neces-

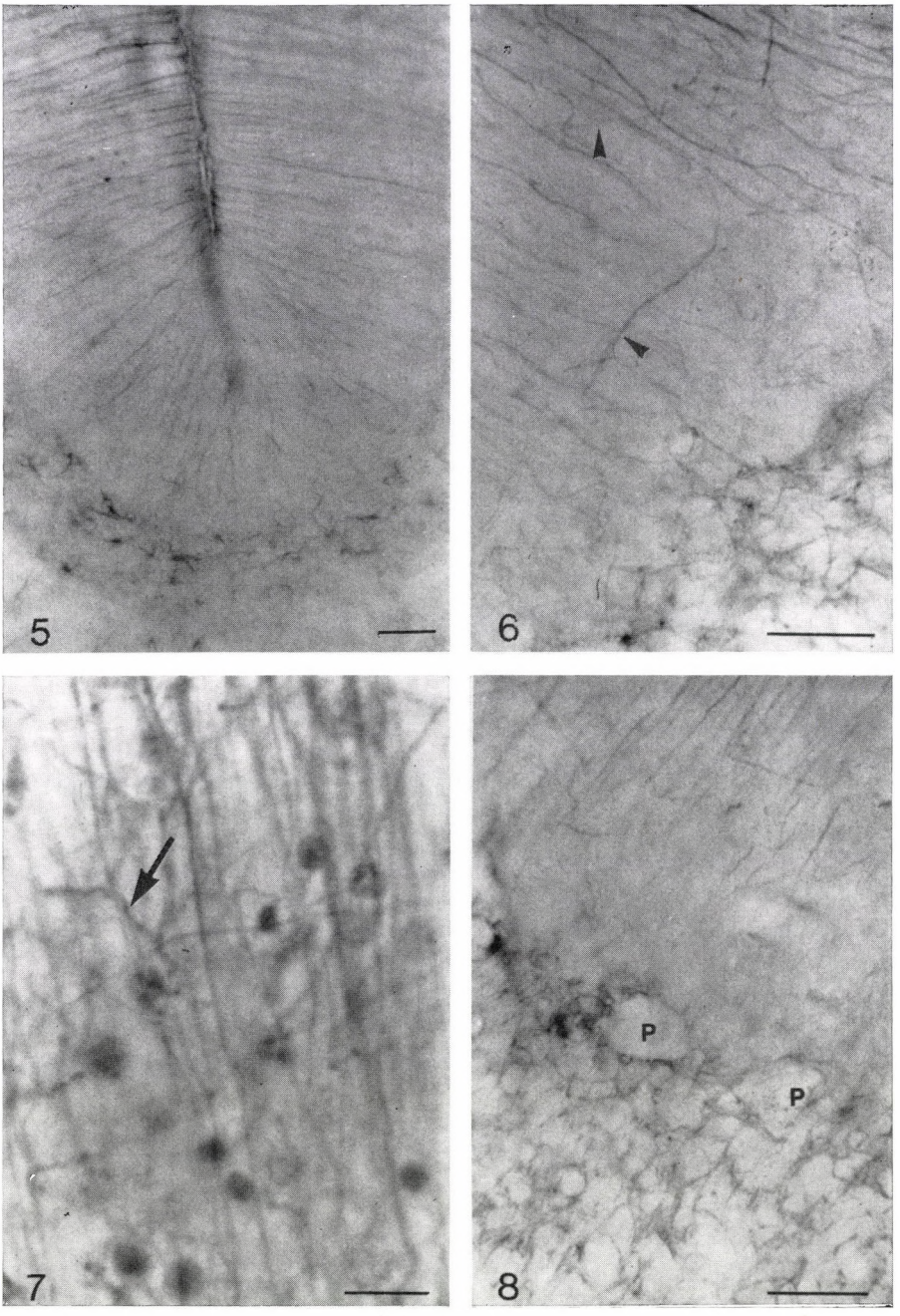

Fig. 5. GFAP-staining in the monkey cerebellum. Immunoreactive Bergmann-fibers are more densely packed at the depth of folia than towards its curvature. Bar scale = 100 μm

Fig. 6. In the monkey cerebellum numerous oblique and transverse side-branches of Bergmann-fibres are to be observed (arrowheads). Bar scale = 100 μm

Fig. 7. Molecular layer of the monkey cerebellar cortex immunostained for GFAP and counterstained with haematoxylin. Some Bergmann-fibres are seen to bend transversely (arrow), while most of them have a perpendicular course. Bar scale = 20 μm

Fig. 8. Pericellular nests of GFAP-positive fibres around the unstained Purkinje-cells (P) of monkey cerebellum. Bar scale = 50 μm

sarily distinguish glia cells according to the state of their GFAP. On the other hand, glial tumours and sites of reactive gliosis [9] are known to contain increased amounts of intermediate filaments owing to which they show a marked GFAP-immunoreactivity. This argues for the primary role of filament-bound GFAP in the immunostaining obtained and explains why glial cell bodies of the intact brain containing much less intermediate filaments than processes, usually do not stain in a well appreciable manner.

The adoption of GFAP immunostaining as a diagnostic tool in neuropathology requires a precise knowledge of reaction patterns in the normal CNS. Data concerning this issue are fragmentary because most studies were carried

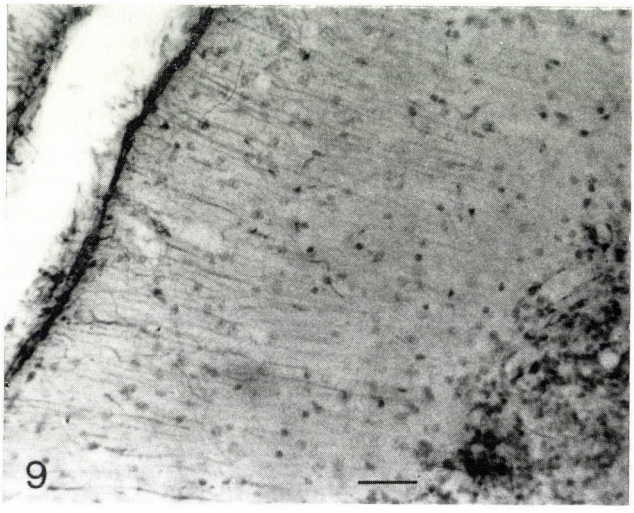

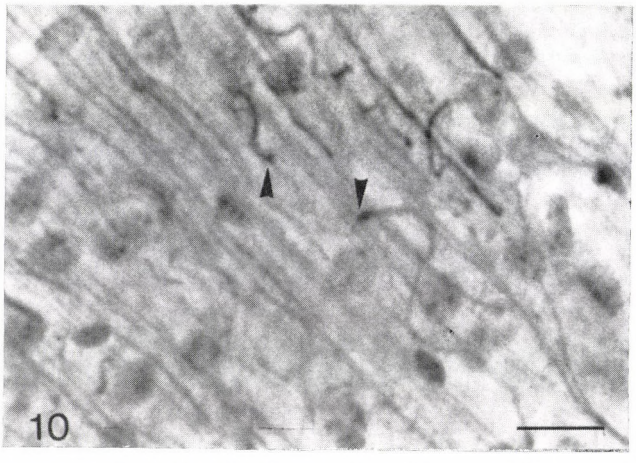

Fig. 9. Survey micrograph of the GFAP-reacted monkey cerebellum counterstained with haematoxylin. Bar scale = 100 μm

Fig. 10. Immunostained Bergmann-fibres of the monkey cerebellum often terminate with club-shaped end-portions (arrowheads) in the molecular layer. Bar scale = 20 μm

out in laboratory rodents, while those performed in the human brain had to rely largely on biopsy and/or autopsy material. However, perfusion fixation appears to be one of the necessary prerequisites of obtaining a specific reaction in a well-preserved structure.

Our present study was intended to provide information as to interspecies differences of GFAP reaction in an area investigated extensively in the rat, i.e. the cerebellum. Observations in the monkey cerebellum suggest that although the basic pattern of immunoreactivity is similar, there are differences worth of notion. First among them the presence of transverse Bergmann glial elements in the monkey but not in the rat has to be mentioned. While vertical Bergmann fibres have been shown to participate in positioning migrating granule cells during cerebellar maturation, the role of transverse elements is unclear. A future better understaining of glial functions in relation to neuronal transmission and metabolism [8, 13, 16] will perhaps help to interpret our immunohistochemical findings.

Another difference between GFAP-distributions in the rat and monkey cerebellum is the less coherent glial network in the monkey than in the rat granular layer. This can be explained by the larger cerebellar glomeruli of the monkey than of the rat since astroglia of the granular layer is mainly constituted by processes surrounding these complex synaptic structures. All other differences observed appear to be due to different geometries of cerebella in the two species.

It is thus concluded that current methods for staining immunoreactive GFAP are sensitive enough to disclose differences in glioarchitectonics of the CNS in different species. With its relevance to the human situation the monkey brain is worth of special attention. Therefore, comparative GFAP studies in the rat and monkey brain concerning further areas such as the cerebral cortex and hippocampus are in progress in our laboratory.

REFERENCES

Bascó E, Woodhams PL, Hajós F, Balázs R: Immunocytochemical demonstration of glial fibrillary acidic protein in mouse tanycytes. Anat Embryol, 162: 217—222, 1981

Bignami A, Dahl D: Differentiation of astrocytes in the pyramidal tracts of the newborn rat: an immunofluorescence study with antibodies to a protein specific to astrocytes. Brain Res 49: 393—402, 1973

Bignami A, Dahl D: Astrocyte-specific protein and radial glia in the cerebral cortex of newborn rat. Nature, 252: 55—56, 1974

Bignami A, Dahl D: Astrocyte-specific protein and neuroglial differentiation: an immunofluorescence study with antibodies to the glial fibrillary acidic protein. J Comp Neurol, 153: 27—38, 1974

Choi B, Lapham L: Radial glia in the human fetal cerebrum: a combined Golgi, immunofluorescent and electron microscopic study. Brain Res, 148: 295—311, 1978

Das GD: Differentiation of Bergmann glia cells in the cerebellum: a Golgi study. Brain Res 110: 199—213, 1976

Eng LF, Vanderhaeghen JJ, Bignami A, Gerstl B: An acidic protein isolated from fibrous astrocytes. Brain Res 28: 351—354, 1971

Fedoroff S, Vernadakis, Y: Astrocytes. Academic Press, New York 1986
Goebel HH, Schlie M, Eng LF: Immunopathologic spectrum of the glial fibrillary acidic protein in neurooncology. Acta Histochemica (Suppl. 5,) XXXIV: 81—93, 1987
Hajós F, Bascó E: The surface-contact glia. Adv Anat Embryol Cell Biol Vol. 84. Springer-Verlag Berlin, Heidelberg, New York, Tokyo 1984
Hajós F, Kálmán M: Distribution of glial fibrillary acidic protein-immunoreactive astrocytes in the rat brain. Exp Brain Res (in press)
Ikeda A, Yoshii I, Mishima N: An immunohistochemical study of the Müller cells of the chicken retina. Arch Histol Jap 2: 175—183, 1980
Kimelberg H: Glial Cell Receptors. Raven Press, New York
Patel AJ, Weiz MD, Hunt A, Tahourdin CSM, Thomas DGT: Distribution of glutamine synthetase and glial fibrillary acidic protein and correlation of glutamine synthetase with glutamate decarboxylase in different regions of the rat central nervous system. Brain Res 331: 1—10, 1985
Rakic P: Neuronal-glial interaction during development. Trends Neurosci, 7: 184—187, 1981
Varon SS, Somjen GG: Neuron-glia interactions. Neurosci Res Prog Bull 17: 1—239, 1979

Acta Morphologica Hungarica 37 (1—2), pp. 93—99 (1989)

EXPERIMENTALLY INDUCED ACUTE CHANGES IN VEINS STUDIED BY SCANNING MICROSCOPY

U. FUCHS[1], H. JELLINEK[2], Anna KÁDÁR[3]

[1]INSTITUTE OF PATHOLOGIC ANATOMY, KARL MARX UNIVERSITY LEIPZIG, GDR,
[2]2ND PATHOLOGIC INSTITUTE SEMMELWEIS MEDICAL ACADEMY, BUDAPEST, HUNGARY AND
[3]2ND CENTRAL DEPARTMENT FOR ELECTRON MICROSCOPY, SEMMELWEIS MEDICAL ACADEMY BUDAPEST, HUNGARY

(Received 8 February 1988)

Endothelial damage caused by hypoxia and the local administration of Varicocid®, or by using vascular clamps on the jugular vein of rabbits, was studied under a scanning electron microscope.

Adhering platelets and fibrin were found only in the acutely damaged veins with endothelial defects. Swelling and vacuolization of endothelial cells did not induce intravascular coagulation.

Adhering thrombocyte aggregates and fibrin strands can be found on the venous wall after acute changes under a scanning microscope only if part or all of the endothelial lining has been lost. Intravascular coagulation is not induced by swelling or vacuolization. The jugular vein of rabbits was studied after hypoxia, the administration of Varicocid® and the use of vascular clamps.

Keywords: Venous wall, acute change, phlebothrombosis, hypoxia, Varicocid®, vascular clamp, scanning electron microscope

Introduction

Under normal conditions, the veins remain free from thrombotic deposits for decades. Different explanations have been given of how phlebothromboses originate (for a survey see Fuchs [5]) either by intravascular or parietal initiation The former case is primarily assumled if the blood is hypercoagulable or ADP is released from a slow or turbulent bloodstream. Damage to the vessel wall caused by hypoxia, trauma, inflammation, and immunological or toxic factors may activate the parietal coagulation system in the veins. Finally, local intravascular coagulation may spread to the veins from microcirculation. Consequently, the endothelial lesions observed are interpreted either as the cause or the effect of a thrombosis. The present study concerns itself with acute damage to the vessel wall as seen under the scanning electron microscope, and with beginning coagulation and the endothelial damage observed.

Send offprint requests to: Doz. Dr. U. Fuchs, Institute of Pathologic Anatomy, Karl Marx University, Liebigstr. 26, DDR 7010 Leipzig

Materials and methods

Bilateral jugular veins were exposed in 9 rabbits and given different treatments. One segment was cut off from circulation for one hour by proximal and distal ligature. This temporary hypoxia was followed by one hour of recirculation (group A). In group B, 1 ml of Varicocid® made by AWD Dresden was injected into the vein which remained clamped off for the time being.

In group C the vessels were squeezed with the aid of a vascular clamp, and the test duration was 2 h for all groups. Two untreated controls were also examined. The vessels were double fixed in glutaraldehyde and OsO_4, subjected to critical point drying and examined with a scanning attachment for the JEM 100 electron microscope.

Results

The normal furrowed relief of the venous wall (Fig. 1 — control) appear less regular after all types of lesions. In a focal pattern, the ridges become wider and higher (Fig. 2a — hypoxia) and show severe local swelling (Fig. 2b — hypoxia). The surface loses its fine markings (Fig. 1) and displays a large number of crater-type cavities from the rupture of intracellular vacuoles during dissection (Fig. 3a — hypoxia). Apart from these smaller phenomena there are also protrusions with large craters (Figs 2b — hypoxia, 3b — Varicocid® administration) apparently due to different degrees of swelling, the rupture of big

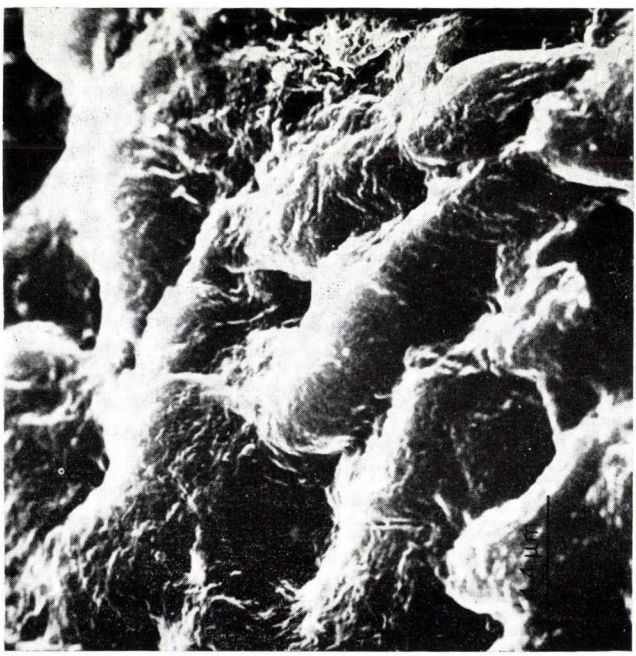

Fig. 1. The normal interio relief of the venous wall (×44 500)

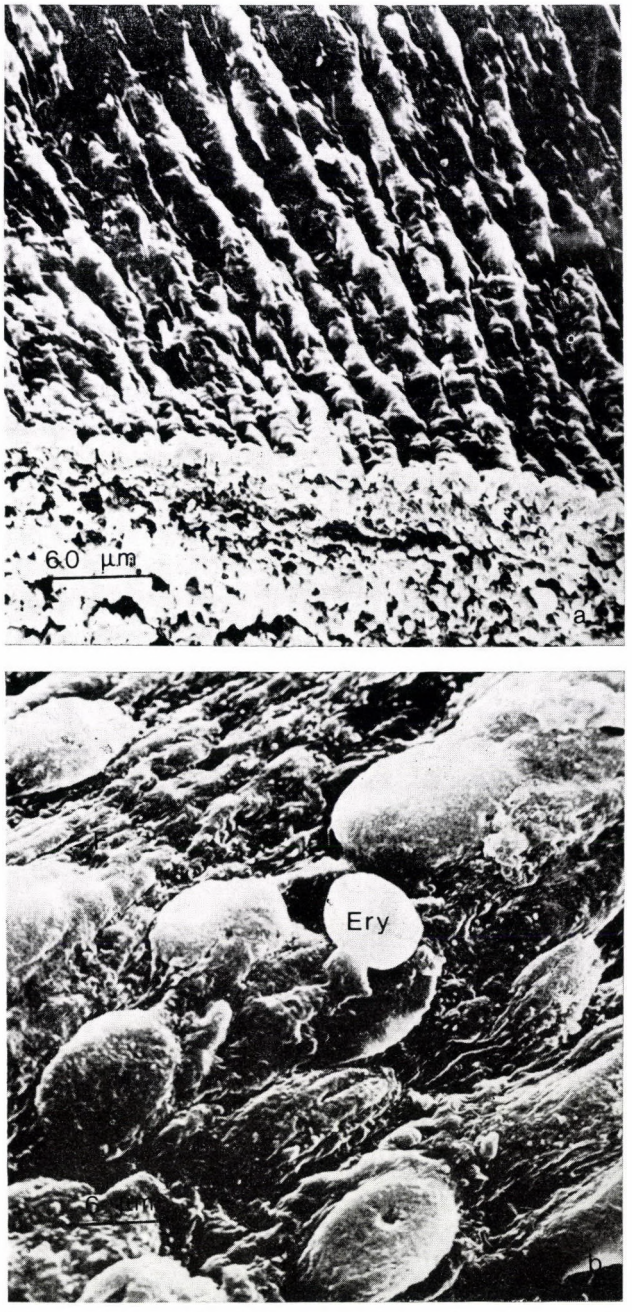

Fig. 2. The upfolded interior relief seen as a top view and in cross section (a) with various degrees of oedematous swelling leading to "ballooning degeneration" of the endothelium (b). D: endothelial defects; Ery: erythrocytes; F: endothelial appendices; a, b: hypoxia (a: ×300, b: ×3 200)

vacuoles and even the loss of nuclei or parts of cells. [3] Over shorter or longer stretches, the endothelia have been lost altogether (Figs 2b — hypoxia. 4a, b — vessel clamping). The remaining endothelial cells extend long appendices (Fig. 2b — hypoxia), which initiate cell migration as the first step in covering the endothelial cell defects. Thrombocytes (Fig. 4b — vessel clamping) and macrophages from the blood become attached to the exposed subendothelium. Finally, fibrin strands (Fig. 4c — vessel clamping, 4d — varix) can be detected between the thrombocytes and other blood cells. Severe endothelial swelling and many craters are regularly found after Varicocid® administration and hypoxia, endothelial defects occur in all examinations, and larger parietal coagulations are common after clamping and Varicocid® administration.

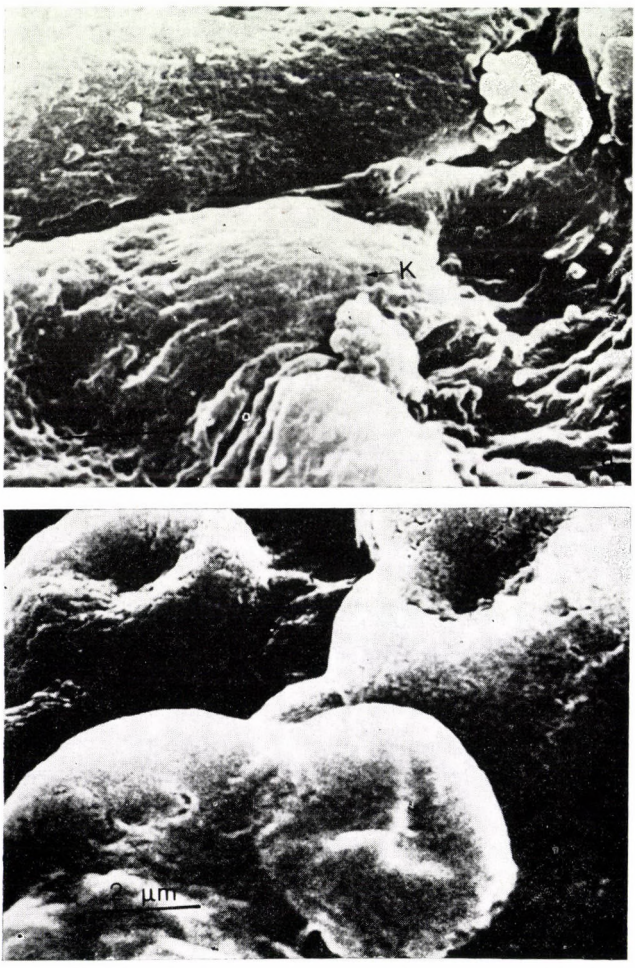

Fig. 3. Small craters (K, Fig. a) and protrusions with large craters (Fig. b). Hypoxia (Fig. a). Varicocid® administration (Fig. b). (a, b: ×10 000)

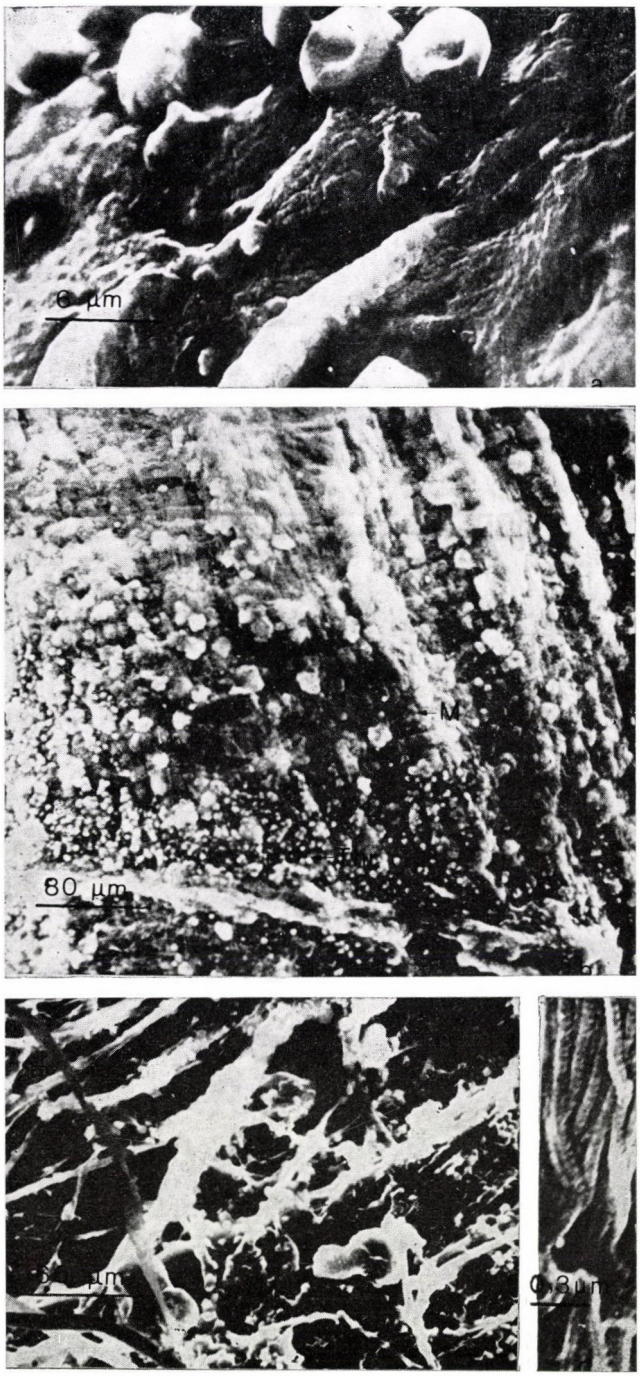

Fig. 4. Endothelial defects (a, b). Attached macrophages (M) and thrombocytes (Thr, Fig. b). Fibrin network with thrombocytes and macrophages (c). For comparison striped fibrin from a human varix (d). Ery: erythrocyte; vessel wall clamping (a, b, c). Human varix (d) (a: ×3 200; b: ×250; c: ×300; d: ×30 000)

Discussion

The relief on the inner surface of arteries [4, 8] and veins, and their pathologic reaction are comparable in view of the similar experimental set-ups outlined in the following. Elemér, Kerényi and Jellinek [1, 2] have all found craters and endothelial losses after one-hour ligature of the abdominal aorta, followed by recirculation over periods from 1 h to 2 days. The surviving endothelial cells attempt to abridge the endothelial defects with appendices. Regeneration sets in after 2 h and, after a severe trauma, may take more than 2 weeks [3]. Where endothelium has been lost, thrombocytes, leucocytes, monocytes and lymphocytes accumulate, but no obstructing thrombi have been reported [2] involving the venous wall.

In our own experiments, and in those conducted on the arteries by Elemér, Kerényi and Jellinek [1, 2], thrombocytes cover the exposed ground substance but not the swollen vacuolized endothelia. Kjeldsen, Astrup and Wanstrup [10], by contrast, have found thrombocytes also on top of damaged cells, as well as arranged in rows and, therefore, probably situated in extended intercellular joints. While obstructing thrombi are not reported for arteries [1, 2], larger parietal coagulations occur in veins after extremely serious lesions. While the endothelium is still there, clotting is inhibited by the high fibrinolytic activity of the venous wall [6] and the production of aggregation inhibiting PgI_2.

The comparable reactivity of veins and arteries is not limited to the acute experiment described here. Arteriosclerotic venopathy occurs in places where the vein is in immediate contact with an affected artery [7, 9], or if it is transplanted by way of operation into the arterial bloodstream subject to arteriosclerosis. During the first 5 years, the cumulative occlusion rate in aortocoronary venous bypass vessels is between 20 and 25%. Occlusion at a very early date is blamed on intravascular clotting, after about a year it is caused by intimal hyperplasia [11]. The fact that veins are less disposed to develop arteriosclerosis than arteries is attributed to their position in the low-pressure system, the greater clearance provided by thinner vessel walls, and their high fibrinolytic and aggregation-inhibiting capacity.

In the present studies thrombosis is caused by coagulation which in turn originates from the exposed subendothelium when defects have occurred in the endothelial complex. The endothelial lesion, then, is the primary event followed by coagulation.

REFERENCES

1. Elemér G, Kerényi T, Jellinek H: Effect of temporary hypoxia on the permeability of the rat aorta. Path Europ 10: 123, 1975
2. Elemér G, Kerényi T, Jellinek H: Scanning and transmission electron microscopic studies on post-ischemic endothelial lesions following recirculation. Atherosclerosis 24: 219, 1976

3. Fonkalsrud EW, Sanchez M, Zerubavel R, Lassaletta L, Smeesters C, Mahoney A: Arteria endothelial changes after ischemia and perfusion. Surg Gynecol Obstet 42: 715, 1976
4. Fuchs U: Das innere Relief der normalen und arteriosklerotischen Aorta im Rasterelektronenmikroskop. Exp Path 7: 45, 1972
5. Fuchs U: Das Kreislaufsystem. In: Holle G. (ed.) Allgemeine Pathologie, Jena: Fischer (in the press)
6. Fuchs U, Graff J: Gefäßwand und Fibrinolyse — Pathologische Aspekte. Fol Haemat 113: 176, 1986
7. Geiringer F: Venous atheroma. Arch Path 48: 410, 1949
8. Jellinek H: Arterial surface changes examined by SEM and TEM. In: GW Manning and MD Haust (eds) Atherosclerosis, Plenum New York 1977 p. 324
9. Kappert A: Lehrbuch und Atlas der Angiologie. Huber Bern, Stuttgart, Wien 1969
10. Kjeldsen K, Astrup P, Wanstrup J: Ultrastructural changes in the rabbit aorta after a moderate carbon monoxide exposure. Atherosclerosis 16: 67, 1972
11. Nienaber CA, Siebes M, Bleifeld W: Perkutane transluminale Angioplastie von koronaren Bypass-Gefässen. Dtsch med Wschr 111: 1469, 1986

Acta Morphologica Hungarica 37 (1—2), pp. 101—109 (1989)

IMMUNE COMPLEX NEPHROPATHIES IN PATIENTS WITH MALIGNANT TUMOURS

L. Kun, Judit Nagy, M. Schmelczer, C. Trinn, T. Burger

2nd DEPARTMENT OF MEDICINE, UNIVERSITY MEDICAL SCHOOL, PÉCS, HUNGARY

(Received 23 March 1988)

The authors have studied the incidence of changes related to immune complex glomerulonephritis in postmortem kidney specimens from 23 patients with malignant tumours (18 solid tumours and 5 leukaemias), using light microscopy and immunofluorescence. As revealed by light microscopy, 4 kidneys had diffuse, 2 focal mesangial proliferative glomerulonephritis and 1 IgA glomerulonephritis.

Granular deposition of immunoglobulin in the mesangium was observed in 5 kidneys, on 3 occasions together with C_3. In only 2 patients were, in addition to glomerular damage, clinical symptoms observed. No CEA and alpha FP were found in the diseased kidneys. The results suggest that glomerular damage with no or only occasional clinical symptoms is not rare in patients with malignant tumours.

Introduction

It has been known for more than fifty years that malignant tumours can lead to renal diseases, most commonly to that known as the paraneoplastic nephrotic syndrome observed in 5—11% of patients with nephrotic syndrome [3, 7, 10, 11, 12, 19, 27, 35]. Haematuria, as a clinical manifestation, can also be found occasionally; however, it is generally associated with proteinuria or the nephrotic syndrome.

Regarding the histological characteristics of the renal changes, in addition to carcinomas, membranous glomerulonephritis (GN) belonging to the GNs of immune complex origin, has most frequently been reported [5, 7, 8, 9, 11, 14, 16]. Minimal changes have been found mainly in patients with Hodgkin's disease, non-Hodgkin lymphomas and leukaemias [8, 9, 17, 21, 22, 29, 34]. IgA GN was observed by Sinniah [30] in mucus-producing adenocarcinoma, and by Mustonen et al [23] in carcinomas of the bronchi, tongue and pancreas as well as in retroperitoneal liposarcoma and nasopharyngeal papilloma.

Various malignant tumours and associated nephropathies have generally produced symptoms simultaneously; however, it was sometimes found that the symptoms of the nephrotic syndrome preceded those of tumours.

Send offprint requests to: Dr. L. Kun, 2nd Dept. of Medicine, University Medical School, Pécs, H-7621, Hungary

Only few data are available concerning the incidence of glomerular lesions with no clinical symptoms in malignancies. The same paucity of data characterizes the frequency of the clinical picture of oligosymptoms, which can be detected only by special examinations [23, 27, 31, 33].

For the present work postmortem kidney specimens from 23 patients with malignant tumours (18 with solid tumours and 5 with leukaemias) were used. In addition to routine light microscopic examination, an immunofluorescence method was used to detect changes related to GN of mainly immune complex origin. Besides antibodies of different subclasses, C_3 and fibrinogen, the presence of carcino-embryonic antigen (CEA) and that of alpha foetoprotein (alpha FP) in the glomeruli were also examined.

Materials and methods

Kidney specimens taken from the autopsies of 18 patients with solid tumours and 5 patients with leukaemias were studied using light microscopy and an immunofluorescence method to search for changes related to the presence of immune complexes and other glomerular abnormalities. The ages of the 12 male and 11 female patients ranged from 6 to 76 years. Among the 18 solid tumours there were 6 gastrointestinal carcinomas, 4 urogenital carcinomas, 2 lung carcinomas, 1 thyroid tumour, 1 gall bladder tumour, 1 cerebral tumour, 1 hypopharyngeal tumour, 1 malignant melanoma, and 1 hepatoma. Out of 5 patients with leukaemias, 3 suffered from acute myeloid leukaemia, 1 from acute lymphoid, and 1 from chronic myeloid leukaemia. To eliminate false-negative and false-positive changes resulting from autolytic processes, only the cases wherein autopsy had been performed within 24 h after death were selected.

The method of examination of the material was the same as that used for kidney biopsies and described in detail elsewhere [24]. In brief: for *light microscopy*, sections were cut from kidney pieces, fixed in formalin, embedded in paraffin, and stained with haematoxylin-eosin, Jones's silver staining and PAS reaction. For *immunofluorescence*, cryostat sections of 4—5 μ thickness were cut from unfixed kidney pieces. After washing in phosphate buffered salive (PBS), they were treated with FITC-labelled anti-human IgG, IgA, IgM, IgE, C_3, fibrinogen/fibrin antisera (Cappel USA; Dakopatts, Denmark; Behring, FRG). In addition, to identify the assumed antigen component of the immune complex GN, sections were examined with rabbit anti-human CEA antibody (Behring, FRG) and, in a second step, with antirabbit immunoglobulin labelled with FITC (Cappel, USA) and other sections were studied for anti-human alpha FP (Behring, FRG) using a direct method. Intensity of the fluorescent stainings was expressed according to a semiquantitative scale as follows: 0 = negativ, +/− = traces, + = small amount, ++ = moderate amount, +++ = large amount. Owing to the increased background staining observed in the postmortem material examined, only the reactions rated as + — +++ were included.

Kidneys from 25 patients who had no tumours and died of diseases other than renal served as controls.

Results

Clinical symptoms and laboratory results

The case histories were studied with the aim of finding data on previous renal diseases. Of the laboratory findings, serum CN, creatinine, urinary protein, pus and sediment were evaluated. No circulating immune complex examinations were made.

In 7 cases out of 23, glomerular abnormalities were observed by light microscopy.

Among the abnormalities involving the mesangium in all cases, a histological picture characteristic of diffuse mesangial proliferative GN was demonstrated by *light microscopy* in 4 kidneys, and in 2 that of the focal form of GN. Proliferation of the mesangial cells and the matrix was generally moderate. In the seventh kidney the diffuse mesangial cell proliferation was accompanied by crescent formation on 47 per cent of the glomeruli. In some of the glomeruli the mesangial proliferation had spread to the portions of the glomerular basement membrane immediately adjacent to the mesangium. However, no tramtrack alterations or thickening of the wall was observed in the peripheral basement membranes (Figs 1, 2).

Immunofluorescent staining revealed granular deposition of immunoglobulins in 5 patients; the same picture was associated with the presence of C_3 in 3 patients, and in 1 with that of fibrinogen. Fibrinogen alone was found in the glomeruli of 2 kidneys. These alterations developed in the mesangium in all cases but one. The relationship between the type of malignancy and the positive immunohistological findings is presented in Table I. Figs 3 and 4 illustrate the immunofluorescent findings.

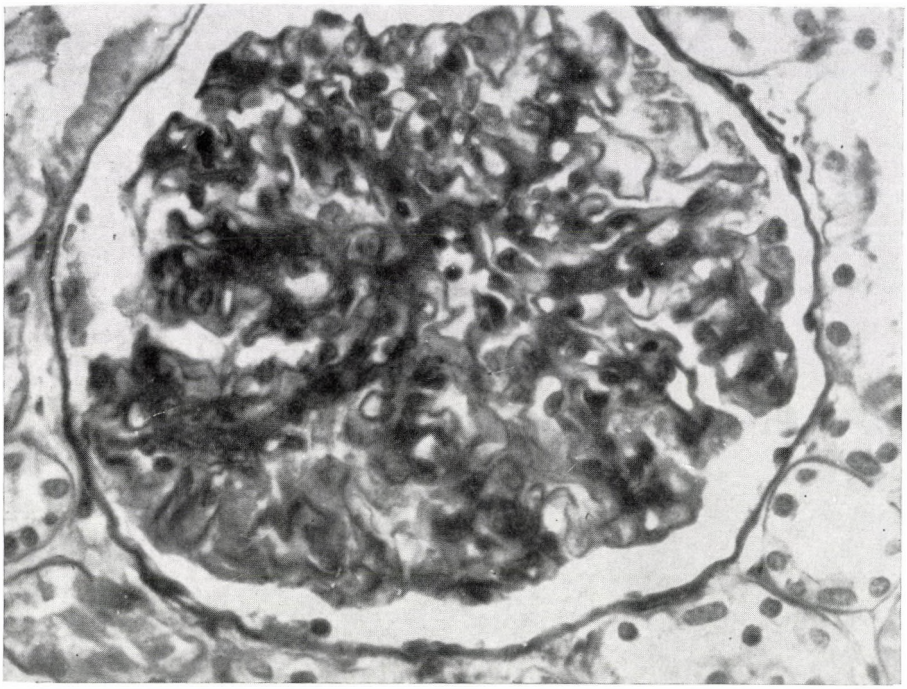

Fig. 1. Various degrees of proliferation of the mesangial matrix and moderate proliferation of the mesangial cells, spreading over almost all segments of glomeruli (PAS, ×250)

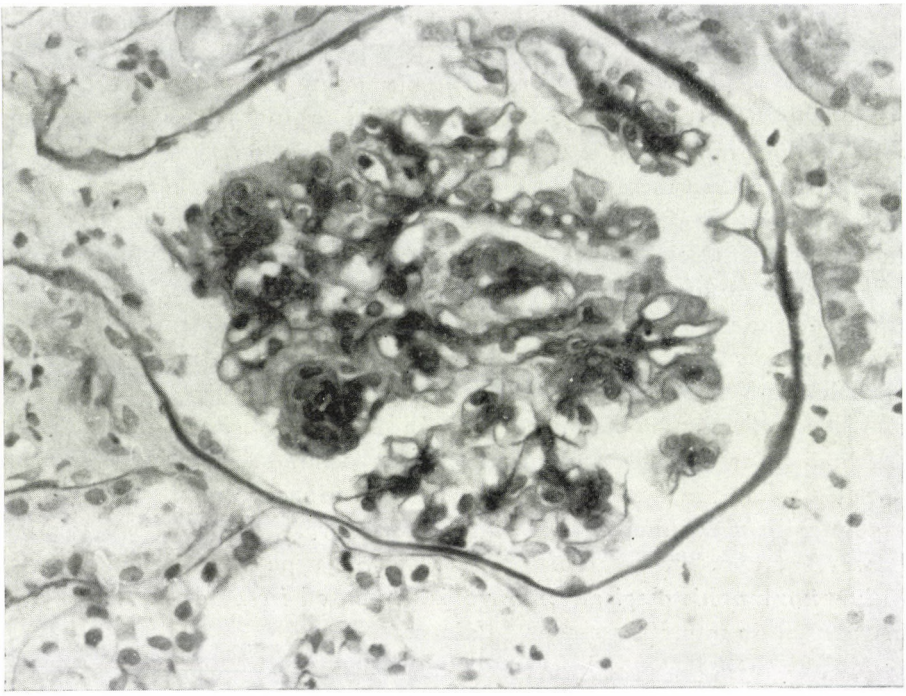

Fig. 2. Focal proliferation of mesangial cells and matrix in glomerulus. Thickness of peripheral glomerular basement membranes is normal (Jones, ×250)

In no single case could CEA and alpha FP be demonstrated in the glomeruli.

Table I

Types of malignancy and immunofluorescent findings

Types of malignancy	Immunofluorescent findings				
	IgG	IgM	IgA	C_3	Fibrinogen/fibrin
Ca of kidney	++	—	++	+++	+++
Ca of colon	—	++	—	++	—
Ca of rectum	—	—	—	—	++
Ca of hypopharynx	+	—	+	—	—
Ca of cholecyst	—	—	—	—	++
Ca of thyroid	++	—	—	—	—
AML	—	++	—	++	—
Total	3	2	2	3	3

AML: acute myeloid leukaemia

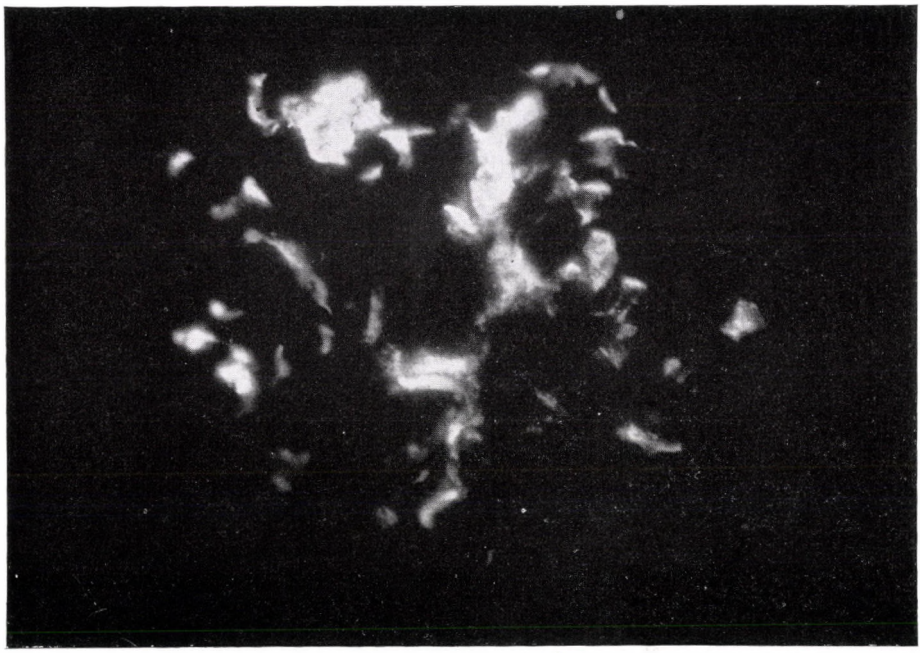

Fig. 3. Large amount of granular deposition of IgA in glomerulus, exclusively in mesangium except for some short portions of glomerular basement membrane (×500)

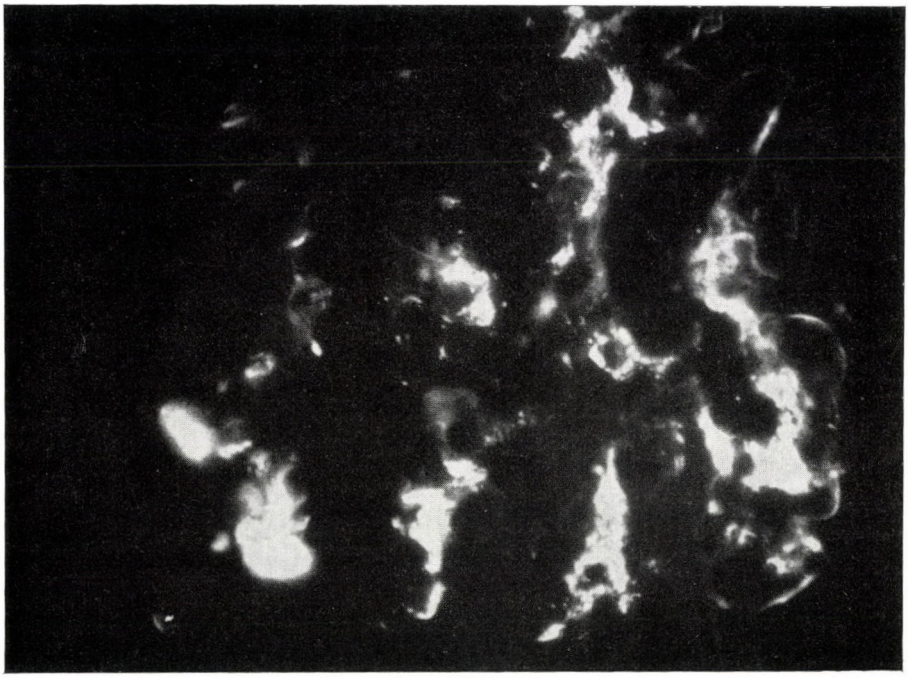

Fig. 4. Granular, partly coalescent deposition of IgM not uniformly distributed in mesangium of glomerulus (×500)

A study of the patients' case histories did not reveal data relevant to any previous renal lesions. The laboratory findings of five patients provided evidence of renal involvement. Apart from the abnormalities observed in urine, histological examinations showed glomerular damage related to the presence of immune complexes in 2 patients only (Table II.). In 1 of the 3 other patients,

Table II

Relationship between histological and clinical findings in glomerular damage related to presence of immune complexes

Immune complex related glomerular damage, histologically:	Clinical manifestation		
	PP	PP + PH	Acute renal failure
Positive (2 patients)	1	0	1
Negative (3 patients)	2	1	0
Total	3	1	1

PP: persistent proteinuria
PH: persistent haematuria

immunofluorescence demonstrated no immunoglobulins, only fibrinogen in addition to focal mesangial proliferation. Chronic pyelonephritis was diagnosed histologically as the cause of the clinical symptoms in the other 2 patients. Resection of a rectal tumour in one patient resulted in the disappearance of his proteinuria, which did not recur even when a second malignant tumour leading to death developed. Histological changes were not accompanied by increased serum CN and creatinine except in the patient dying from acute renal failure.

In the patient with renal carcinoma, IgA GN was diagnosed on the basis of the morphological appearance (light microscopy showed mesangial proliferation of GN with 47% crescent formation; by immunofluorescence, a large amount of C_3 and fibrinogen, and a moderate amount of IgA and IgG deposits in the glomeruli were found).

In none of the 25 control kidneys were changes related to immune complex GN found.

Discussion

Immunoprotein deposition in the glomeruli was observed in 20% of patients with solid tumours by Sinniah [30], and in 1.6% by Sutherland et al [33]; the same authors [33] found immunoprotein deposition in 14.1% of patients with leukaemias, while Davies et al [6] observed no precipitation at all. However, when immunohistological examination was combined with elec-

tron microscopy, involvement of the kidneys was detected in 55% of patients with malignant disease by Pascal et al [27], and in 30% by Helin et al [13].

No electron microscopic examinations were performed in the present study. Immunofluorescence revealed staining of a granular character, related to the presence of immune complexes in 5 out of the 23 kidneys studied. No such staining was found in the 25 controls. Light microscopy provided evidence of glomerular abnormalities in the kidneys of 7 tumour patients; the histological changes characteristic of mesangial proliferative GN were diffuse in 4 of them and focal in 2. One more patient suffered from IgA GN.

There was no membranous GN among our cases. This fact is not surprising, since in the references mentioned in the introduction [5, 7, 8, 9, 11, 14, 16] membranous GN was clinically associated with either nephrotic syndrome or considerably severe proteinuria not yet resulting in nephrotic syndrome, which had generally been recognized during the patient's lifetime. All of our patients but one showed only slight urinary alterations, as in the retrospective study by Pascal et al. [27]. According to the data available to them, the patients of Sutherland et al. [31, 33] were clinically free from symptoms. In a study of a similar character Sinniah [30] did not publish laboratory data.

Based upon our studies and the references detailed above it is doubtless that chiefly in association with solid tumours glomerulopathy accompanied by no or only mild clinical symptoms is not rare.

The depositions which were in all our cases of the granular type, are suggestive of a causal role of antigen-antibody immune complexes. The possible antigens are mainly tumour-associated antigens, re-expressed oncofoetal antigens (e.g. CEA, alpha-FP), oncogenic or other viral antigens and autologous non-tumour antigens (e.g. renal tubular epithelial antigen). Apart from data from animal experiments, few cases are known where the antigen of immune complexes deposited in the kidney was identified in humans. Using antibodies produced against the homogenate of the tumour tissue, Lewis et al. [20] found a tumour associated antigen in the renal glomeruli of patients with bronchogenic carcinoma. Constanza et al. [4] and Couser et al. [5] found CEA in the glomerular immune complexes of membranous GN patients with colonic tumour. Ozawa et al [26] identified renal tubular epithelial antigen-antibody immune complexes in the glomeruli of patients with renal tumours. Regarding the role of virus antigens in humans, there are also only sporadic data available. The virus-associated antigens forming immune complexes must have originated from viruses which presumably had either played a role in tumour formation [25] or caused intercurrent infection [15]. The present study examined the glomerular incidence of CEA and alpha FP in immune complexes assumed in the glomeruli; however, in no case could their presence be demonstrated.

Immune complexes in the circulation were also found in a variable proportion of patients with solid tumours and lymphomas/leukaemias, at the most

in 82% [1]. However, it is unknown in which of these patients were the immune complexes deposited in the glomeruli. It also requires further clarification which state causes renal deposition of immune complexes clinical symptoms.

Some authors also raise the question of whether autopsy material may be suitable for immunohistological examination. Sutherland et al [32] emphasize their observation that in kidneys examined 2—3 h after death, background staining can be so pronounced that it hinders objective evaluation of a specific staining if this is faint. On the other hand, frequent IgA GN have been described [2] in kidneys of patients who died of cirrhosis. These authors consider postmortem material suitable for immunohistological examination. We and others [18, 28] did not experience any difficulty in differentiating between specific and background staining; however, considering the issues mentioned above, we rejected all material showing only minimal positive staining. As controls, postmortem tissue specimens from patients without tumours were also chosen, so that we might assess the "subclinical" immune complex GNs occurring in patients without tumours or clinical renal disease. No such cases were found in our controls comprising a relatively small number of patients.

The relationship between tumours and IgA GN will be dealt with in detail in a separate paper.

Acknowledgements

We thank the Department of Pathology of Pécs University Medical School for the postmortem kidney specimens; Dept. I. of Medicine, Dept. of Paediatrics, Dept. of Neurosurgery, Depts I. and II. of Surgery and Dept. of Urology of Pécs University Medical School for permission to use their clinical records.

REFERENCES

1. Baldwin RW, Price MR: Tumor antigens and tumor-host relationship. Ann Rev Med 27: 151, 1976
2. Callard P, Feldman G, Prandi D, Belair MF, Mandet C, Weiss Y, Druet P, Benhamou JP, Bariety J: Immune complex type glomerulonephritis in cirrhosis of the liver. Am J Pathol 80: 329, 1975
3. Cameron JS, Ogg CS: Neoplastic disease and the nephrotic syndrome. Q J Med 44: 630, 1975
4. Constanza ME, Pinn V, Schwartz RS, Nathanson L: Carcinoembryonic antigen-antibody complexes in a patient with colonic carcinoma and nephrotic syndrome. N Eng J Med 289: 520, 1973
5. Couser WG, Wagenfeld LB, Spargo BH, Lewis EJ: Glomerular deposition of tumor antigen in membranous nephropathy associated with colonic carcinoma. Am J Med 57: 962, 1974
6. Davis S, Marquet E, Rambotti P, Sobel HJ: Electron microscopic and immunohistochemical analysis of glomerular deposits in patients with bronchogenic carcinoma. Ultrastructural Pathol 1: 527, 1980
7. Eagen JW, Lewis EJ: Glomerulopathies of neoplasia. Kidney Internat 11: 297, 1977
8. Editorial: Tumor related renal lesions. Ann Int Med 81: 550, 1974
9. Editorial: Non-renal neoplasms and the kidney. Lancet i: 24, 1975

10. Fer MF, McKinney TD, Richardson RL, Hande KR, Oldham RK, Greco FA: Cancer and the kidney: Renal complications of neoplasms. Am J Med 71: 704, 1981
11. Gagliano RG, Costanzi JJ, Beathard GA, Sarles HE, Bell JD: The nephrotic syndrome associated with neoplasia; an unusual paraneoplastic syndrome. Am J Med 60: 1026, 1976
12. Ghosh L, Muehrcke RC: The nephrotic syndroma: A prodrome to lymphoma. Ann Int Med 72: 379, 1970
13. Helin H, Pasternack A, Hakala T, Penttinen K, Wager O: Glomerular electron-dense deposits and circulating immune complexes in patients with malignant tumours. Clin Nephrol 14: 23, 1980
14. Higgins MR, Randall RE, Still WJS: Nephrotic syndrome with oat-cell carcinoma. Br Med J 3: 450, 1974
15. Hyman LR, Burholder PM, Joo PA, Segar WE: Malignant lymphoma and nephrotic syndrome: A clinicopathologic analysis with light, immunofluorescence and electron microscopy of the renal lesions. J Pediatr 82: 207, 1973
16. Kaplan BS, Klassen MB, Gault MH: Glomerular injury in patients with neoplasia. Ann Rev Med 27: 117, 1976
17. Kiely JM, Wagoner RD, Holley KF: Renal complications of lymphoma. Ann Int Med 71: 117, 1976
18. Lászik Z, Iványi B, Ormos J: Immunofluorescent examination of the kidney postmortem. Histol Histopath 2: 13, 1987
19. Lee JC, Yamauchi H, Hopper J: The association of cancer and the nephrotic syndrome. Ann Int Med 64: 41, 1966
20. Lewis MG, Loughride LW, Phillips TM: Immunological studies in nephrotic syndrome associated with extrarenal malignant disease. Lancet ii: 134, 1971
21. Lowry WS, Munzenrider JE, Lynch GA: Nephrotic syndrome in Hodgkin's disease. Lancet i: 1127, 1971
23. Mustonen J, Pasternack A, Helin H: IgA mesangial nephropathy in neoplastic diseases. Contrib Nephrol 40: 283, 1984
24. Nagy J: A Vesebetegségek Citopatológiája. In: Barta I (ed.), Citopatológia. Medicina, Budapest 1979, p. 387
25. Oldstone MBA, Theofilopoulos AN, Gunven P, Klein G: Immune complexes associated with neoplasia: presence of Epstein—Barr virus antigen-antibody complexes in Burkitt's lymphoma. Intervirology 4: 292, 1974
26. Ozawa T, Pluss R, Lacher J, Boedecker E, Guggenheim S, Hammond W, McIntosh: Endogenous immune complex nephropathy associated with malignancy: I. Studies on the nature and immunopathogenic significance of glomerular bound antigen and antibody and circulating immune complexes. Q J Med 44: 523, 1976
27. Pascal RR, Innaccone PM, Rollwagen FM, Harding TA, Bennet SJ: Electron microscopy and immunofluorescence of glomerular immune complex deposits in cancer patients. Cancer Res 36: 43, 1976
28. Sheibani K, Tubbs RR, Valenzuela R, Deodhar S: Reliability of immunofluorescence of renal tissue obtained at autopsy. Am J Clin Path 72: 222, 1979
29. Sherman RL, Susin M, Waksler ME, Becker EL: Lipoid nephrosis in Hodgkin's disease. Am J Med 52: 699, 1972
30. Sinniah R: Mucin secreting cancer with mesangial IgA deposits. Pathology 14: 303, 1982
31. Sutherland JC, Mardiney MR: Immune complex disease in the kidneys of lymphoma-leukaemia patients: The presence of an oncornovirus-related antigen. JNCI 50: 633, 1973
32. Sutherland JC, Markham RV, Mardiney MR: Subclinical immune complexes in the glomeruli of kidneys postmortem. Am J Med 57: 436, 1974
33. Sutherland JC, Markham RV, Ramsey HE, Mardiney MR: Subclinical immune complex nephritis in patients with Hodgkin's disease. Cancer Res 34: 1179, 1974
34. Szabó T, Erdei I, Szabó J, Szegedi Gy: Hodgkin-betegséghez társult nephrosis syndroma. O. H. 114: 2729, 1973
35. Walker JF: Glomerulopathies of neoplasia. Ir Med J 74: 119, 1981

Acta Morphologica Hungarica 37 (1—2), pp. 111—116 (1989)

CHRONOMORPHOLOGY OF THE DUODENUM IN MAN

A. MARKIEWICZ[1, 2], Anna LELEK[2], Barbara PANZ,[3] J. WAGIEL[4]
H. BOLDYS[2], M. HARTLEB[2], M. KAMIŃSKI[4]

[1]DISTRICT RAILWAY HOSPITAL, KATOWICE, [2]DEPTS OF GASTROENTEROLOGY, [3]ELECTRON MICROSCOPY, [4]HISTOLOGY AND EMBRIOLOGY, SILESIAN SCHOOL OF MEDICINE, KATOWICE, POLAND

(Received 19 May 1988)

The aim of the present study was to investigate the possible existence of rhythmicity of some morphological structures of the jejunum in man. The height of intestinal villi was found to vary significantly during the 24 h time span, being higher during the day than during the night, when the proportion between small and medium size villi changed ($p < 0.05$). The highest mitotic activity was found at 2^{00} and at 6^{00}, and the lowest at 10^{00} and 14^{00} ($p < 0.01$). Both height and width of microvilli did not change during the 24 h span, while thickness of the glycocalyx was slightly higher during the day when compared to the night. There were no significant circadian changes of Paneth cell granularity. We conclude that circadian rhythmicity of jejunum morphology in man is less distinct than in animals, but that significant circadian changes in some parameters do exist.

Introduction

The activities of different digestive enzymes, including those bound to the intestinal brush border, show clear circadian variations, being high at night and low in the daytime in rats fed ad libitum. The circadian rhythm of jejunal function in man and rats might be expected to be out of phase by about half a day because of the nocturnal feeding habits of rats. In previous studies [4, 5] we confirmed this supposition. In addition, a circadian rhythm in the activity of four marker enzymes were found in the lower duodenum in man. All enzymes tested (acid and alkaline phosphatase, 5 nucleotidase, and NADPH) were more active during the waking than resting span.

No structural change in the small bowel morphology was observed in rats sacrificed at different times of the day [1]. On the contrary, Stevenson, et al. [12] reported on the measurement of villous height and the number of columnar cells lining the villus in the jejunum of rats over a 24 h span. They found that both villus height and cell number were 50 to 65% greater just before feeding when compared to their state 12 h later. The authors concluded that these fluctuations might be related to the previously reported peak in jejunal digestive enzyme activity at the feeding time.

Send offprint requests to: Dr. A. Markiewicz, District Railway Hospital, Panewnicka 65, 40-760 Katowice, Poland

The above mentioned data led us to investigate whether the villi, microvilli and glycocalyx of human enterocytes exhibit variability of their morphological structure over the circadian time frame. In addition, the mitotic activity and an estimate of Paneth cell secretory activity were measured in the biopsy specimens.

Materials and methods

i) *Retrospective analysis:* Our earlier reported studies [4, 5] were carried out on 11 healthy men, aged 20—22. We took lower duodenal biopsy specimens with a Crosby—Evans capsule [3] for the measurement of activity of four marker enzymes at 8 h intervals for 2.5 consecutive days, starting at 18^{00} in 4 subjects, at 22^{00} in 5, and at 2^{00} in the last 2. The different starting times for the subjects in the group resulted in data accumulated at every 4 h interval, i.e. each patient was sampled 6 times during the 24 h span. During the sampling period a standard meal was served 7 and a half h before each biopsy. At least 2 sections of each specimen were examined for enzyme activity and photographs of the intestinal villi were taken.

In a retrospective analysis only 154 out of 1300 photos were selected. These photos demonstrated 258 longitudinally sectioned villi, in which the lamina propria were seen reaching the muscularis mucosae and could be measured for villous height (original magnification ×150, Quantimet 700, Cambridge Instruments; [11]. At the same time the mitotic activity in the jejunal crypts was estimated (×400).

ii) *Prospective study:* We repeated the study on another group of 8 healthy men, aged 20—22. The purpose and nature of the study was explained to all participating subjects and all freely gave their consent. Biopsy specimens from lower duodenum were taken according to the above mentioned schedule, i.e. at 6^{00}, 10^{00}, 14^{00}, 18^{00}, 22^{00}, and 2^{00}. At each timing interval at least 2 villi were examined by electron microscopy and photographs of microvilli of enterocytes located on the tips and sides (at 1/2 of the villi) were taken for morphometric analysis (original magnification ×15 000; [11]. We also measured the area occupied by Paneth cell granules in 20 crypts in each biopsy specimen (original magnification ×400, Quantimet 700; [9, 11]).

Results and discussion

As evidenced from the retrospective study (Fig. 1), the height of the villi in man significantly varied during the day, being higher in the day than in the night. This was due primarily to a change in the proportion between the small and medium size villi. However, the day-night differences were not as large as observed in rats [12].

A correlation between enzyme activity and mitotic activity in the human intestinal epithelium was not found. The number of villus cells is the result of cell generation, migration and extrusion. If circadian rhythmicity in both cell generation and removal exists, then the two rhythms should be out of phase with one another. These findings, therefore, are in agreement with those authors who found that mitotic activity of the intestinal epithelium was highest at times of minimum feeding activity. However, the literature is controversial on this issue. Some previous studies [7] have indicated that there is no circadian variation of mitotic activity in the gastrointestinal epithelium. More recent ones [10] demonstrated the presence of a circadian rhythm in both

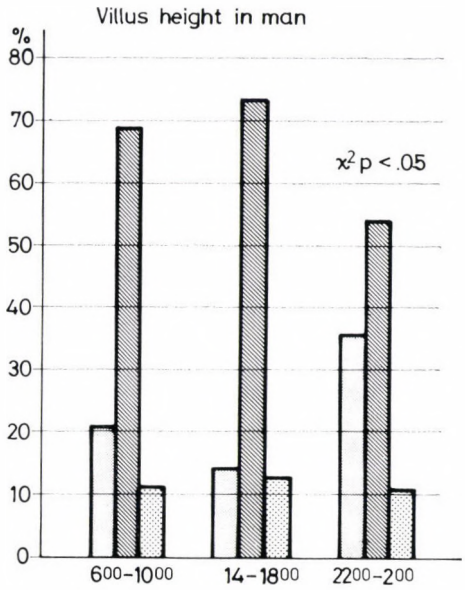

N° of villi	<0.3mm	0.3mm–0.45mm	>0.45mm
M 111	23 20.7%	76 68.5	12 10.8
A 71	10 14.1	52 73.2	9 12.7
N 76	27 35.5	41 53.9	8 10.6

Fig. 1. Percentage distribution of villi sizes (small < 0.3 mm, medium, and high > 0.45 mm) in M (morning), A (afternoon), and N (night) group tested. A retrospective analysis of 154 photos which represented 258 longitudinally sectioned villi, × 150, and could be measured for villous height [5]. Biopsy specimens were taken from the lower duodenum in 11 men

mitotic and DNA synthesizing activities of the rodent gut with peak activity documented at the transition from the dark (active) to the light (rest) phase.

In our material of 11 men, the highest mitotic activity was observed at 2^{00} and 6^{00}, and the lowest at 10^{00} and 14^{00} (*t*-paired test, $p < 0.01$; Fig. 2).

The results of electron microscopic studies are presented in Figs 3—4. Both height and width of microvilli (Fig. 3) did not significantly change over a 24 h time frame. As expected, the only differences were between the height in the tip and side of microvilli, which are usually short and thick or high and slim, respectivily. The glycocalyx thickness was slightly but not significantly higher during the doy than during the night (Fig. 4). These findings seem to be in agreement with the observations of bot higher brush border enzyme activity [5] and enhanced absorption in man [6, 8] at those circadian time stages.

Figure 5 shows that there were no marked changes in Paneth cell secretory granular area during the 24 h time span. It is noteworthy, howerer, that a

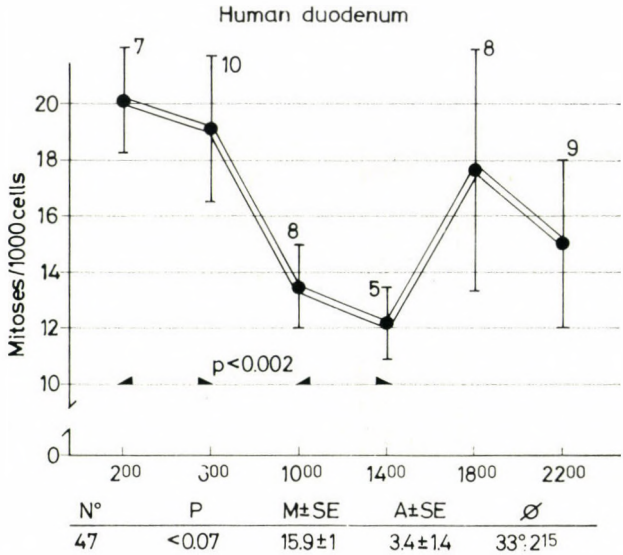

Fig. 2. Chronogram and single cosinor [2] summary of mitosis rhythm in the duodenum of 11 men. M, mesor = computer determined mean value of the rhythm defined by a cosine curve; A, amplitude = one half of the difference between the highest and lowest point in the rhythm defined by a cosine curve, expressed in the same units as the variable analyzed; 0, acrophase = timing of the highest point in the rhythm, hence the peak of the cosine curve expressed in degrees and clock hours

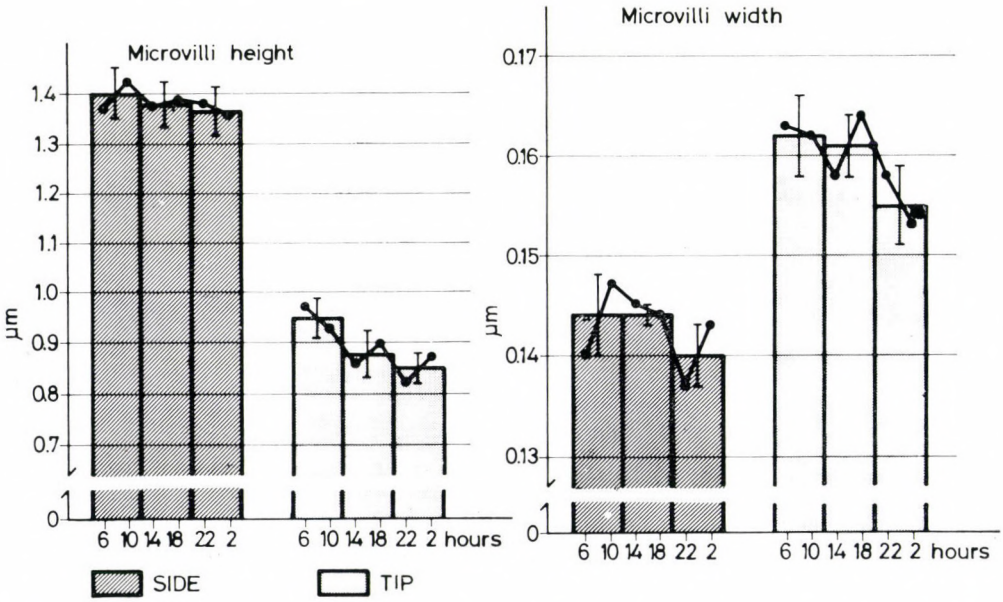

Fig. 3. The 24-h variance of microvilli height and width. Electron micrographs of microvilli of enterocytes located on the tips and sides (at 1/2 of the villi) were taken for morphometric analysis, ×15 000. Biopsy specimens from the lower duodenum in 8 normals

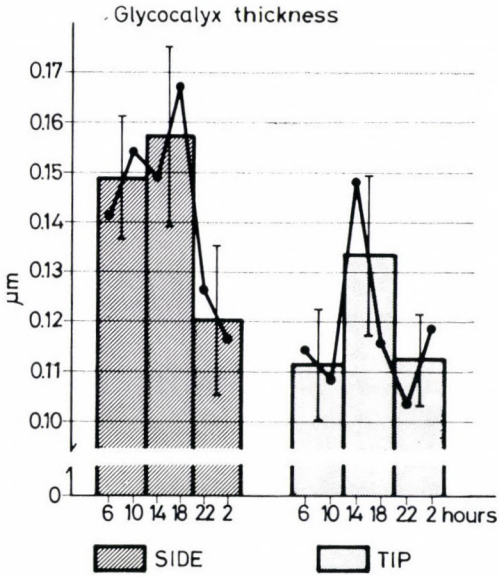

Fig. 4. The 24-h variance of glycocalyx thickness (see Fig. 3)

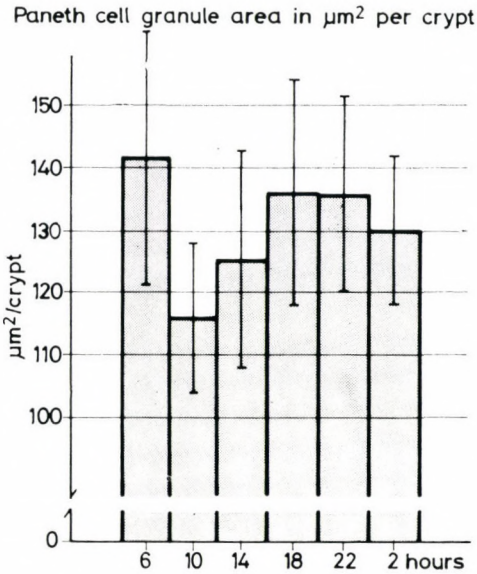

Fig. 5. The 24-h variance of Paneth cell granularity in the lower duodenum of 8 normals. The area occupied by the secretory granules in 20 crypts in each biopsy specimen was measured by a quantimeter, ×400

sligthtly greater area was found at 6^{00} than at 10^{00} and at 14^{00}. The interpretation of increased or decreased Paneth cell function based on estimation of the granular area must be cautiously interpreted because each biopsy specimen was taken 7 and a 1/2 h after a standard meal. This schedule eliminates the possibility of direct estimation of the influence of a meal on Paneth cell granularity. Further studies will be necessary to clarify this point.

Acknowledgements

The authors would like to thank Professor J. G. Moore (Salt Lake City, Utach) for his valuable advice and help in the improvement of the manuscript.

REFERENCES

1. Becciolini A, Romano S, Porciani S, Buricchi L, Benucci A, Casati V: Circadian rhythms of some enzymes in the small intestine of rat. In: Halberg F (ed.) XIII International Conference I.S.C. Pavia 1977 Proceedings, Il Ponte, Milano 1981, p. 11
2. Cornelissen G, Halberg F, Stebbings J, Halberg E, Carandente F, Hsi B: Chronobiometry with pocket calculators and computer systems. 10: 333, 1980
3. Evans N, Farrow LJ, Harding A, Stewart JS: New techniques for speeding small intestinal biopsy. Gut 11: 88, 1970
4. Markiewicz A, Kamiński M, Tarquini B, Halberg F: Circadian rhythm of enzymatic activity in human jejunum (Abstr.). Notiziario S I Bio C 5: 849, 1981
5. Markiewicz A, Kamiński, Chociłowski W, Gomoluch T, Bołdys H, Skrzypek B: Circadian rhythms of four marker enzymes activity of the jejunal villi in man. Acta Histochem 72: 91, 1983
6. Markievicz A: Pharmacokinetic data have rhythms: are they important? Pol J Pharmacol Pharm 36: 27, 1984
7. Pilgrim C, Erb W, Maurer W: Diurnal fluctuations in the numbers of DNA synthesizing nuclei in various mouse tissues. Nature 199: 863, 1963
8. Reinberg A, Smolensky MH: Circadian changes of drug disposition in man. Clin Pharmacol 7: 401, 1982
9. Satoch Y: Ultrastructure of Paneth cells in germ-free rats, with special reference to the secretory granules and lysosomes. Arch Histol Jap 47: 293, 1984
10. Sigdestad CP, Bauman J, Lesher SW: Diurnal fluctuations in the number of cells in mitosis and DNA synthesis in the jejunum of the mouse. Exp Cell Res 58: 159, 1969
11. Slavin G, Sowter C, Robertson K, McDermott S, Paton K: Measurement in jejunal biopsies by computer-aided microscopy. J Clin Pathol 33: 254, 1980
12. Stevenson NR, Day SE, Sitren H: Circadian rhythmicity in rat intestinal villus length and cell number. Internat J Chronobiol 6: 1, 1979

Acta Morphologica Hungarica 37 (1–2), pp. 117–124 (1989)

S-100 PROTEIN IMMUNOREACTIVITY IN HUMAN ISLETS OF LANGERHANS

Z. LÁSZIK,[1] T. KRENÁCS[1], E. DOBÓ[2]

[1]DEPARTMENT OF PATHOLOGY, [2]CENTRAL RESEARCH LABORATORY, ALBERT SZENT-GYÖRGYI MEDICAL UNIVERSITY, SZEGED, HUNGARY

(Received 20 October 1988)

S-100 protein-containing cells were demonstrated by immunogold silver staining in human islets of Langerhans from patients with chronic pancreatitis (CP) with (n = = 6) (Group I) or without (n = 6) (Group II) diabetes mellitus, (DM) and from non-diabetic, non-pancreatic controls (n = 6) (Group III). In all three groups S-100 protein containing cells were observed in all islets of Langerhans throughout the pancreas. Quantitative analysis of cell composition of islets did not reveal significant differences in S-100 protein cell content between the three groups. When double immunohistochemical staining was used to demonstrate different endocrine cell types (insulin, glucagon and pancreatic polypeptide) and S-100 protein immunoreactive cells, the latter proved to be a distinct cell type. Somatostatin-producing cells and S-100 protein-containing cells were usually also present as two distinct cell populations, but positive staining for both S-100 protein and somatostatin was occasionally observed within the same cells.

Keywords: S-100 protein, endocrine pancreas

Introduction

During the past decade, a wealth of immunohistochemical data has been reported on the cell composition of human islets of Langerhans, relating to both normal and pathological conditions [1, 14, 16, 20, 25, 27]. Besides the four main endocrine cell types (B, A, D, and PP cells), D_1 [2, 4], C [13] and P cells [2] have been described as occurring rarely in human islets. Although certain investigators have postulated the presence of gastrin cells in human islets [8, 12], it is generally agreed that they do not contain gastrin cells [20]. In this study, we have demonstrated the presence of S-100 protein in some human pancreatic islet cells, by applying immunogold silver staining (IGSS) [15]. Additionally, the nature of this cell type was characterized by double labelling, using IGSS for S-100 protein and immunoperoxidase techniques for various islet cell hormones.

Send offprint requests to: Dr. Z. Lászik, Departm. of Pathology, Albert Szent-Györgyi Medical University, H-6701, POB 401, Szeged, Hungary

Materials and methods

Tissues preparation

Surgical specimens of the pancreases removed from 12 patients with CP and 6 pancreases from autopsy cases were investigated. Six of the 12 chronic pancreatitic patients (Group I) had subclinical DM, while another 6 patients (Group II) had manifest DM. Autopsy cases (Group III) had suffered neither from CP nor from DM. Pancreatic tissue pieces of 1 cm^3 were either frozen in liquid nitrogen and cut by cryostat, or were fixed in 4% neutral buffered formalin and paraffin-embedded according to routine histological procedures. From both frozen and paraffin-embedded material, consecutive sections of 5 μm thickness were cut for immunohistochemistry. Before immunostaining, some of the frozen sections were treated with 100% ammonium sulphate at 37 °C for 2 h, after 4% buffered neutral formalin fixation for 15 min to remove S-100 protein selectively.

Immunohistochemical reagents

Rabbit antisera against glucagon, somatostatin, bovine S-100 protein, as well as guinea-pig anti-insulin, swine anti-rabbit immunoglobulin, and peroxidase-rabbit-antiperoxidase (PAP) complex were obtained from Dakopatts (Glostrup, Denmark), and rabbit anti-pancreatic polypeptide from BioGenex Laboratories (Dublin, CA, USA). Immunogold conjugate for the detection of rabbit immunoglobulin was prepared as follows: Rabbit immunoglobulin G (IgG) was purified by chromatography on a DEAE-Sephadex A-50 (Pharmacia, Uppsala, Sweden) column according to the method of Levy and Sober [21]. Purified antibodies mixed with Freund's complete adjuvant was administered to male Wistar rats every second week for two months. Specific anti-rabbit IgG was obtained from sera of rats by purification through an AcA-22 gel-glutaraldehyde-rabbit IgG column, followed by fractionated elution with 0.1 M glycine-hydrochloric acid buffer (pH 2.3), and a glycine-hydrochloric acid and dioxanes (9 : 1) solution, respectively. The most avid anti-immunoglobulin fractions collected in the second stage of the elution were conjugated with colloidal gold by the method of De Mey et al. [6]. 5 μm diameter gold particles were prepared by reduction with phosphorus according to Zsigmondy [32].

Immunohistochemistry

The sections were stained with the immunogold-silver staining (IGSS) method of Holgeta et al. [15] for S-100 protein, with the unlabelled PAP method of Sternberger et al. [29] for glucagon, somatostatin and pancreatic polypeptide, and with the indirect immunoperoxidase (IPO) method for insulin. Double immunolabelling procedures were carried out with sequential use for IGSS method for S-100 protein, and the PAP or IPO method for one of the other antigens. In IGSS, the physical silver development was performed according to the original paper of Danscher [3], except that silver nitrate was used instead of silver lactate and gum arabic was omitted. Peroxidase was visualized with 3-amino-9-ethylcarbazole (AEC) according to the prescription of Graham et al. [11]: 0.02% AEC with 0.015% H_2O_2 in acetate buffer (50 mM) pH 5.0.

Controls

Negative control sections were treated with non-immune rabbit serum instead of specific antibody in each immunostaining procedure. Physical silver development was carried out on untreated pancreas sections as well.

Quantification

Quantitative determination of the S-100 protein positive cell content was performed through counting of the nuclei of the S-100 protein positive and negative cells in 10 islets in each patients. The mean number of S-100 protein positive cells in the three groups was then used to calculate the percentage occupied by S-100 protein positive cells. Quantitative measurements were compared via analysis of variance (ANOVA).

Results

Figure 1 illustrates S-100 protein-positivity in pancreatic nerves and also in islets of Langerhans. The ovoid or polyglonal S-100 protein-positive cells are scattered throughout the islets. The immunoreactive product is located in both the cytoplasm and the nucleus. The S-100 protein-containing cells are found in most of the islets in different parts of the pancreata. The number of S-100 protein immunoreactive cells varied from one islet to another (0—14.5%); its mean percentage lay in the range 3.01—9.59% in the individual cases. Significant differences were not observed between the three groups (Table I).

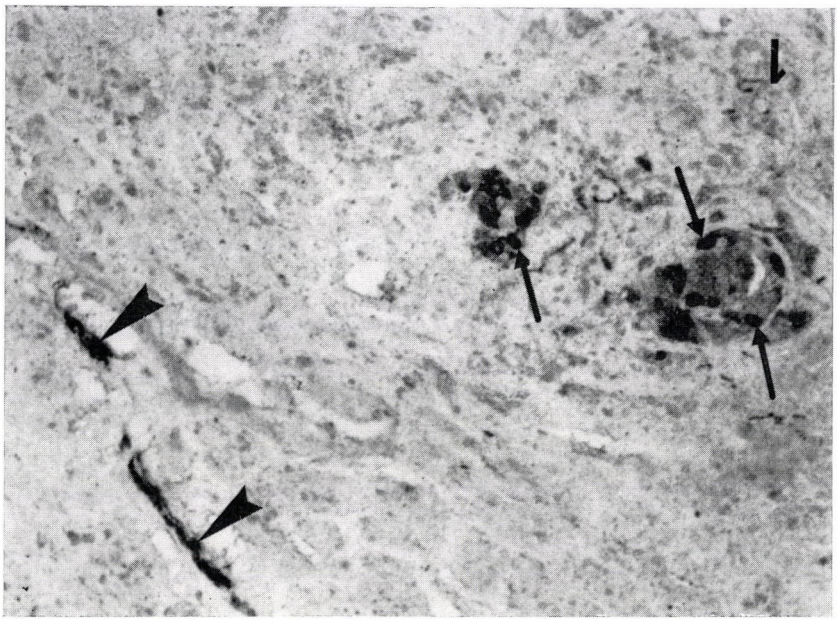

Fig. 1. S-100 protein staining in nerves (arrowheads) and in some cells of Langerhans islets (arrows). Immunogold-silver staining technique. Original magnification ×220

Double immunohistochemical staining with antibodies to S-100 protein and various islet cell hormones (insulin, glucagon and pancreatic polypeptide) showed distinct positivities (Fig. 2a-c). There was no cross-reaction between different endocrine and S-100 protein-containing cells. The somatostatin-producing cells and S-100 protein-positive cells usually comprised two distinct cell populations, but in some cells positive staining for both S-100 protein and somatostatin could be seen. If one of the frozen sections was treated with 100% ammonium sulphate before immunostaining, only somatostatin-positivity could be detected, whereas staining for both somatostatin and S-100 protein

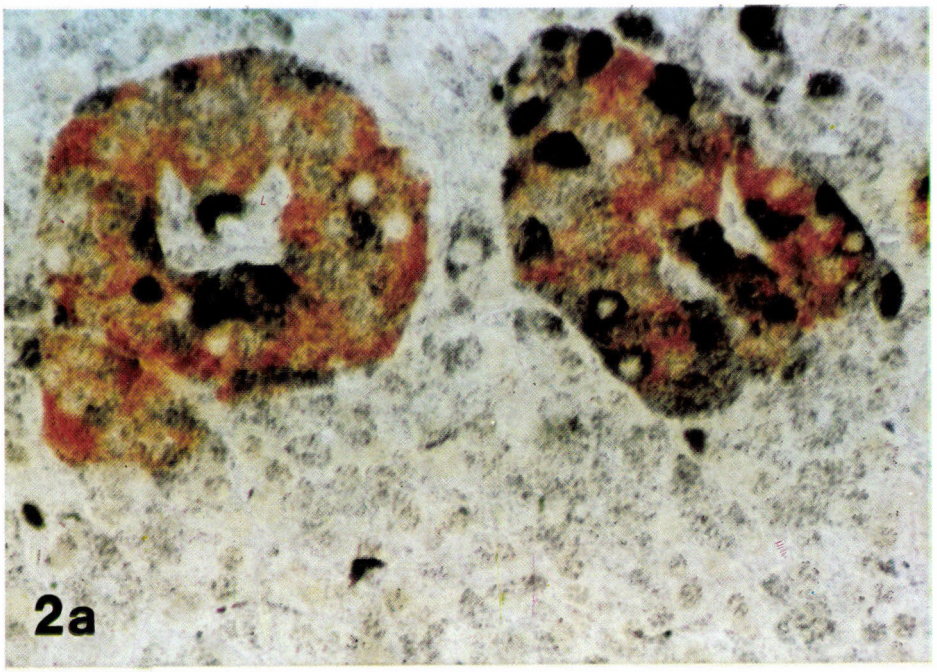
2a

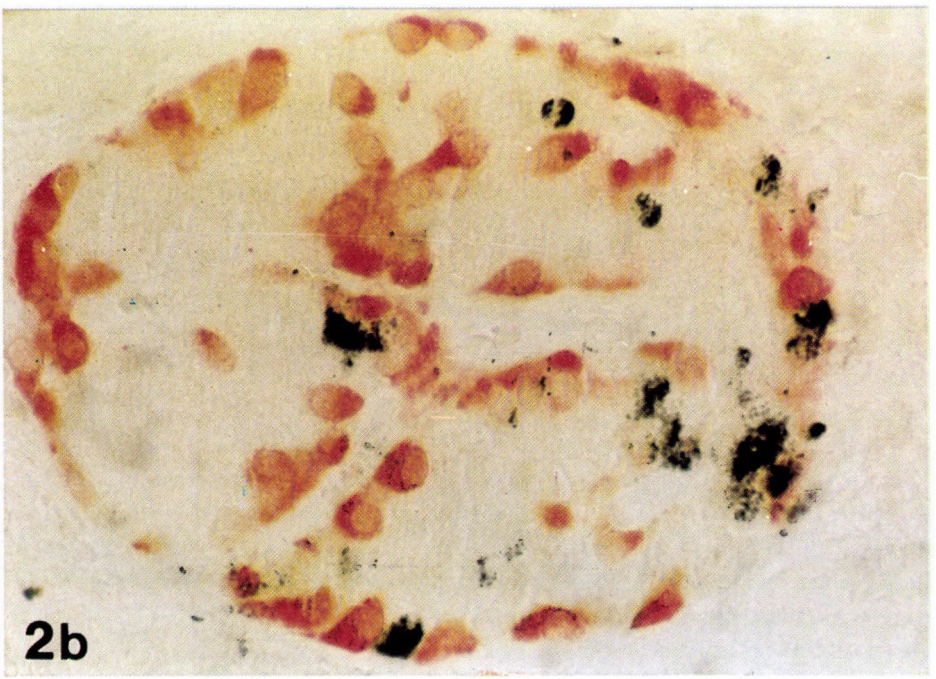
2b

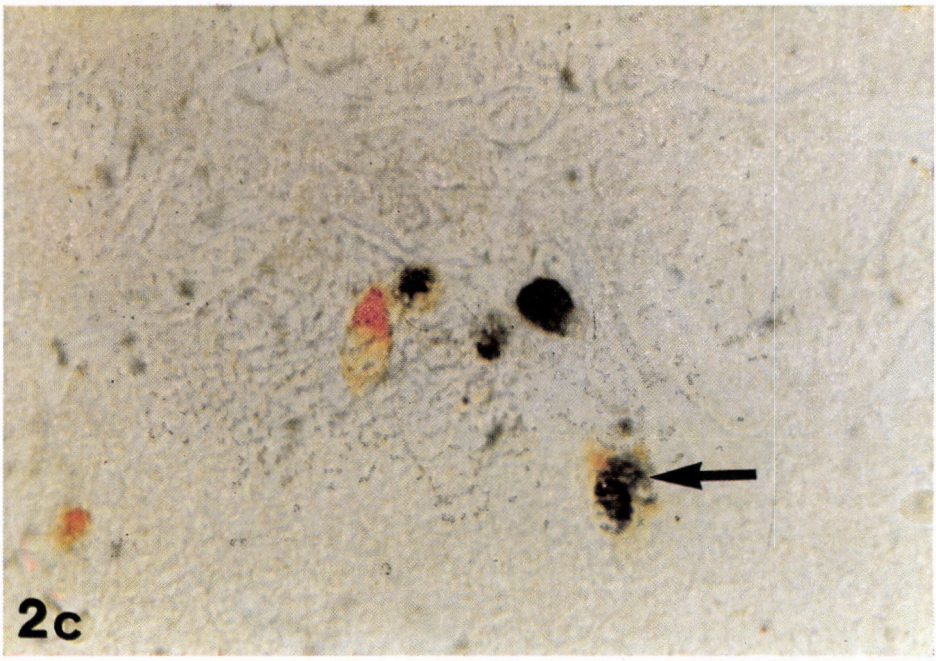

Fig. 2. Sections of pancreas double stained with antibodies (a) to insulin and S-100 protein, (b) to glucagon and S-100 protein, and (c) to somatostatin and S-100 protein. Arrow indicates double staining in one cell. Indirect peroxidase or peroxidase-antiperoxidase and immunogold-silver staining technique. Black colour indicates S-100 protein positivities. Original magnifications (a—b) ×560; (c) ×720

Table I

Data of quantitative analysis. Number of S-100 protein positive cells (% of total) in islets of Langerhans

Case No.	Controls	Chronic pancreatitic diabetic patients	Chronic pancreatitic non-diabetic patients
1.	4.41±2.78	7.30±2.85	5.08±3.83
2.	4.35±2.55	6.96±5.36	6.61±5.30
3.	5.19±3.71	9.31±4.74	5.65±4.53
4.	3.81±2.61	4.84±2.82	8.26±2.63
5.	4.14±2.06	9.59±4.04	5.94±3.19
6.	4.37±3.31	3.01±2.63	3.13±2.29
Average	4.37±2.83[a]	6.83±3.74[b]	5.77±2.94[c]

[a, b, c] There is no significant difference ($P > 0.05$) using analysis of variance

in the same cell was found in an adjacent section that had not been treated for S-100 protein removal. This selective removal of S-100 protein from the sections was possible only in frozen material. A few of the nerves also exhibited double staining (weak somatostatin and stronger S-100 protein-positivity).

Discussion

The cell compositions of human pancreatic islets in normal and pathological conditions have been reported previously [1, 14, 16, 19, 25, 27] and will merely be reviewed briefly here. In human islets, there are four main endocrine cells (insulin, glucagon, somatostatin and pancreatic polypeptide), with more rarely occurring D_1, C and P cells. To our knowledge, occurrence of S-100 protein-containing cells in human pancreatic islets has not been mentioned in the literature, with the exception of a brief report by Vanstapel et al. [31], who described scattered S-100 protein-positivity without any comment. However, Girod et al. [10] have recently detected S-100 protein-containing cells in the islets of *Macaca irus* monkeys. In our present study, by means of light microscopic immunocytochemistry we have demonstrated the occurrence of S-100 protein-containing cells in human islets of Langerhans. Our results indicate that S-100 protein-containing cells represent a distinct cell type in human islets of Langerhans. S-100 protein is not an antigen specific for a particular tissue, since it has been demonstrated in a variety of normal and pathological conditions [7, 9, 17, 18, 22, 23, 24, 26, 28, 30, 31]. The function of S-100 protein-containing cells in the islets of Langerhans is unclear. Their number in the islets of diabetic and non-diabetic chronic pancreatitic patients was the same as in healthy pancreata (non-diabetic non-pancreatitic patients). Accordingly, it seems that they do not play a role in the pathogenesis of diabetes mellitus in chronic pancreatitis.

Girod et al. [10] have suggested that S-100 protein-positive cells in monkeys might be identical with the C cells observed by Grube and Bohn [13] in guinea pig, rat and man. In the latter study C cells did not show immunostaining with any of the pancreatic hormones. However, our results also indicate that there is a „subpopulation" of somatostatin-producing cells which also contain S-100 protein. The simultaneous occurrence of somatostatin and S-100 protein has never been mentioned within somatostatin-producing cells. The functional sisgnificance of this situation is unknown; it is also an open question as to whether the occurrence of S-100 protein within some of the somatostatin-producing cells is permanent or transitional. In the latter case it might reflect a functional state, while in the former it could indicate a real subpopulation of somatostatin-producing cells.

REFERENCES

1. Abdul-Karim FW, Dahms BB, Velasco ME, Rodman HM: Islets of Langerhans in adolescents and adults with cystic fibrosis: A quantitative study. Arch Pathol Lab Med 110: 602, 1986
2. Capella C, Solcia E, Friferio B, Buffa R, Usellini L, Fontana P: The endocrine cells of the pancreas and related tumours. Ultrastructural study and classification. Virchow's Arch (A) 373: 327, 1977

3. Danscher G: Localization of gold in biological tissue. A photochemical method for light and electron microscopy. Histochemistry 71: 81, 1981
4. Deconinck JF, Potvliege PR, Gepts W: The ultrastructure of the human pancreatic islets of adults. Diabetologia 7: 266, 1971
5. Deconinck JF, van Assche FA, Potvliege PR, Gepts W: The ultrastructure of the pancreatic islets. II. The islets of neonates. Diabetologia 8: 326, 1972
6. De Mey JR: The preparation of immunoglobulin gold conjugates (IGS reagents) and their use as markers for light and electron microscopic immunocytochemistry. In: Cuello AC, (ed.) Immuno Histochemistry. IBRD Handbook Series: Methods in Neurosciences, Wiley and Sons, Chicester 1983, p. 347
7. Egan MJ, Newman J, Crocker J, Collard M, Birmingham E: Immunohistochemical localization of S-100 protein in benign and malignant conditions of the breast. Arch Pathol Lab Med 111: 28, 1987
8. Erlandsen SL, Hegre OD, Parsons JA, McEvoy RC, Elde RP: Pancreatic islet cell hormones distribution of cell types in the islet and evidence for the presence of somatostatin and gastrin within the D cell. J Histochem Cytochem 24: 883, 1976
9. Girod C, Trouillas J, Dubois MP: Immunocytochemical localization of S-100 protein in stellate cells (folliculostellate cells) of the anterior lobe of the normal human pituitary. Cell Tissue Res 241: 505, 1985
10. Girod C, Durand N, Raccurt M: Immunostaining of a cell type in the islets of Langerhans of the monkey *Macaca irus* by antibodies against S-100 protein. Cell Tissue Res 247: 11, 1987
11. Graham RC, Lundholm U, Karnovsky MJ: Cytochemical demonstration of peroxidase activity with 3-amino-9-ethylcarbazole. J Histochem Cytochem 13: 150, 1965
12. Greider MH, McGuigan JE: Cellular localization of gastrin in the human pancreas. Diabetes 20: 389, 1971
13. Grube D, Bohn R: The microanatomy of human islets of Langerhans, with special reference to somatostatin (D-) cells. Arch Histol Jap 46: 327, 1983
14. Hara M, Tsutsumi Y: Immunohistochemical studies of endocrine cells in heterotopic pancreas. Virchow's Arch (A) 408: 435, 1986
15. Holgate CS, Jackson P, Cowen PN, Bird CC: Immunogold-silver staining: New method of immunostaining with enhanced sensitivity. J Histochem 31: 938, 1983
16. Ianucci A, Mukai K, Johnson D, Burke B: Endocrine pancreas in cystic fibrosis: An immunohistochemical study. Hum Pathol 15: 278, 1984
17. Jundt G, Schulz A, Paul E, Cochran AJ, Herschman HR: S-100 protein in amelanotic melanoma. Path Res Pract 181: 37, 1986
18. Kahn HJ, Marks A, Thom H, Baumal R: Role of antibody to S-100 protein in diagnostic pathology. Am J Clin Pathol 79: 341, 1983
19. Klöppel G, Bommer G, Commandeur G, Heitz P: The endocrine pancreas in chronic pancreatitis. Immunocytochemical and ultrastructural studies. Virchow's Arch (A) 377: 157, 1978
20. Klöppel G. Lenzen S: Anatomy and physiology of the endocrine pancreas. In: Klöppel G, Heitz PU (eds), Pancreatic Pathology. Churchill Livingstone, Edinburgh London Melbourne and New York 1984, p. 133
21. Levy HB, Sober HA: A simple chromatographic methods for preparation of gammaglobulin. Proc Soc Exp Biol 103: 250, 1960
22. Nakajima T, Sato Y, Watanabe S, Shimosato Y, Ishihara K, Isobe T: Immunoelectron microscopical demonstration of S-100 protein in epidermal Langerhans cells. Biomed Res 3: 266, 1982
23. Nakajima T, Watanabe S, Sato Y, Kameya T, Hirota T, Shimosato Y: An immunoperoxidase study of S-100 protein distribution in normal and neoplastic tissues. Am J Surg Pathol 6: 715, 1982
24. Nakamura Y, Becker LE, Marks A: S-100 protein in tumors of cartilage and bone. Cancer 52: 1820, 1983
25. Pelletier G: Identification of four cell types in the human endocrine pancreas by immunoelectron microscopy. Diabetes 26: 749, 1977
26. Santa Cruz D, Clark B, Hartman BK, Moore BW: S-100 protein — an immunohistochemical marker for neural tumors and tumor-like conditions of the skin. Arch Dermatol 118: 951, 1982
27. Stefan Y, Orci L, Malaisse-Lagae F, Perrelet A, Patel Y, Unger RH: Quantitation of endocrine cell content in the pancreas of nondiabetic and diabetic humans. Diabetes 31: 694, 1982

28. Stefansson K, Wollmann R, Jerhovic M: S-100 protein in soft tissue tumours derived from Schwann cells and melanocytes. Am J Pathol 106: 261, 1982
29. Sternberger LA, Hardy PH Jr, Cuculis JJ, Meyer HG: The unlabelled antibody enzyme method of immunohistochemistry. Preparation and properties of soluble antigen-antibody complex (horseradish peroxidase-antiperoxidase) and its use in identification of spirochetes. J Histochem 18: 315, 1970
30. Takahashi K, Isobe T, Ohtsuki Y, Akagi T, Sonobe H, Okuyama T: Immunohistochemical study on the distribution and subunits of S-100 protein in human neoplasm and normal tissue. Virchow's Arch (B) 45: 385, 1984
31. Vanstapel MJ, Gatter KC, DeWolf-Peeters C, Mason DY, Desmet VD: New sites of human S-100 immunoreactivity detected with monoclonal antibodies. Am J Clin Pathol 85: 160, 1986
32. Zsigmondy R: Zur Enkenntnis der Kolloide. Gustav Fischer, Jena, 1905

ANNOUNCEMENT

FIRST INTERNATIONAL CONGRESS ON VERY ULTRA LOW DOSAGE

Bordeaux, FRANCE, September 20–22, 1990

Further inquiries: Prof. Ch. Doutremepuich, Haematology Laboratory,
Faculty of Pharmacy,
3, Place de la Victoire
33076 Bordeaux, France

PRINTED IN HUNGARY

Akadémiai Kiadó és Nyomda Vállalat, Budapest

INSTRUCTIONS TO AUTHORS

Form of manuscript

Contributors are requested to supply two complete copies of the manuscript including all tables and illustrations. Manuscripts should be typed double-spaced with margins of at least 4 cm. Pages should be numbered consecutively.

The *headline* should include the title of the paper, authors' names, and name and short postal address of the institute where the work was done.

An *abstract* of not more than 200 words should be supplied typed before the text. It should briefly describe the purpose of the investigations, the methods utilized, the results obtained, and the authors' principal conclusions.

Abbreviations and symbols

Abbreviations should be spelled out when first used in the text or, alternatively, a list of abbreviations might be given. The *International System of Units (SI)* should be used for all measurements. Symbols for physical quantities are to be printed in italics and should, therefore, be underlined in the manuscript. Unusual symbols should be identified on the margin.

References

References should be numbered in alphabetical order, and these numbers only should be inserted in the text (in parentheses). In the reference list each item should include the names and initials of all authors; the title of the article; the title of the journal abbreviates according to the style used in *Index Medicus* (a list of the journals indexed is printed annually in the January issue); the volume number; the first page number; and the year of publication.

Kaplan AP, Kay AB, Austen KF: A pre-albumin activator of prekallikrein. J Exp Med 135:81, 1972

Titles of books should be followed by the publisher; place of publication; and the year.

Oláh I, Röhlich P, Törő I: Ultrastructure of Lymphoid Organs. Akadémiai Kiadó, Budapest 1975

Halász B: The endocrine effects of isolation of the hypothalamus from the rest of the brain. In: Frontiers in Neuroendocrinology, eds Ganong WF, Martini L, Oxford University Press, Oxford 1969, p. 307

Tables and illustrations

Tables should be comprehensible to the reader without reference to the text. The headings should be typed above the table. Tables should be numbered with Roman and illustrations with Arabic numerals.

Figures should be identified by number and authors' name written lightly in pencil on the back. The top should be indicated on the back of prints. The letters a, b etc. should be placed in the lower left-hand corner of prints. Staining techniques and the original magnification of photomicrographs should be stated. Figure captions should be typed on a separate sheet. The approximate place of figures and tables in the text should be indicated in the manuscript on the left-hand margin.

Proofs and reprints

Reprints and proofs will be sent to the first author unless otherwise indicated. A hundred reprints of each paper will be supplied free of charge.

Periodicals of the Hungarian Academy of Sciences are obtainable at the following addresses:

AUSTRALIA
C.B.D. LIBRARY AND SUBSCRIPTION SERVICE
Box 4886, G.P.O., *Sydney N.S.W. 2001*
COSMOS BOOKSHOP, 145 Ackland Street
St. Kilda (Melbourne), Victoria 3182

AUSTRIA
GLOBUS, Höchstädtplatz 3, *1206 Wien XX*

BELGIUM
OFFICE INTERNATIONAL DES PERIODIQUES
Avenue Louise, 485, *1050 Bruxelles*
E. STORY-SCIENTIA P.V.B.A.
P. van Duyseplein 8, *9000 Gent*

BULGARIA
HEMUS, Bulvar Ruszki 6, *Sofia*

CANADA
PANNONIA BOOKS, P.O. Box 1017
Postal Station "B", *Toronto, Ont. M5T 2T8*

CHINA
CNPICOR, Periodical Department, P.O. Box 50
Peking

CZECHOSLOVAKIA
MAD'ARSKA KULTURA, Národni třida 22
115 66 Praha
PNS DOVOZ TISKU, Vinohradská 46, *Praha 2*
PNS DOVOZ TLAČE, *Bratislava 2*

DENMARK
EJNAR MUNKSGAARD, 35, Nørre Søgade
1370 Copenhagen K

FEDERAL REPUBLIC OF GERMANY
KUNST UND WISSEN ERICH BIEBER
Postfach 46, *7000 Stuttgart 1*

FINLAND
AKATEEMINEN KIRJAKAUPPA, P.O. Box 128
00101 Helsinki 10

FRANCE
DAWSON-FRANCE S.A., B.P. 40, *91121 Palaiseau*
OFFICE INTERNATIONAL DE DOCUMENTATION ET LIBRAIRIE, 48 rue Gay-Lussac
75240 Paris, Cedex 05

GERMAN DEMOCRATIC REPUBLIC
HAUS DER UNGARISCHEN KULTUR
Karl Liebknecht-Straße 9, *DDR-102 Berlin*

GREAT BRITAIN
BLACKWELL'S PERIODICALS DIVISION
Hythe Bridge Street, *Oxford OX1 2ET*
BUMPUS, HALDANE AND MAXWELL LTD.
Cowper Works, *Olney, Bucks MK46 4BN*
COLLET'S HOLDINGS LTD., Denington Estate,
Wellingborough, Northants NN8 2QT
WM DAWSON AND SONS LTD., Cannon House
Folkstone, Kent CT19 5EE
H. K. LEWIS AND CO., 136 Gower Street
London WC1E 6BS

GREECE
KOSTARAKIS BROTHERS INTERNATIONAL BOOKSELLERS, 2 Hippokratous Street, *Athens-143*

HOLLAND
FAXON EUROPE, P.O. Box 167
1000 AD Amsterdam
MARTINUS NIJHOFF B. V.
Lange Voorhout 9-11, *Den Haag*
SWETS SUBSCRIPTION SERVICE
P.O. Box 830, 2160 Sz Lisse

INDIA
ALLIED PUBLISHING PVT. LTD.
750 Mount Road, *Madras 600002*
CENTRAL NEWS AGENCY PVT. LTD.
Connaught Circus, *New Delhi 110001*
INTERNATIONAL BOOK HOUSE PVT. LTD.
Madame Cama Road, *Bombay 400039*

ITALY
D. E. A., Via Lima 28, *00198 Roma*
INTERSCIENTIA, Via Mazzé 28, *10149 Torino*
LIBRERIA COMMISSIONARIA SANSONI
Via Lamarmora 45, *50121 Firenze*
SANTO VANASIA, Via M. Macchi 58
20124 Milano

JAPAN
KINOKUNIYA COMPANY LTD.
Journal Department, P.O. Box 55
Chitose, *Tokyo 156*
MARUZEN COMPANY LTD., Book Department
P.O. Box 5050 Tokyo International, *Tokyo 100-31*
NAUKA LTD., Import Department
2-30-19 Minami Ikebukuro, Toshima-ku, *Tokyo 171*

KOREA
CHULPANMUL, *Phenjan*

NORWAY
TANUM-TIDSKRIFT-SENTRALEN A.S.
Karl Johansgata 43, *1000 Oslo*

POLAND
WĘGIERSKI INSTYTUT KULTURY
Marszalkowska 80, *00-517 Warszawa*
CKP I W, ul. Towarowa 28, *00-958 Warszawa*

ROUMANIA
D. E. P., *Bucuresti*
ILEXIM, Calea Grivitei 64–66, *Bucuresti*

SOVIET UNION
SOYUZPECHAT — IMPORT, *Moscow*
and the post offices in each town
MEZHDUNARODNAYA KNIGA, *Moscow G-200*

SPAIN
DIAZ DE SANTOS Lagasca 95, *Madrid 6*

SWEDEN
ESSELTE TIDSKRIFTSCENTRALEN
Box 62, *101 20 Stockholm*

SWITZERLAND
KARGER LIBRI AG, Petersgraben 31, *4011 Basel*

USA
EBSCO SUBSCRIPTION SERVICES
P.O. Box 1943, *Birmingham, Alabama 35201*
F. W. FAXON COMPANY, INC.
15 Southwest Park, *Westwood Mass. 02090*
MAJOR SCIENTIFIC SUBSCRIPTIONS
1851 Diplomat, P.O. Box 819074,
Pallas, Tx. 75381-9074
READ-MORE PUBLICATIONS, INC.
140 Cedar Street, *New York, N. Y. 10006*

YUGOSLAVIA
JUGOSLOVENSKA KNJIGA, Terazije 27, *Beograd*
FORUM, Vojvode Mišića 1, *21000 Novi Sad*

Index: 26.017

Acta Morphologica Hungarica

VOLUME 37, NUMBERS 3–4, 1989

EDITOR-IN-CHIEF
K. LAPIS

COPY-EDITOR
ERZSÉBET L. JUHÁSZ

EDITORIAL BOARD
I. TÖRŐ (Chairman), E. BEREGI, B. CSILLIK, P. ENDES, B. HALÁSZ, H. JELLINEK, GY. RAPPAY, GY. ROMHÁNYI, P. RÖHLICH, E. SOMOGYI, J. SUGÁR, GY. SZÉKELY, J. SZENTÁGOTHAI, I. TARISKA

Akadémiai Kiadó, Budapest
ACTA MORPH. HUNG. HU ISSN 0236—5391

ACTA MORPHOLOGICA
HUNGARICA

A QUARTERLY OF THE HUNGARIAN ACADEMY OF SCIENCES

Acta Morphologica publishes original papers on experimental morphology and pathology in English.

Acta Morphologica is published in yearly volumes of four issues by

AKADÉMIAI KIADÓ
Publishing House of the Hungarian Academy of Sciences
H-1117 Budapest, Prielle K. u. 19—35.

Manuscripts and editorial correspondence should be addressed to

Acta Morphologica
Ist Institute of Pathology and Experimental Cancer Research, Semmelweis Medical University,
1085 Budapest, Üllői út 26, Hungary

Subscription information

Orders should be addressed to

KULTURA Foreign Trading Company
H-1389 Budapest P.O. Box 149

or to its representatives abroad

Acta Morphologica Hungarica is abstracted/indexed in Biological Abstracts, Chemical Abstracts, Chemie-Information, Current Contents–Life Sciences, Excerpta Medica, database (EMBASE), Gerontological Abstracts, Index Medicus

---

© *Akadémiai Kiadó, Budapest*

CONTENTS

Normal and experimental morphology

Endocervical cytology: characterization of the cells by image analyzer. *Veronika Tóth, M. Bodó, Gy. Lehoczky, B. Molnár, J. Sugár* 125

Alteration of the submandibular glands of female mice during pregnancy and lactation. A histological, histometric and histochemic study. *J. A. Rossi, L. C. Bruschi* 135

GAP junction between human T-colony cells. *T. Neumark, D. C. Huynh* 147

Analyses of the tidemark on human femoral heads. I. Histochemical, ultrastructural and microanalytic characterization of the normal structure of the intercartilaginous junction. *R. Oettmeier, K. Abendroth, Sabine Oettmeier* 155

Analyses of the tidemark on human femoral heads. II. Tidemark changes in osteoarthrosis — A histological and histomorphometric study in non-decalcified preparations. *R. Oettmeier, K. Abendroth, Sabine Oettmeier* 169

Morphology of supravital brain slices pre-incubated in a physiological solution prior to fixation *F. Hajós, J. Garthwaite, G. Garthwaite, A. Csillag* 181

Pathology

Cadmium influence on the rat liver. *M. Vojtíšek, D. Hulínská, D. Bitternová, M. Cikrt, V. Hulínský* 201

Ultrastructure of the Ito cells in liver disease associated with fibrosis. *I. Bartók, Sz. Virágh, Cs. Hegedűs, Katalin Bartók* 219

Renal complications in mutiple myeloma. *B. Iványi* 235

Antifreeze (ethylene glycol) intoxications in Baltimore. Report of six cases. *F. Introna, J. A. Smialek* 245

Haemophagocytic sinus histiocytosis with massive lymphadenopathy: Early lesions, progression and involution. *G. Kelényi, L. Olasz* 265

Acta Morphologica Hungarica 37 (3—4), pp. 125—133 (1989)

ENDOCERVICAL CYTOLOGY: CHARACTERIZATION OF THE CELLS BY IMAGE ANALYZER

VERONIKA TÓTH[1], M. BODÓ[1], GY. LEHOCZKY[2], B. MOLNÁR[3], J. SUGÁR[3]

[1]DEPARTMENT OF CYTOPATHOLOGY, [2]DEPARTMENT OF GYNECOLOGY,[3] DEPARTMENT OF PATHOLOGY NATIONAL ONCOLOGICAL INSTITUTE, BUDAPEST, HUNGARY

(Received 20 October 1988)

Authors report on 359 patient's endocervical smears taken by cytobrush. Stormby's endocervical brush did not cause bleeding disturbance or preventing colposcopic examination. The smears contained numerous, well evaluable squamous and endocervical cells. Out of seven cytologically positive cases three proved to be negative by colposcopy. Histology, however, confirmed the cytological diagnosis. Cytology was followed by histology in 42 cases. Cytological and histological diagnoses were compared, there was one false negative.

For the more precise characterization of endocervical cells 13 features were measured by a Robotron type image analyzer and the results were statistically analyzed. The respective cell groups can be separated from each other by morphometric and densitometric parameters.

Results of this study have produced a data base that can be extended further on. It may give help in case of differential diagnostic problems since it is capable of distinguishing certain cell groups, consequently these data can be incorporated into a diagnostic program.

Keywords: Cytobrush, reserve cell hyperplasia, image analysis

Introduction

Recently the incidence of cervical squamous cancer is decreasing in contrast to adenocarcinomas that show relatively increasing tendency [7]. Colposcopy, in combination with cytology, plays an important role in the detection of premalignant and malignant ectocervical lesions but it cannot yield sufficient information about processes localized to the endocervical region [9]. It has been proved that adequate sampling technique is of crucial importance in the detection of endocervical dysplasias, in situ adenocarcinomas and early microinvasive and invasive carcinomas of the cervix uteri [4, 11].

In this paper we report our results obtained with the cytobrush. With the aim to get more and objective information about endocervical cell groups after light microscopic characterization, these clusters were evaluated by a digital analyzer. It is, however, not clear, whether there is a transition region between the benign and the suspicious cell lines [4].

Send offprint requests to: Dr. Veronika Tóth, Res. Institute of Oncopathology, Natl. Oncological Inst., Dept. of Cytopathology, Ráth Gy. 7—9, Budapest, H-1122, Hungary

The goal was the detection of the subvisual onset of the cellular transformation of metaplastic squamous and columnar cells. It has been supposed that this system, after the establishment of a data base, may be helpful in solving some differential diagnostic problems in endocervical and bronchial cytology.

Materials and methods

From 1 April 1986 to 30 September 1987 we examined cytological preparation from 359 patients. Samples were randomly taken and in the first period of the examinations (6 months, 100 cases) the cytobrush (Medscand AB, Malmö, Sweden) and cotton swab techniques ran parallel. The smears were prepared using the conventional Papanicolaou method. In 42 cases cytology was followed by histology. Biopsy specimens were routinely fixed, embedded and stained with HE.

Groups of endocervical cells were studied with a Robotron A 6471 type digital TV image analyzer. The objects were measured with a green filter under $\times 500$ magnification. The transformed light intensities were digitalized into 64 gray — levels and stored on 512×712 image points in the memory of PDP 11 computer by a SZK-40 type video camera.

We selected 13 object features. Further on they will be abbreviated as in Table II. In fact, our objects were groups of cells. The measured parameters, however, relate always to a single cell. We have examined five codes:

Code 1: columnar endocervical cells	134 groups
Code 2: reserve cells	142 groups
Code 3: hyperplasia of reserve cells	169 groups
Code 4: squamous metaplasia	155 groups
Code 5: atypical squamous metaplasia	122 groups

Results were statistically analyzed by methods supplied in the software AMBA/R (Robotron Co) [1]. We applied bivariate tests such as Student's F- and *t*-test and multivariate methods for simplifying the structure of the data i.e. hierarchic classification and principal components analysis.

Results

With Stormby's endocervical cytobrush we obtained plentiful samples of good quality (Figs 1, 2). Bleeding disturbing colposcopic examinations were not observed.

Distribution of cytological diagnoses (Table I) clearly demonstrates that 85.38% of the cases were P_1—P_2, i. e. negative, 11.6% suspect (P_3) and 7 (1.94%) positive. There were altogether three smears (0.83%) which did not contain endocervical cells due to technical error.

Out of the seven cytologically positive cases three turned to be negative by colposcopy. Histological examination, however, confirmed the cytological diagnosis. There was one false negative (underdiagnosed) case (P_2) that proved to be severe dysplasia by histology.

During the evaluation of our results the problem of reserve cell processes got into the focus of our interest. In certain cases it may be difficult to separate

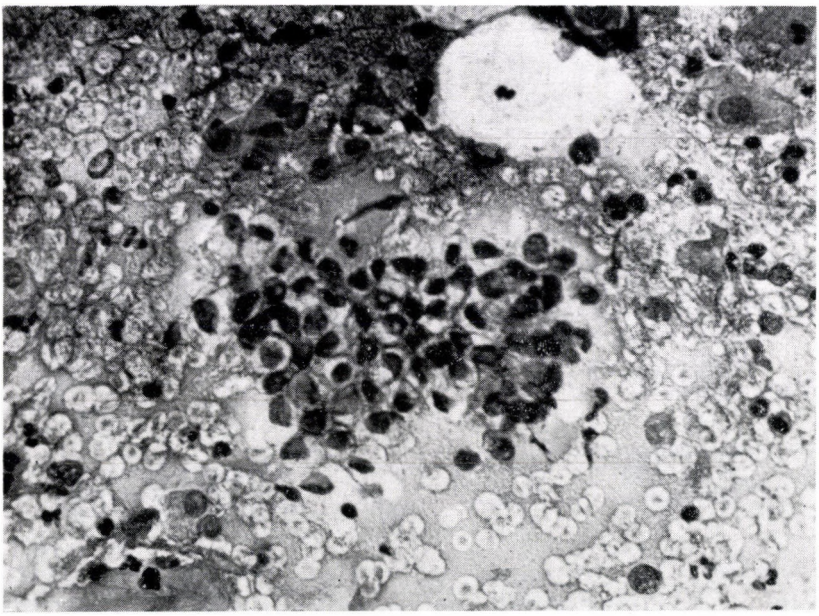

Fig. 1. Group of typical endocervical cells. Papanicolaou staining, ×350

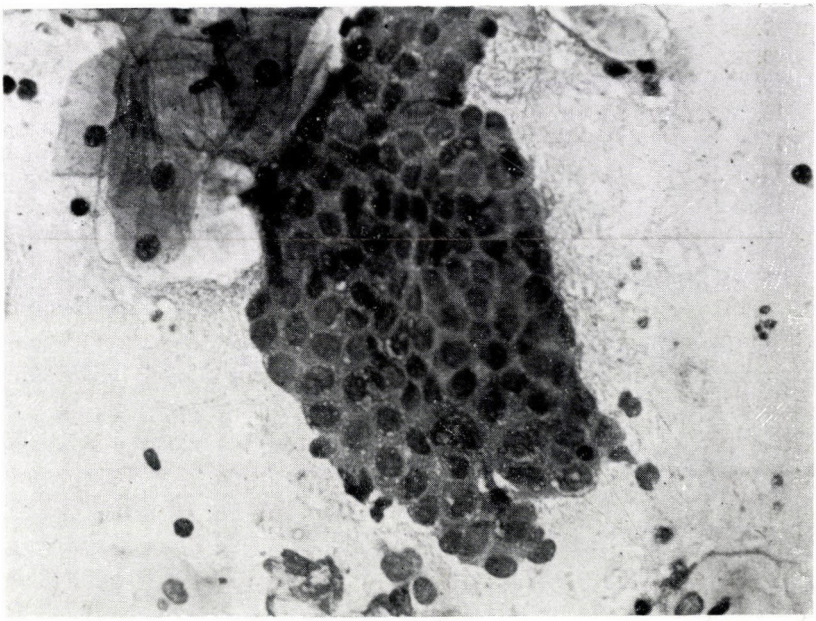

Fig. 2. Cytological picture of reserve cell hyperplasia. Papanicolaou staining, ×350

Table I

Distribution of cytological diagnoses

Diagnoses	Case Number	%
P_1	2	0.55
P_2	301	84.0
P_3	42	11.6
P_4	3	0.83
P_5	4	1.11
After irradiation: negative	3	0.83
Suspect tumour cells visible	1	0.25
Endocervical cells absent	3	0.83
Total	359	100.00

Table II

Object features

1.	Level	—	Threshold
2.	Length	—	Length of contour
3.	Areag	—	Area within contour
4.	Convg	—	Shape factor
5.	Formg	—	Form factor
6.	Contg	—	Gray value gradient at contour
7.	Numbc	—	Cell number of the group
8.	Area1	—	Area of one cell
9.	Mgv	—	Mean gray value
10.	Sgrv	—	Sum of gray values
11.	Maxgv	—	Range of gray values
12.	Holeg	—	Relative hole area
13.	Comp	—	Compactness

by light microscopy the different endocervical cells appearing in clusters or sheets. The question arose whether the columnar, basal, or reserve cells could be distinguished and what parameters were discriminating when an image analyzer was used.

The seven positive cases were not evaluated because the squamous like tumour cells did not form groups and the smear from the single one case of adenoacanthoma did not contain sufficient number of cells for statistical evaluation.

According to our program 13 object features were selected (Table II). Some of them were morphometric, the others densitometric features. The measured values were analyzed by statistical tests. (Table III shows the

results of the principal components analysis. Based on the highest eigenvalues there were chosen two principal components which contain eigenvalues eigenvectors of the corresponding variance co-variance matrix. The values of eigenvectors show relationships among variables, features. We can demonstrate closed connections between Lenght, Areag i. e. morphometric, and Sgrv i.e. densitometric features, whereas the second component contains only gray level parameters (Mgv, Maxgv, Comp).

Table III

Principal Components Analysis

Feature No. Object No.	13 722					
Eigenvalues						
	4.179	3.451	1.649	1.244	0.949	0.771
	0.284	0.209	0.155	0.067	0.028	0.011
	0.004					
Eigenvectors						
	0.061	0.448	0.433	0.329	0.314	0.173
1.	0.300	0.080	0.170	0.443	0.214	0.056
	0.025					
	0.212	0.197	0.088	0.272	0.268	0.344
2.	0.181	0.306	0.480	0.061	0.392	0.058
	0.357					

1. Principal Component
2 — Length
3 — Areag
10 — Sgrv

2. Principal Component
9 — Mgv
11 — Maxgv
13 — Comp

Table IV

Results of Hierarchic Classification

Code Groups	Features	Ratio of cells discriminated correctly (%)
1—2	Contg Areal	80.2
1—3	Areal Contg	73.0
2—3	Areal Sgrv	89.0
4—5	Numbc Areag	73.2

These different codes can be separated also by hierarchic classifier. For the distinction of our objects, the computer selected the optimal main parameters: the area of one cell (Area 1), the number of the cells (Numbc), the area of cell group (Areag), the gray value gradient (Contg), and the sum of the gray values (Sgrv) (Table IV).

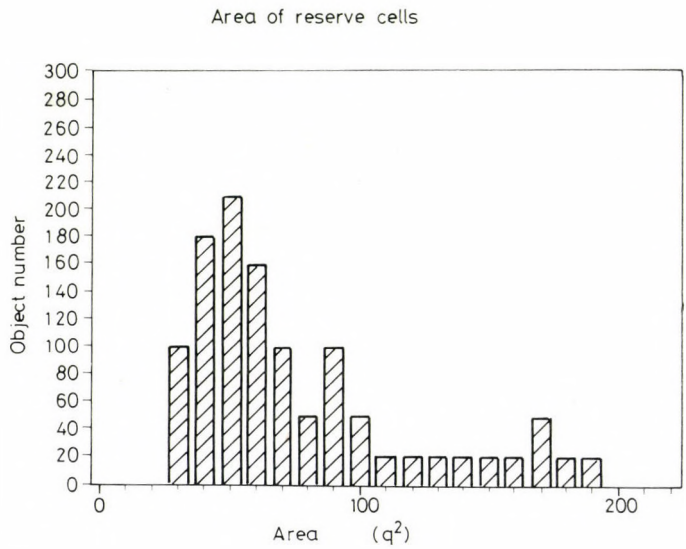

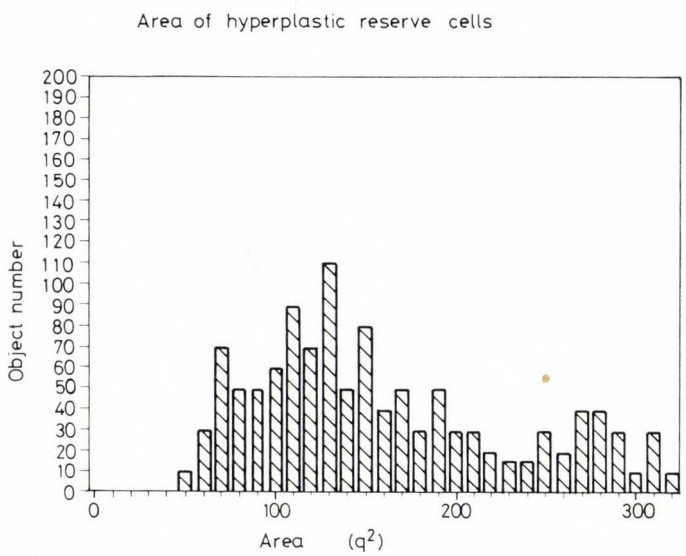

Fig. 3. Histograms of reserve cells and reserve cell hyperplasia groups. *t*-test $p < 0.05$

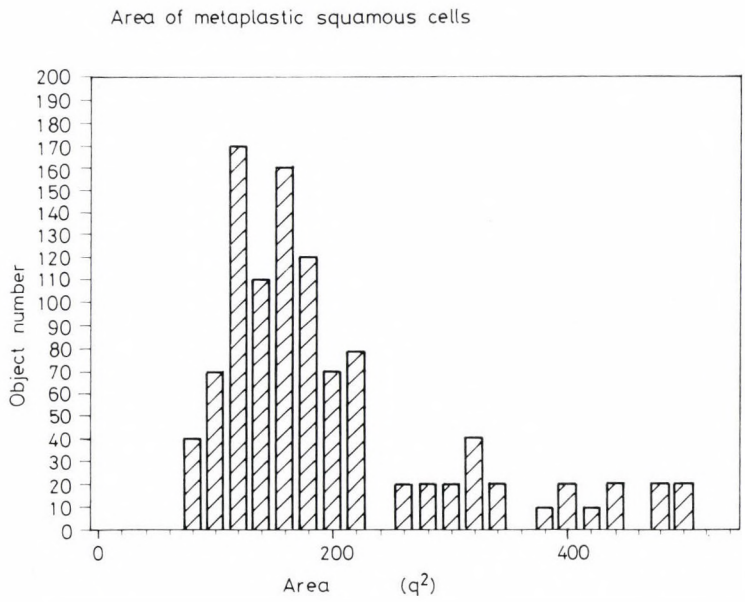

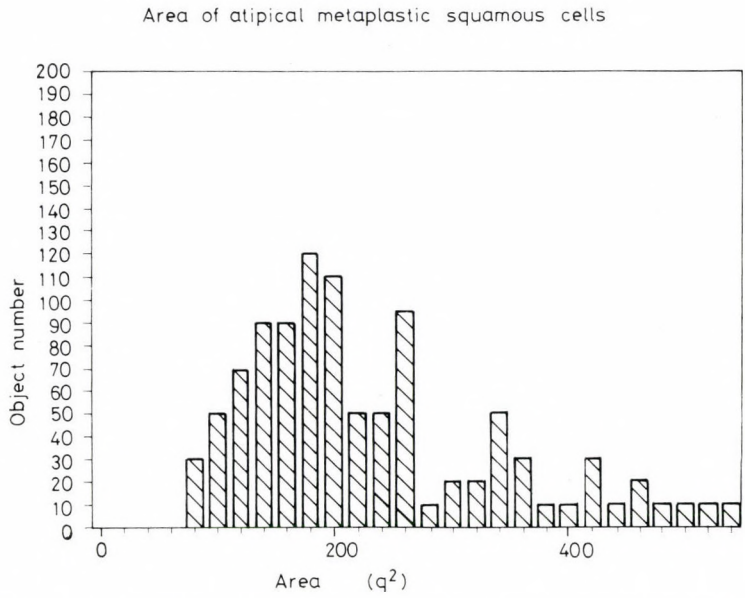

Fig. 4. **Histograms of squamous metaplasia and atypical metaplasia cell groups.** *t*-test $p < 0.05$

By the use of the bivariate tests, cells of codes 1, 2, codes 2, 3 and codes 4, 5 can be separated at significant level if the area of one cell is considered (Figs 3, 4,).

Discussion

Stormby's endocervical brush is especially designed to obtain with its small nylon brushes sufficient endocervical material for cytological examinations. Using this cytobrush we obtained smears containing numerous ecto- and endocervical cells suitable for evaluation.

Similarly favourable results were reported by Ros et al. [11] and Trimbos and Arentz [12]. Boon and Vooijs stress the importance of the sampling technique in the establishment of more precise diagnosis [3, 13].

Endocervical cells are known to appear in clusters [5]. Our smears contained simultaneously quite a number of mucin producing columnar, reserve cells, hyperplastic reserve cells and squamous metaplastic cells in clusters or sheets. The appearance of fine morphological changes (slight nuclear enlargement, mild hyperchromasia and minimal anisokaryosis) may indicate dysplasia or well differentiated adenocarcinoma [8].

Features presented in this paper may play and important role in detecting the reserve cell processes because of their fine morphological differences.

This system may serve further on as a data base. It may be helpful in differential diagnostic problems. With sufficient number of positive cases the system may be extended then it will probably be suitable for the better characterization of reserve cell processes.

REFERENCES

1. AMBA/R — Dialog/programming System, user Manual VEB Robotron-Vertrieb, Berlin, 1987.
2. Bartels PH: Numerical evaluation of cytologic data. IX. Search for data structure by principal components transformation. Analyt Quant Cytol 3: 167, 1981.
3. Boon ME, Rietveld-Sheffers PEM: Improving the quality of cervical smears made by general practitioners: Introduction of the cytobrush method. European Cytology Congress, Madrid, 1985 (Abstract).
4. Burger G, Jütting U, Rodenacker K: Changes in benign cell populations in cases of cervical cancer and its precursors. Analyt Quant Cytol 3: 261, 1981.
5. Kivlahan C, Ingram E: Papanicolaou smears without endocervical cells. Are they inadequate? Acta Cytol 30: 258, 1986.
6. Koss LG: Diagnostic cytology and its histopathologic bases. JB Lippincott Company, Philadelphia. (3rd Ed.) 1979.
7. Marehevsky AM, Gil I, Jeanty H: Computerized interactive morphometry in Pathology: Current instrumentation and methods. Human Pathol 18: 320, 1987.
8. Ng ABP: Microinvasive adenocarcinoma and precursors of adenocarcinoma of the uterine cervix. Compedium on diagnostic cytology. In: Wied GL, Koss LG, Reagan JW (eds) Tutorials of Cytology. (5th Ed.) Chicago, 1983. pp 148—154.
9. Patten FS Jr: Morphologic subclassification of preinvasive cervical neoplasia. Compendium on diagnostic cytology. In: Wied GL, Koss LG, Reagan JW (eds) Tutorials of Cytology. (5th Ed.) Chicago, 1983. pp 108—117.

10. Reagan JW, Ng ABP: Cellular detection of glandular neoplasms of uterine cervix. Compendium on diagnostic cytology. In: Wied GL, Koss LG, Reagan JW (eds) Tutorials of Cytology. (5th Ed.) Chicago, 1983. pp 155—163.
11. Ros E, Jumenez Ayala M, Vilaplana E, Saiz-Pardo F, Losite L, Garcia Andrade MC, Navarro E, Rodriguez C: New technique for endocervical cytological sampling with Stormby's bruch. Preliminary results. Citologia, 9: 20, 1983.
12. Trimbos JB, Arentz NPW: The efficiency of the cytobrush versus the cotton swab in the collection of endocervical cells in cervical smears. Acta Cytol 30: 261, 1986.
13. Vooijs GP, Elias A, van der Graaf Y, Poelen-van-der Berg M: The influence of sample takers on the cellular composition of cervical smears. Acta Cytol 30: 251, 1986.

Acta Morphologica Hungarica 37 (3—4), pp. 135—145 (1989)

ALTERATION OF THE SUBMANDIBULAR GLANDS OF FEMALE MICE DURING PREGNANCY AND LACTATION A HISTOLOGICAL, HISTOMETRIC AND HISTOCHEMICAL STUDY*

J. A. Rossi, L. C. Bruschi

DEPARTMENT OF HISTOLOGY, STATE UNIVERSITY OF LONDRINA, PARANÁ STATE, BRAZIL

(Received 23 November 1988)

The submandibular glands of mice show "masculinization" during pregnancy and lactation. In this work involving morphological, morphometric and histochemical analyses we observed an increase in the volume fraction and area of the granular ducts and the apical granulation of their cells. The maximum response to the masculinization occurred on the 15th day of pregnancy. From this day on a decrease in the volume fraction of the granular ducts starts, even though the gland keeps the "masculine pattern" throughout the end of the lactation phase. Our observations support the intermodulation between striated and granular ducts. In our opinion, the "masculinization" process of the submandibular gland is related to the progesterone increase which takes place during pregnancy; its maintenance during lactation is also connected to prolactin.

Keywords: Salivary gland, submandibular gland, pregnancy and lactation

Introduction

The submandibular gland of mice consist of morphofunctional units composed by acini, intercalated ducts, granular ducts, striated ducts and excretory ducts.

In adult mice this gland shows a sexual dimorphism which is morphologically evident in its segments called granular ducts (GD) which are more numerous and thicker in the male than in the female [26, 28, 46].

This dimorphism is androgen-dependent, since castration of these animals changes these ducts into striated ducts [9, 17, 25] and after the replacement of exogenous testosterone the granular ducts recover their standard pattern [5, 8, 27, 29].

However, not only androgens, but also other steroid or anabolizant drugs exert a stimulation on this cell system [13, 22, 23, 31, 35].

The hormone fluctuations during pregnancy and lactation bring about a male pattern of the glands, i.e., pregnant or lactating females have bigger granular ducts than virgin, non-pregnant or non-lactating females [11, 46].

Send offprint requests to: J. A. Rossi, Dept. of Histology, State University of Londrina, Paraná State, POB 6001-86051, Brazil

* This work was supported by grants from CPG — UEL (124.875)

The present study describes the quantitative and morphological variations of the submandibular gland parenchyma due to the masculinization during pregnancy and lactation. To assess changes histological, morphometric and histochemical analyses of the granular ducts were carried out.

Materials and methods

Forty-five adult female mice of the Swiss strain were randomly assigned in nine groups of five animals each and classified as follows:

P0 = control groups, non-pregnant animals
P5 = 5-day- pregnant females
P10 = 10-day- pregnant females
P15 = 15-day- pregnant females
N = 21-day- pregnant females (birthday of offspring)
L5 = 5-day- lactating females
L10 = 10-day- lactating females
L15 = 15-day- lactating females
L21 = 21-day- lactating females (date of weaning)

Body weight was taken at the end of each experimental period. All animals were sacrificed by cervical dislocation, the pairs of the salivary glands were dissected, cleaned and weighed. The left glands were fixed in Helly's fluid, embedded in paraffin and stained with hematoxylin-eosin and Mallory trichrome.

The right glands were fixed in formolsaline (0.1 M) and used for tryptophan aminoacid determination by the method described by Adams [1]. The control of the reaction was made by performic acid, in accordance with Toennies [45].

The histometric analysis was made following Henning [20], using an eyepiece integrating Zeiss I Kpl, 8×, type II with 100 hits. The minimum number of points (P) counted for each animal groups [7600] in order to reach a 5% precision, was estimated according to Schaefer [41] by

1. a previous counting of 200 points (N) with the inside number of points (PN) falling on granular ducts;
2. the determination of the approximate points fraction (PF = PN);
3. the calculus of P from the formula:

$$P = \frac{1 - PF}{e_A^2 \cdot PF}$$, where e_A is the desired relative error (0.05).

Diameter determinations of striated and granular ducts were made using a PZO-K 15× eyepiece. For each duct which was cut transversally, two measures of the orthogonal diameters were taken, according to Piza [37]. This author proposes that the diameter measures should, not be taken through the intersection lines of the eyepiece micrometer but using just the base lines, in order to assure the orthogonality between both diameters.

The area was obtained using the formula:

$$S = \frac{\pi}{4}\left[\frac{D1 + D2}{2}\right]^2$$

The data were treated statistically by the analysis of variance, followed, when needed, by Tukey multiple-range test [42]. The ratios were transformed in degrees by means of a table of angular arco-seno transformation [16] before the analysis of variance within $P < 0.05$.

Results

Table I shows the data obtained concerning body weight, absolute and relative gland weights.

The statistical analysis enables us to infer that female mice show an increase in their body weight during pregnancy, most significant from their

Table I

Average and standard deviation of the body, absolute and relative glandular weights of the female mice in several groups

Groups	Body weights (G) *D- 4.896	Absolute gland weights (G) D- 0.02	Relative gland weights D- 0.439
P0	30.45 ± 1.11	0.091 ± 0.013	0.301 ± 0.049
P5	32.63 ± 1.22	0.089 ± 0.002	0.274 ± 0.022
P10	36.50 ± 1.13	0.102 ± 0.013	0.280 ± 0.037
P15	41.58 ± 3.72	0.118 ± 0.015	0.290 ± 0.057
N	41.00 ± 3.81	0.110 ± 0.006	0.271 ± 0.024
L5	39.26 ± 2.45	0.102 ± 0.008	0.261 ± 0.028
L10	39.75 ± 1.71	0.092 ± 0.011	0.232 ± 0.022
L15	39.77 ± 2.80	0.092 ± 0.006	0.231 ± 0.022
L21	39.90 ± 1.73	0.092 ± 0.008	0.231 ± 0.024

* D of Tukey [42] (Minimal difference significance among the averages)

15th day of pregnancy until the day of birth of their offspring. There is no significant decrease during the lactation period. The submandibular glands also show an increase of absolute weight, more significant on the 15th day of pregnancy. However, from this day on, there is a reduction of weight which by the time of birth equals that of the animals in the control group (P0). There is no significant change in the relative weight of glands, once there is an analogy between the phases of further increase of glandular weight and the increase of body weight.

Histological data

Starting on the 10th day of pregnancy, there is an increase in the quantity and in the diameter of the granular ducts. There is also a significant increase of apical granulation in their cells. This is more pronounced on the 15th day of pregnancy. The development of granular ducts is accomplished with the decrease of striated ducts. During the intense development of granular ducts, we could see clear signs of transformation of striated ducts into granular

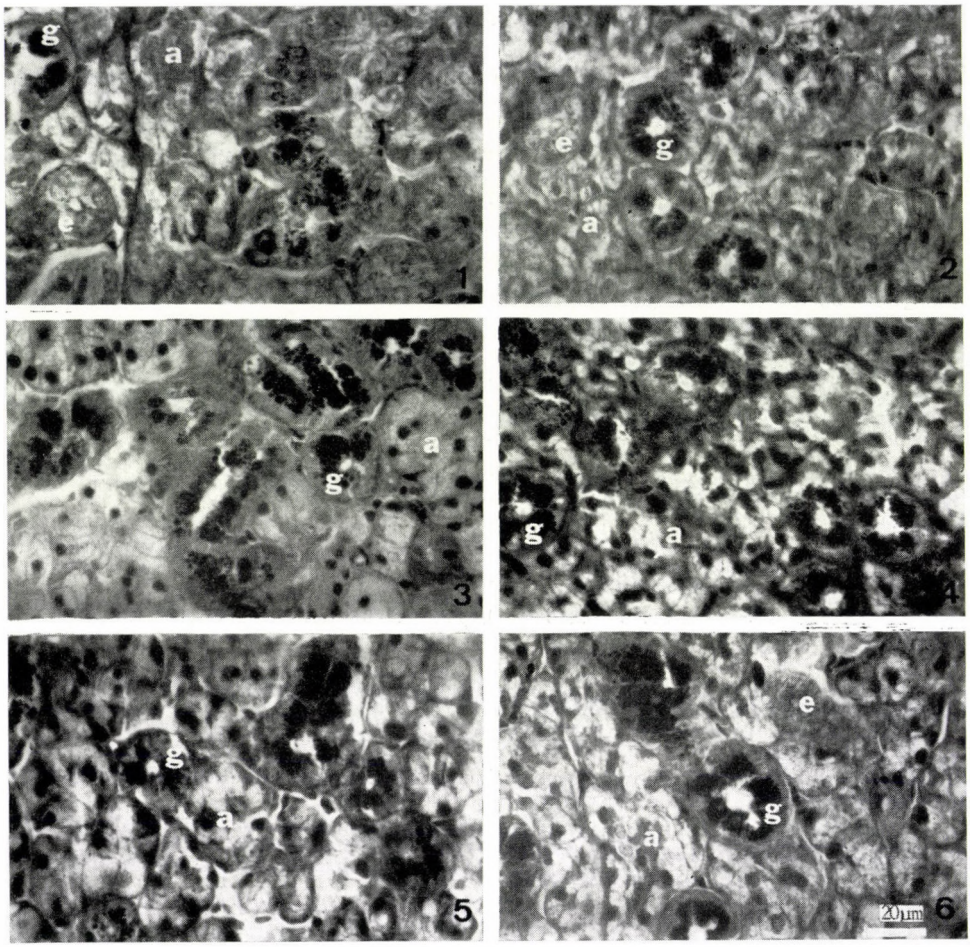

Figs. 1—6. Mallory's trichrome stain of the submandibular glands of female mouse (×500) in the control group (Fig. 1), on the 10th day of pregnancy (Fig. 2), on the day of birth of the offspring (Fig. 3), on the 5th, 10th and 21st days of lactation (Figs 4, 5, 6). Granular duct (g), striated duct (e) and acini (a)

ducts, i.e., loss of basal striation, displacement from the nucleus to the base of the cell, as well as apical vacuolization.

From the 10th day of lactation, we observed a reduction of granular ducts and at the same time an increase of striated ducts. The other parenchymal components do not alter their forms (Figs 1—6).

Histochemical data

The result obtained from the reaction of tryptophan is shown in Table II. The reaction of granular duct cells is higher in relation to the control

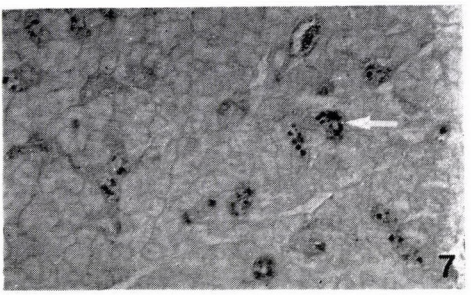

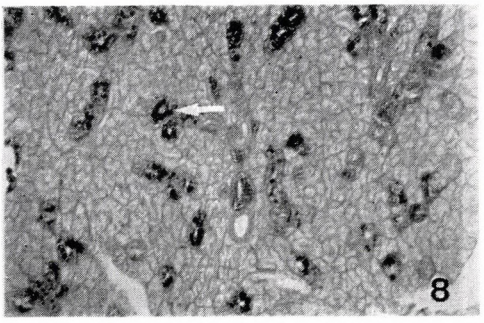

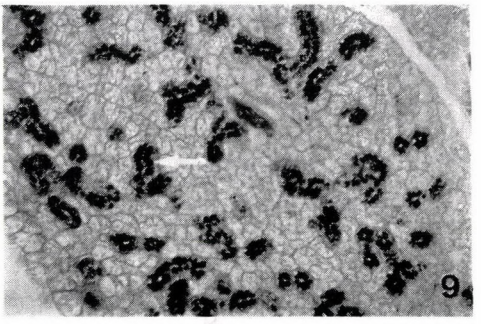

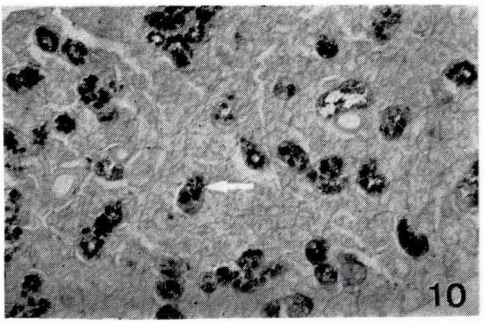

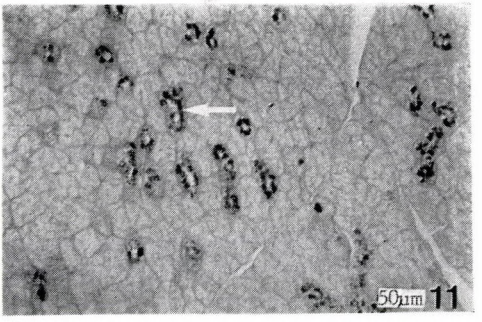

Figs. 7—11. Tryptophan in the granular ducts (arrows) of the submandibular gland of female mouse (×130), in control groups (Fig. 7) on the 10th and 15th day of pregnancy (Figs 8, 9) on the 10th and 21st day of lactation (Figs 10, 11)

group (P0), even since the 10th day of pregnancy and reaches its peak on the 15th day of pregnancy. Even in the period of cessation of lactation, the reaction is relatively higher than in the control animals (Figs 7—11).

Histometric data

The volume fraction of SMG components of several groups is shown in Table III. The distribution of volume fraction occupied by granular and striated ducts in the groups is shown in Fig. 12.

From the data analysis, we may consider the following regarding the control group (P0):

Table II

Results from the reaction to the tryptophan in submandibular gland of female mice in several groups

Groups	Acini	Intercalated ducts	Granular ducts	Striated ducts	Excretory ducts	Stroma
P0	—	—	+	—	—	—
P5	—	—	+	—	—	—
P10	—	—	++	—	—	—
P15	—	—	++++	—	—	—
N	—	—	+++	—	—	—
L5	—	—	+++	—	—	—
L10	—	—	+++	—	—	—
L15	—	—	++	—	—	—
L21	—	—	++	—	—	—

a) The volume fraction of acini is reduced from the 10th day of pregnancy to the 21st day of lactation, reaching a lower percentage between the 15th day of pregnancy and the 5th day of lactation.

b) The volume fraction of granular ducts increases significantly since the 10th day of pregnancy until the 21st day of lactation, reaching its highest percentage between the 15th day of pregnancy and 5th day of lactation.

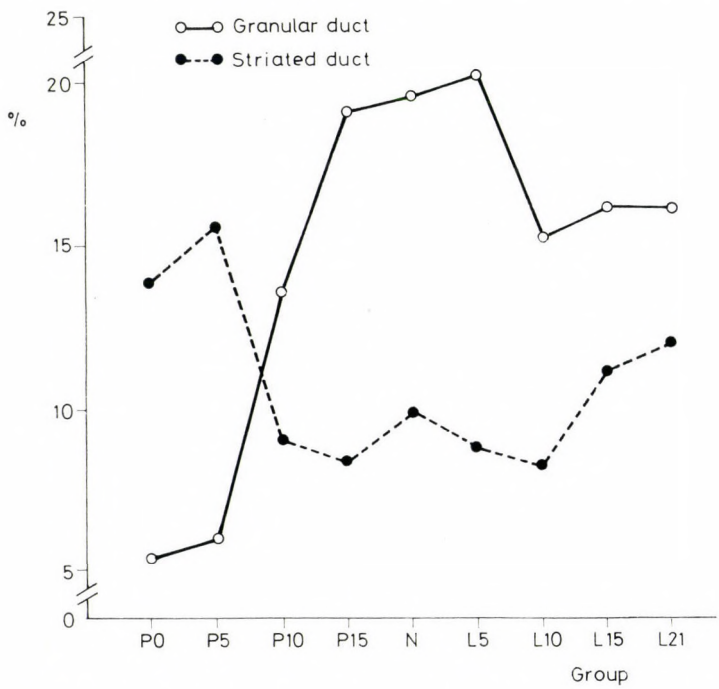

Fig. 12. The volume fraction of granular and striated ducts in several groups

Table III

Average and standard deviation of the volume fraction of SMG components in several groups

Groups	Acini	Intercalated ducts	Granular ducts	Striated ducts	Excretory ducts	Stroma
	*D- 5.652	D- 0.268	D- 5.425	D- 3.214	D- 0.455	D- 1.411
P0	76.89 ± 1.62	0.41 ± 0.06	5.46 ± 0.91	13.95 ± 1.18	0.56 ± 0.55	2.68 ± 0.62
P5	75.16 ± 1.78	0.29 ± 0.20	5.98 ± 1.33	15.65 ± 0.71	0.35 ± 0.22	2.53 ± 0.55
P10	72.69 ± 2.23	0.49 ± 0.06	13.58 ± 2.49	9.03 ± 0.57	0.35 ± 0.42	3.81 ± 0.55
P15	66.84 ± 4.88	0.54 ± 0.15	19.01 ± 4.12	8.36 ± 1.67	0.34 ± 0.42	4.88 ± 0.91
N	65.23 ± 2.02	0.63 ± 0.06	19.46 ± 2.07	9.91 ± 1.33	0.61 ± 0.82	4.10 ± 0.49
L5	65.78 ± 3.23	0.69 ± 0.15	20.11 ± 3.12	8.75 ± 1.15	0.65 ± 0.64	3.96 ± 0.71
L10	71.08 ± 1.62	0.69 ± 0.11	15.05 ± 2.78	9.15 ± 1.13	0.24 ± 0.33	3.71 ± 0.66
L15	68.08 ± 1.82	0.62 ± 0.11	16.01 ± 2.58	11.05 ± 3.07	0.45 ± 0.49	3.55 ± 0.95
L21	67.42 ± 3.21	0.69 ± 0.08	15.98 ± 2.43	11.99 ± 1.42	0.63 ± 0.55	3.24 ± 0.24

* D of Tukey [42] (Minimal difference significance among the averages)

c) There is a reduction of the number of the striated ducts from the 10th day of pregnancy until the 10th day of lactation, however, the return to the standard pattern of control group occurs on the 15th day of lactation.

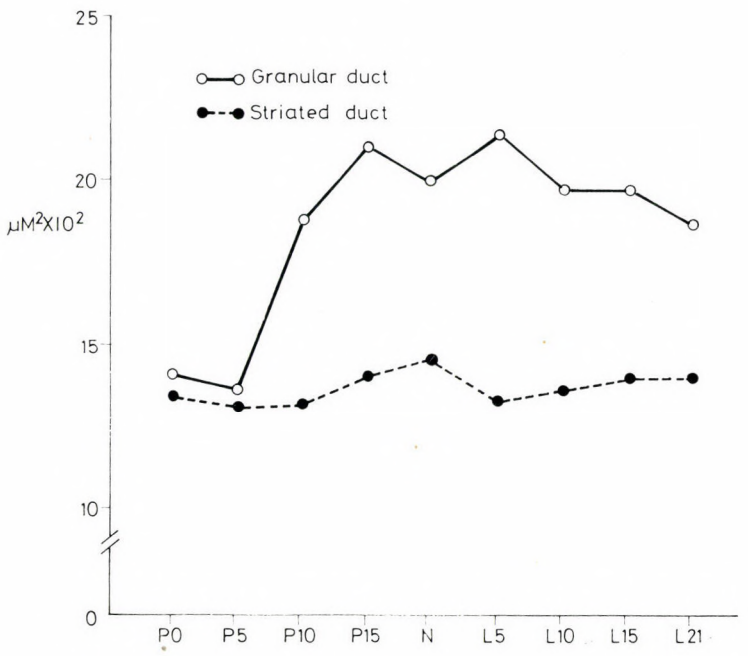

Fig. 13. The granular and striated ducts area in several groups

Ductometric data

The measuring of the granular ducts presents a significant increase which starts on the 10th day of pregnancy and remains until the 21st day of lactation. The striated ducts do not show any relevant change in area during the analyzed periods (Fig. 13).

Discussion

The submandibular glands of mice (SMG) have a sexual dimorphism which begins at puberty when a differentiation of granular ducts from striated ducts occurs [9, 17, 25]. Male animals will have more granular ducts than the females as soon as the level of testicular androgen rises [4, 14]. In mice, this starts on the 21st day of life [24].

The SMG are typical androgen-target organs, following a general mechanism of androgenic activity. The SMG presents receptors for the androgens which are characterized and quantified [15, 43, 48].

Although Desclin [12] reports that progesterone does not have any masculinization effect on SMG of female mice either with or without an ovary other authors have shown that progesterone is also stimulating the SMG. Raynauld [38] obtained a partial regression of the SMG with progesterone in castrated animals and Travill [46] believes that masculinization effect of the glands of pregnant animals is due to high levels of progesterone which occur during this period.

Studies in mice Tfm/y also show that the SMG of these animals is insensitive to progestagens [6, 33] which suggest that progesterone acts via androgenic receptors.

The progesterone could interact directly with the receptors for androgens or after biotransformation into steroids C 19. In fact, progesterone can be converted in 5-α-dihydrotestosterone in some androgen-target organs such as the pre-pubertal glands of mice, showing that the masculinization effects of progesterone can take place after conversion into androgens [33].

In vitro, the SMG can take up cholesterol and make it into dihydroepiandrosterone, it can also convert pregnenolone into progesterone and dihydroepiandrosterone and convert progesterone into androstenedione [39, 40]. Thus, the supposition that progesterone may be biotransformed into SMG before its binding to receptors of androgens is reasonable.

We can also say that the oestrogens have some effect on the SMG in a similar way as that of the androgens. Nevertheless, the response to them is moderate when compared to that of the male hormones [19]. Moreover, the prolonged treatment with oestrogen mimicks castration [9]. This must be

due to the LH inhibition promoted by oestrogen. Once LH secretion becomes reduced, the androgen production is also reduced [32].

Our results have shown that masculinization during pregnancy and lactation, although evident, does not reach the same level observed in the gland of a normal adult male animal.

The segments altered during those phases are the granular ducts. Since the 10th day of pregnancy of the animal they show an increase in quantity and diameter and an increment of this cellular granules content.

This initial hypertrophy, is compatible with the progestational peak which occurs on the 6th day of pregnancy [30], and these alterations become more significant on the 15th day of pregnancy. The SMG shows then a slight reduction of the granular duct volume fraction and of reaction towards tryptophan, not reducing however, the area of the remaining ducts. Up to the end of the lactation, the SMG keeps a masculinized pattern. This masculinization is understandable since even though the levels on the progesterone start decreasing on the 17th day of pregnancy, the concentration of progestin is very high in the SMG between the 15th day and 22nd day of pregnancy in the rat, being higher that in the concentration in the ovarian blood [36].

Taking into account the period of 10 days to obtain a full post-castration gland atrophy [44], it appeared that the hormone retention in the glandular tissue would enable the masculinization maintenance in the phase of the plasmatic progesterone reduction.

We also have to consider the maintenance of the relative masculinization of the gland during lactation which may be prolactin-dependent.

In fact, in the young rat, the weight of sexual accessory organs increases when the levels of prolactin becomes higher [34]. The treatment with antiprolactin from birth, causes a weight decrease of the prostate and seminal vesicle of rats [21]. Barañao et al. [3] claim that, at least in the prostate, the prolactin increases the testosterone metabolism, besides increasing the androgenic receptors. Another point to take into consideration is that the prolactin stimulates the glucocorticoid and dihydroepiandrosterone production in the cortex of the adrenal [10, 47]. Considering that during the lactation period the prolactin level is high a hyperfunction of the adrenal is likely to help maintain the masculine pattern of SMG. Moreover, high doses of prolactin may stimulate the progesterone synthesis by the ovaries [18], and the presence of prolactin may inhibit in the female rat the induction of enzymes which degradate the progesterone into 3 β and 20 α-hydroxysteroid dehydrogenase and 5 α-reductase [2].

Based on our results and on literature reviews the masculinization of SMG which took place in pregnant and lactating female mice seems to be due to the variation of progesterone concentration during pregnancy. It is also likely that during lactation, the progesterone retention within the SMG, its

slow metabolism and prolactin action through either adrenal stimulation or other already considered actions are enough for the maintenance of a glandular masculinization.

REFERENCES

1. Adams CWM: A p-dimethylaminobenzoaldehyde-nitrite method for the histochemical demonstration of tryptophane and related compounds. J Clin Path, 10: 56, 1957
2. Aires MM: Fisiologia Básica. Rio de Janeiro, Guanabara Koogan, 1985 p. 564
3 Barañao JLS, Chemes HE, Tesone M, Chiauzzi VA, Scacchi P, Calvo JC, Faigon MR, Moguilevski JA, Charreau EH, Calandra RS: Effects of androgen treatment of the neonate on rat testis and sex accessory organs. Biol Reprod, 25: 851, 1981
4. Bhoola KD, Dorey G: Age related increase and androgen dependence of enzymes in the mouse submandibular gland. J Physiol (London), 225: 26, 1972
5. Bruschi LC: Efeitos de dose única de testosterona na modulacao estrutural e bicquimica dos ductos granulosos da glândula submandibular do camundongo castrado. São Paulo, 1979. p. 113 (Tese de Doutoramento — Instituto de Ciências Biomédicas, USP.)
6. Bullock LP, Barthe PL, Mowszowicz I, Orth DN, Bardin CW: The effect of progestins on submaxillary gland epidermal growth factor: demonstration of androgenic, synandrogenic and antiandrogenic actions. Endocrinology, 97: 189, 1975
7. Calandra RS, Blaquier JA: Hormonas esteroideas sexuales. In: RS Calandra F Nicola (eds). Endocrinologia Molecular. Bueanos Aires, El Ateneo 1980 p. 199
8. Chrétien M: Actio de la testostérone sur la structure fine d'un effecteur: la glande sous-maxillaire de la souris mâle. II. Réaction des tubes sécréteus a l'injection de testottérone chez le casrat. J Microsc (Paris), 14:55, 1972
9. Chrétien M: Action of testosterone on the differentiation and secretory activity of a target organ: the submaxillary gland of the mouse. In Rev Cytol, 50:353 1977
10. Colby HD: Mechanism of action of prolactin on adrenocortical steroid secretion in hypophysectomized female rat. Endocrinology, 104: 1299—303, 1979
11. Desclin Jr. J: Recherches sur la masculinization spontanée et expérimentale des glandes sous-maxillaires chez la souris femelle. Arch Biol, 71: 235—68, 1960
12. Desclin Jr. J: Action de la progestérone sur la structure des glandes sous-maxillaires chez la souris. C R Hebd Seances Acad Sci, 264: 367—9, 1967
13. Doine AI, Fava-de-Moraes F: Histochemistry of the submandibular salivary gland of castrated male mice treated with androgens and anabolic steroids. Arch Oral Biol, 24: 569, 1979
14. Dunn JF, Wilson JD: Development study of androgen responsiveness in the submandibular gland of the mouse. Endocrinology, 96: 1571, 1975
15. Dunn JF, Goldstein JL, Wilson JD: Development of increased cytoplasmic binding of androgen in the submandibular gland of the mouse with testicular feminization. J Biol Chem, 248: 7819, 1973
16. Fisher RA, Yates F. Tabelas estatisticas para pesquisa em biologia, medicina e agricultura. São Paulo, Poligono, Ed. da Univ. de São Paulo 1971, p. 151
17. Gresik W: Postnatal developmental changes in submandibular glands of rats and mice. J Bioch Cytochem, 28: 860, 1980
18. Grota LJ, Eik-Nes KB: Plasma progesterone concentrations during pregnancy and lactation in the rat. J Reprod Fertil, 13: 83, 1967
19. Harfin JF: Regulación hormonal e nerviosa del tamano y estructura de las glandulas submaxilares. Buenos Aires 1969. (Tesis de Doutorado — Fac. de Odontologia, Univ. Buenos Aires.)
20. Henning A: Kritische Betrachtung zur Volumen-und Oberfläche Messung in der Mikroskopie. Zeiss Werkz Schr, 6: 78, 1958
21. Hostetter MW, Piacsek BE: The effect of prolactin deficiency during sexual maturation in the male rat. Biol Repro, 17: 374, 1977
22. Houssay AB, De Harfin JF, Montuori E, Epper CE: Effects of anabolic steroids upon submandibular glands in C3H/Ep mice. Acta Physiol Lat Am, 16: 52, 1966
23. Houssay AB, Bozzolo E, Curbelo HM: Effects of anabolic steroids upon the iodine uptake by submaxillaries in mice. Acta Endocrin Pan Amer, 1: 33, 1970
24. Jean-Faucher CH, Berger M, Turchheim M, Veyssiere G, Jean U: Developmental patterns of plasma and testicular testosterone in mice from birth to adulthood. Acta Endocrinol, 89: 780, 1978

25. Kumegawa M, Takuma T, Takagi Y: Precocious induction of secretory granules by hormones in convoluted tubules of mouse submandibular glands. Am J Anat, 148: 111, 1977
26. Lacassagne A: Dimorphisme sexuel de la glande sous-maxillaire chez la souris. C R Seances Soc Biol Fil, 133: 180, 1940
27. Lacassagne A, Chamorro A: Réaction á la testosterone de la glande sous-maxillaire, atrophiée, consecutivement a l'hypophysectomie chez la souris. C R Seances Soc Biol Fil, 134: 223, 1940
28. Leite PEP, Fava-de-Moraes F, Doine AI: Estudo estrutural, histoquimico e bioquimico da glandula submandibular da camundonga portadora de sindrome anovulatória androgênica. An Farm Quim São Paulo 17 (Supl): 107, 1977
29. Lyon MF, Hendry I, Short RV: The submaxillary salivary glands as test organs for response to androgen in mice with testicular feminization. J Endocrinol, 58: 357, 1973
30 McCormack JT, Greenwald GS: Progesterone and Oestradiol-17β concentrations in the peripheral plasma during pregnancy in the mouse. J Endocr, 62: 101, 1974
31. Melhado RM: Efeitos do anti-andrógeno acetato de ciproterona na glândula submandibular do camundongo. Araçatuba, Faculdade de Odontologia — UNESP 1980. (Tese Livre-Docência.)
32. Minetti CASA: Modulacão andrógeno-tiroidiana da expressão androgênica na glãndula submandibular do camundongo. São Paulo 1985 p. 110 (Tese de Doutorado — Instituto Ciencias Biomédicas da Universidade de São Paulo.)
33. Mowszowicz I, Bieber DE, Chung KW, Bullock LP, Bardin CW: Synandrogenic and antiandrogenic effect of progestins: comparison with non-progestational antiandrogens. Endocrinology, 95: 1589, 1974
34. Negro-Villar A, Waad SA, McCann SM: Evidence for a role of prolactin in prostate and seminal vesicle growth in immature male rats. Endocrinology, 100: 729, 1977
35. Nogueira-Campos CR: Efeitos do progestágeno acetato de medroxiprogesterona na glãndula submandibular e no tecido de granulação de ferida cirúrgica cutănea em camundongos. Estudo Ponderal, Histológico e Histoquimico. Araçatuba, Faculdade de Odontologia — Unesp, 1982 (Tese de Mestrado)
36. Paulo E, Szoltys M: Steroid hormone content in the submandibular gland of normal and pregnant rats. Archs Oral Biol, 27: 887, 1982
37. Piza IG: Determinacao de diametros médios em micrometria. I — Obtencao da ortogonalidade entre o maior e o menor diametro, através de ocular micrométrica simples. Semina, 4: 467, 1984
38. Raynauld J: Controle hormonal de la glande sous-maxillaire de la souris. Bull Biol Fr Belg, 94: 399, 1960
39. Rosner JM, Camara SA, Cardinali DP, Diégues ME: *In vitro* biosynthesis of androgens by rat submaxillary glands. Acta Physiol Latino Am, 15: 221, 1965
40. Rosner JM, Macome JC, Cardinali DP: *In vitro* biosynthesis of steroids and steroids by rat submaxillary glands. Endocrinology, 85: 1000, 1969
41. Schaefer A: Micro-stereology. The mathematical basis of stereology. New Dev Techn (Wild Heerbrug Ltd Precision. Instruments Makers Microscopy Division), 7: 3, 1970
42. Snedecor GW: Statistical methods. (5th Ed.) Iowa State College Press 1956, p. 557
43. Takuma T, Nakamura R, Hosoi K, Kumegawa M: Binding protein for 5-α-dihydrostestosterone in mouse submandibular gland. Biochim Biophys Acta, 496: 175, 1977
44. Tames DR: Efeitos da castracão na modulação estrutural e bioquimica dos ductos granulosos da glandula submandibular do camundongo. Sao Paulo, 1979. p. 94 (Tese de Doutoramento Instituto de Ciências Biomédicas, USP.)
45. Toennies G: The oxidative convertion of casein into protein free of methionine and tryptophane. J Biol Chem, 145: 667, 1942
46. Travill A: The effect of pregnancy on the submandibular glands of mice. Anat Rec, 155: 217, 1966
47. Vermeulen A, Ando S: Prolactin and adrenal androgen secretion. Clin Endocrinol, 8: 295, 1978
48. Wilson JD, Gosdstein JL: Evidence for increased cytoplasmic androgen binding in the submandibular gland of the mouse with testicular feminization. J Biol Chem, 247: 7342, 1972

Acta Morphologica Hungarica 37 (3—4), pp. 147—153 (1989)

GAP JUNCTIONS BETWEEN HUMAN T-COLONY CELLS

T. NEUMARK, D. C. HUYNH

NATIONAL INSTITUTE OF RHEUMATOLOGY AND PHYSIOTHERAPY, BUDAPEST, HUNGARY

(Received 6 December 1988)

T-cell colonies formed in liquid or semisolid cultures of stimulated human blood mononuclear cells were investigated under electron microscope. Typical gap junctions with five-layered structure were demonstrated between colony cells embedded in water miscible resin. The overall thickness of the junctional zones was less than 25 nm. The intercellular gap was demonstrated by lanthanum nitrate staining. Close membrane associations were observed after normal embedding with a junctional width of 20—35 nm corresponding to gap junctions.

The functional importance of free communication between colony cells is discussed.

Keywords: Gap junction, T-colony cells

Introduction

Lymphocytes undergo blastic transformation and divide intensively after proper stimulation. Phytohaemagglutinin (PHA) is a well-known stimulant for T-cells, resulting in cell division associated with transformation and colony formation. The interaction of cells and the appearance of clusters of transformed T-cells suggest that intercellular communications may be involved in the process of cell division and differentiation. The exchange of biologically active substances through intercellular junctions is a possible mechanism involved in cellular immune actions [1].

The gap junction represents a close membrane interaction at distinct sites of plasma membranes facilitating the transport of both ions and larger molecules [2, 3, 4, 5]. This type of cell cooperation is believed to play an important role in many biological processes involved in the control of ontogeny of the immune responses as well [6]. Morphological evidence has been presented on close contacts between rabbit spleen lymphocytes in culture [7].

The present study describes the occurrence of gap junctional structures between PHA-stimulated human T-colony cells.

Send offprint requests to: Dr. T. Neumark, Dept. of Electron Microscopy, National Inst. of Rheumatology and Physiotherapy, Budapest 114, POB 54, H-1525, Hungary

Materials and methods

1. Peripheral blood mononuclear cells (PBMC)

Mononuclear cells were isolated from peripheral heparinized blood of healthy persons on a Ficoll-Hypaque gradient. The PBM cells consisted of both lymphocytes (85—90%) and monocytes (about 10%). The viability of cells as tested by trypan blue exclusion, was greater than 95%.

2. PHA colony formation in liquid culture

10^5 PBMC were suspended in 1 ml of RPMI-1640 medium containing 20% heat inactivated foetal calf serum (FCS, Human, Hungary) and 5×10^{-5} M 2-mercaptoethanol (Serva, Germany). The suspension was incubated with 5 μl of PHA-P (1 mg/ml) (Difco, USA) at 37 °C in humidified air with 5% CO_2 for 18 h. The sedimented PHA-treated cells were resuspended and cell aggregates dispersed gently. The suspension was then plated, in flat bottom 96 well microculture plates (100 μl per well). Cultures were incubated for 6 days in Assab incubator containing 5% CO_2.

3. Lymphocyte stimulation with PHA in agar culture

PBMCs were suspended at a concentration of 10^6 per ml in RPMI-1640 containing 10% FCS and were incubated with 0.5% PHA at 37 °C in humidified air with 5% CO_2 for 18 h. The PHA-pretreated cells were washed twice and resuspended. Viable cells were counted. One million of PHA stimulated PBMC were added to 1 ml of mixture of double strength RPMI-1640 and 0.6% agar (Difco, USA) in double distilled water previously boiled for 2 min, and held at 37 °C. It was poured into a 10 × 35 mm sterile Petri dish and allowed to gel. The culture was kept at 37 °C in 5% CO_2 humidified air for 6 days.

In both agar and liquid medium cultures, round shape aggregates containing more than 50 cells were counted as colonies under an inverted microscope.

4. Electron microscopy

On the sixth day of culture, colonies were harvested and washed twice in RPMI-1640 and fixed as follows:

a) The largest colonies were picked out from the liquid medium and fixed in a 1.5% paraformaldehyde-glutaraldehyde mixture in 0.1 M sodium cacodylate buffer at pH 7.2 for 1 h at room temperature. After fixation the colonies were pre-embedded in 2.5% agar in distilled water.

b) The largest colonies grown in the agar medium were cut out of the gel, dissected in about 2 × 2 mm size and fixed as mentioned above.

In both cases lanthanum-containing fixatives were also used according to Neaves [8]. After fixation, colonies were washed three times in 0.1 M sodium cacodylate buffer at pH 7.2 and dehydrated partly with graded series of water miscible Durcupan in distilled water and in graded series of ethanol and propylene oxide.

Finally, all the colonies were embedded in Spurr's medium. Ultrathin sections were stained with uranyl acetate and lead citrate and investigated under a JEM 100 CX electron microscope equipped with a side entry goniometer with a specimen tilt angle ±60°.

Results

The colonies grown either in agar or in liquid medium showed the same morphological features. The majority of colony-forming cells were lymphoblasts.

The low-power examination of colonies has shown close membrane associations or simple junctional areas between cells (Fig. 1). By using water miscible embedding substance it was clearly seen that the extracellular space

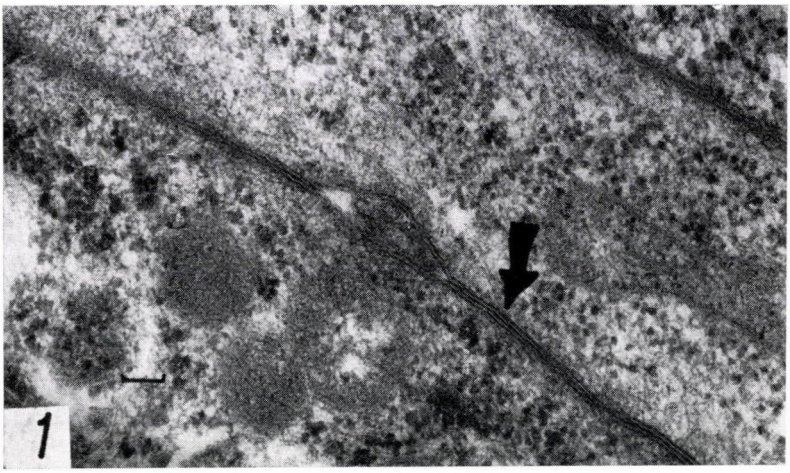

Fig. 1. Extended gap junction between two lymphoblasts (Arrow). Water-miscible embedding. ×50 000

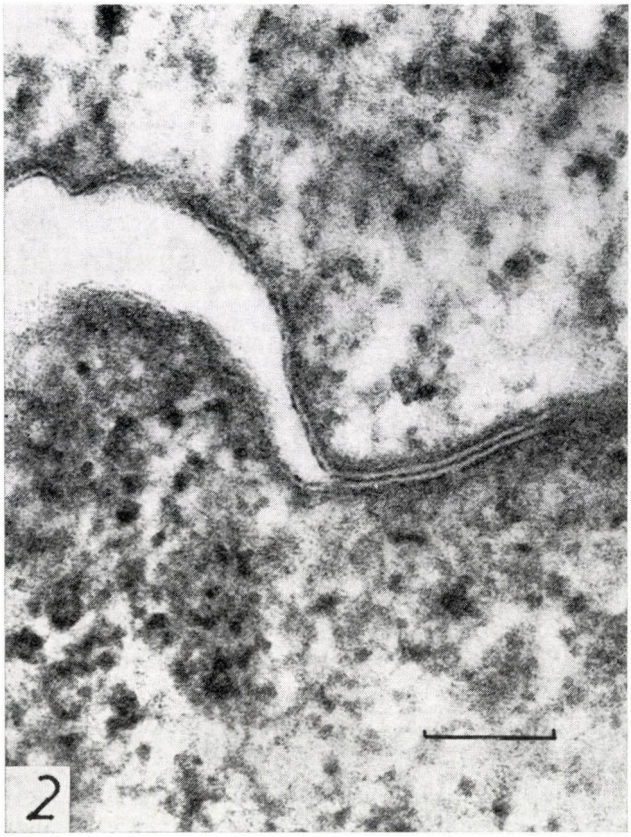

Fig. 2. At high magnification the two membranes appear to fuse. ×165 000

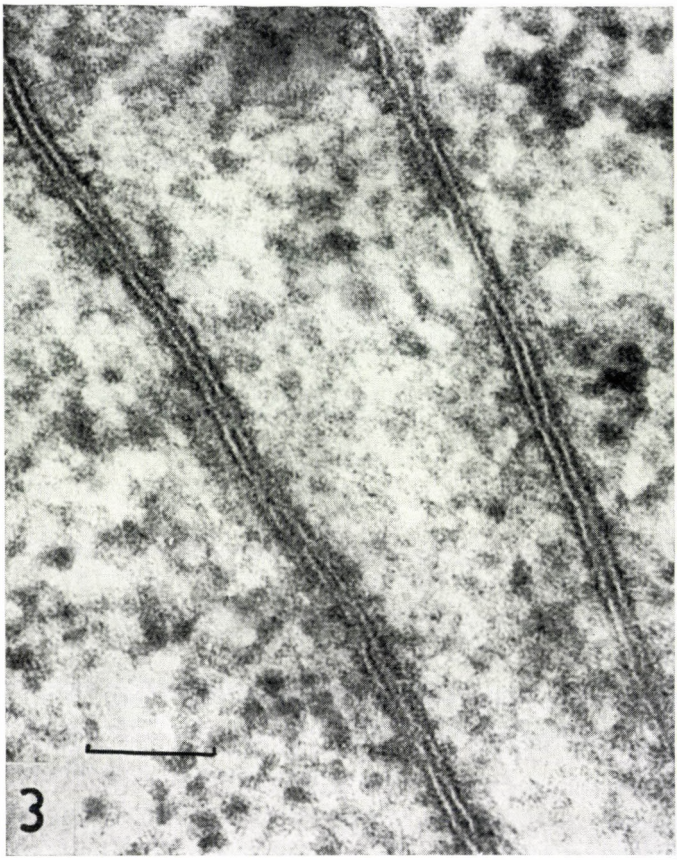

Fig. 3. At high magnification the five layers of the junctional zone characteristic for gap junction is well visible. Water-miscible embedding. ×165 000

between the outer layers of adjacent cytoplasmic membranes was greatly reduced or appeared to fuse. The overall width of the junctional zone was about 25 nm (Fig. 2). By means of the goniometer, its five-layered structure was also proved (Fig. 3). The central electron dense thick layer was composed of the two outer leaflets of cytoplasmic membranes with a narrow gap which was proven with lanthanum nitrate staining (Fig. 4). The thickness of the intercellular space was about 2—3 nm.

In colonies dehydrated in organic solvent, junctional areas similar to gap junctions without central electron dense thick layer were also observed between lymphoblasts (Fig. 5). It was clearly seen that the opposing cell membranes were separated by a rather constant gap which was less than 8 nm wide. Along gap junctions mostly ribosomes and arrays of microfilaments were observed. The colonies did not reveal other types of cell junctions either in water-soluble or in Spurr's medium.

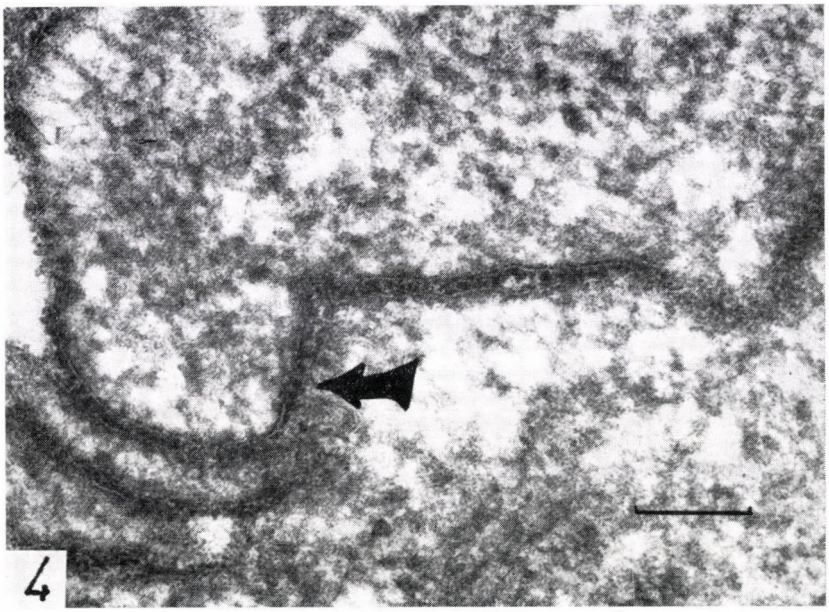

Fig. 4. After lanthanium fixation the septate intercellular gap between opposed cell membranes is clearly visible (Arrow). ×150 000

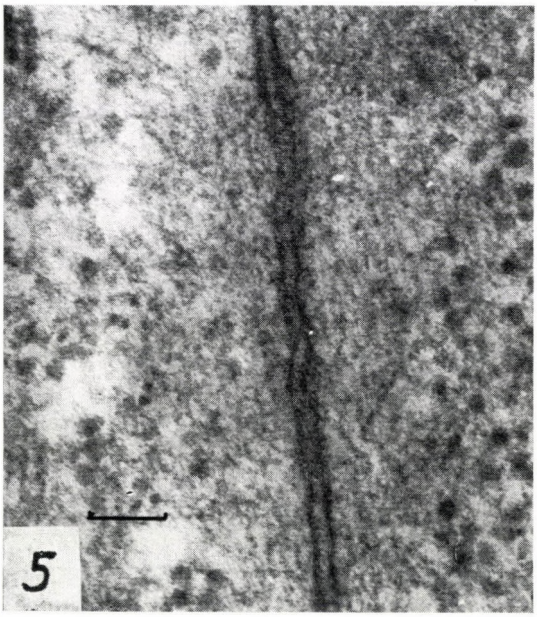

Fig. 5. Cell-cell contact between lymphoblasts in colonies dehydrated in organic solvent. Note the close membrane association between two plasma membranes. ×100 000

Discussion

The occurrence of gap junctions between T-colony cells stimulated by PHA both in agar and in liquid medium is described in this paper. The character of gap junction in colonies formed in two types of culture medium seems to be identical.

The exposure of cells to ethanol probably causes some changes in the characteristic five-layered composition of gap junction. The intercellular gap between outer leaflets of plasma membrane becomes wider as compared to gap junctions in sections prepared avoiding ethanol treatment. The cause of this can be the shrinkage of the cell by ethanol or some alterations of the physicochemical properties of plasma membrane during dehydration. Further studies are needed to clarify this problem.

Concerning the function of gap junctions, there is a great deal of information indicating that gap junctions are involved in intercellular communication. Ionic flow between electrotonically coupled cells is believed to occur at gap junctions [9]. Furthermore, in many cellular systems, gap junctions allow the intercellular exchange of particles larger than ions such as dye molecules and labelled nucleotides [2, 4, 10].

The maximum molecular weight for substances freely passing the gap junctions is about 1000 daltons (1200 according to Simpson et al.) [11]. These include biologically active substances as steroids vitamins and nucleotides [5]. Recent studies have implicated gap junctions in the differentiation of cells in several systems including mesoderm of chick limb bud [12], sebaceous gland [13], wound healing [14], oocyte maturation [15], liver generation [16], and PHA-stimulated rabbit spleen cells [7]. The gap junctions between T-colony cells observed in this study seem to be related to the function of these cells. We suggest that the mutual exchange of nucleotides through gap junctions would be a simple coordinating control over the differentiation of lymphocytes and the growth of colonies. It would be interesting if gap junctions were related somehow to the responsiveness of T-colony cells for the colony stimulating factors. However, the molecular weight of these factors seems to contradict to a passive cell-to-cell transmission via gap junctions.

Acknowledgement

We would like to thank Judit Rahoi for the valuable technical assistance and Dr. Katalin Merétey for the helpful discussions.

REFERENCES

1. Peracchia C, Dulhunty AF: Low resistance junctions in crayfish: Structure changes with functional uncoupling. J Cell Biol 70: 419, 1976
2. Gilula NB, Reaves OR, Steibach A: Metabolic coupling, ionic coupling, and cell contacts. Nature 235: 262, 1972

3. Benett MUL: Function of electronic junctions in embryonic and adult tissues. Fed Proc 32: 65, 1973
4. Staphaelin LA: Structure and function of intercellular junctions. Int Rev Cytol 39: 191, 1974
5. Loewenstein WR: Cellular communications by permeable membrane junctions. In: Wismann G, Claiborne R. (eds) Cell Membranes: Biochemistry, Cell Biology, and Pathology H. P. Publishing Co., New York 1975, p. 105
6. Loewenstein WR: Cellular communication through membrane junctions. Arch Intern Med 129: 299, 1972
7. Kapsenberg ML, Leene W: Formation of B type gap junctions between PHA-stimulated rabbit lymphocytes. Exp Cell Res 120: 211, 1979
8. Neaves W: Permeability of sertoli cell tight junctions to lanthanum after ligation of ductus deferens and ductuli efferentes. Cell Biol 59: 559, 1973
9. Azarnia R, Loewenstein WR: Intercellular communication and tissue growth. J Membr Biol 6: 368, 1971
10. Kalderin N, Epstein ML, Gilula NB: Cell-to-cell communication and myogenesis. J Cell Biol 75: 788, 1977
11. Simpson L, Rose B, Loewenstein WR: Size limit of molecular permeating the junctional membrane channels. Science 195: 294, 1977
12. Kelley RO, Fallon JF: Identification and distribution of gap junctions in the mesoderm of the developing chick limb bud. J Embriol Exp Morph 46: 99, 1978
13. Kitson N, Van Lennep EW, Young JA: Jap junctions in human sebaceous glands. Cell Tissue Res 190: 115, 1978
14. Gabbiani G, Chaponier C, Huttner I: Cytoplasmic filaments and gap junctions in endothelial cells and myofibroblasts during wound healing. J Cell Biol 76: 561, 1978
15. Gilula NB, Epstein ML, Beers WH: Cell-to-cell communication and ovulation. A study of the cumulus-oocyte complex. J Cell Biol 78: 58, 1978
16. Yee AG, Revel JP: Loss and reappearence of gap junctions in regenerating liver. J. Cell Biol. 78: 554, 1978

Acta Morphologica Hungarica 37 (3—4), pp. 155—168 (1989)

ANALYSES OF THE TIDEMARK ON HUMAN FEMORAL HEADS

I. HISTOCHEMICAL, ULTRASTRUCTURAL AND MICROANALYTIC CHARACTERIZATION OF THE NORMAL STRUCTURE OF THE INTERCARTILAGINOUS JUNCTION

R. Oettmeier[1], K. Abendroth[2], Sabine Oettmeier[3]

[1]ORTHOPEDIC CLINIC AND [2]CLINIC OF INTERNAL MEDICINE, DEPARTMENT OF RHEUMATOLOGY AND OSTEOLOGY FRIEDRICH SCHILLER UNIVERSITY OF JENA, [3]DISTRICT DENTAL DEPARTMENT, EISENBERG, EAST-GERMANY

(Received 7 December 1988)

The tidemark as a boundary between non-calcified and calcified articular cartilage has a complicated structure and fulfils various physiological functions. 25 human femoral heads from healthy joints were examined. In non-decalcified preparations three structural components of the tidemark were demarcated: (1) the PAS-positive, proteoglycan-containing tidemark line adjacent to the basal cartilage, (2) the sublinear light-coloured zone and (3) the demarcation line to the calcified cartilage. Using scanning electron microscopy, the tidemark was characterized as an electron-dense impression between hyaline and calcified cartilage. The presence of specific architecture and orientation of collagenous fibres could not be shown.

Concentrations of calcium, phosphorus and sulphur could not be detected in the tidemark by means of an X-ray microanalyzer. A morphological model of the tidemark region was established, which represents the intercartilaginous junction as a double layer of substantially and functionally different surfaces.

Keywords: Tidemark, articular cartilage, electron microscopy, joint, X-ray microanalysis

Introduction

The junction between hyaline articular cartilage and the adjacent calcified cartilage is known as the tidemark (TM) or line of demarcation [9, 11]. On demineralized slices stained with haematoxylin and eosin (HE), the TM appears as a thin, basophilic, undulated line, which separates calcified and non-calcified articular cartilage. The TM was found to contain calcium, phosphate, collagenous fibres, neutral and acidic phospholipids and unsaturated fatty acids [10]. The region was shown to be free of low- and high-molecular mucopolysaccharides. The continuous crossing of collagen fibres from the hyaline to the calcified cartilage was determined by fibre stainings, polarized optical methods and finally by using scanning electron microscopy (SEM) [12].

Send offprint requests to: Dr. Ralf Oettmeier, Friedrich Schiller University, Orthopaedic Clinic, Rudolf Elle Hospital, Eisenberg (Thüringia) 6520, DDR

Apart from these fibres, it was hardly possible to find the submicroscopical correlate of histochemical features. The functional significance of the TM as barrier of mineralization and anchor of the highly compliant hyaline cartilage to its rigid base is generally accepted [6].

Histological examinations of the TM region using paraffin-embedded specimens have the drawback that on account of demineralization, some information about mineralization, composition and morphology of the TM seem to be lost.

In this study we have analyzed the normal structure of the TM on human femoral heads. After processing without decalcification, many histochemical methods, SEM and X-ray microanalysis were used. Drawing conclusions from our own findings and some references of the literature, a structural model of the TM was developed and discussed.

Materials and methods

Altogether 50 bone specimens from 25 human femoral heads were examined. 13 joint heads were resected in the course of total hip arthroplasty from patients with medial femoral neck fracture with an average age of 74.4 years (range 66—84 years). 12 femoral heads were obtained at necropsy showing no macroscopic signs of osteoarthrosis. The average age of the deceased persons was 59.3 years (range 36—72 years). After medial-sagittal bisection of the femoral head we took bone specimens of the load and non-load pressure area. These were fixed for at least 36 h in Carnoy's solution, dehydrated in ethanol and embedded in methyl methacrylate by means of underpressure (in an exsiccator) and ultrasound (3×1 min). With a hard cut microtome (Fi. Jung, Heidelberg/FRG four micron thick slices were obtained, deplastified in toluol and stained by the following methods: HE, trichrome staining method of Ladewig (modified Goldner reaction), Gömöri's silver staining, PAS-reaction, gallamine-blue Giemsa staining, von Kossa, safranin O method and finally the collagen reaction according to Crossmon.

Six plastic-embedded, 7 micron thick sections of normal cartilage-bone tissue were allowed to air dry and then coated with carbon. The determination of concentration and distribution of mineral compounds was carried out on the same sections with the help of an X-ray microanalyzer. It was possible to couple photographically the SEM micrographs with the appropriate distribution pattern of calcium, phosphorus and sulphur.

Results

a) Histology

The trichrome staining method of Ladewig was very useful for TM analyses in non-decalcified preparations. On intact articular cartilage the TM was shown as a continuous demarcation between hyaline and calcified cartilage (Fig. 1). After higher magnification it was possible to subdivide the TM into three parts (i) the granular, undulated *line of the TM* adjacent to basal hyaline cartilage, (ii) the *sublinear light-coloured line* below the TM line and (iii) the *demarcation line to the calcified cartilage*. The colouring of the *TM line* was similar to the osteoid in this staining. In 82% of preparations examined the

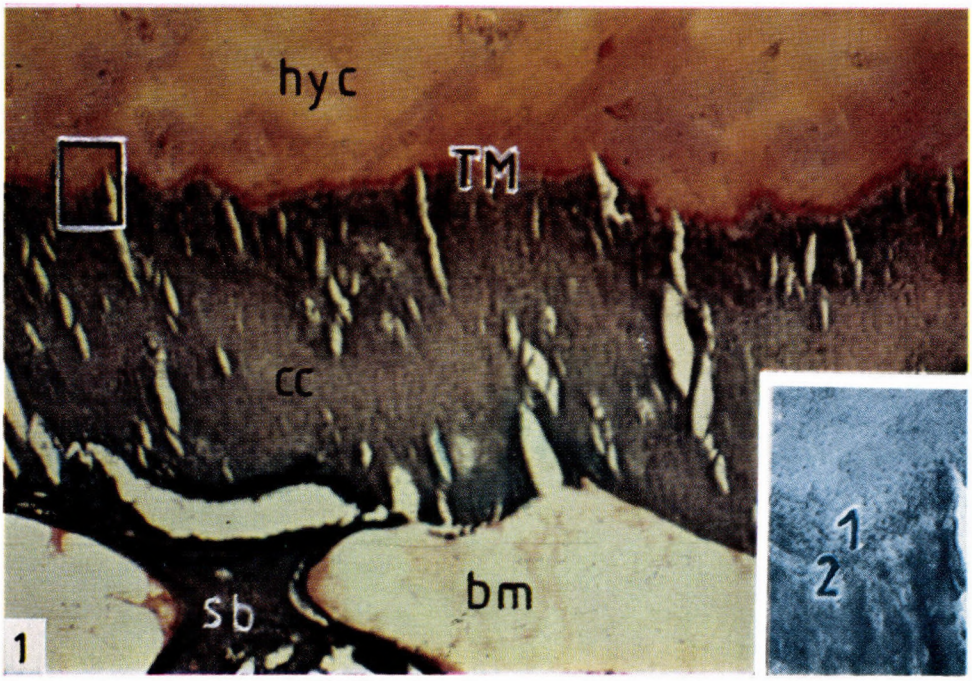

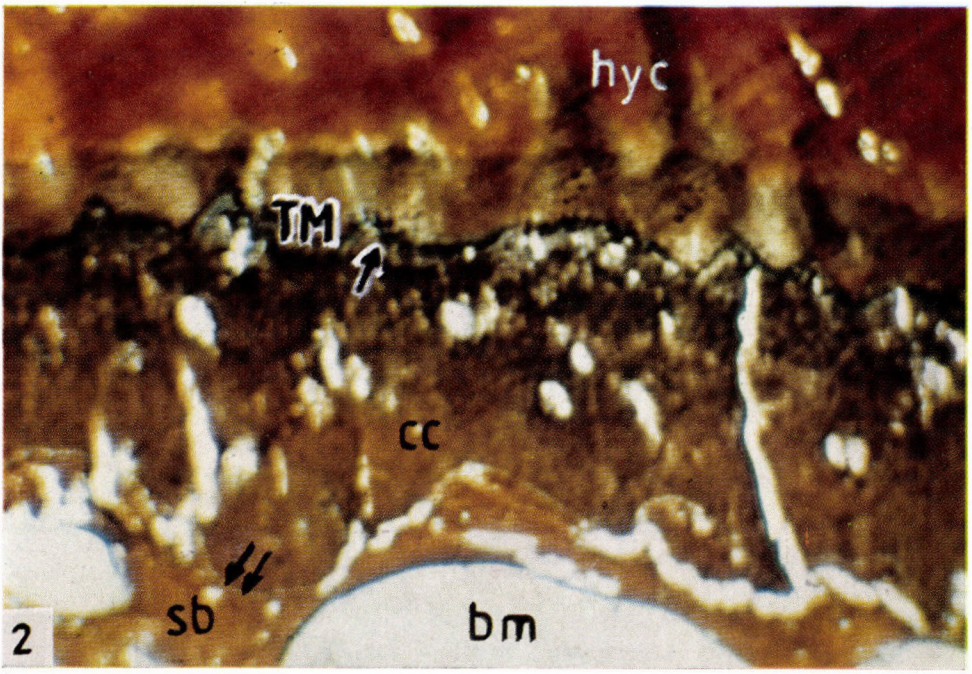

Fig. 1. Photomicrograph demonstrating the two main components of the tidemark (TM): (1) the red-stained *TM line* adjacent to basal hyaline cartilage (hyc) and (2) the *sublinear light-coloured line* adjacent to the calcified cartilage (cc.). Subchondral bone (sb) and fatty bone marrow (bm) are visible (methyl methacrylate, Ladewig's trichrome staining, ×120, inset ×280)

Fig. 2. Photomicrograph of the TM region stained with Gömöri's silver technique. Beside the TM line and sublinear light-coloured line appears the demarcation line to the calcified cartilage (single arrow). Note the similarity between sublinear light-coloured zone and the apparent cement line (double arrows), (abbreviations see Fig. 1, methyl methacrylate, ×120)

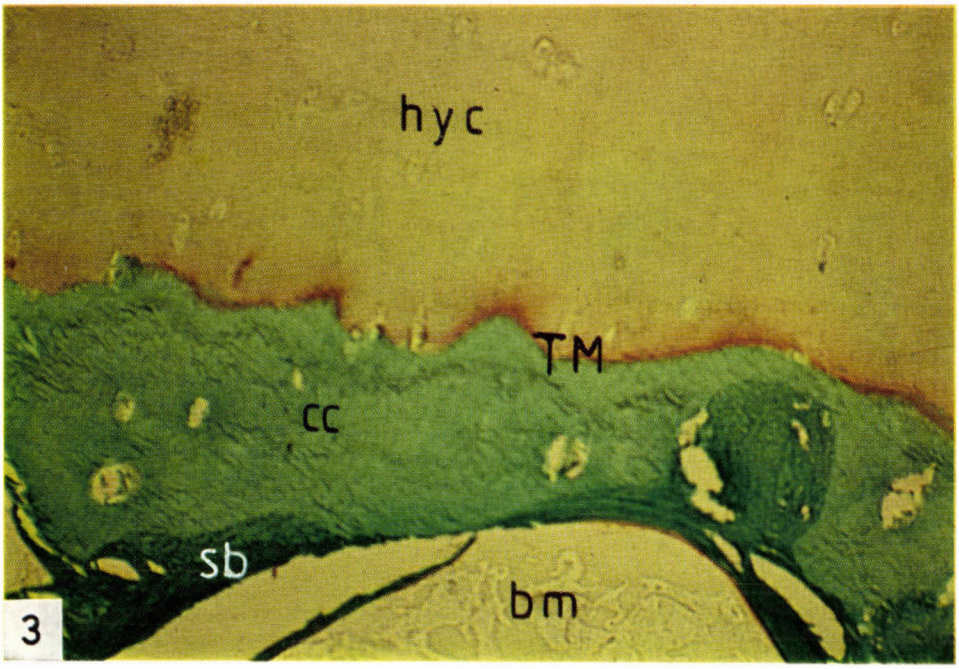

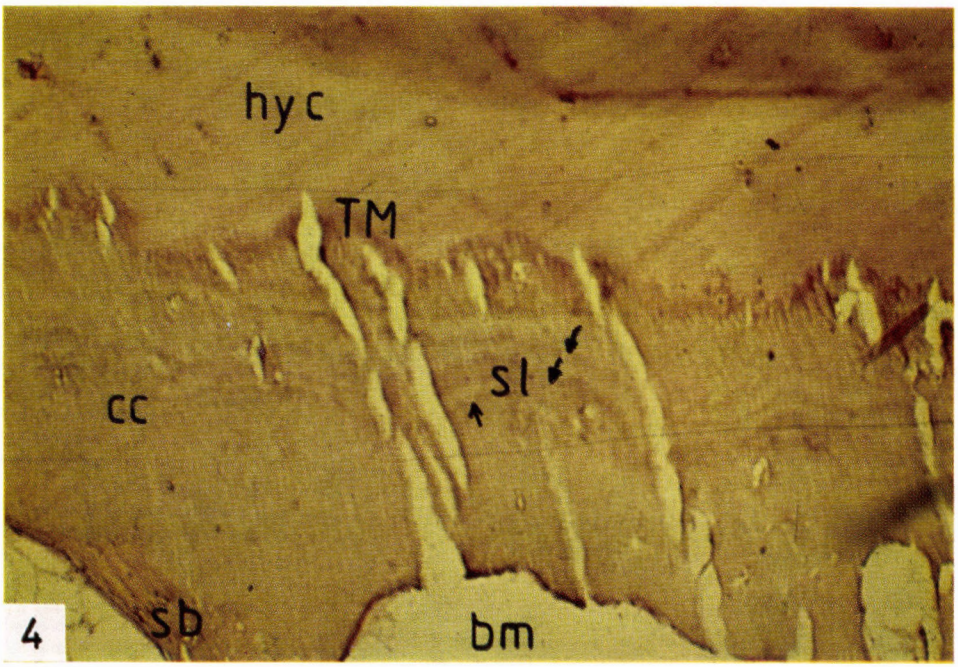

Fig. 3. Intensive collagen reaction of the *TM line* (abbreviations see Fig. 1, methyl methacrylate, Crossmon's staining method, ×120)

Fig. 4. TM region stained with HE on non-decalcified preparation. The TM is only vaguely seen. Weak "secondary lines" (sl) in the calcified cartilage are visible, but demonstrating no true multiplications of the TM (abbreviations see Fig. 1, ×120)

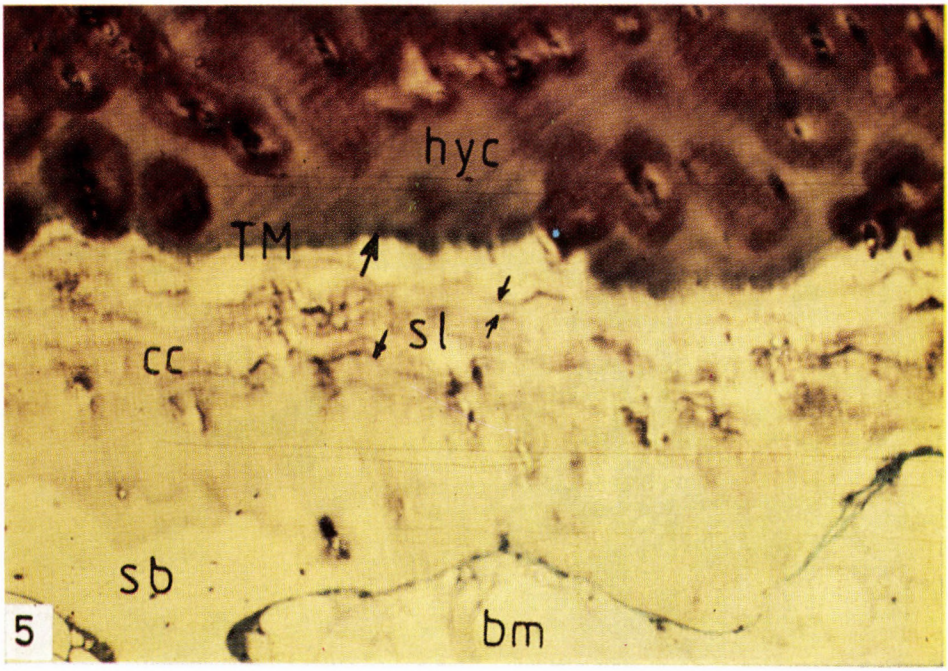

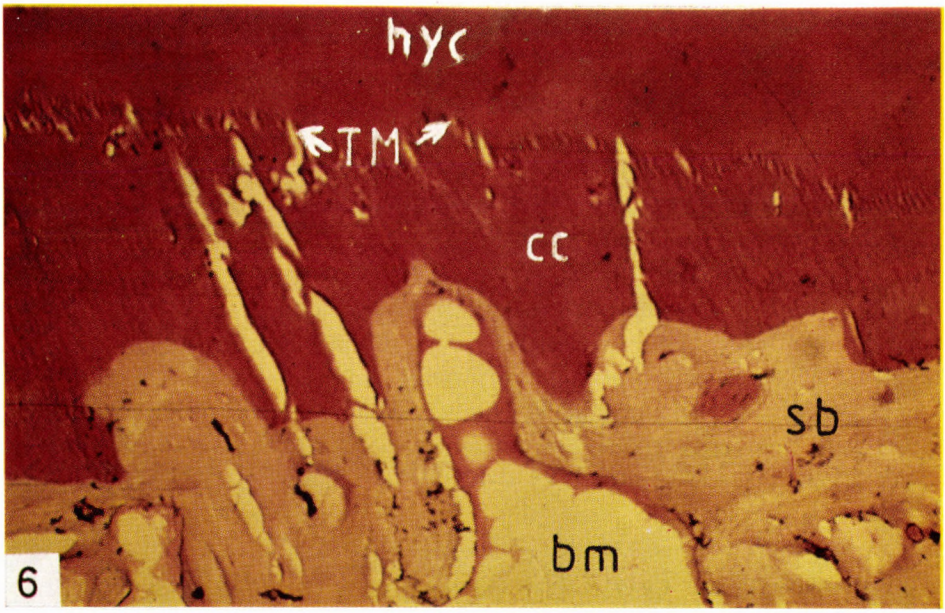

Fig. 5. Photomicrograph of the basal part of normal articular cartilage from the femoral head stained with gallamine-blue Giemsa. Note the positive matrix colouring of the *TM line* (arrow) and the appearance of "secondary lines" (sl) in the calcified layer (abbreviations see Fig. 1, methyl methacrylate, ×120)

Fig. 6. Positive PAS reaction of the TM and of hyaline and calcified cartilage (abbreviation see Fig. 1, methyl methacrylate, ×120)

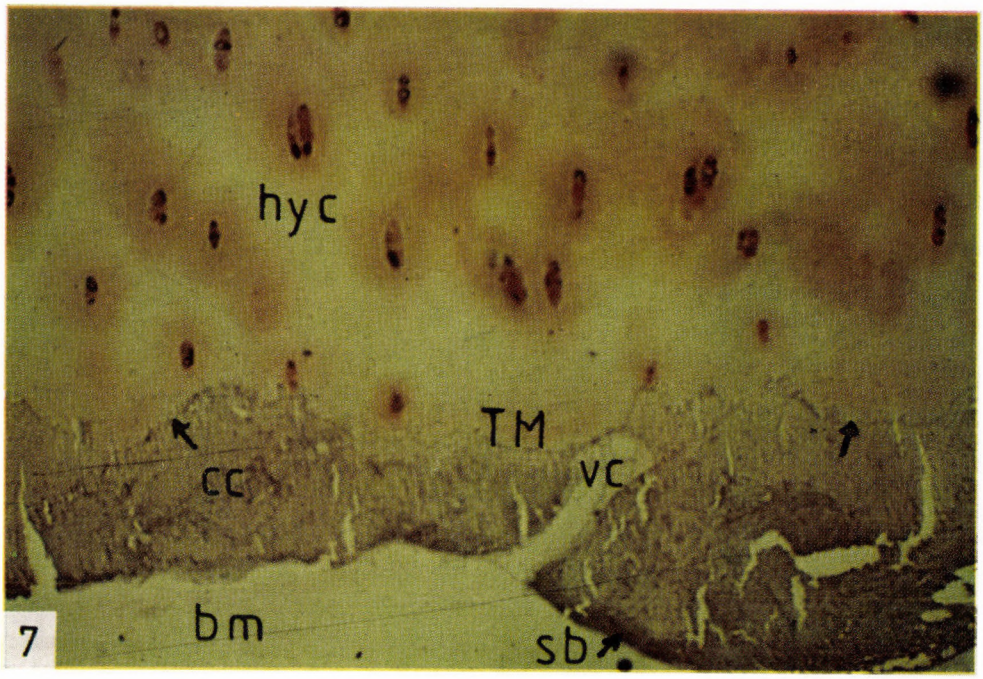

Fig. 7. Photomicrograph of the TM region stained with safranin O. Note the pericellular proteoglycan staining stops abruptly at the *sublinear light-coloured line.* Additionaly, the demarcation line to the calcified cartilage (arrow) and a large vascular channel (vc) are visible (abbreviations see Fig. 1, methyl methacrylate, ×120)

TM could be subdivided into the above mentioned three components, showing no signs of duplications and other TM changes. These parts could also be shown by silver staining after Gömöri (Fig. 2) and collagen reaction after Crossmon (Fig. 3). Note that the *light-coloured line* was similar to the cement line between calcified cartilage and subchondral bone plate. The representation of the TM in the HE staining was poor (Fig. 4). In the gallamine-blue and HE staining we often found weak lines in the calcified cartilage (Figs 4, 5). We called them "secondary lines", because they were not multiplications of the TM. Especially in the non-loaded zone of the joint heads these "secondary lines" were frequently observed. Together with the hyaline and calcified cartilage, the TM was mostly PAS-positive (Fig. 6). In the *TM line* we could clearly show proteoglycan, using the safranin O reaction (Fig. 7). In the von Kossa staining, calcified cartilage and subchondral bone plate appeared homogeneously black. Phosphate-containing granules could be demonstrated in the intercartilaginous junction (Fig. 8). Additionally, this staining allowed to see argyrophilic star-like particles in the hyaline cartilage demarcated from the TM. These particles were concentrated around chondrons, seemed to be fibre-oriented and their size decreased towards the surface (Fig. 8).

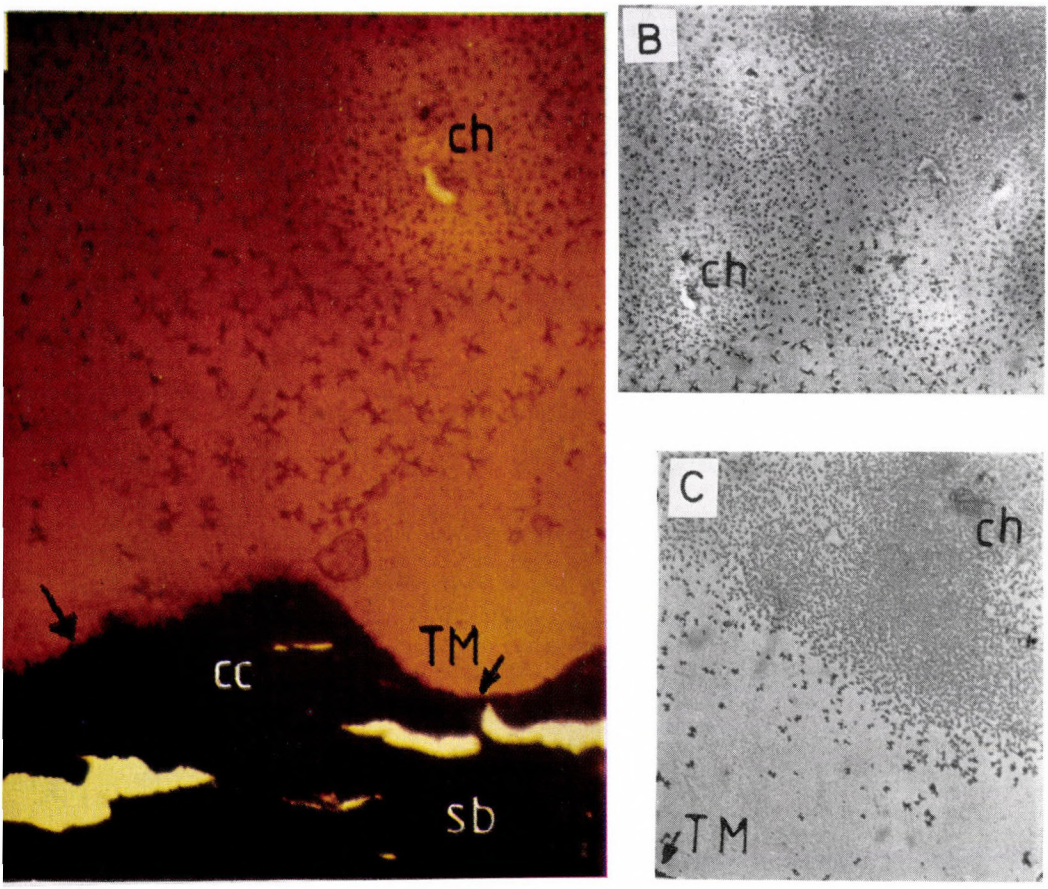

Fig. 8. Photomicrograph of a plastic-embedded section stained with the von Kossa method. A. The red *TM line* with some phosphate granules (arrows) is visible. Starlike argyrophilic particles are concentrated arround chondrons and are demarcated from the TM (counterstained with Masson's trichrome method, ×120). B. Argyrophilic particles surrounding the chondrocytes (ch) in the intermediate zone of hyaline cartilage (×200). C. Another portion showing clearly the argyrophilic particles and their demarcation from the TM (abbreviations see Fig. 1, ×200)

b) SEM observations

In non-decalcified slices the TM could be clearly identified with SEM (Fig. 9). The electron-dense depression adjacent to basal cartilage was attributed to the *TM line*. Some differences were observed in the structural features of hydroxyl apatite in calcified cartilage and subchondral bone. Because of the embedding of minerals and matrix compounds no conclusions could be drawn concerning the specific orientation of collagenous fibres in the TM region.

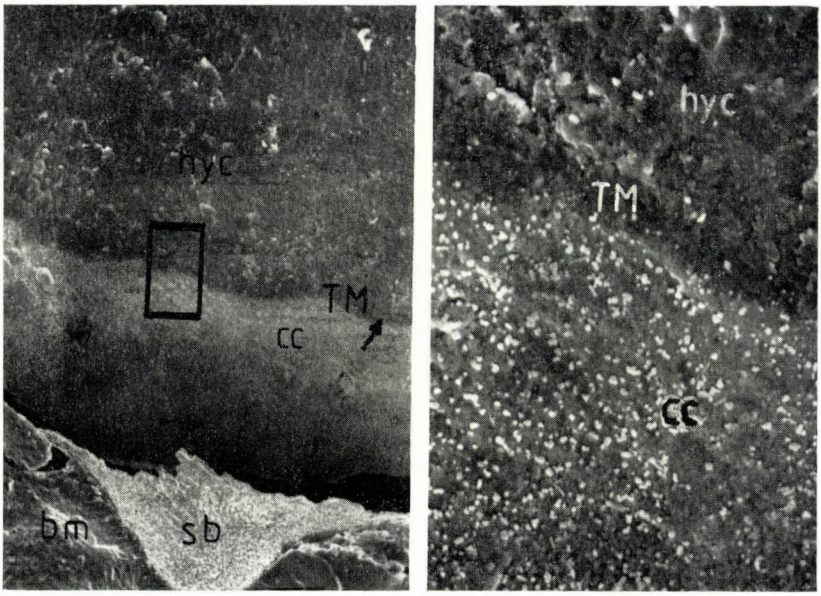

Fig. 9. SEM micrograph of the TM region on non-decalcified cartilage-bone tissue showing the TM as a dark depression (arrow) between the non-calcified (hyc) and calcified cartilage (cc). Note the hydroxyl apatite crystals in the calcified layer (A ×300, B ×3000)

c) X-ray microanalysis

The most important chemical elements in the TM region were calcium (380 counts/100 s), phosphorus (315 counts/100 s) and sulphur (425 counts per 100 s). Low concentrations of silicon (235 counts/100 s), iron (220 counts/100 s), chlorine (215 counts/100 s) and magnesium (205 counts per 100 s) were also detected. The distribution pattern of these main elements could be demonstrated in Fig. 10 in comparison to the appropriate SEM micrograph. The concentration of calcium and phosphorus was not different in the calcified cartilage and subchondral bone plate. Because of the sulphated matrix compounds, sulphur was especially concentrated in the hyaline cartilage. At higher magnification no concentrations of calcium, phosphorus or sulphur demonstrated specific for the TM (Fig. 11).

Discussion

According to Dmitrovsky et al. [10] the TM was found to have two histologically distinct components: (i) an indistinct and wider granular zone adjacent to the non-calcified cartilage, and (ii) a continuous smooth line approximately 5 microns wide adjacent to the calcified layer. Additionally

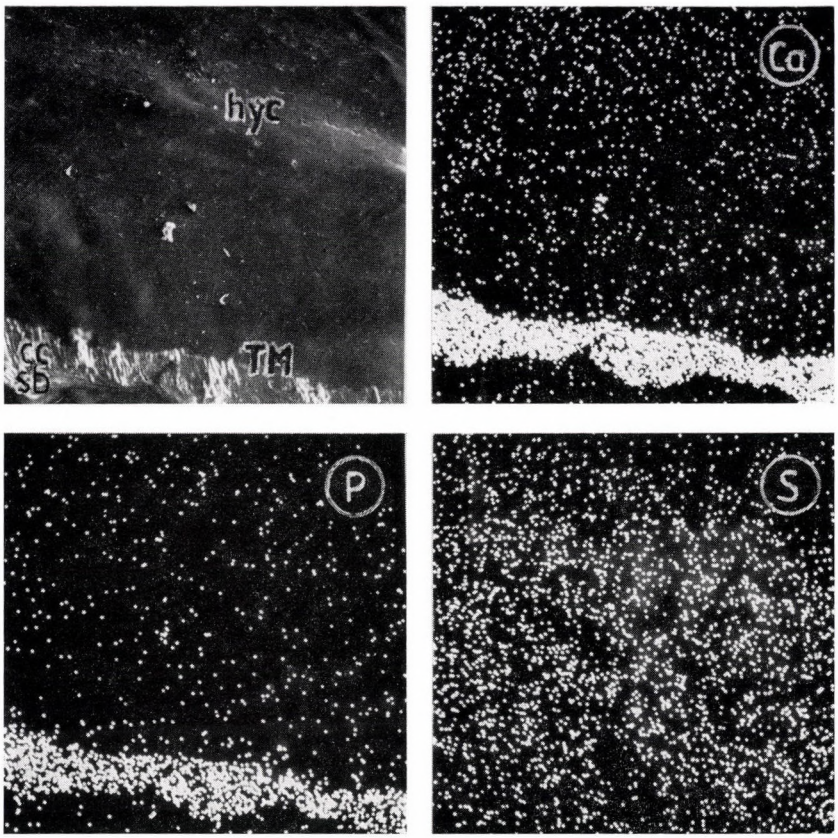

Fig. 10. SEM micrograph and the appropriate X-ray microanalysis of this region showing the distribution pattern of calcium (Ca), phosphorus (P) and sulphur (S). Note the concentration of sulphur in the hyaline cartilage (hyc). The concentration of calcium and phosphorus in the calcified cartilage (cc) and subchondral bone (sb) is fairly similar (plastic-embedded section, ×60)

we have determined the demarcation line to the calcified cartilage, which is mostly visible as a separate structure in various histological stainings. Polarized optical observations have corroborated the continuous crossing of collagenous fibres through the TM region [12, 15, 16]. Redler et al. [21] have observed by SEM three distinct morphological orientations of collagenous fibrils in the TM.

In accordance with Hough et al. [16], we demarcated submicroscopically the TM only as an electron-dense depression between the calcified and non-calcified articular cartilage. The embedding of matrix and mineral components is the reason for the poor representation of fibre architecture in non-decalcified preparations. On the other hand, the clear determination of the TM cannot be reliably made with SEM after demineralization [14].

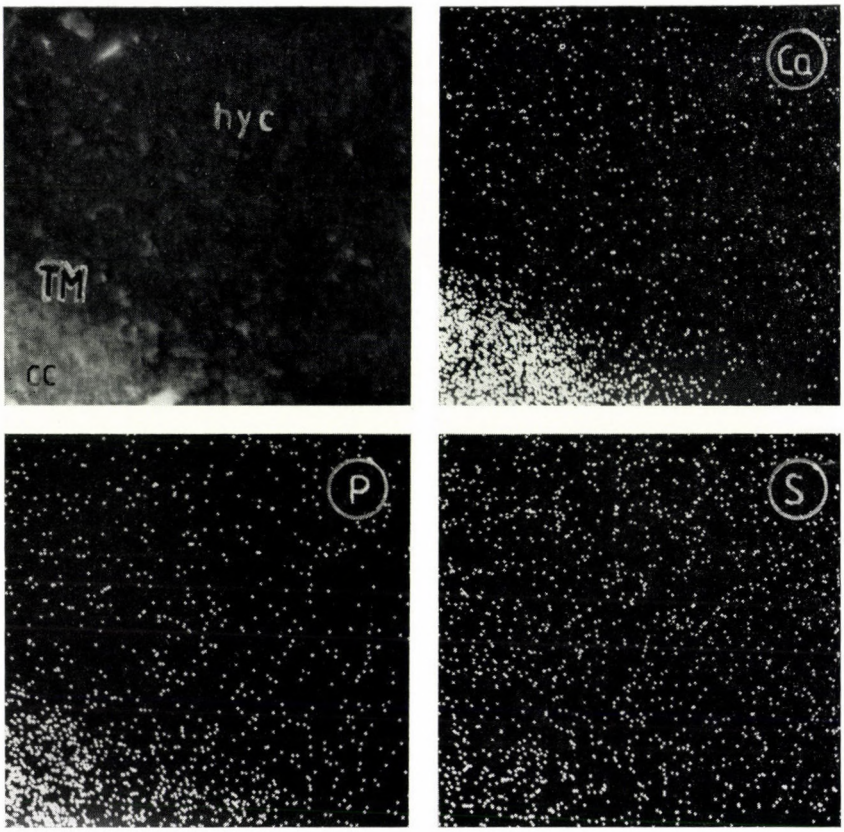

Fig. 11. The TM region of the same sample as shown in Fig. 10 after higher magnification. No separate concentrations of determined elements in the TM are visible (SEM and X-ray microanalysis, plastic-embedded section, ×1000)

Histologically, the enrichment of collagen in the *TM line* was obvious (see Fig. 3). Although structure and composition of collagen in the TM show according to Boskey et al. [4] no significant differences in comparison to the articular cartilage, the reactivity with collagen dyes is increased. Partially unmasked collagenous fibrils are perhaps responsible for this phenomenon. Contrary to the results of Dmitrovsky et al. [10], the TM, especially the *TM line*, shows a positive PAS-reaction in our examinations. We suppose that the *TM line* contains proteoglycan contrary to the *sublinear light-coloured line*. These high molecular substances are often masked by other compounds, like pyrophosphate, hydroxyl apatite and phospholipid-calcium complexes.

Using 2% osmium tetroxide and Nile-blue sulphate on fresh frozen specimens, the TM stained strongly for neutral and acidic lipids and unsaturated fatty acids [10]. Lipids and especially calcium-phospholipid-phos-

phate complexes could also be shown in other mineralization fronts. These complexes are claimed to play an important role as promotors of calcification [3, 5]. Indeed, the total lipid amount shows no differences between articular cartilage and TM [4]. After normal fixation the lipids are removed from the tissue [12]. However, phospholipid-calcium complexes are able to stay partially in the TM region which explains some of the observed staining phenomena [2]. It is our opinion that in unfixed native preparations the lipids and lipid complexes are concentrated in the described *light-coloured line*. This view is supported by the observation of some authors that manipulations on bone-cartilage slices lead to lacerations in the TM region [6, 14]. The TM seems to be a highly vulnerable zone.

As reported by Dmitrovsky et al., the TM did not stain for proteoglycan and the pericellular and intercellular matrix staining failed to appear at the TM. We suppose that this arrest of glycosaminoglycan dyes takes place on the *sublinear light-coloured line*. It is necessary to stress our observation that the colouring of the *TM line* in Ladewig's trichrome staining is similar to the osteoid containing glycosaminoglycans and collagen fibrils.

Matrix vesicles could be shown only near the TM [4, 10]. As reported by Wuthier et al. [23] and Boskey et al. [3], the complex lipid compounds can suggest the existence of matrix vesicles or some parts of them. The TM has also high alkaline phosphatase and ATPase activities [8, 10]. According to the hypothesis of Anderson [1], it is possible that the TM possesses products of matrix vesicles.

After demineralization the content of calcium in the TM seems to be increased [16]. Using X-ray microanalysis, on non-decalcified sections we found no distinct concentrations of calcium, phosphorus and sulphur specific for the TM region. We agree with Haynes [15] that the mineral contents in the calcified cartilage and mineralized subchondral bone plate are similar. Hough et al. [16] have not described significant differences in the sulphur contents in calcified and non-calcified cartilage. Our distribution analyses of sulphur clearly show the increased concentration in the hyaline cartilage especially in the intermediate zone (see Fig. 10). The sulphated matrix components of intact hyaline cartilage are responsible for this result.

The silver method of von Kossa stains PO_4^{---} specifically [10]. Phosphate granules were found in the *TM line* as well as in the hyaline cartilage around the chondrons (argyrophilic particles). These particles could mainly be pyrophosphate, which is known as an inhibitor of mineralization [4]. It was surprising that the HE staining of non-decalcified preparations showed only vague *TM lines*. The demineralization seems to promote the reaction of the dye with acidic and basic molecule groups in the TM. Furthermore, rests of calcium-phospholipid-phosphate complexes are also able to react with haematoxylin [4].

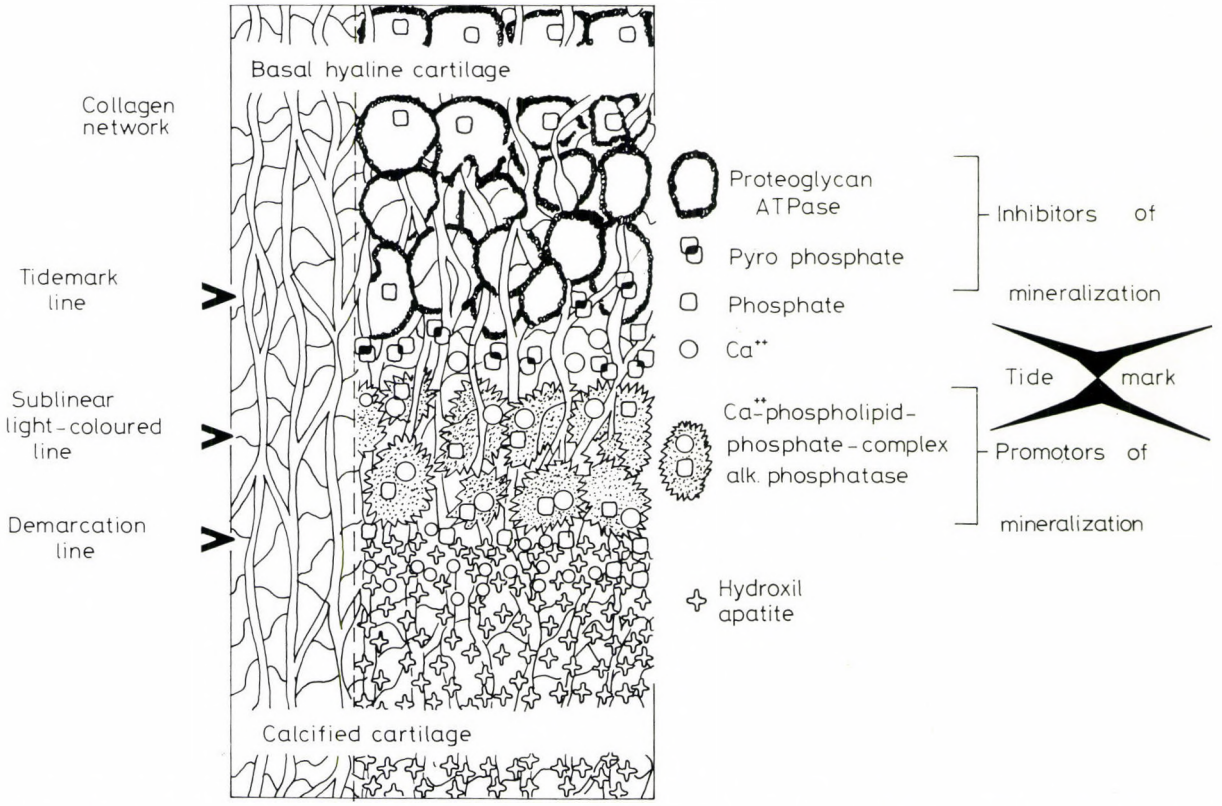

Fig. 12. Morphological and functional model of the TM in normal human cartilage. Crossing collagen fibres (see left) ensure the connection of the functionally complementary surfaces. Unmasked collagen fibrils, proteoglycans and other inhibitors of mineralization represent the *TM line*. In the *sublinear light-coloured zone* lipids, lipid complexes and other promotors of mineralization are concentrated

The described "secondary lines" in the calcified cartilage seem to represent markers of physiological subchondral remodelling and enchondral ossification. Some studies with tetracyclin-labelling showed a life-long turnover in the calcified cartilage and subchondral bone plate [15, 17, 18]. It is important for the nomenclature of the TM region that the "secondary lines" are either duplications or multiplications of the TM.

Summarizing our results and the findings from the literature we can establish the morphological model of the TM region shown in Fig. 12. The TM is not a separate membrane as reported by Havelka et al. in 1982 [13]. In agreement with Spinelli [22] we share the opinion that the TM represents a double layer of two morphologically and functionally complementary surfaces. The connection is ensured by crossing collagen fibres. Spinelli [22] has demonstrated granular and gelatinous substances on the surface of the calcified cartilage by SEM observations, which are probably calcium-phospholipid-phosphate complexes and hydroxyl apatite. These substances represent the *sublinear light-coloured line* light microscopically. In conclusion, we support the hypothesis by Boskey et al. [4] and Bullough et al. [7] that in the TM there exists a balanced system of factors promoting calcification (matrix vesicles, glycoproteins, calcium-phospholipid-phosphate complexes, alkaline phosphatase, phosphoproteins, proteolipids and others) and of calcification inhibitors (proteoglycan, ATPase, pyrophosphate, nucleotide triphosphate and others). The cells on both sides of the mineralization barrier are capable to produce these antagonistic factors and are responsible for the physiological dynamic steady state. Excessive progression of the calcification front probably results from disturbances in this equilibrium, as is shown in our following study on TM changes in osteoarthrosis [20].

Acknowledgements

The authors would like to thank the scientific assistants Mrs. Schütz and Mrs. Heinisch for making the histological preparations and Mrs. Bimberg from the Architecture and Building College in Weimar for ther generous realization of ultrastructural examinations.

REFERENCES

1. Anderson HC: Matrix vesicle calcification. Fed Proceedings 35, 105, 1976
2. Boskey AL, Posner AS: Extraction of a calcium-phospholipid-phosphate complex from bone. Calcif Tissue Res 19: 273, 1976
3. Boskey AL, Posner AS: The role of synthetic and bone extracted calcium-phospholipid-phosphate complexes in hydroxyl apatite formation. Calcif Tissue Res 23: 251—258, 1977
4 Boskey AL, Bullough PG, Dmitrovsky E: The biochemistry of the mineralization front. In: WSS Jee and AM Parfitt, (eds) Bone Histomorphometry, 3rd Int. Workshop. Suppl Metabol Bone Dis Rel Res, 1980, pp 61—68

5. Boskey AL, Posner AS, Lane JM, Goldberg MR, Cordella DM: Distribution of lipids associated with mineralization in bovine epiphyseal plate. Arch Biochem Biophys 199: 305, 1980
6. Broom ND, Poole CA: A functional-morphological study of the tidemark region of articular cartilage maintained in a non-viable physiological condition. J Anat 135: I, 65, 1982
7. Bullough PG, Jagannath A: The morphology of the calcification front in articular cartilage. J Bone Jt Surg 65-B: 72, 1983
8. Christensen SB: Osteoarthrosis — changes of bone, cartilage and synovial membrane in relation to bone scintigraphy. Acta Orthop Scand Suppl 214, 56: 6, 1985
9. Collins DH: The Pathology of Articular and Spinal Disease.Arnold and Co., London, 1949
10. Dmitrovsky E, Lane LB, Bullough PG: The characterization of the tidemark in human articular cartilage. Metabol Bone Dis Rel Res 1: 115, 1978
11. Fawns HT, Landells IW: Histological studies of rheumatic conditions. Observations of the fine structure of the matrix of normal bone and cartilage. Ann Rheumat Dis 12: 105, 1953
12. Green WT, Martin GN, Eanes ED, Sokoloff L: Microradiographic study of the calcified layer of articular cartilage. Arch Path 90: 151, 1970
13. Havelka S, Valouch P, Módis L: Zur Remodellation der Knochen-Knorpelgrenze bei Gelenkerkrankungen. Prim. Coll Osteol Jenense 1980 Wiss. Beitr. der FSU Jena. 1982, pp 74—82
14. Havelka S, Horn V, Spohrova D, Valouch P: The calcified-noncalcified cartilage interface: the tidemark. Acta Biol Hung 35, 271, 1984
15. Haynes DW: The mineralization front of articular cartilage. In: WSS Jee and AM Parfitt (eds) Bone Histomorphometry, 3rd Int. Workshop Suppl. Metabol Bone Dis Rel Res, 1980 pp 55—60,
16. Hough AJ, Banfield WG, Mottram FC, Sokoloff L: The osteochondral junction of mammalian joints. Lab Invest 31: 685, 1974
17. Lemperg R: The subchondral bone plate of the femoral head in adult rabbits. I. Spontaneous remodeling studied by microradiographic and tetracycline labelling. Virch. Arch. Abt A: Path Anat 352: 1, 1971
18. Lemperg R: The subchondral bone plate of the femoral head in adult rabbits. II. Changes induced by intracartilaginous defects studied by microradiography and tetracycline labelling. Virch Arch Abt A: 352: 14, 1971
19. Lillie RD: Histopathologic Technique and Practical Histochemistry. Philadelphia, Blakiston Div Mc Grav Hill Book and Co. 1965
20. Oettmeier R, Abendroth K, Oettmeier S: Analyses of the tidemark on human femoral heads. II. Tidemark changes in osteoarthrosis — A histological and histomorphometric study in non-decalcified preparations. Acta Biol Morph Acad Sci Hung, in press
21. Redler I, Mow VC, Zimny ML, Mansell I: The ultrastructure and biomechanical significance of the tidemark of articular cartilage. Clin Orthoped Rel Res 112: 357, 1975
22. Spinelli R: Nuovi aspetti strutturali della cartilagine articolare. II. "Tidemark" visto al microscopio elettronico a scansione. Giorn Ital Orthoped Traumatol 2: 393, 1976
23. Wuthier R, Gore ST: Partition of inorganic ions and phospholipids in isolated cell, membraned matrix vesicle fractions: evidence for calcium-phospholipid-phosphate complexes. Calcif Tissue Res 24, 163—171, 1977

Acta Morphologica Hungarica 37 (3–4), pp. 169–180 (1989)

ANALYSES OF THE TIDEMARK ON HUMAN FEMORAL HEADS

II. TIDEMARK CHANGES IN OSTEOARTHROSIS – A HISTOLOGICAL AND HISTOMORPHOMETRIC STUDY IN NON-DECALCIFIED PREPARATIONS

R. Oettmeier[1], K. Abendroth[2], Sabine Oettmeier[3]

[1]ORTHOPAEDIC CLINIC AND [2]CLINIC OF INTERNAL MEDICINE, DEPARTMENT OF RHEUMATOLOGY AND OSTEOLOGY, FRIEDRICH SCHILLER UNIVERSITY OF JENA, [3]DISTRICT DENTAL DEPARTMENT, EISENBERG, GDR

(Received 7 December 1988)

Histological and histomorphometric examinations were carried out on 88 human femoral heads, 63 from patients with osteoarthrosis and 25 controls. The changes of the tidemark were found to be multiform in the osteoarthrotic process and could be classified into three degrees of severity. Low-grade tidemark changes were characterized by reduplications of the tidemark and discontinuities of the tidemark line, occurring also in about one third of the controls. Vascular invasion into the tidemark as well as incipient calcification of basal hyaline cartilage were observed in middle-grade tidemark alterations. High-grade changes were distinguished by the disappearance of the tidemark, advanced mineralization and ossification of basal hyaline and calcified cartilage and finally by the "tidemark and bone bald". Measuring the thickness of intact and osteoarthrotic hyaline cartilage, calcified layer and subchondral bone plate, it was possible to determine some correlations between the tidemark state and the structures measured. Variations in subchondral bone volume could also influence the tidemark and cartilage changes. The important role of the intercartilaginous junction in the pathogenesis and progress of osteoarthrosis is stressed.

Keywords: Tidemark, articular cartilage, osteoarthritis, histomorphometry, pathology of cartilage, calcified cartilage

Introduction

The tidemark (TM) is early involved in the process of cartilage destruction in inflammatory and degenerative joint diseases. Fibrillation of cartilage, increased remodelling of calcified cartilage and subchondral bone are important factors which initiate such pathologic changes. It is discussed in the literature that in some cases the TM changes occur primarily and subsequently, cause the destruction of articular cartilage [5, 12, 14, 15, 28]. Reduplications of the TM were described already in 1942 by Bennett et al. [3]. TM multiplications were often found in osteoarthrosis (OA) [9, 12, 19, 25], rheumatoid arthritis [1, 11] and Pierre-Marie-Strümpell-Bechterew's disease [2]. Their frequent occurrence was seen in both young and elderly adults [3, 18, 19].

Send offprint requests to: Dr. R. Oettmeier, Friedrich Schiller University Orthopaedic Clinic, Rudolf Elle Hospital, Eisenberg (Thüringia) 6520, DDR

Starting from the normal structure of the TM in femoral heads [27], TM changes in OA will be described and graduated in this study. The dependence of TM structure on the thickness of intact and degenerated hyaline cartilage, calcified cartilage and subchondral bone plate and, finally, on the subchondral trabecular bone volume will be determined using histomorphometry.

Materials and methods

Altogether 88 human femoral heads were examined. The joint heads were resected in the course of total hip joint replacement from 63 patients with primary coxarthrosis (average age 65.3 years) and from 13 patients after medial femoral neck fracture (mean age 74.4 years). Approximately 1 cm thick bone-cartilage specimens of the medial-sagittally bisected joint heads from the loaded and non-loaded zone were fixed in Carnoy's solution, dehydrated in ethanol and embedded in methyl methacrylate. Four micron thick sections were obtained, deplastified in toluol and stained by the method of Ladewig, gallamine-blue Giemsa, Gömöri, PAS, safranin O and von Kossa.

Using an eyepiece gradicule (Fi. Zeiss, Jena/GDR), we have determined the thickness of osteoarthrotic and normal cartilage, calcified cartilage and subchondral bone plate. In an area of about 2.5 mm^2 below the subchondral bone plate, the trabecular bone volume (TBV) was determined by means of the eyepiece gradicule of Merz [22]. The results were compared with the TM state in the region measured.

Results

a) Histology

According to the indication for hip joint replacement, in the osteoarthrotic femoral head, all degrees of cartilage destruction have been found. Mostly, the TM was involved in this process. It was useful to classify the TM changes into three degrees of severity (Table I). Frequent *low-grade* TM changes were duplications and multiplications of TM components, but we have seldom seen a true TM duplication (Fig. 1). The duplicated lines were

Table I

Classification of TM changes into three degrees of severity

Degree 1	Degree 2	Degree 3
low-grade changes	middle-grade changes	high-grade changes
+ reduplication and multiplication of TM components	+ loss of TM components	+ total loss of the TM
+ dimmed TM lines	+ partial mineralization of hyaline cartilage	+ advanced mineralization of hyaline cartilage
+ TM splitting and flocculation	+ vascular invasion in the TM and basal hyaline cartilage	+ ossification of calcified cartilage
+ different width of TM components		+ TM and bone "bald"

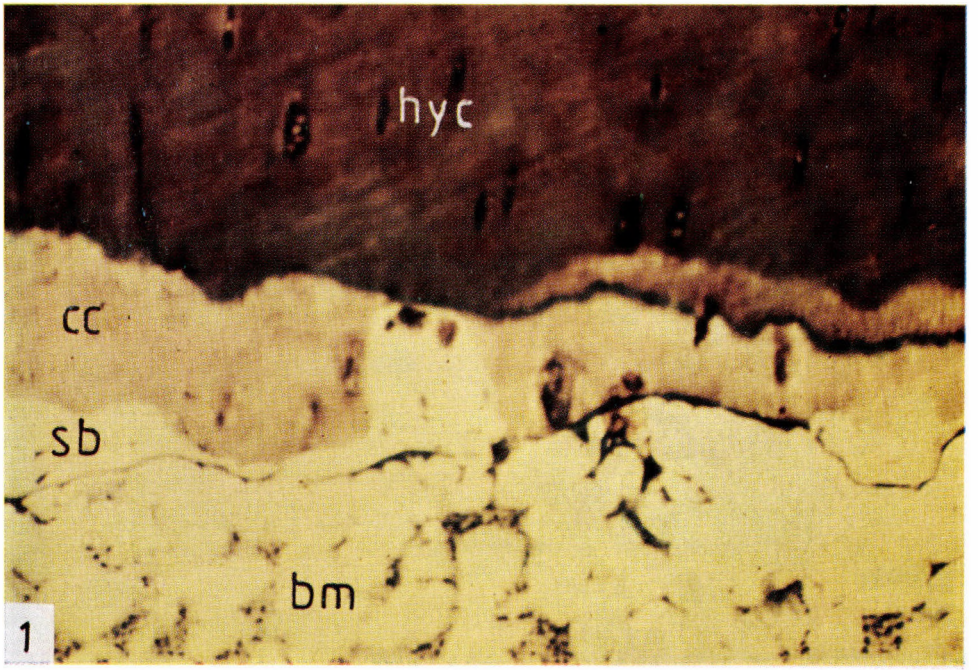

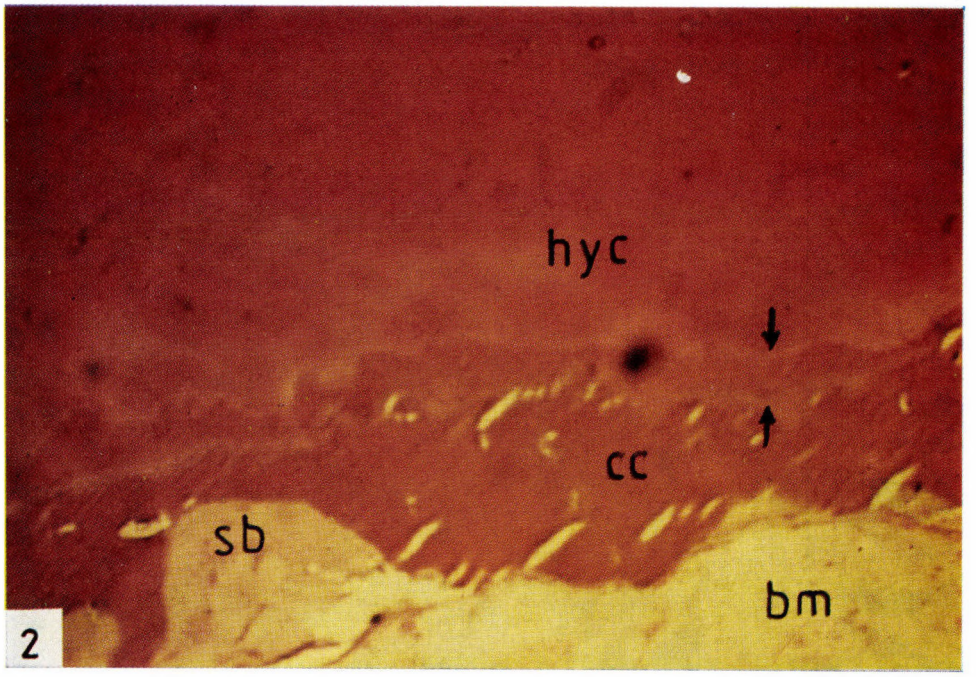

Fig. 1. Low-grade TM change showing a true duplication of all TM components (hyc — hyaline cartilage, cc — calcified cartilage, sb — subchondral bone, bm — bone marrow), (methyl methacrylate, gallamine-blue Giemsa, ×120)

Fig. 2. Low-grade TM change. The duplicated TM lines are PAS negative (arrows), (abbreviations see Fig. 1, methyl methacrylate, PAS reaction, ×120)

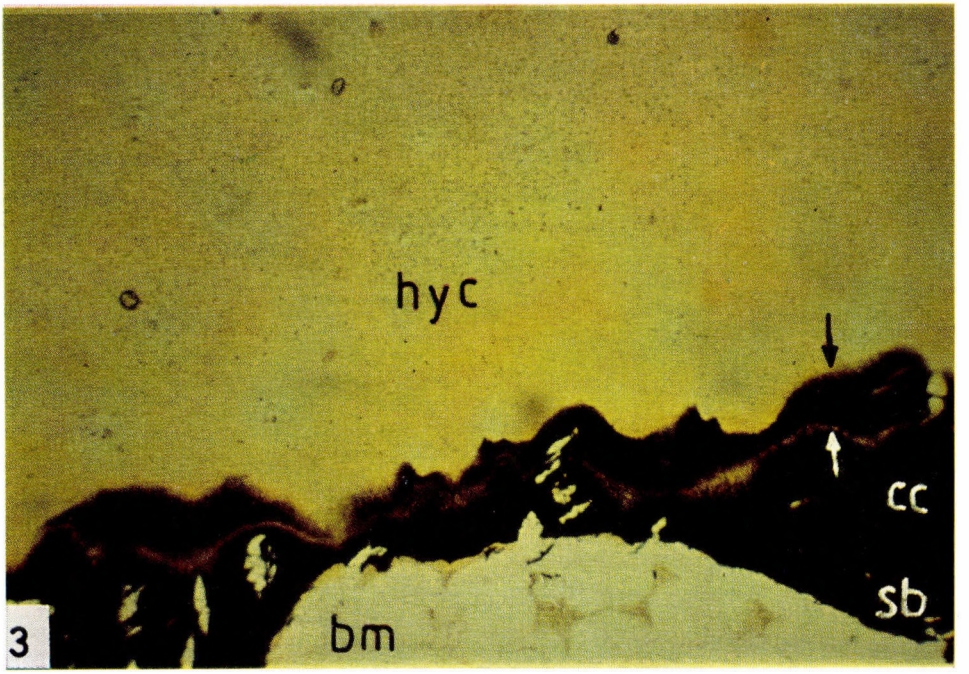

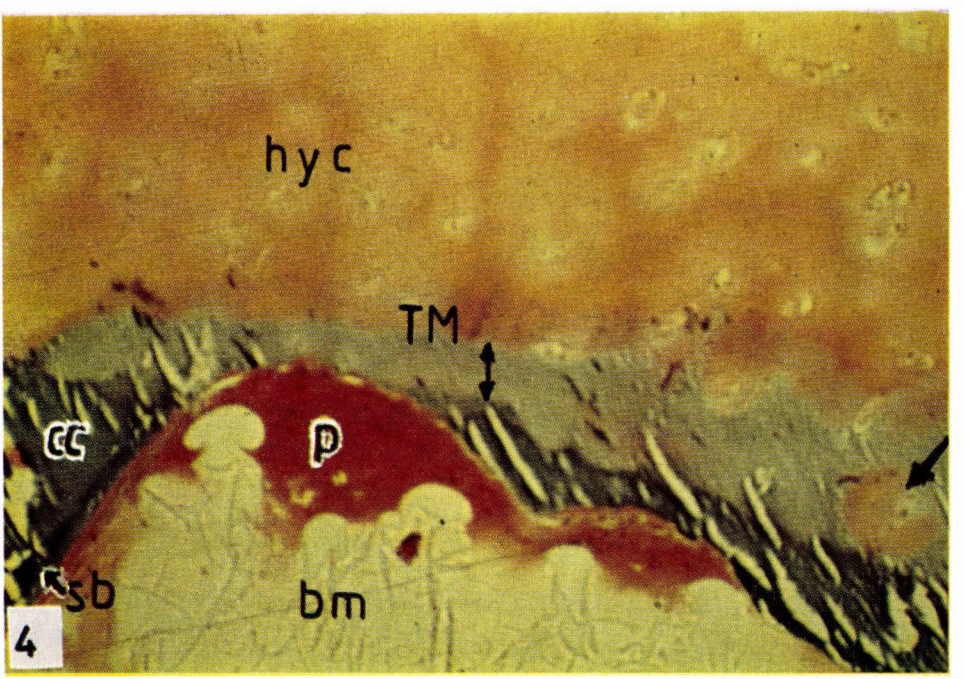

Fig. 3. The interface between the duplicated TM is mineralized (arrows), (abbreviations see Fig. 1, methyl methacrylate, von Kossa, ×120)

Fig. 4. Middle-grade TM change. The TM line is disappeared and an entombed chondron into the mineralized basal cartilage is visible (arrow). Note the avascular, fibrinoid "plug" (p) adjacent to subchondral bone (sb) and calcified cartilage (cc), (methyl methacrylate, Ladewig, ×120)

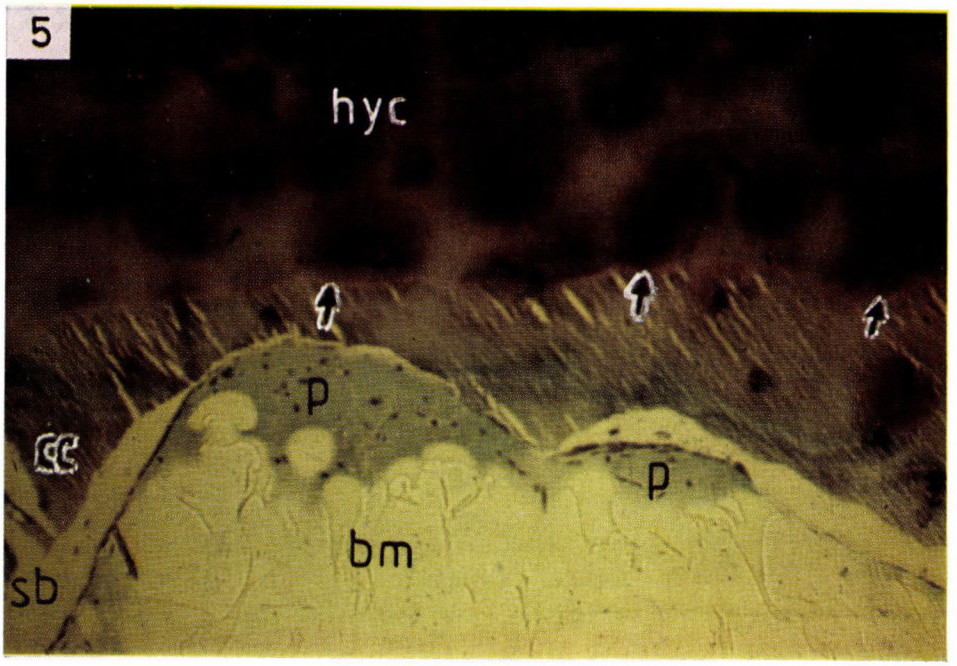

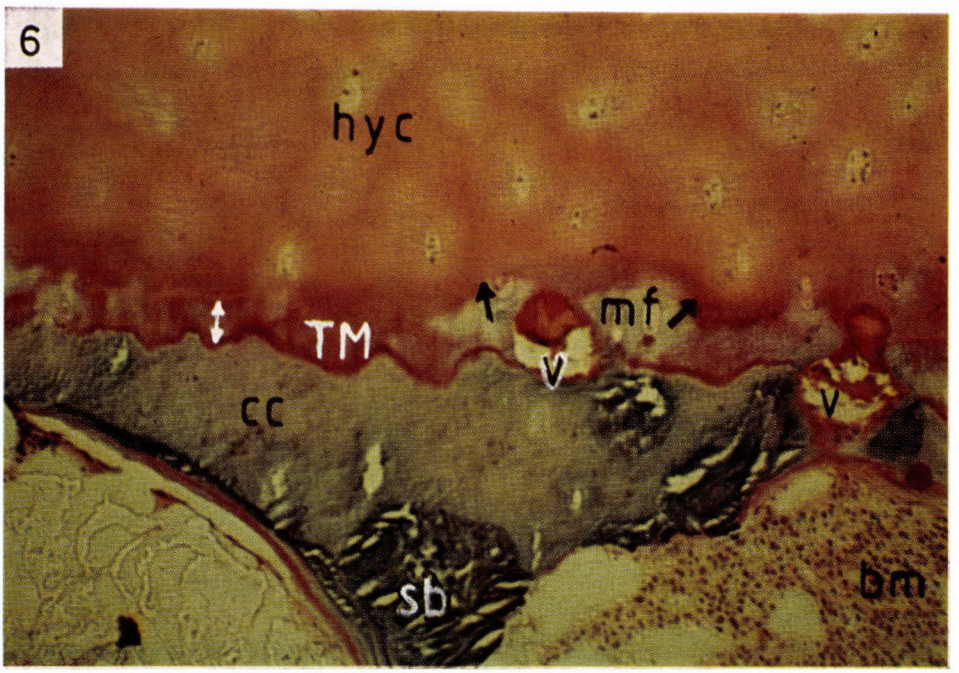

Fig. 5. Same sample as shown in Fig. 4 stained with gallamine-blue Giemsa demonstrating the relative intact limit of the low-grade alterated TM for mineralization (arrows). The "plugs" (p) are also visible (abbreviations see Fig. 4, ×120)

Fig. 6. Low-grade TM changes (left part) and middle-grade TM alterations (right part). Note the vascular invasion (v) in the TM and basal hyaline cartilage (hyc) behind the progression of mineralization front (mf), (methyl methacrylate, Ladewig, ×120)

Table II

Frequency of TM changes in normal and osteoarthrotic femoral heads

Diagnosis	Number	Degree of TM alteration			% TM
	(n)	I	II	III	changes
Control persons					
— load area	12	3	1	—	33
— non-load area	12	5	—	—	42
Femoral neck fracture					
— load area	13	5	2	—	53
— non-load area	13	6	2	—	61
Coxarthrosis					
— load area	63	1	1	58	95
— non-load area	63	22	18	2	66

PAS-negative (Fig. 2) and the interface between the lines was already mineralized as shown by the von Kossa staining (Fig. 3). Other low-grade TM alterations were dimmed, flocculent and splitted TM lines (Table I). These changes were also found in about one third of control persons, but in 25% of osteoarthrotic femoral heads in the non-loaded zone (Table II). In the *middle-grade* stage of TM changes there were only parts of TM components visible. Areas of calcified basal cartilage occurred with entombed chondrons and larger penetrating vessels appeared in the calcified cartilage and TM (Figs 4 and 6).

For demarcation from high-grade TM alterations, it was important that this stage still showed a relatively intact limit of the TM for mineralization (Fig. 5). Especially in the load area of the degenerative femoral head all kinds of *high-grade* TM destructions were present (Table I). These were characterized by fragmentation or total loss of the TM, advanced mineralization and ossification of basal hyaline and calcified cartilage, and, finally, after total abrasion of cartilage, we could see the so-called "TM and bone bald" according to Franz [7] (Fig. 7).

b) Histomorphometry

The results of measurements are summarized in Table III. Most important for intact TM was especially only low-grade fibrillated cartilage, i.e. fibrocartilaginous covering. With decreasing hyaline cartilage and increasing fibrocartilaginous tissue the TM destruction advanced. Variations in total thickness of articular cartilage were wide and therefore the standard deviation relatively high. For this reason it was useful to evaluate the percentage of

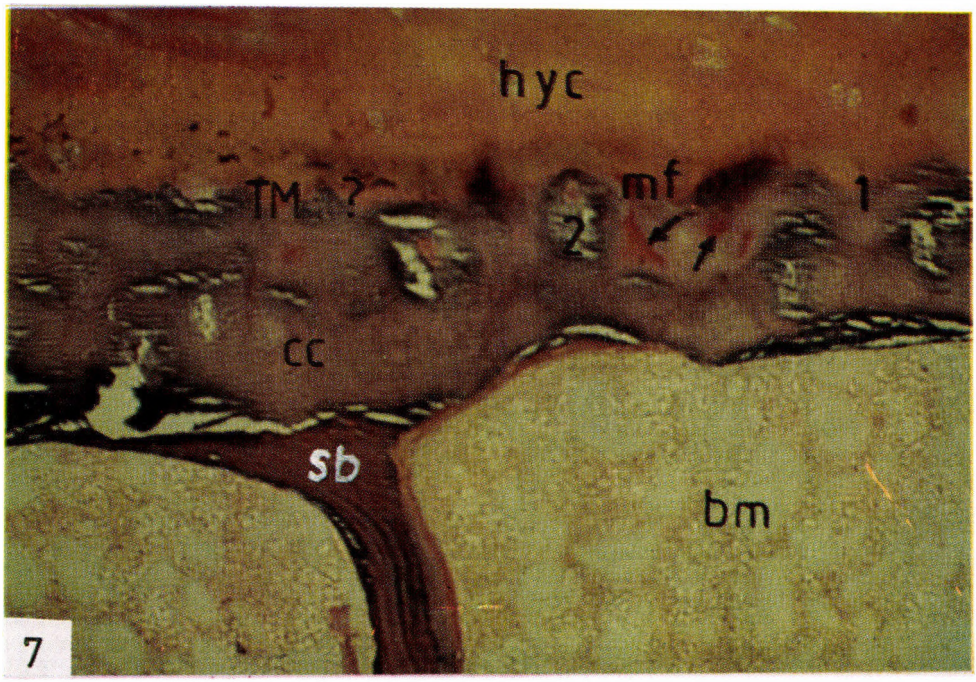

Fig. 7. High-grade TM alteration. Note the total loss of the TM, the advanced mineralization (1) and ossification (2) of basal hyaline cartilage. Rests of hyaline cartilage in the mineralization front (mf) are visible (arrows) (abbreviations see Fig. 1, methyl methacrylate, Ladewig, ×120)

Table III

Influence of thickness of fibrocartilaginous tissue (osteoarthrotic cartilage), intact hyaline cartilage, calcified cartilage and subchondral bone plate as well as subchondral trabecular bone volume (TBV) on the TM state

Parameter	TM normal	Degree of tidemark alteration		
	(51)[a]	I (42)	II (24)	III (60)
Fibrocartilaginous tissue (μm)	70 ± 40[b]	202 ± 142	380 ± 230	605 ± 310
Hyaline cartilage (μm)	1020 ± 170	714 ± 295	320 ± 212	70 ± 49
Calcified cartilage (μm)	161 ± 9	141 ± 15	132 ± 24	112 ± 46
Subchondral bone plate (μm)	140 ± 24	86 ± 17	54 ± 21	281 ± 68
Subchondral TBV (mm^3/cm^3)	20 ± 4.4	12.4 ± 3.1	13.6 ± 4.8	49.1 ± 11.2

[a] number of measured slices; [b] mean ± SD

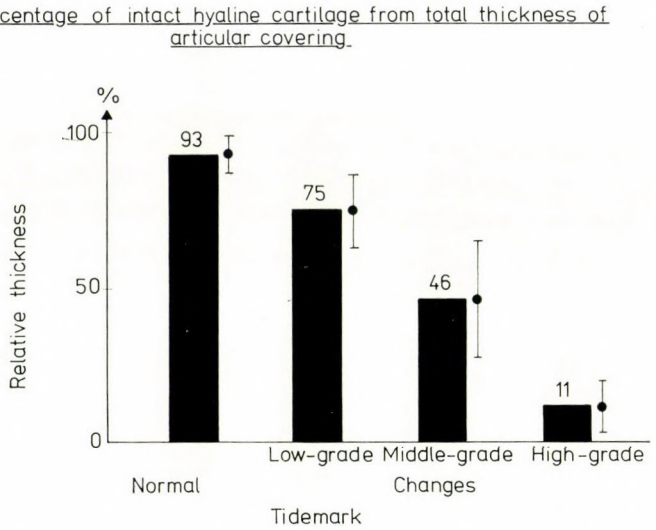

Fig. 8. Percentage of intact hyaline cartilage from total thickness of articular covering in comparison to the TM state

intact from the total thickness of cartilage (Fig. 8). The differences between all groups were now significant. The thickness of calcified cartilage remained fairly constant despite of low- and middle-grade TM changes (Table III).

Only normal TBV in the subchondral spongy area was accompanied by intact TM structure. Osteopenia, both in femoral neck fracture and the non-load area of femoral heads in OA, as well as in osteosclerosis (in the load area of osteoarthrotic joint heads) were accompanied by TM alterations (Table III).

Discussion

We confirm that the reduplication of TM components is the most common TM change at the early stage of OA. Its occurrence in healthy joints is focally possible. As reported by Green et al. [9] in the human patella there are, on average, 1.13 ± 0.06 TM lines. In fibrillated articular cartilage their number increased to 1.58 ± 0.09.

The distance between the duplicated lines ranges from 2 μm to 150 μm [9]. TM reduplications occur often in young adults, as was stated by Haynes [13] and Lane et al. [18]. Some authors describe an increase in TM multiplications with ageing (3.11, 13.18). All patients examined in this study were older than 50 years. In about one third they have shown low-grade TM alterations including TM reduplication despite of intact cartilaginous surface. Nevertheless, true duplications of all TM components were rarely observed.

We can also confirm the opinion that distinct TM multiplications are often accompanied by fibrillation of articular cartilage [9, 13]. Low-grade TM changes must be interpreted as early signs of the disturbed barrier function at the mineralization front. The accelerated mineralization and ossification of basal articular cartilage towards its surface have been demonstrated by Haynes [13] using triple labelling. On the basis of our previous study [27], we emphasize the morphological and functional concept of the TM as the limit of promotors and inhibitors of mineralization. Under pathological conditions the articular cartilage is only partly able to ensure this dynamic equilibrium. By developing new structures, similar to the original TM, the articular cartilage can stop or delay the mineralization of basal hyaline cartilage. This process reflects the reparative mechanisms on the cartilage-bone boundary in OA. After the breakdown of this stage, the basal cartilage is not able to limit pathological mineralization. Marked vascular invasion and disturbances of mineralization in calcified cartilage and subchondral bone as well as accelerated enchondral ossification and subchondral osteosclerosis can promote these events decisively.

TM splitting and dimmed TM lines are other TM changes described in the literature [12, 21] in analogy to the low-grade TM alterations reported in this study. In Heberden's arthrosis, Irlenbusch [15] and Dominick [5] observed some cases with TM "flaking". It is a further hint to the generally accepted vulnerability of the TM zone [4, 27, 31].

In 5 of 63 patients with coxarthrosis we observed only low-grade TM alterations in the load area of the femoral head despite of nearly total abrasion of cartilaginous covering. In these cases the cartilage destruction seems to be a purely mechanical one. On the other hand, this phenomenon may point to individual differences in reactivity and reparative potency of the TM region, as was shown in osteological examinations of subchondral bone in OA [26].

TM changes seem to be the secondary effect of cartilage fibrillation and elevated subchondral bone turnover [9, 12, 32]. But Johnson [16] supposes the disturbed remodelling of the bone-cartilage boundary to be the causal factor of OA. Predominantly structural and biochemical TM changes can exert primary influence on the pathogenesis of OA [5, 15, 28, 32]. As shown by histomorphometry in this study, it is hardly possible to determine which of the phenomena is the primary. We suppose a complex and mutually inductive behaviour of the neighbouring morphological structures. Independently of the place of primary lesion, be it in the subchondral bone, calcified cartilage, TM or hyaline cartilage, the disturbance gains greater significance only after including neighbouring structures.

In the calcified layer of articular cartilage, blood vessels are present extending in close proximity to chondrocytes [8]. Under physiological conditions Lane et al. [17] have found on an average 300—400 small vessels per

64 mm^2 in the calcified cartilage of femoral heads. In OA hypervascularity of the subchondral bone and marked vascular invasion in the cartilage were noted by some authors [10, 20, 30, 33]. Not only the penetration of larger vessels into the calcified cartilage represents a sensitive standard of the histological stage of OA, as reported by Pommer [29], but also all other described TM changes. The role of the TM in the progress of the osteoarthrotic disease seems to be more important. After the breakdown of the inhibitory function of the TM for mineralization, the cartilage will be more rigid and directs the joint finally on a pathway of mechanical self-destruction [13].

Green et al. [9] have reported the normal thickness of the calcified layer of articular cartilage to be 134 ± 7 microns as measured in paraffin sections. They could not see significant differences with ageing, contrary to Lane and co-workers [18]. Müller-Gerbl et al. [23] have established that the thickness of the calcified layer corresponds closely to that of the total cartilage. The value of the calcified layer expressed as a percentage of the total cartilage volume varied in human femoral heads by as much as 5.08% (range: 3.72%—8.8%).

The volume of the calcified zone was not only constant for one joint, but also in all the joints of a single individual [23, 24]. Also after life-long migration of the TM region in direction to the surface, the thickness of calcified cartilage seems to remain fairly constant [13]. We agree with Green et al. [9] that this phenomenon is functionally controlled. The relatively constant thickness of the calcified cartilage despite of low- and middle-grade TM alterations was already observed in the early stage of OA by Green et al. [9]. The thickness of the calcified cartilaginous layer depends upon mechanical factors [26, 27, 34]. Only in animal experiments could be a selective increase induced in the thickness of calcified cartilage [6].

In high-grade osteopenia, the bone-marrow space abuts directly on the calcified layer of articular cartilage without any sign of fractures (see Fig. 4). This phenomenon was only observed in femoral samples, most often in the non-weight-bearing areas, in agreement with the observations of Stougard [4] mostly accompanied by middle-grade TM changes. We observed the so-called "plugs" in the non-load area of osteoarthrotic femoral heads (see Figs 4 and 5). According to Green et al. [9] these "plugs" are avascular, necrotic tissue components which adjoin the subchondral bone plate or directly the calcified cartilage. Fibrinoid "plugs" were described by Abendroth [1] also in rheumatoid arthritis.

Summarizing our examinations we showed that, under pathological conditions, the mineralization of articular cartilage progressed towards the joint surface. It would be very interesting to study wether this mechanism in osteomalacia, for example, will proceed the opposite-direction by hypomineralization of calcified cartilage and bone.

Acknowledgements

We are particulary grateful to Mrs. Schütz and Mrs. Heinisch for their technical assistance.

REFERENCES

1. Abendroth K: Beitrag zur Pathogenese der Osteopenie bei Rheumatoidarthritis. Diss. B, Friedrich-Schiller-Universität Jena, 1980
2. Bély M: Multiplication of Tidemark Lines in Bechterew's Disease. CIC Edizoni Internationali, EULAR — Symposium, Roma 1986, pp 95.
3. Bennett GA, Waine H, Bauer W: Changes in the Knee Joint at Various Ages. Commonwealth Fund, New York, 1942
4. Broom WD, Poole CA: A functional-morphological study of the tidemark region of articular cartilage in a non-viable physiological condition. J Anat 135: 65, 1982
5. Dominick G: Veränderungen der Tidemark im Verlauf des Arthroseprozesse — ein histomorphologische Studie. Tertium Coll. Osteol. Jenense 1986, Wiss. Beitr. der FSU Jena, 1988
6. Fiorani-Gallotta G: Su alcuni particolari aspetti della cartilagine articolare in animali trattati con estrogeni. Arch Orthop 68: 324, 1955
7. Franz R: Tierexperimentelle Untersuchungen zum Übergang einer präarthrotischen Deformität in den Arthroseprozeß. Diss. B, Dresden, 1979
8. Gilmore RSC, Palfrey AJ: A histological study of human femoral condylar articular cartilage. J Anat 155: 77, 1987
9. Green WT, Martin GN, Eanes, ED, Sokoloff L: Microradiographic study of the calcified layer of articular cartilage. Arch Path 90: 151, 1970
10. Harrison MHM, Schajowicz F, Trueta J: Osteoarthritis of the hip: a study of the nature and evolution of the disease. J Bone Jt Surg 35-B: 598, 1953
11. Havelka S, Valouch R, Módis L: Zur Remodellation der Knochen-Knorpelgrenze bei Gelenkerkrankungen. Prim. Coll. Osteol. Jenense 1980, Wiss. Beitr. der FSU Jena, 74, 1982
12. Havelka S, Horn V, Spohrova D, Valouch P: The calcified-non-calcified cartilage interface: the tidemark. Acta Biol Hung 35: 272, 1984
13. Haynes DW: The mineralizationfront of articular cartilage. In: WSS Jee and AM Parfitt (eds) Bone Histomorphometry 3rd Int. Workshop Suppl Metabol Bone Dis Rel Res 1980, p 55
14. Inoue H, Kodama T: Sterioscopic observations of osteochondral junction in healthy and degenerated articular cartilage. 14rd Int. Congress of Rheumatology, San Francisco 1977, pp 312—313
15. Irlenbusch U: Epidemiologische, klinische, genetische und morphologische Untersuchungen zur generalisierten Osteoarthrose. Diss. B, Leipzig, 1987
16. Johnson LC: Kinetics of osteoarthritis. Lab Invest, 8: 1223, 1959
17. Lane LB, Villacin A, Bullough PG: The vascularity and remodelling of subchondral bone and calcified cartilage in adult human femoral and humeral heads. J Bone Jt Surg 59-B: 272, 1977
18. Lane LB, Bullough PG: Age related changes in the thickness of the calcified zone and the number of tidemarks in adult human articular cartilage. J Bone Jt Surg 62-B: 372, 1980
19. Macys JR, Bullough PG, Wilson PD: Coxarthrosis: a study of the natural history based on a correlation of clinical, radiographic and pathologic findings. Sem Arthr Rheum, 10(1): 66, 1980
20. Mankin HJ: The reaction of articular cartilage to injury and osteoarthritis. New England J Medicine, 291: 1285 and 1335, 1974
21. Meachim G, Bentley G: Horizontal splitting in patellar articular cartilage. Arthritis and Rheum, 21: 669, 1978
22. Merz WA, Schenk RK: Quantitative structural analysis of human cancellous bone. Acta Anat (Basel), 75: 54, 1970
23. Müller-Gerbl M, Schulte E, Putz R: The thickness of the calcified layer of articular cartilage: a function of the load supported? J Anat, 154: 103, 1987
24. Müller-Gerbl M, Schulte E, Putz R: The thickness of the calcified layer in different joints of a single individual. Acta Morphol Neerl-Scand, 25: 41, 1987
25. Oettmeier S, Oettmeier R, Ziller R: Tidemark-Analysen an resezierten Femurköpfen. Tertium Coll Osteol Jenense 1986, Wiss. Beitr. der FSU Jena, 1988
26. Oettmeier R, Abendroth K: Osteoarthritis and bone: osteologic types of osteoarthitis of the hip. Skeletal Radiol, 18:165, 1989

27. Oettmeier R, Abendroth K, Oettmeier S: Analyses of the tidemark on human femoral heads. I. Histochemical, ultrastructural and microanalytic characterization of the normal structure of the intercartilaginous junction. Acta Morphol Hung, (in press)
28. Otte I: Atiologische und pathogenetische Vorstellungen bei der Arthrose. Z Rheumatol, 42: 242, 1983
29. Pommer G: Über die mikroskopischen Kennzeichen und die Entstehungsbedingungen der Arthritis deformans. Virch Arch Path Anat, 263: 434, 1927
30. Stevens J: Osteoarthritis of the hip. Clin Orthop Rel Res, 71: 152, 1970
31. Spinelli R: Nuovi aspetti strutturali della cartilagine articolare. II. "Tidemark" visto al microscopio elettronico a scansione. Giorn Ital Ortoped Traumatol, 2: 393, 1976
32. Sokoloff L: The biology of degenerative joint disease. Univ. of Chicago Press, Chicago, 1969
33. Sokoloff L: The general pathology of osteoarthritis. In: SY Ali, MW Elvis, DH Leaback (eds) Proceedings of the Symposium on Normal and Osteoarthrotic Articular Cartilage. London, 1973, Institute of Orthopaedics, 1984 pp 111—123
34. Stougard J: The calcified cartilage and subchondral bone under normal and abnormal conditions. Acta Path Microbiol Scand Section A, 82: 182, 1974

Acta Morphologica Hungarica 37 (3—4), pp. 181—199 (1989)

MORPHOLOGY OF SUPRAVITAL BRAIN SLICES PRE-INCUBATED IN A PHYSIOLOGICAL SOLUTION PRIOR TO FIXATION

F. Hajós[1], J. Garthwaite[2], G. Garthwaite[2], A. Csillag[1]

[1]1ST DEPARTMENT OF ANATOMY, SEMMELWEIS UNIVERSITY MEDICAL SCHOOL, BUDAPEST, HUNGARY.
[2]DEPARTMENT OF VETERINARY PHYSIOLOGY AND PHARMACOLOGY, UNIVERSITY OF LIVERPOOL, UNITED KINGDOM

(Received 6 February 1989)

Slices of 400 μm thickness were prepared from various regions of the adult rat brain using a vibratome, and incubated in oxygenated Krebs-Henseleit medium for 3 h prior to processing for light and electron microscopy. Previous findings in cerebellar slices suggest that the structural recovery requires at least a 1 h period of incubation. In the present study, vibratome-cut slices of other brain areas such as the hippocampus, parietal cortex, striatum and median eminence were shown to display after this period a gross and fine structure comparable to in situ fixed tissues, and to retain it for at least 3 h of incubation. These areas are thought to be promising for further in vitro functional morphological experimentation.

Keywords: Brain, tissue slices, ultrastructure

Introduction

The potentialities of working with incubated brain slices have amply been exploited in neurophysiology and neurochemistry [see for References 3] but not in neuromorphology. The delayed recognition of the usefulness of these preparations follows from the general attitude of morphologists towards the way of preservation of structure at the EM level. The main goal of EM fixation procedures is to prevent structural disintegration by minimizing the time elapsing between cessation of blood supply and exposure to fixative. To achieve this, initially, small tissue samples were excised from anaesthetized animals and immersed immediately into the fixative. By the mid 70s it was, however, realized that in spite of all efforts to hurry with sampling the slow penetration of fixatives through cell membranes leaves time for hypoxic and other post mortem alterations [9, 17, 21]. As an alternative, the vascular perfusion of the fixative (usually an aldehyde or a mixture of aldehydes) under anaesthesia, followed by the immersion of excised tissue blocks into osmic acid solution has been proposed [18]. This procedure has widely been accepted and is to date the method of choice in most morphological laboratories.

Send offprint requests to: Dr. F. Hajós, Dept. of Anatomy and Histology, Veterinary University, Budapest, P.O. Box 2, H-1400, Hungary

In previous studies we have demonstrated [6, 8] that rat cerebellar slices maintained in vitro need a recovery period before they show a reasonable functional performance as judged by recording electrical activity and measuring nucleotide synthesis. Parallel light- and electron microscopic studies have revealed a process of structural restitution taking as a reference the appearance of in situ aldehyde-perfused, osmium-postfixed nervous tissue. This observation enabled us to study the morphological effects of agents applied to the incubation medium in cerebellar slices maintained in vitro [4, 5, 6, 14].

Conditions of producing viable slices of the rat cerebellum were discussed in an earlier work by Garthwaite et al. [8]. From these studies it emerged that cutting by hand, vibratome or chopper makes a difference to viability, to an extent which depended on the age of the animal. While 8-day-old cerebella could readily be sliced by a mechanical chopper, at an older age this method yielded no viable slices. On the other hand, vibratome slices of the cerebellum showed a structural and functional recovery even in the adult.

Encouraged by the results obtained in the cerebellum, we attempted to cut vibratome slices from various brain areas and incubated them to see if they were capable of structural recovery. By this we intended to explore new CNS regions suitable for in vitro functional morphological studies.

Materials and methods

Brains of adult albino rats (250 g body weight, either sex) were removed from the skull and dissected into the following parts: cerebellum, hippocampus, parietal cortex, striatum, hypothalamus, mesencephalon-pons and medulla. The tissue was fixed by cyanoacrylate glue to a specimen stage and in some cases covered with 3% agar in saline kept liquid at 37 °C by continuous stirring. Vibratome sections of 400 μm thickness were cut in various planes using a Vibroslice (Campden Instruments), and incubated for 3 h in a Krebs-Henseleit solution in a 37 °C shaking water bath. The incubation medium contained (mM): NaCl (118), KCl (4.7), $CaCl_2$ (2.5), $NaHCO_3$ (25), KH_2PO_4 (1.19), $MgSO_4$ (1.18) and glucose (11) and was equilibrated with 5% CO_2 in O_2. Slices were fixed by a mixture of 4% paraformaldehyde and 2.5% glutaraldehyde in 0.1 M phosphate buffer (pH 7.4). After an overnight wash in phosphate buffer they were immersed for 1 h into 1% osmic acid, dehydrated with graded ethanol and propylene oxide and embedded flat in Durcupan (Fluka). Ultrahin and 0.5—1 μm semithin sections were cut with a Tesla ultramicrotome and stained with uranyl acetate — lead citrate and 1% toluidine blue, respectively. Electron micrographs were made with a Tesla BS 500 electron microscope.

Results

In all slices the cut surfaces showed considerable structural damages down to a 5—15 μm depth and were not evaluated. The rest of the tissue was of even quality.

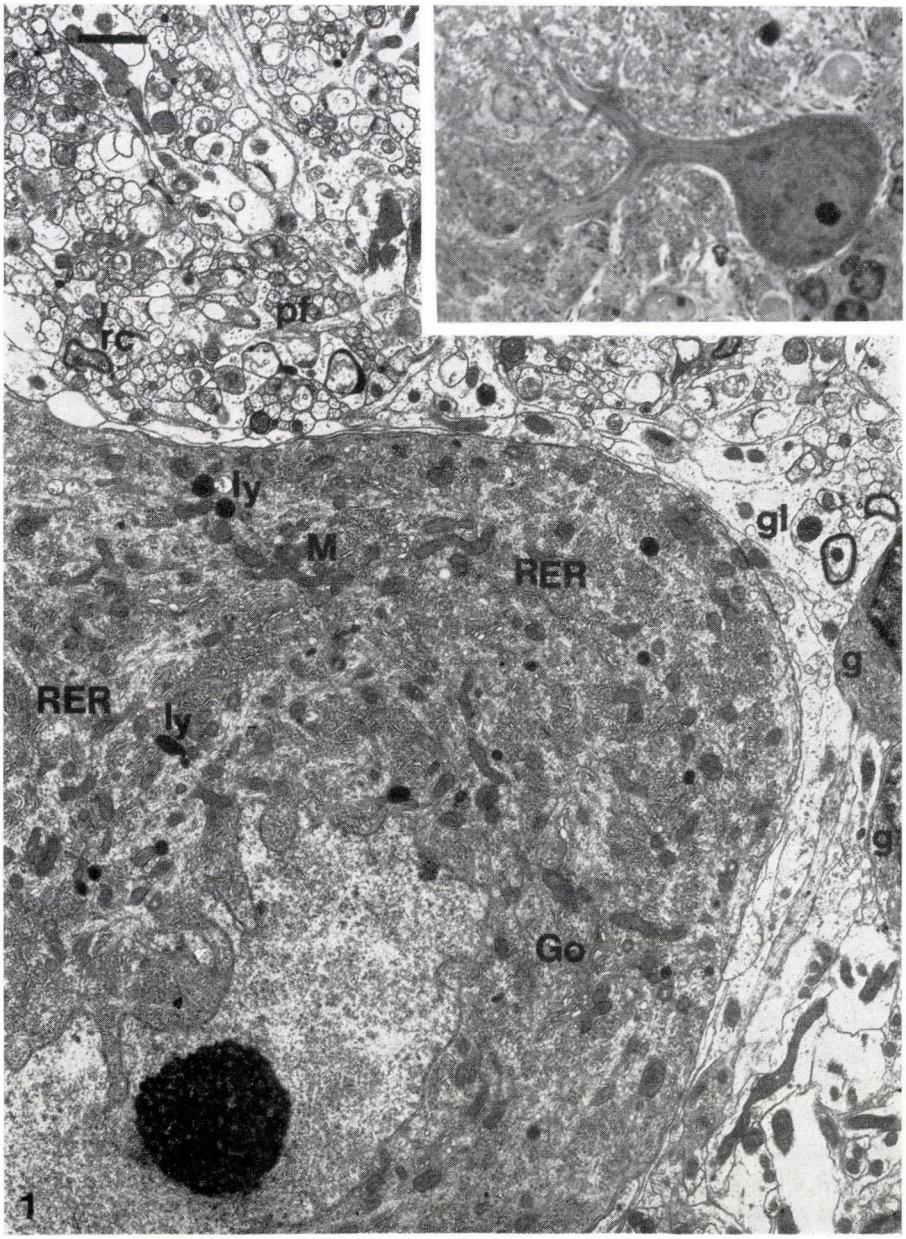

Fig. 1. Cerebellar slice (sagittal), 3 h incubation. Inset shows the light microscopic appearance (×1.100) of a Purkinje-cell in a toluidine blue-stained semithin section. A portion of this cell can be seen in a low-power electron-micrograph. Cell membrane is intact, the nucleus is indented particularly at its aspect facing the origin of the main dendritic shaft, the nucleolus is prominent. Mitochondria (M) appear as dark oval or bacilliform profiles. Cisternae of the rough endoplasmic reticulum (RER) are scattered throughout the cytoplasm often surrounded by clouds of free ribosomes. The Golgi apparatus (Go) consists of parallel elongated sacs and numerous vesicles, lysosomes (ly) are dark. The Purkinje-cell is surrounded by a glial envelope (gl) leaving room only for a few presynaptic terminals (arrows) to contact the cell body. At top an area of the lower molecular layer is visible with cross-sectioned bundles of parallel fibres (pf). Double arrow points at a typical axon-spine synapse between parallel fibre and Purkinje-cell dendritic spine. Recurrent collaterals of the Purkinje-axon (rc) are the only myelinated elements of this neuropil region. At extreme right a portion of the granular layer is to be seen with characteristic granule cells (g). ×9.000

Cerebellum

Cerebellar slices were cut in either the sagittal plane or longitudinally from the pial surface of the vermis and yielded similar results upon incubation. In semithin sections (Fig. 1, inset) all cell types of the cerebellar cortex were recognized by their typical appearance. Purkinje-cells had a prominent nucleolus and a cytoplasm packed with organelles up to the main dendritic shaft. The nuclear structure of microneurons and glial cells was characteristic. Granule cells had round, small nuclei with darkly staining clumps of chromatin. The light, indented nucleus of molecular layer interneurons was clearly visible. Astroglial cells including the Bergmann glia were conspicuous by their pale nuclei, with well-outlined nuclear envelope and excentrically located nucleolus. The light, "watery" cytoplasm of astroglia was also evident.

The electron microscopic structure of incubated cerebellar slices (Figs 1, 2) apparently did not differ from that of the in situ fixed cerebellum. Purkinje-cells were loaded with aggregations of free ribosomes and condensed mitochondria, nuclear folds were facing the origin of the dendritic shaft. The Purkinje-cell body was surrounded by a glial sheath. In the molecular layer Purkinje dendrites and cross sections of parallel fibres were seen, a few of them synapsing with dendritic spines. The granular layer (Fig. 2) contained, in addition to normal-looking granule cells, large mossy terminals synapsing with several dendritic appendages in the typical glomerular formation. Myelin sheaths were well preserved even at their terminal sites and Ranvier-nodes. An elaborate astroglial system enmeshed the granular layer. No swelling of glial cells or processes was encountered. Glycogen granules occurred scattered in glial processes.

Hippocampus and dentate gyrus

Slices were cut transversely to the longitudinal axis of the hippocampal formation. Both survey and oil immersion light microscopy revealed a good overall and cellular preservation of the hippocampus. Pyramidal cells of CA1 (Fig. 3 A) stained lightly, their large, round nuclei with one or more nucleoli were prominent. Under oil immersion mitochondria and lysosomes could be perceived. Astrocytes in the pyramidal layer, but not elsewhere in the hippocampus and dentate gyrus, were dark, granule cells and the neuropil of the dentate gyrus showed no pathological alteration (Fig. 3 B).

Electron microscopy corroborated the impression of good preservation. Pyramidal cells (Fig. 4) had a smooth-contoured nucleus with evenly distributed chromatin and prominent nucleoli, scattered RER, mitochondria and lysosomes located mainly at the origin of the apical dendrite. On the cell body and dendritic shafts numerous synapses were observed. The neuropil of the

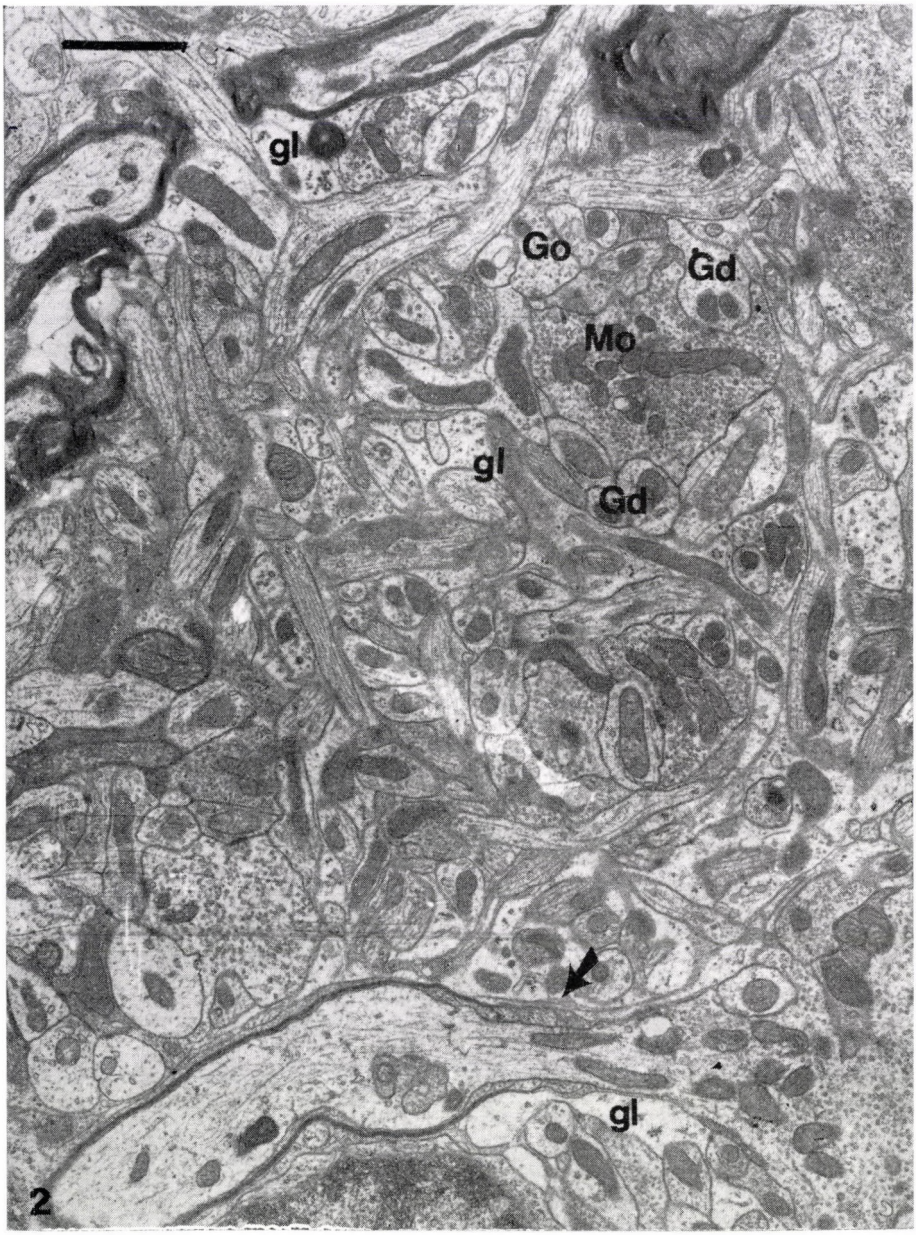

Fig. 2. Cerebellar slice (sagittal), 3 h incubation. The neuropil of the granular layer contains profiles of giant terminals of mossy fibres (Mo) surrounded by the postsynaptic protrusions of granule cell dendrites (Gd). The mossy terminal at the bottom is seen to emerge from the myelinated mossy fibre. The ending of the myelin sheath (arrow) is fully preserved showing the individual lamellae to turn back so as to enclose a small amount of oligodendroglial cytoplasm. Mossy terminals contain numerous round synaptic vesicles and elongated mitochondria. Golgi terminals (Go) can be recognized by contacting the peripheral side of the granule cell dendrites and by containing pleomorphic synaptic vesicles. Glial processes (gl) are found throughout the neuropil containing glycogen granules. At bottom a portion of a granule cell is visible. $\times 20.000$

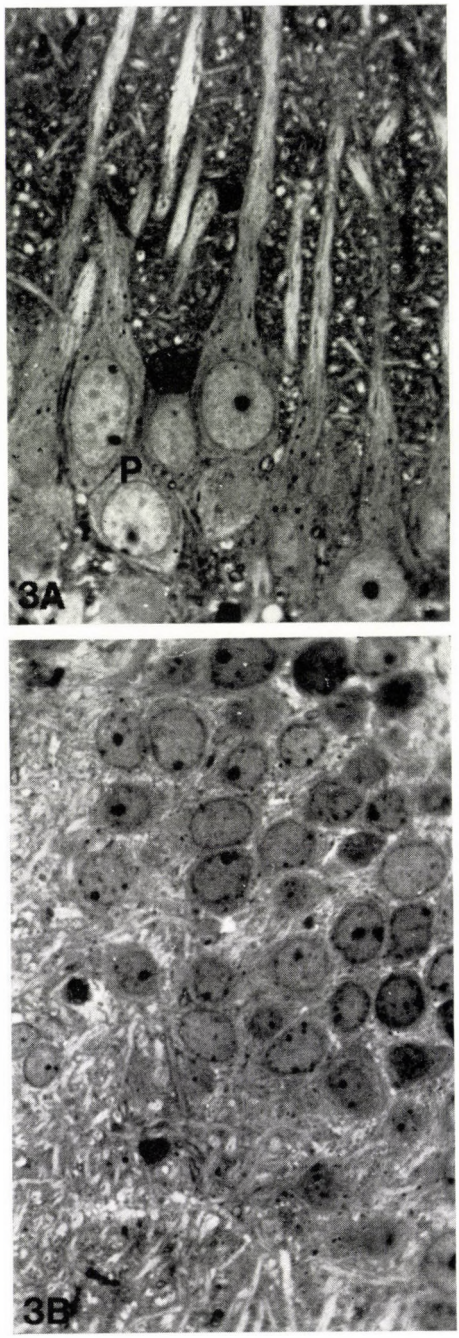

Figs 3 A, B. Hippocampal slice (transverse), 3 h incubation. Oil-immersion picture of the CAl area in toluidine blue-stained semithin sections. A: Pyramidal cells (P) look normal, perikaryal and dendritic mitochondria appear as dark dots (×1.100). B: Granule cells from the upper limb of the dentate gyrus (×1.100)

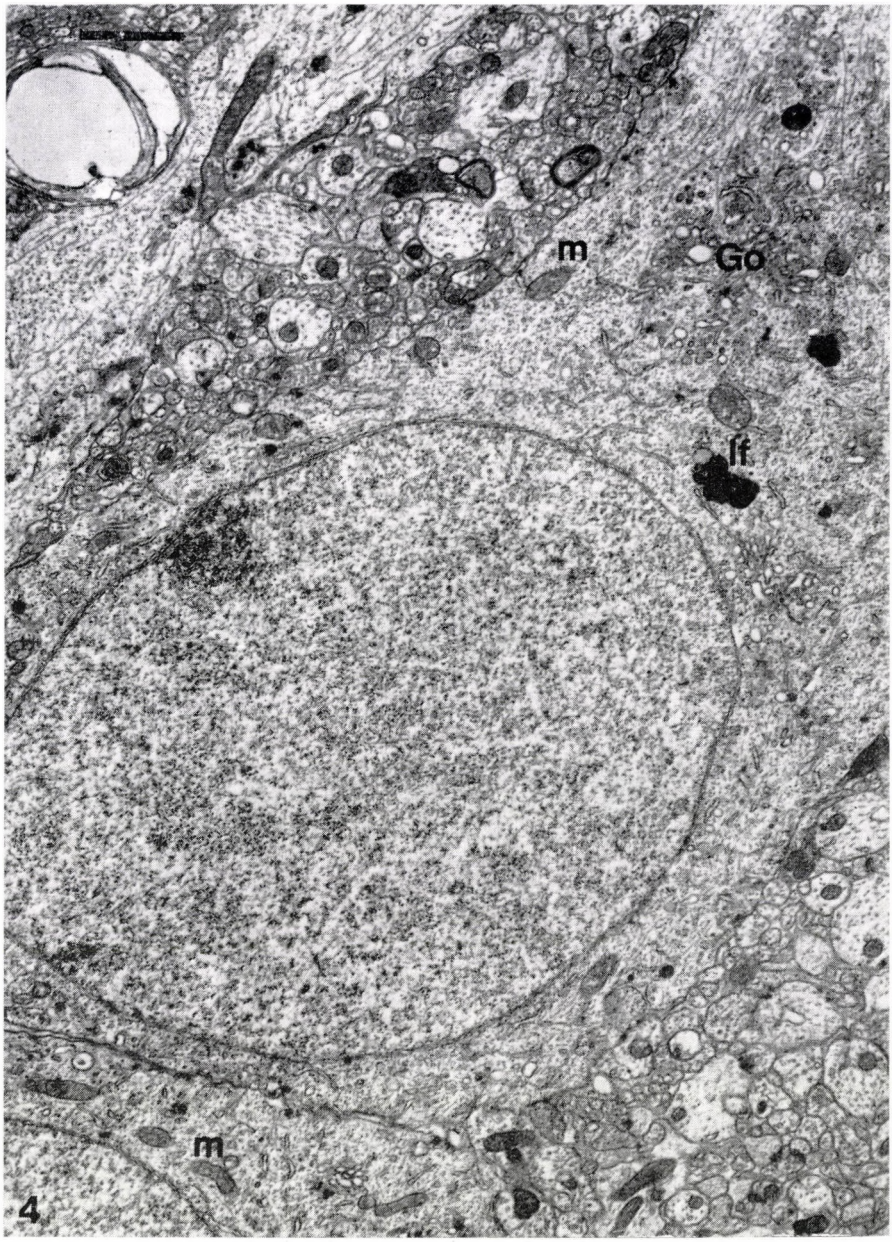

Fig. 4. Electron micrograph of a pyramidal cell from the hippocampal slice (transverse) incubated for 3 h. The cytoplasm contains scattered cisternae of RER, Golgi vesicles (Go), mitochondria (m) and lipofuscin granules (lf). The nucleus is ovoid with sparsely distributed chromatin and eccentrically located nucleolus. ×16.000

pyramidal layer and of the stratum radiatum and oriens looked ultrastructurally intact except for some cross-sectioned myelinated fibres which were lacking axonal cytoplasm. Similarly well-preserved was the fine structure of the dentate gyrus. The molecular layer (Fig. 5) where a particularly high number of neuronal processes and synapses are densely packed, showed no obvious sign of damage.

Cerebral cortex

In the present study frontal slices of the parietal cortex were incubated. In this brain area incubation resulted in a swelling of dendrites in layer I, while the overall structure of deeper layers appeared intact both light- and electron microscopically (Fig. 6). In semithin sections (Fig. 6, inset) neither cellular nor neuropil disintegration were seen. Under the electron microscope the cell bodies appeared well-preserved. Perikaryal mitochondria were somewhat less condensed than mitochondria in the neuropil. Pyramidal dendrites were followed for considerable distances from their cells of origin (Fig. 7). Their synapses and surrounding looked normal.

Striatum

Striatal slices cut in both frontal and horizontal planes showed no gross structural damage after incubation. Upon light microscopic examination (Fig. 8, inset) the neurons and their surrounding neuropil were found in good condition. This finding was supported by electron microscopy (Fig. 8). Nevertheless, in the bundles of myelinated fibres of the pericellular areas were intact. In the unmyelinated neuropil of striatum (Fig. 9) all fine structural details were found preserved.

Hypothalamus

From the hypothalamus proper no slices were obtained with an acceptable gross or fine structure. In sharp contrast to this, the median eminence, a region notorious for its poor fixation by perfusion, displayed in vitro a remarkable degree of fine structural preservation. This applied not only for slices of either plane but also for the excised whole median eminence indicating the extraordinary in vitro viability of this brain area. In semithin sections cut in the frontal plane (Fig. 10, inset) all layers of the incubated median eminence could be surveyed, from the ependymal lining of the infundibular recess down to the zone of portal capillaries near the basal surface. Electron microscopically the internal and middle zones were seen to contain microvillous ependymal cells and sectioned profiles of nerve fibres, respectively

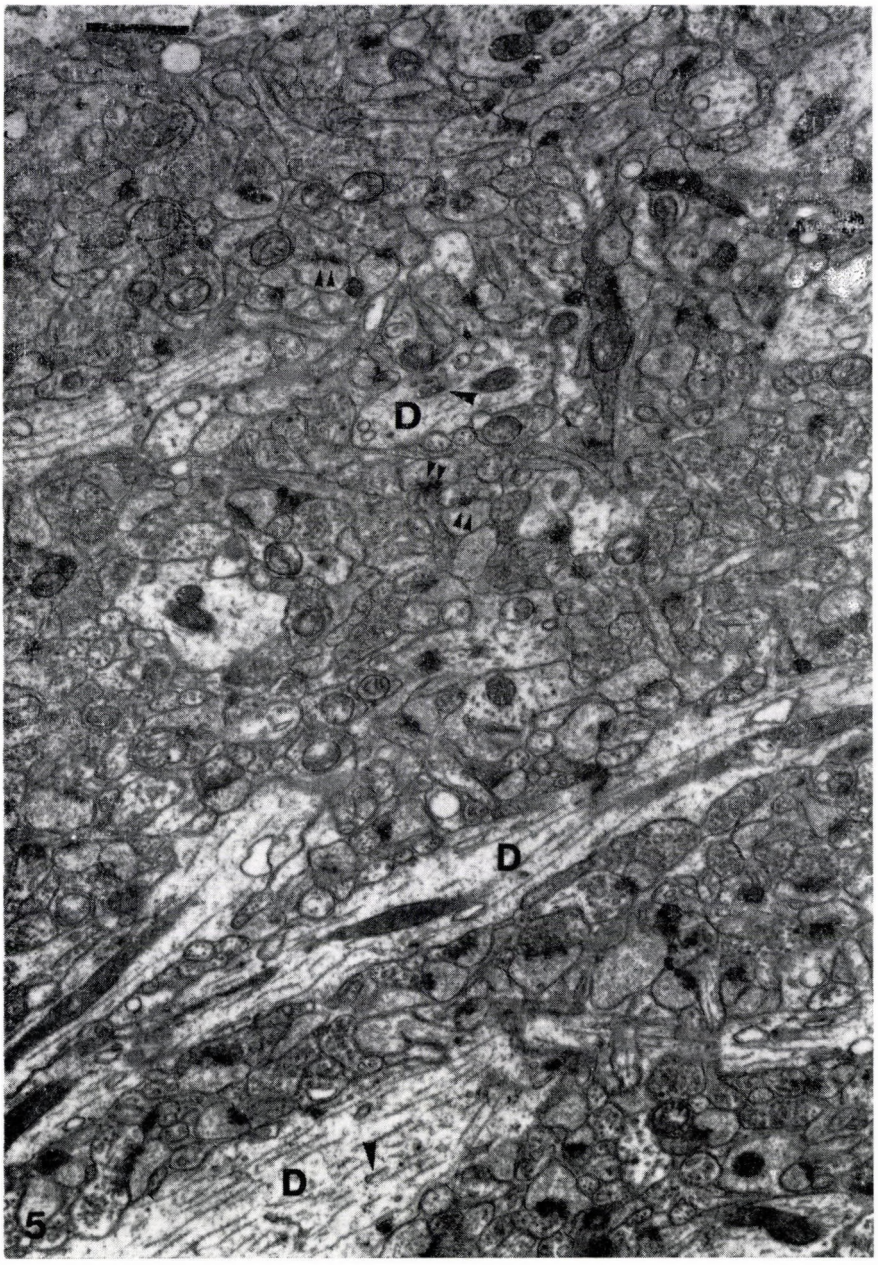

Fig. 5. Molecular layer of the upper limb of dentate gyrus in the hippocampal slice (transverse) incubated for 3 h. Large dendrites (D) can be recognized on the basis of their perpendicular course, elongated mitochondria, arrays of microtubules and occasional RER (arrows). Numerous axo-dendritic spine synapses (double arrow) can be observed. Presynaptic axon terminals contain synaptic vesicles and often a moderately swollen mitochondrion. ×16.000

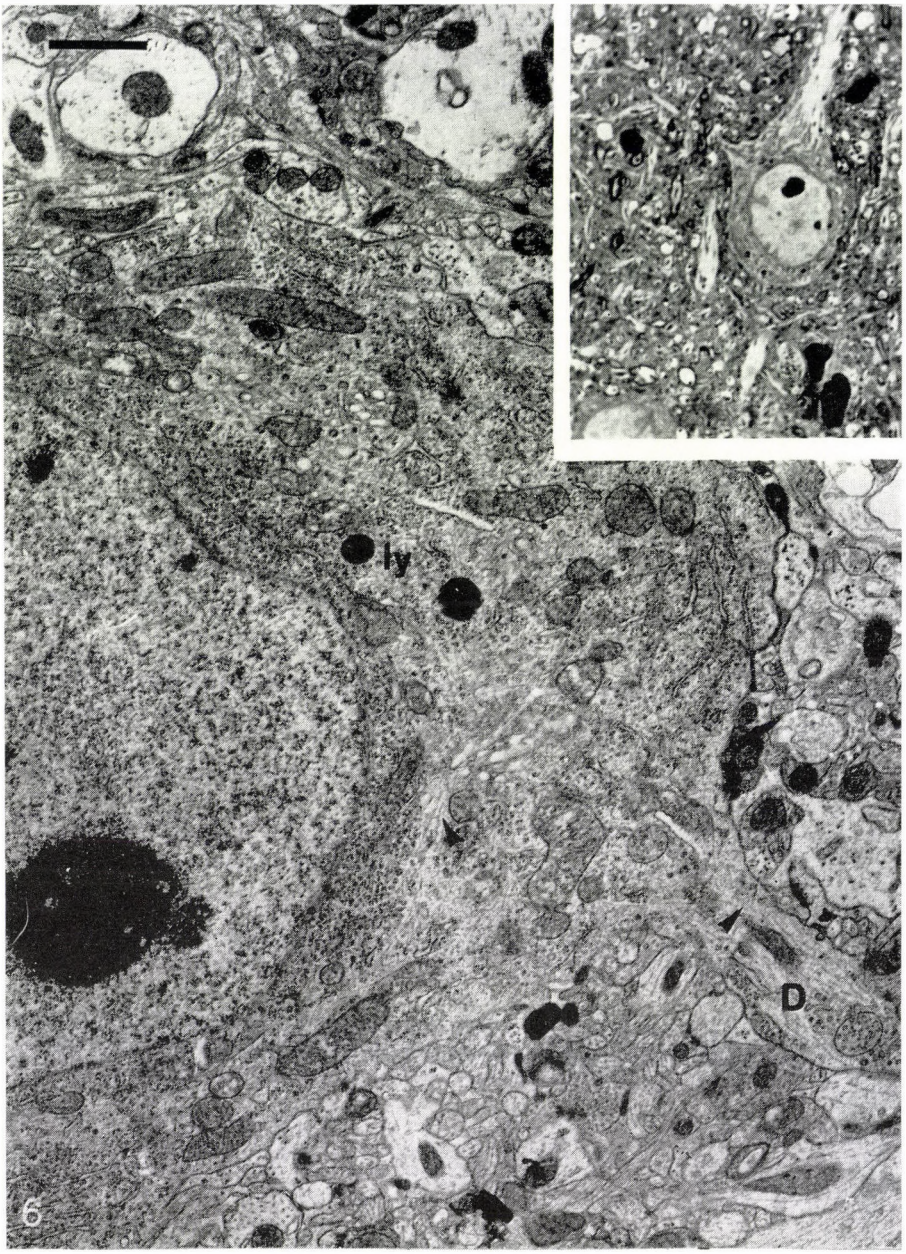

Fig. 6. Small pyramidal cell from lamina III of a slice (frontal) from the parietal cortex incubated for 3 h. Inset shows the overall structure of the cell and its surrounding neuropil in a toluidine blue-stained semithin section (×1.100), while the electron micrograph enlarges on a portion of this cell. The cytoplasm contains flattened cisternae of RER, lysosomes (ly) and aggregations of free ribosomes. The ribosome-free areas are permeated by neurofilaments and neurotubules (arrows) arranged in parallel bundles at the origin of a dendrite (D). The nucleus is oval with evenly distributed, sparse chromatin and a prominent nucleolus. The neuropil adjacent to the cell body shows a good preservation only some dendrites look slightly swollen. ×16.000

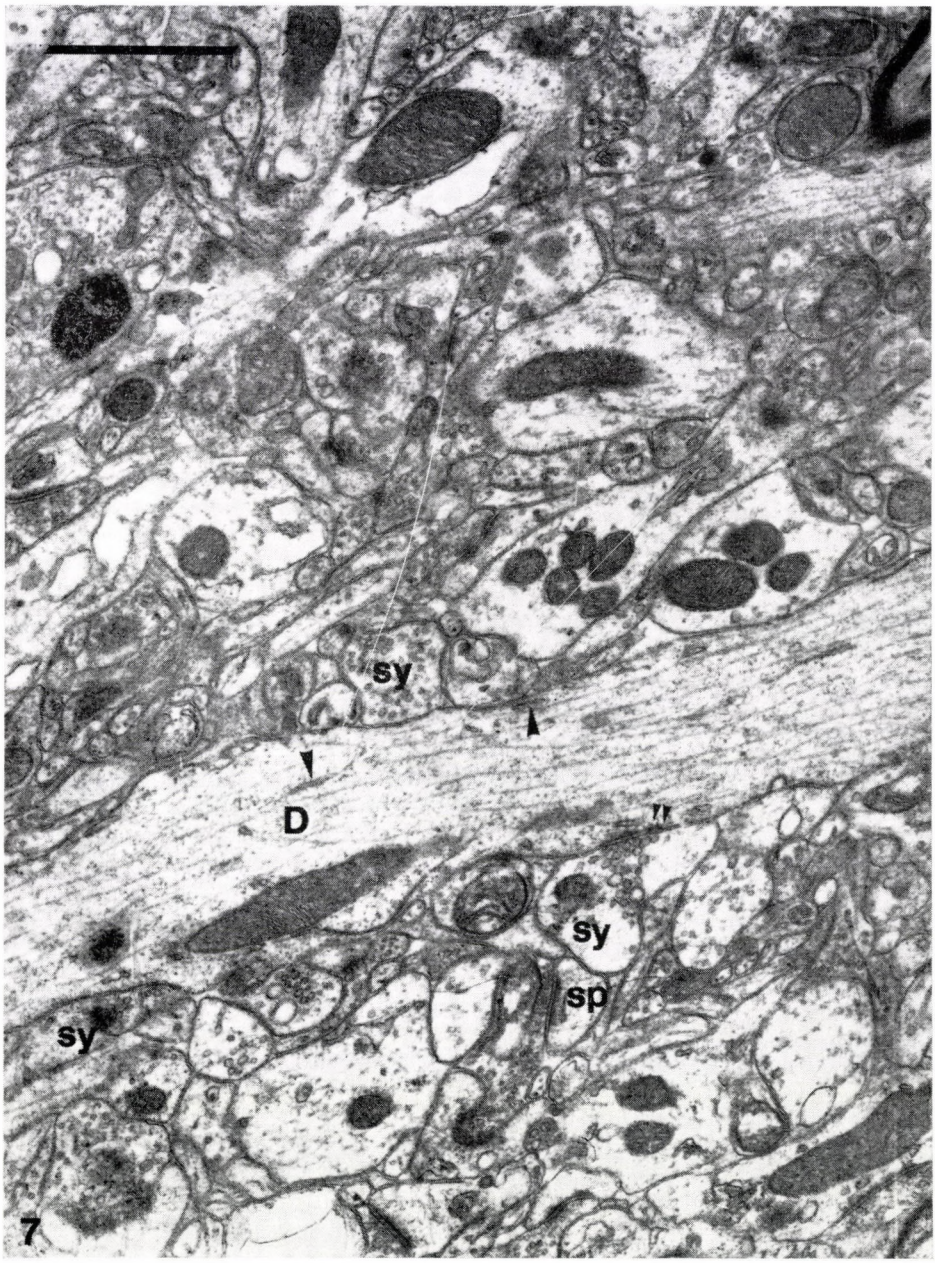

Fig. 7. Parietal cortical slice (frontal) incubated for 3 h. The neuropil is to be seen around the pyramidal basal dendrite (D) in lamina V. The dendrite contains numerous microtubules and some RER (arrows). The shaft of the dendrite is contacted by several presynaptic boutons (sy) one of which forms a synapse (double arrow). In the vicinity of the dendrite, presynaptic boutons form synapses with dendritic spines (sp) ×32.000

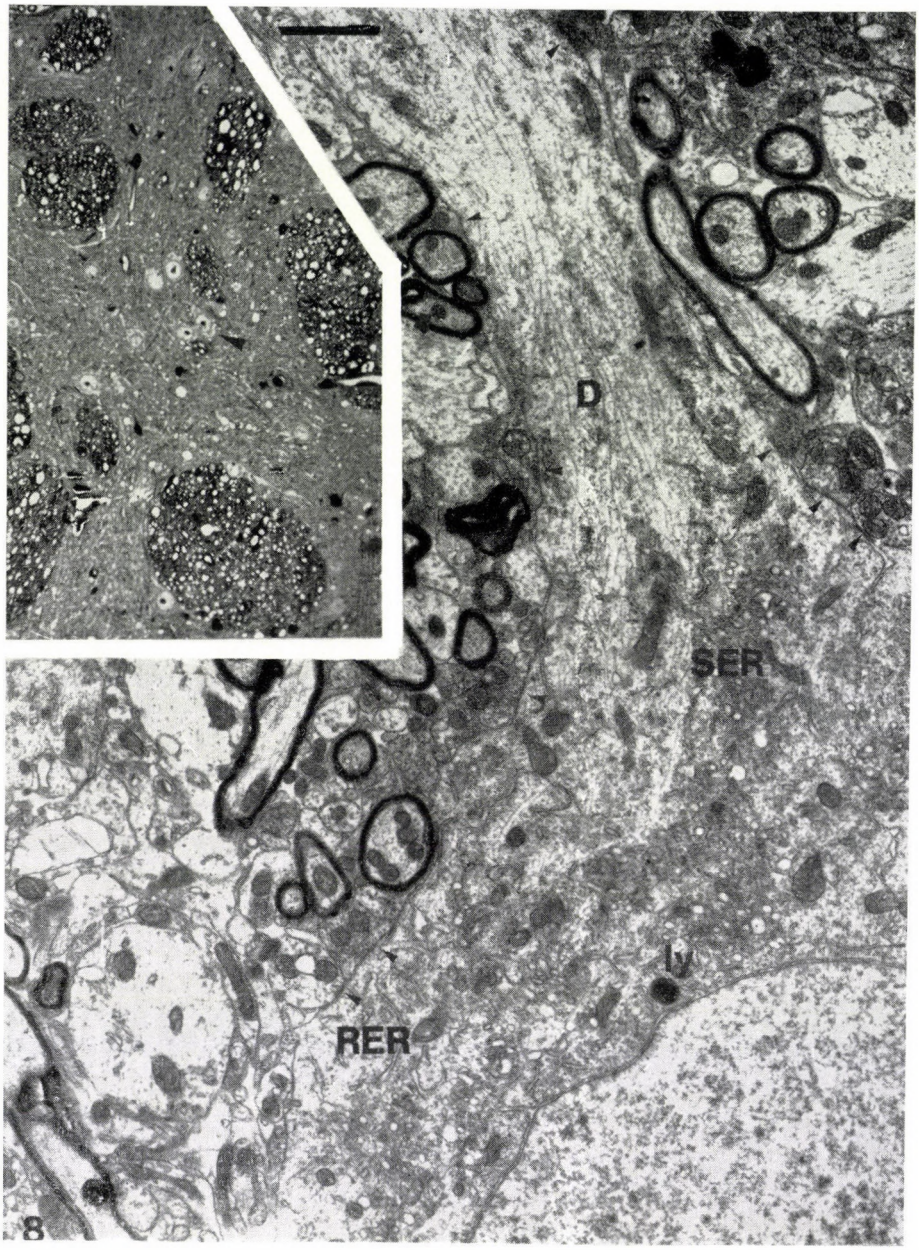

Fig. 8. Striatal slice (frontal) incubated for 3 h. Inset: light microscopic view (×420) of a striatal region in toluidine blue-stained semithin section. The cell indicated by arrow is shown in the electron micrograph. The cytoplasmic area where a dentrite (D) originates from can be seen to contain elongated cisternae of RER, mitochondria, lysosome (ly) and an accumulation of smooth endoplasmic reticulum (SER) vesicles. The cell body and the dendritic shaft is richly supplied with synaptic axon terminals (arrows), the dendrite contains bundles of microtubules. The surrounding neuropil appears to be normal. ×16.000

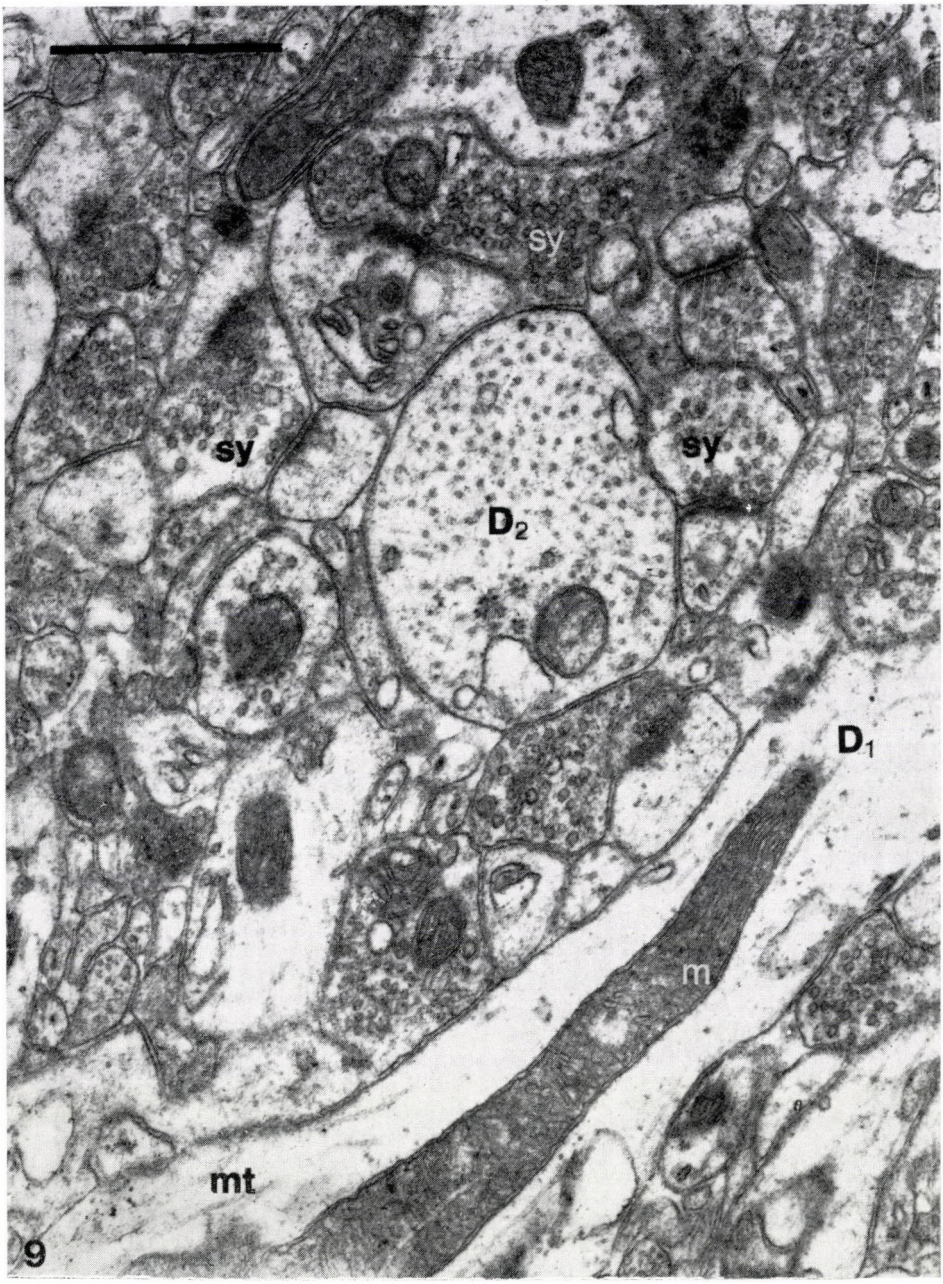

Fig. 9. Neuropil of the striatal slice (frontal) incubated for 3 h. The large dendrite cut longitudinally (D_1) contains an elongated mitochondrion (m) and microtubules (mt). Several presynaptic boutons (sy) are visible synapsing with dendritic appendages. In the middle, a largi-dendrite is in cross section (D_2). ×40.000

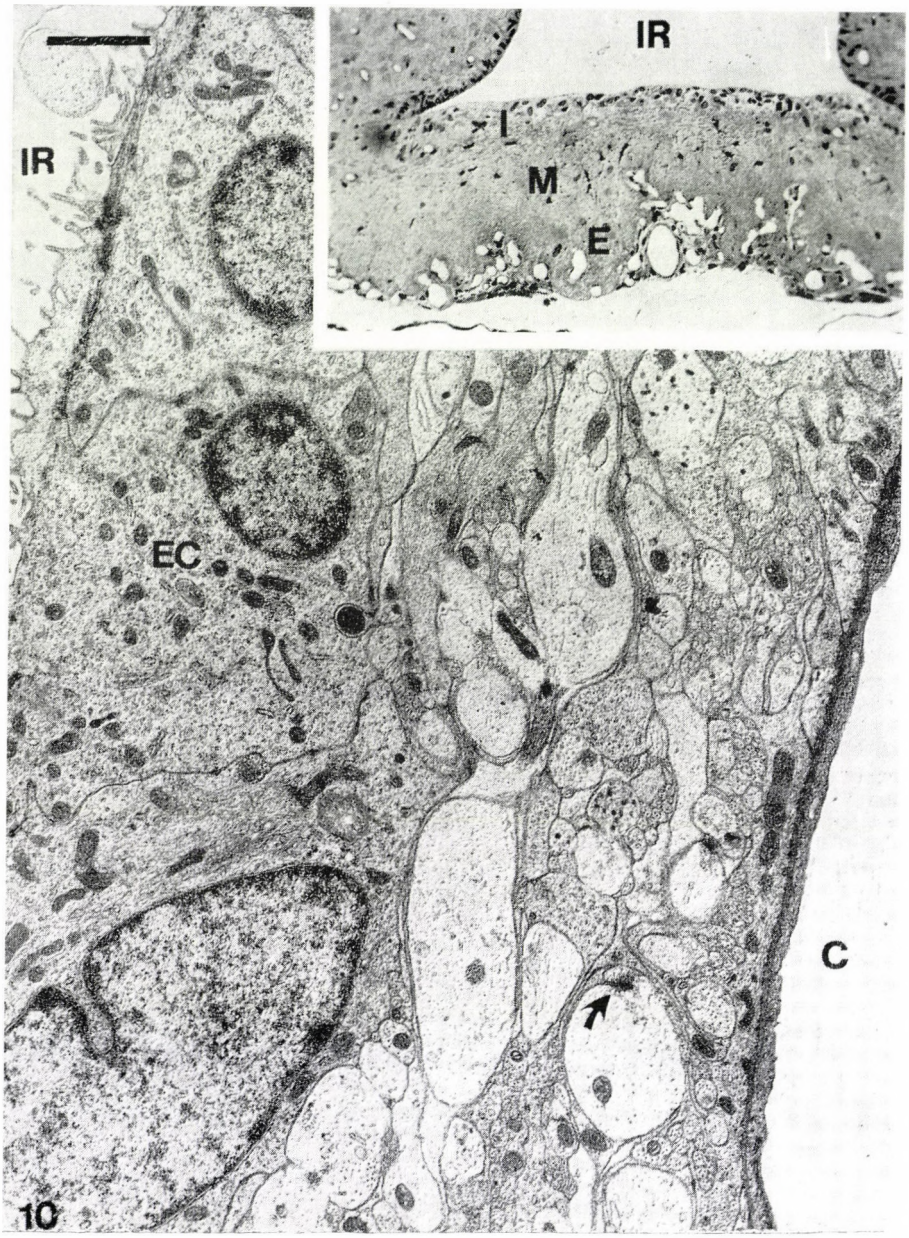

Fig. 10. Inset shows the median eminence slice (frontal) incubated for 3 h as seen in a toluidine blue stained semithin section. The infundibular recess (IR) of the IIIrd ventricle is bordered from below by the median eminence consisting of internal (I), middle (M) and external (E) zones. The ependymal lining of the ventricular floor and the capillary loops of the external zone can well be seen (×90). In the electron micrograph the internal zone is shown adjacent to the floor of the infundibular recess (IR). The ependymal lining formed by microvillous ependymal cells (EC) is well preserved. Underneath the ependyma a variety of profiles can be seen some containing granulated vesicles. Arrow points at a synapse rather infrequent in this region. At right a dilated capillary lumen (C) is to be observed (×16.000)

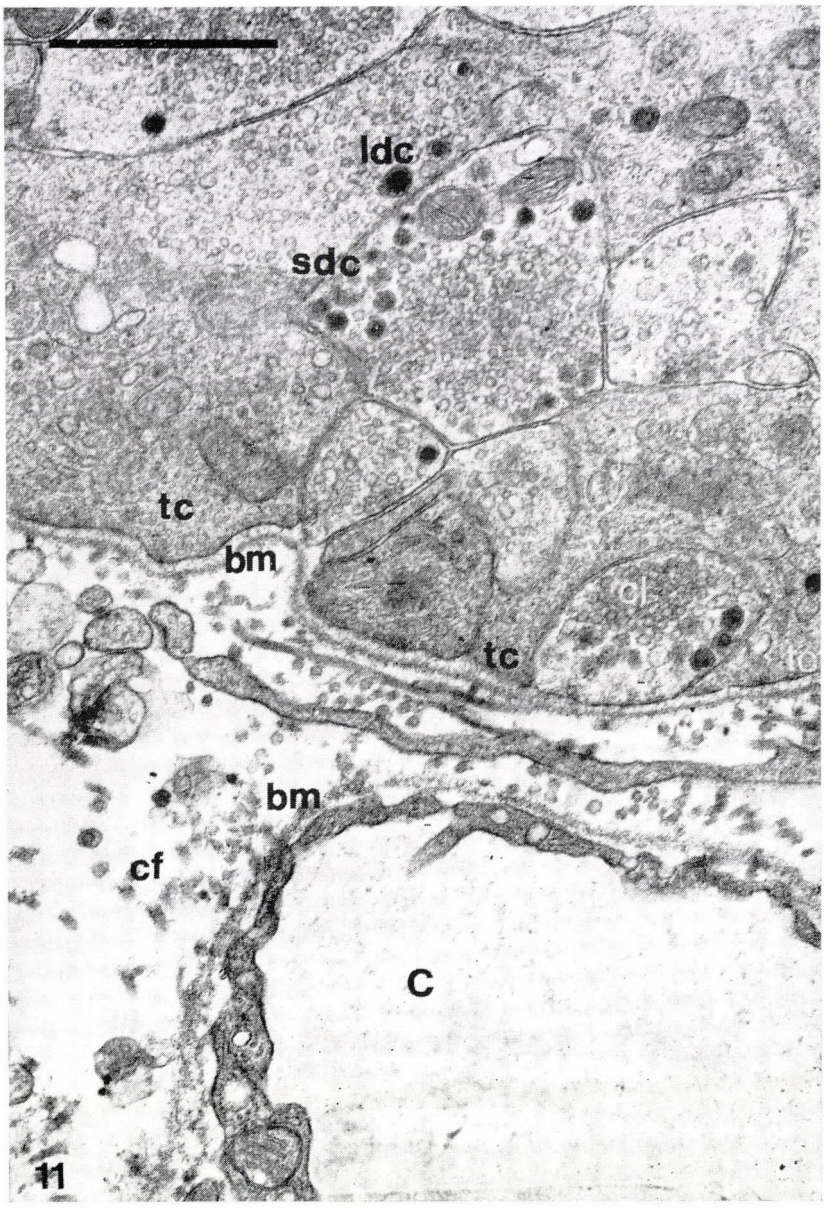

Fig. 11. Median eminence slice (frontal) incubated for 3 h. Electron micrograph of the external zone. The capillary loops (C) are surrounded by a large extracellular space interwoven by collagenous fibres (cf). Note the two basement membranes (bm) demarcating the extracellular space from the capillary and nervous tissue, respectively. In the upper part of the picture vesicle-containing profiles are found in great abundance. Vesicles are of the clear (cl), small dense-core (sdc) and large dense-core (ldc) type. Fibres face the basement membrane only at certain points (arrows) as tanycyte processes (tc) isolate them almost completely from the extracellular space. ×40.000

(Fig. 10). Fibres were of various diameter, some of them were filled with neurosecretory granules and/or other types of clear and dense-cored vesicles. Around capillaries of the internal and middle zones a narrow extracellular space was found contacted by end-feet of tanycytes. The external (palisadic) zone of the incubated median eminence (Fig. 11) was of particular interest due to the high degree of preservation of ultrastructural details. The collagenous pericapillary space was characteristically bordered by two basement laminae, one surrounding the portal capillary the other situated at the border of the nervous tissue. The fenestration of the capillary endothelium was evident. The neuropil of this zone consisted of densely packed varicose nerve fibres and tanycyte processes. Within the nerve fibre varicosities, aggregations of clear, dense-cored and neurosecretory vesicles were seen. At the surfaces of varicosities contacting the basement lamina, membrane invaginations occurred indicative of exo- or endocytosis.

Mesencephalon-pons and medulla

Slices from these areas were cut exclusively in the frontal plane. After incubation they were found totally disintegrated with swollen extracellular spaces, dark, shrunken neurons and empty myelin rings. Glial cells had pyknotic nuclei and severely swollen, 'blown-up' perikarya.

Discussion

Slices of various brain areas cut and incubated under identical conditions proved to be of different viability as judged by their structural preservation after 3 h of incubation.

While incubated slices of the cerebellum, hippocampus — dentate gyrus, cortex, striatum and median eminence displayed a structure comparable to in situ fixed preparations of these areas, those of the hypothalamus, mesencephalon-pons and medulla were found severely damaged.

Structural preservation was assessed relying on criteria such as the basophilia and electron-density of cell bodies, swelling of glial and dendritic elements, width of extracellular spaces, nuclear fine structure and configuration of mitochondria. According to the findings of Cammermeyer [2] and of Brierley et al. [1] dark and electron-dense cells at the light and electron microscopic levels, respectively, represent cellular injury due to hypoxia, oligaemia and hypoglycaemia. Similar alterations were found to be brought about by toxic depolarization by glutamate analogues [5, 6, 14] suggesting an ionic imbalance underlying altered cytoplasmic staining. Swelling of glial elements is also part of CNS tissue reaction to different types of damaging effects [15, 19]. Mito-

chondrial configuration [10] is a most sensitive indicator of local oxygen supply, the condensed from being the structural correlate of unimpaired function [13]. Accordingly, slices considered as structurally recovered were devoid of populations of dark cells, swollen glial or dendritic elements and contained condensed mitochondria throughout.

Among the possible reasons of in vitro structural recovery of some but not all brain areas studied, the different amount and orientation of myelinated fibres seems to be a decisive factor. Regions such as cerebral and cerebellar cortices do not contain bundles of myelinated axons. Afferent fibres are myelinated but once they have left the white matter they take an individual course to reach their targets. Myelinated efferents have unmyelinated initial segments and their myelinated portions gather in the white matter. By contrast, in the mesencephalon, pons and medulla, an abundance of myelinated fibre tracts is present which appear not to slice easily and their compression or dragging by the vibrating blade damages the interposed grey matter territories. Even within slices capable of structural recovery, there appears to be a gradient of sensitivity of structures to damaging effects. Neuronal and glial cell bodies are the most sensitive followed by dendrites and glial processes. Interestingly, unmyelinated axons and synaptic terminals seem to be the most resistent to slicing and in vitro conditions. This observation is in agreement with earlier findings in incubated synaptosomes [12] and explains why the median eminence consisting almost exclusively of axons survives even in toto after excision.

In earlier studies aimed at the observation of conditions of recovery of cerebellar slices [11, 14] we were enlarging on the extent and nature of structural alterations which could be regarded as the "point of no return". Dark cytoplasm and mitochondrial swelling occurring after 1 h of incubation either under hypoxic conditions or in the presence of neurotoxic agents were found to be remarkably reversible, while the dilatation of Golgi cisterns and clumping of nuclear chromatin marked the beginning of irreversible structural deterioration. This seems to be at variance with the conclusion of Brierley et al. [1], who claim that mitochondrial swelling is the leading phenomenon in irreversible nerve cell injury. However, the extreme swelling they document is far beyond the degree of mitochondrial changes we mean under "swelling". Transformations of mitochondria in our system correspond to the function-dependent reversible swelling-contraction cycles observed in vitro by Hackenbrock et al. [10]. It is also worth of notion that inhibitory interneurons such as cerebellar Golgi-cells, were always the first to be affected irreversibly by non-physiological conditions [14].

As far as the time factor is concerned, our previous observations have shown that the structure of freshly cut slices was inferior to that of incubated slices (unpublished data). This suggests that the structure seen after incubation

is a result of recovery from the trauma of slicing or excision and not, as could be argued, a fortunate preservation at the beginning of the process.

Data suggest [3] that over a 12 h period of time recovered slices can be maintained without decay of structure and functional performance. This should obviously vary with regions but a 2 h period after the 1 h recovery time was found in all viable preparations to pass without major alterations in structure. This seems to be sufficient for experimentation.

Although incubated slices have for long been used in CNS research [for References see 3, reviewed also by 16] — the hippocampal slice is a routine preparation in electrophysiology [20], striatal and hypothalamic slices are frequently used in neuropharmacology — it is difficult to extrapolate from our studies as to the experimental morphological value of these preparations. Undoubtedly, for the electrophysiologist one single cell from which proper electrical activity can be recorded is enough. This, however, is not the case in neurochemical and neuropharmacological experiments where values measured refer to the whole tissue and structurally damaged slices are likely to produce artifacts. Our findings suggest that all kinds of functional experiments and measurements are more relevant if performed after a period of structural recovery. Concerning brain areas which in our hands failed to recover, data in the literature must be interpreted with caution unless investigators can prove a reasonable structural preservation of their preparations.

For the purpose of functional morphology the usefulness of the cerebellar slice preparations seems to be well established [7]. Some pioneering work has been performed on the in toto excised median eminence by Zamora et al. [22]. Less convincing are the sporadic reports on the experimental morphology of hand-cut or mechanically chopped hippocampal and cortical slices. The application of a vibratome and the recognition of the significance of the recovery period added to the number of brain areas from which structurally well-preserved slices can be prepared. However, there still remained some regions of interest where in vitro studies require further methodological sophistication.

REFERENCES

1. Bierley JB, Brown AW, Meldrum BS: The nature and time course of neuronal alterations resulting from oligaemia and hypoglycaemia in the brain of Macaca mulatta. Brain Res 25: 483, 1971
2. Cammermeyer J: Differential response of two neuron types to facial nerve transection in young and old rabbits. J Neuropathol Exp Neurol 12: 203, 1963
3. Dingledine R (ed.) Brain Slices. Plenum Press, New York, London, 1984
4. Garthwaite J, Garthwaite G: Neurotoxicity of excitatory amino acid receptor agonists in rat cerebellar slices: dependence on calcium concentration. Neurosci Letts 66: 193, 1986
5. Garthwaite J, Garthwaite G, Hajós F: Amino acid neurotoxicity: relationship to neuronal depolarization in rat cerebellar slices. Neuroscience 18: 449, 1986

6. Garthwaite G, Hajós F, Garthwaite J: Ionic requirements for neurotoxic effects of excitatory amino acid analogues in rat cerebellar slices. Neuroscience 18: 437, 1986
7. Garthwaite J, Woodhams PL, Collins MJ, Balázs R: A morphological study of incubated slices of rat cerebellum in relation to postnatal age. Devl Neurosci 3: 90, 1980
8. Garthwaite J, Woodhams PL, Collins MJ, Balázs R: On the preparation of brain slices: Morphology and cyclic nucleotides. Brain Res 173: 373, 1979
9. Grote J, Reneau D, Thews G (eds): Oxygen Transport to Tissue. Plenum Press, New York, London, 1976
10. Hackenbrock CR, Rehn TG, Weinbach EC, Lemasters JJ: Oxidative phosphorylation and ultrastructural transformation of mitochondria in the intact ascites tumor cells. J Cell Biol 51: 123, 1971
11. Hajós F: Proliferative activity in incubated slices of immature rat cerebellum. Neurosci Letts 71: 153, 1986
12. Hajós F, Csillag A: Structural changes in vitro of isolated nerve endings. I. Effect of cations. Brain Res 112: 207, 1976
13. Hajós F, Csillag A: Variations of matrix electrondensity in brain mitochondria. Acta Morph Acad Sci Hung 26: 107, 1978
14. Hajós F, Garthwaite G, Garthwaite J: Reversible and irreversible neuronal damage caused by excitatory amino acid analogues in rat cerebellar slices. Neuroscience 18: 417, 1986
15. Klatzo I, Piraux A, Laskowski EJ: The relationship between edema, blood-brain barrier and tissue elements in a local brain injury. J Neuropathol Exp Neurol 17: 548, 1958
16. Lynch G, Schubert P: The use of in vitro brain slices for multidisciplinary studies of synaptic function. Ann Rev Neurosci 3: 1, 1980
17. Nevis AH, Collins GH: Electrical impedance and volume changes in brain during preparation for electron microscopy Brain Res 5: 57, 1967
18. Pease DC: Buffered formaldehyde as a killing agent and primary fixative for electron microscopy. Anat Rec 142, 1962
19. Raimondi AJ, Evans JP, Mullen S: Studies of cerebral edema. III. Alterations in the white matter: an electron microscopic study using ferritin as labelling compound. Acta Neuropathol (Berl) 2: 177, 1962
0. Skrede KK, Westgeard RH: The transverse hippocampal slice: A well defined cortical structure maintained in vitro. Brain Res 35: 589, 1971
21. Van Harreveld A, Ochs S: Cerebral impedance changes after circulatory arrest. Amer J Physiol 187: 180, 1956
22. Zamora AJ, Garosi M, Ramirez VD: Poststimulatory endocytosis, microvesicle repopulation and changes in smooth endoplasmic reticulum in nerve endings of the median eminence superfused in vitro. Neurosci 13: 105, 1984

Acta Morphologica Hungarica 37 (3—4), pp. 201—217 (1989)

CADMIUM INFLUENCE ON THE RAT LIVER

M. Vojtíšek, D. Hulínská, D. Bittnerová, M. Cikrt, V. Hulínský

INSTITUTE OF HYGIENE AND EPIDEMIOLOGY, PRAGUE VŠCHT, LABORATORY OF ELECTRON MICROANALYSIS, PRAGUE, CZECHOSLOVAKIA

(Received 4 October 1988)

Influence of cadmium on the intestinal and hepatic tissue of rat was studied in acute injection and oral as well as subchronic and chronic oral experiments with the purpose of better understanding of the penetration mechanisms of cadmium into these tissues.

Acute single oral dose of $CdCl_2$ 32.5 $mg \cdot kg^{-1}$ inhibited in vitro the respiration of intestinal scrapings (44%) and in liver slices (25.7%). In combined oral doses of 32.5 $mg \cdot kg^{-1}$ + 162.5 $mg \cdot kg^{-1}$ inhibition in the intestine increased with exposure time, while in the liver it decreased. Amount of presumable metallothionein in the liver was approximately ten times higher than that in the intestine. Respiration was measured by a Clark electrode. Binding of cadmium to metallothionein was determined by column chromatography and spectrophotometry.

Physiological findings are in agreement with morphological ones. In cases when, following an acute single oral dose, a 50% change was detected in the absorptive jejunal zone, a 10% change was observed in the liver parenchyma. In the case of combined oral dose of 60—70% of absorptive villi zone is damaged by cadmium, which penetrates by passive diffusion into lamina propria and by blood to the liver, where it acts toxically in 30%. Active transport of cadmium after chronic application is preserved. Correlation of physiological and morphological findings was evident.

Keywords: Clark electrode, metallothionein ,mitochondrial swelling, X-ray microanalysis

Introduction

Toxicological importance of cadmium is nowadays fully recognized [5]. The liver belongs to the tissues, which has a long biological half-life: 10—20 years [15]. Some in vitro studies are dealing with cadmium influence on oxidative and energy metabolism in liver mitochondria [9, 18]. Cadmium also decreases cellular oxygen consumption in isolated hepatocytes [14].

Diamond and Kench [2] observed respiration of liver mitochondria with succinate under the influence of cadmium. In oxygen consumption there is a great increase for low cadmium concentration but in rats chronically poisoned with cadmium there is no apparent stimulation. Sabbioni et al. [17] conclude from results of chronic cadmium exposure tests that cadmium associates with cellular organelles.

Send offprint request to: M. Vojtíšek, Inst. of Hygiene and Epidemiology, CHPNP, 100 42 Prague, Šrobárova 48, Czechoslovakia

The aim of this work is to contribute to the knowledge of mechanism of absorption and cellular localization of cadmium in the liver under various experimental conditions.

In the focus of interest there was also the comparison of the cadmium influence on the liver as compared to the intestine [8].

Materials and methods

Experiments were performed on female Wistar rats, average weight 200—250 g. Rats were maintained on standard pellet diet, water ad lib.

In acute oral test with a single dose, rats were given in ether narcosis 32.5 mg · kg^{-1} $CdCl_2$ on the first day by gavage. This dose was effective for 24 h. In acute test with combined doses, rats were premedicated with an oral dose of 32.5 mg · kg^{-1} $CdCl_2$ 24 h before the application of second oral dose of 162.5 mg · kg^{-1} by gavage. Second cadmium dose was effective for 1, 3, 24 h or 5 days.

In acute injection test, dose of 0.5 mg of $CdCl_2$ in 0.5 ml of saline was injected into ligated jejunal segment under ether narcosis. Control rats were injected with saline only.

In subchronic tests rats were given orally by gavage 0.5 mg of $CdCl_2$ in 0.5 ml of saline for 3 weeks, control rats were given saline only.

In chronic tests rats were drinking 10 ml on average of a solution with 250 mg · l^{-1} $CdCl_2$ for 3 months. Control rats were drinking distilled water only.

There were six rats in each experimental and control group.

Oxygen consumption was measured by a Clark electrode on a scraping of jejunal mucosa or sections of medial liver lobe maintained in Krebs-Ringer buffer pH 7.4 at 37 °C. Determination of metallothionein was performed according to Squibb et al. [19].

Cytosol from the liver or intestinal tissue was separated by means of column chromatography (Sephadex G-75). All fractions were analyzed by spectrophotometry (Unicam SP-1800) at 250 and 280 nm and then by atomic absorption spectrophotometry (Varian Techtron AA 175) for their cadmium content. Results from these measurements enable evaluation of metallothionein content, which is deduced from cadmium amount in fractions.

For histochemical study jejunum and liver were frozen in liquid nitrogen and cut with a Reichert cryocut. Succinate dehydrogenase (SDH) activity, Mg^{2+} adenosine triphosphatase (ATPase) activity, acidic (AcP) and alcalic (AlP) phosphatase activities were determined according to Lojda and Papoušek [11] in the intestine and liver.

Energy dispersive spectrometer (EDS) together with Jeol LCX II microscope were used for the study of ultrathin sections of liver in transmission (TEM), scanning (SEM) and scanning transmission (STEM) mode like in our previous study [8].

Liver and intestinal tissues were prepared for electron microscopy in the same way as in an earlier X-ray microanalytical study [7].

Results

Table I enables comparison of changes of oxidative metabolism of intestinal and liver tissues under various experimental conditions — exposures to cadmium. It seems, that in vitro intestinal tissue reacted after acute exposure to cadmium more markedly than liver tissue. In chronic tests the physiological reaction to cadmium was comparable in both tissues studied.

Figure 2 is depicting determination of cadmium binding low molecular proteins, presumably metallothioneins, in intestinal and liver cytosol. An approximately ten times higher amount of these proteins was found in liver than in intestine for acute combined and chronic tests.

Table I

Inhibition of respiration by cadmium, comparison in small intestine and liver

Application	$CdCl_2$	Exposure period	Inhibition	
Acute single			Intestine	Liver
Controls	0		0	0
Experiment	32.5	24 h	44.03	25.71
Acute combined				
Controls	0		0	0
Experiment	32.5 + 162.5	24 + 1	50.35	43.21
Experiment	32.5 + 162.5	24 + 3	56.28	27.38
Experiment	32.5 + 162.5	24 + 24	70.84	4.0
$CdCl_2$ doses in acute experiments are related to: $mg \cdot kg^{-1}$				
Chronic				
Controls	0		0	0
Experiment	250	3 months	38.43	39.5
$CdCl_2$ dose in drinking water related to: $mg \cdot l^{-1}$, average consumption: 10 ml/day/rat				

All inhibition values are related to 100% value of controls. Statistical significance: *t*-test values: $P < 0.01$

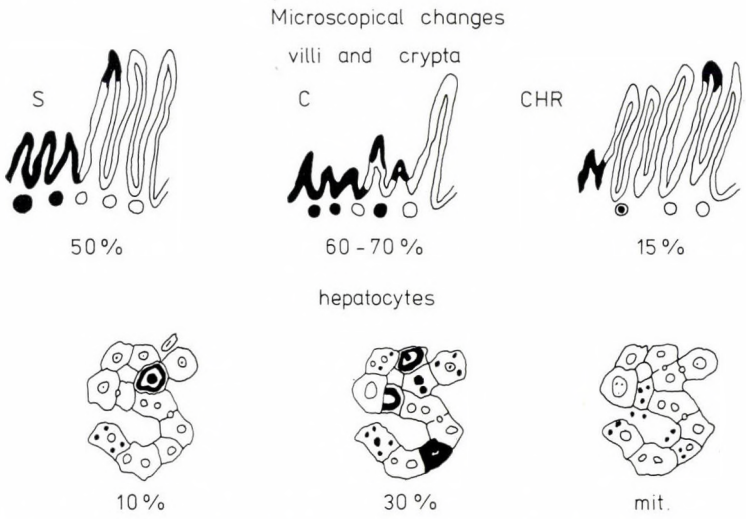

Fig. 1. Diagram, depicting microscopical changes of villi and crypts of intestine and changes in liver hepatocytes. Acute single (S), combined (C), chronic (CHR) cadmium doses, mitochondria (mit.)

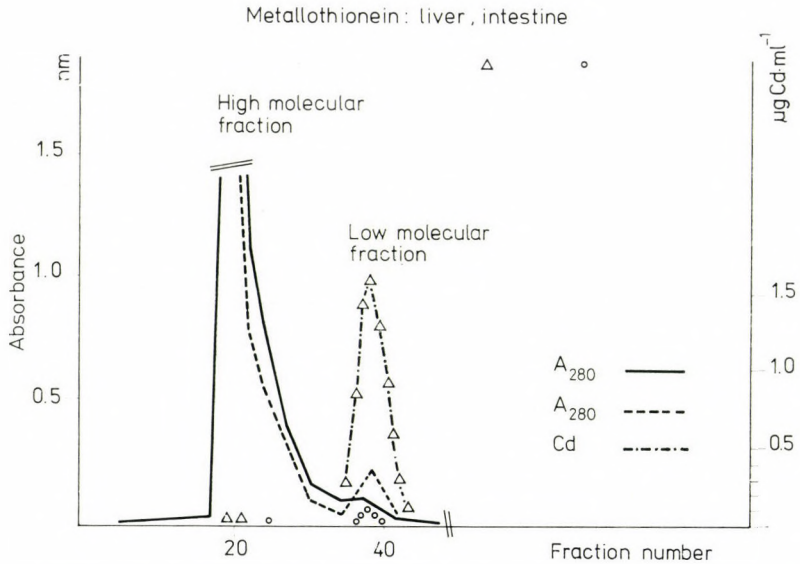

Fig. 2. Diagram, showing cadmium binding low molecular protein, presumably metallothionein in the intestine and the liver

There is a correlation of physiological and morphological findings for both tissues. Histological and histochemical changes in the liver after oral and injection application of cadmium into the intestine are influenced by active or passive penetration throughout the tissues.

In acute injection test cadmium was determined in the liver during half

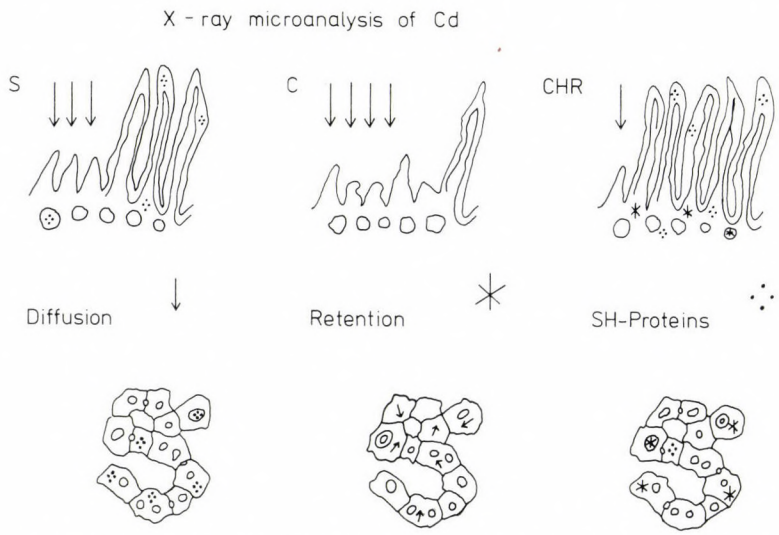

Fig. 3. Diagram, depicting X-ray microanalysis of cadmium penetration through intestinal villi and hepatocytes

an hour [7]. Hypertrophy of the observed medial liver lobe was macroscopically obvious. This hypertrophy was caused by parenchyma vacuolization, dilatation of interlobular and centroacinous veins and in peripheral lobes also dilatation of bile canaliculi, filled with bile.

In the case of passive penetration of acute oral single dose, microscopic findings, e.g. vacuolization of some hepatocytes are similar to findings in intestinal villi where a similar vacuolization of enterocytes occurs.

Combined oral dose of cadmium after 24 h causes focal changes in the liver parenchyma resulting after 5 days in necroses, especially in the region of changed bile canaliculi. In centroacinous and interlobular regions under the influence of venous changes focal fibroses appear. Pathological changes in the parenchyma of medial lobe were not detected after subchronic or chronic cadmium applications with the exception of microscopical changes of cellular organelles. These chronic changes in the liver correlate with changes in intestinal tissue, where only individual enterocytes on the tip of villi are damaged.

Changes after application of acute single, combined and chronic doses of cadmium, concerning villi, crypts and liver lobules are depicted on a diagram (Fig. 1). We presume, that in the case of an 50% change in absorptive jejunal zone after acute single cadmium dose there are 10% changes in liver parenchyma, manifesting as alterations of individual cells only.

In the case of combined dose, when 60—70% of the absorptive villi zone is damaged, cadmium penetrates by passive diffusion into lamina propria and by blood to liver, where it acts toxically in 30%. Longer period (5 days) of exposure to cadmium results in the origin of focal necroses in places of bile canaliculi and venous changes.

Active transport of cadmium is preserved after chronic application, when villi are almost intact. The part of cadmium, which is bound to metallothionein (MT) at the base of mucosa decreases passive cadmium penetration through the jejunal villi and by blood to the liver. After repeated cadmium exposures the liver synthesizes MT (Fig. 2). This may be the reason of only small alteration of the liver parenchyma.

Morphological changes are accompanied by histochemical ones. In acute application of cadmium focal increase of activity of alcalic phosphatase (AlP) in the region of bile canaliculi dilatation in peripheral lobules was observed. In central lobules AlP activity remains positive at the biliary pole of hepatic cells in the vicinity of Herring channels and in the endothelium of capillaries as in controls.

Only in the case of injection of cadmium into ligated intestine is AlP activity in all regions observed decreased as compared to the controls.

Succinate dehydrogenase activity (SDH) is decreased in acute experiments (Fig. 5) in centroacinous hepatocytes and is negative in hepatocytes of peripheral lobules.

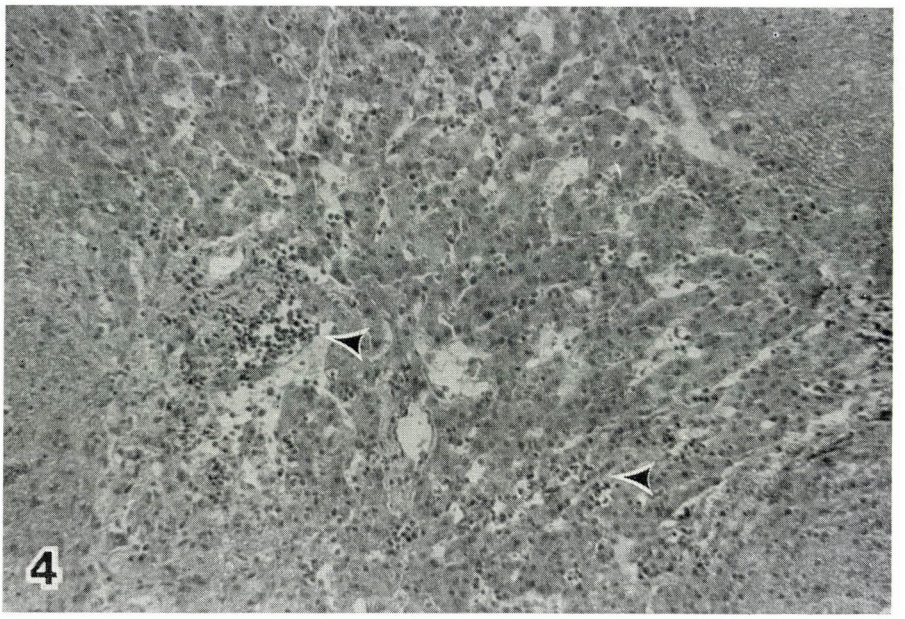

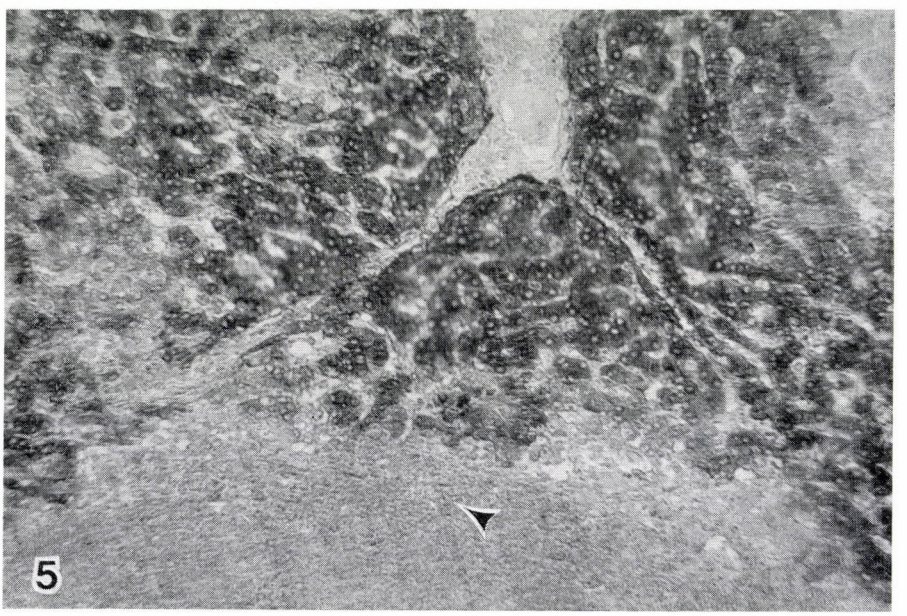

Figs 4—5. Increased activity of acid phosphatase (AcP) in Kupffer cells or in inflammatory infiltration (arrow) and decreased activity of succinate dehydrogenase (SDH) in altered hepatocytes (arrow) after acute combined cadmium dose (×250)

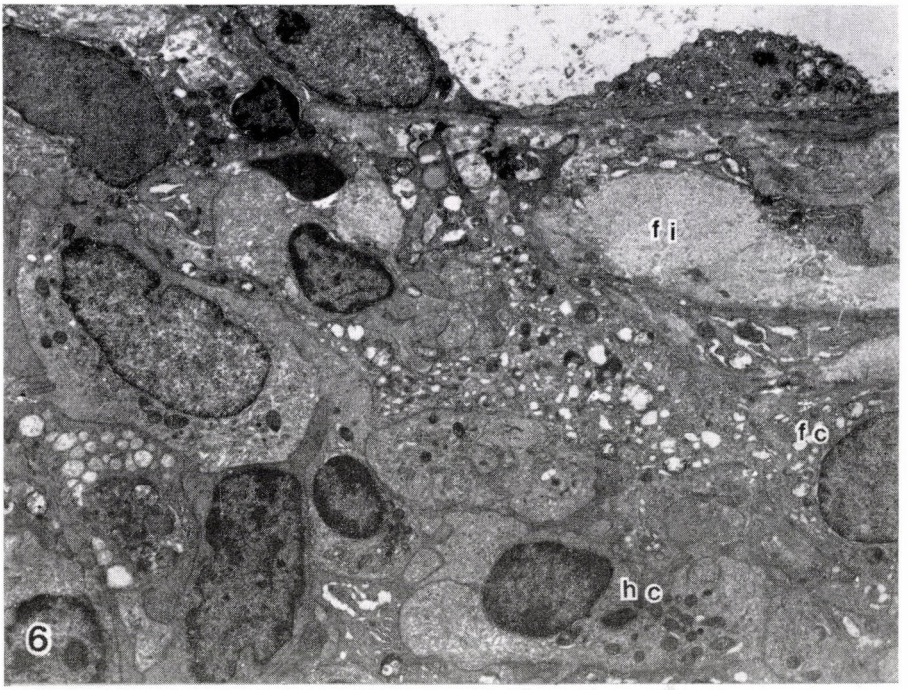

Figs 6—7. Acute single and combined cadmium dose: inflammatory infiltration of the centroacinous zone, containing lymphocytes, histiocytes (hc), fibroblasts (fc) and increased fibrosis (fi) in the vicinity of blood vessels (bd) and bile capillaries (bl) (×2 400)

In the case of acute injection, SDH activity is negative in the parenchyma of central and peripheral part of the medial liver lobe.

Activities of both enzymes are in agreement with the degree of morphological changes of hepatic cells in acute tests after oral and injection applications.

In the case of combined cadmium dose, after a period of 1—3 h, activity of AlP and SDH are decreased but activity of AcP in the portobiliar spaces and capillary endothelium is higher (Fig. 4) as compared to the control. With more prolonged combined treatment (5 days), in the pathologically changed regions there is a highly positive inflammatory infiltration (Fig. 6) and fibrosis (Fig. 7). Lipid droplets accumulate in hepatocytes. In damaged hepatocytes there is no SDH activity (Fig. 5).

In chronic tests AlP activity is increased as compared to controls in endothelial cells only, in other experimental conditions it is unaltered. SDH activity is higher in centroacinal zone than in the peripheral zone, which is in agreement with changes of mitochondria in peripheral hepatocytes. In all experiments hepatic foci were seen to be damaged to various degree but also intact lobules occurred with unchanged enzyme activity in the hepatocytes. It is difficult to determine whether a regeneration process takes place or it is a spot, where cadmium had not penetrated.

Electronoptical studies of medial liver lobe depict hypertrophy of hepatocytes in acute injection cadmium treatment (Fig. 8) as well as in orally applied combined cadmium treatment (Fig. 9) combined with dilatation and hypertrophy of cell organelles. The cellular integrity is undamaged, though. Only after cadmium injection appears a thinning of the cell membrane. The dilatation of smooth (SER) and rough (RER) endoplasmic reticulum and multiplication of prominently dense mitochondrial matrix with dilating cristae were obvious in the case of combined (Fig. 12) as well as injection treatments (Fig. 13).

In the case of oral application of the acute dose, swelling of mitochondria was observed but there was one change of cristae or matrix density. The RER in the vicinity of nuclei is dilated into a vacuolar structure (Fig. 10).

In the case of combined cadmium dose only changes we found not only in the degenerating organellae structures (Fig. 11) but also in the integrity of cells in foci of necroses and increased fibroses (Fig. 7).

In chronic cadmium tests, hepatocyte hypertrophy was not observed (Fig. 16). Their cellular membrane is unchanged, but in the peripheral cytoplasm of these hepatocytes mitochondria are swollen (Fig. 15). The same finding was observed with the subchronic dose (Fig. 14). After the change of cristae mitochondria are being released into the Disse spaces through the cellular wall, creating bleb-like extrusions. Rough endoplasmatic reticulum in the vicinity of nuclei is unchanged (Fig. 17). Centroacinous hepatocytes

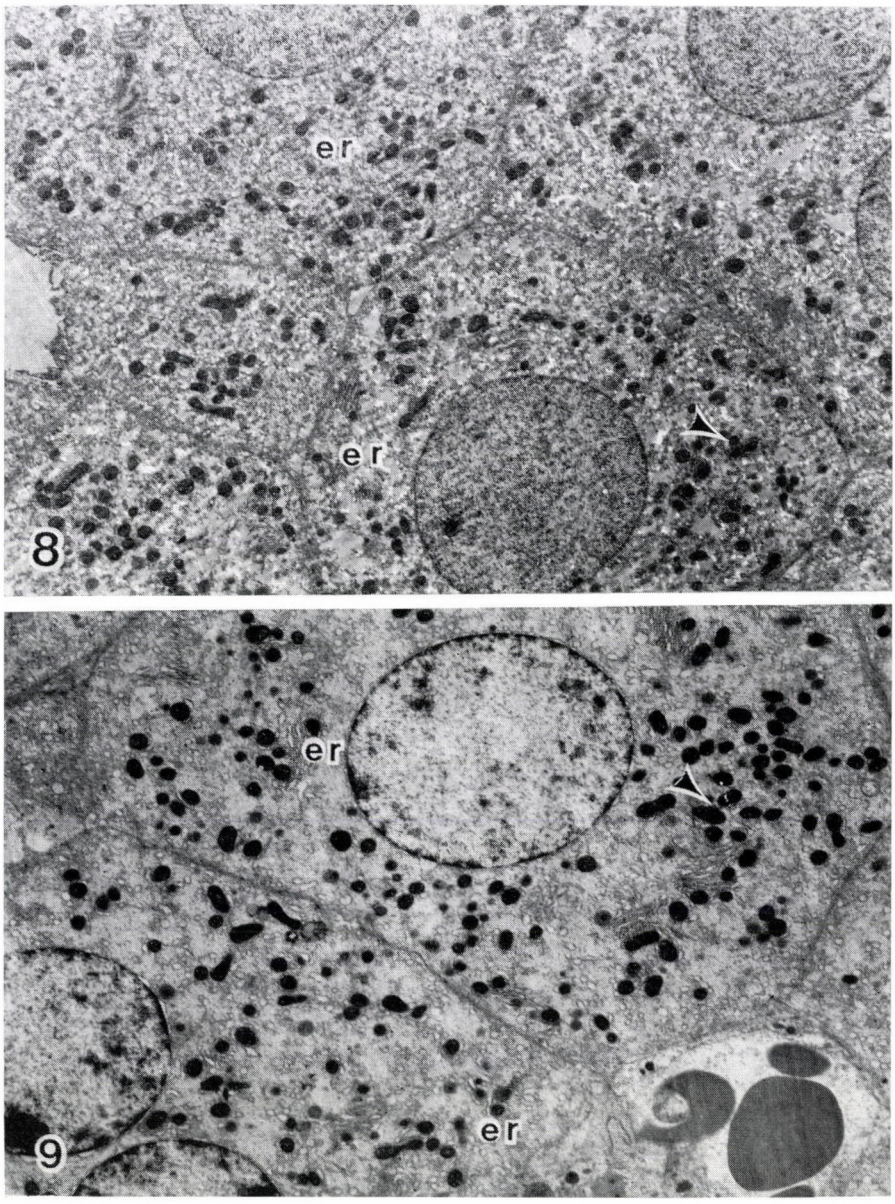

Figs 8—9. Alteration of mitochondria (arrow) and endoplasmatic reticulum (er) in hypertrophic hepatocytes of centroacinous zone after injection dose and after oral combined dose of cadmium (×3 600)

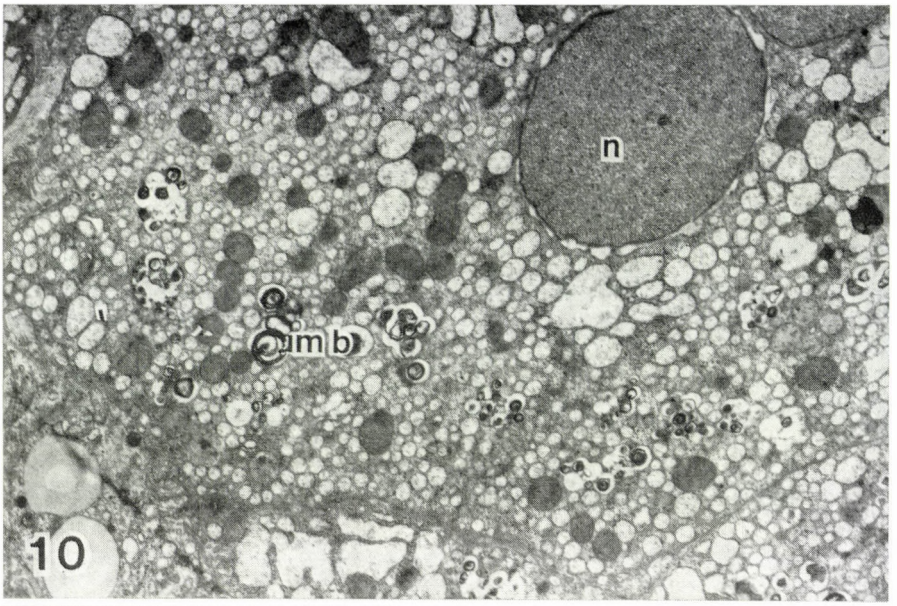

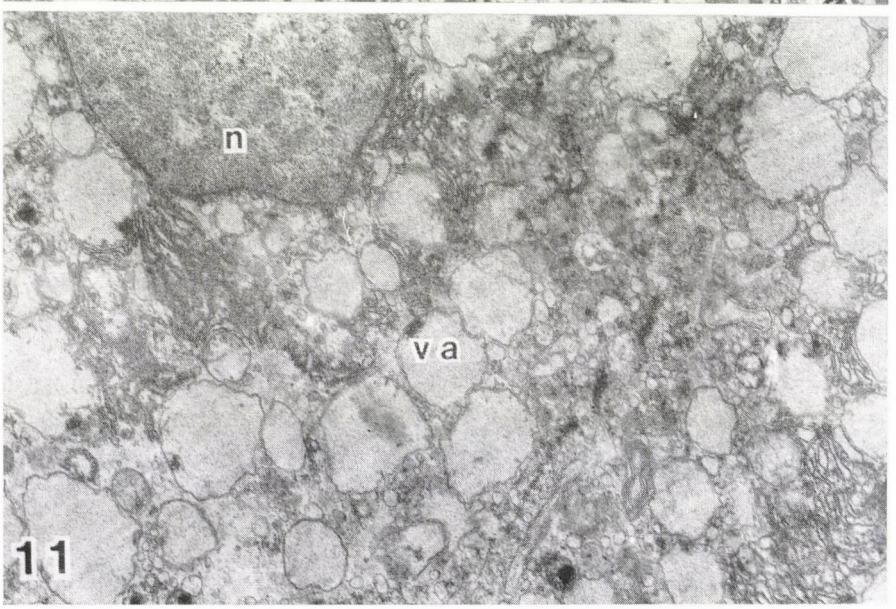

Figs 10—11. Acute single cadmium dose: dilatation of the cisternae of endoplasmatic reticulum (×4 200). In combined cadmium dose vacuolar structures (va) appear around the nucleus (n) arising from mitochondria and formation of myelin-like bodies (mb) in hepatocytes (×13 000)

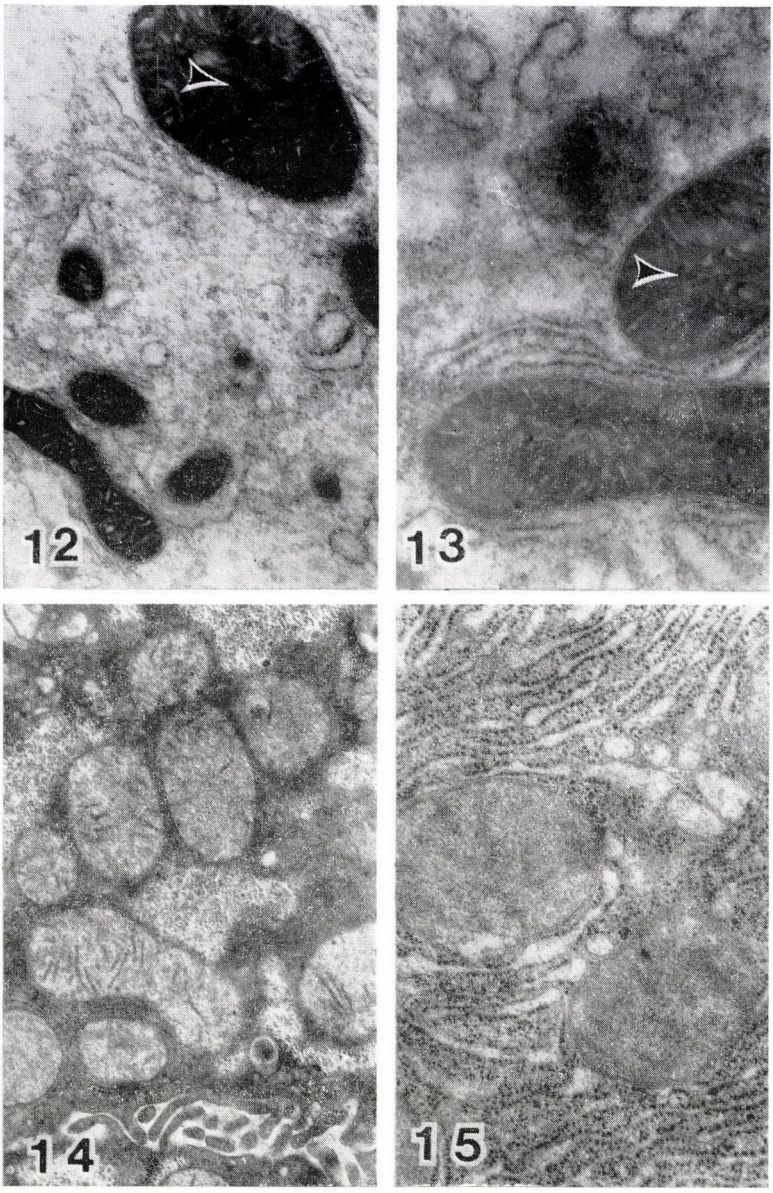

Figs 12—15. The changed, swollen mitochondria with increased density of their matrix (arrow) in the case of injecation and combined doses and unchanged density of mitochondrial matrix and cristae of swelling mitochondria in subchronic and chronic cadmium doses (×29 000)

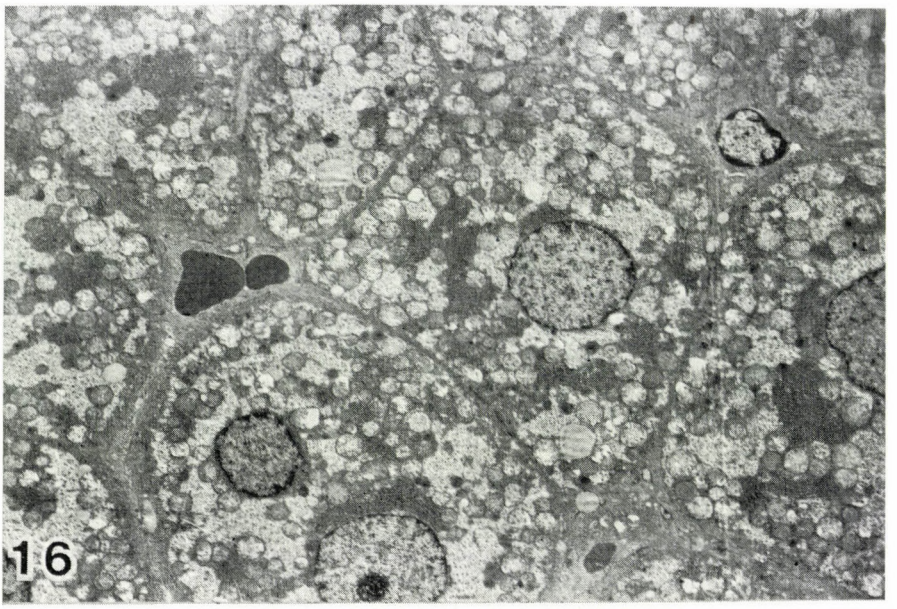

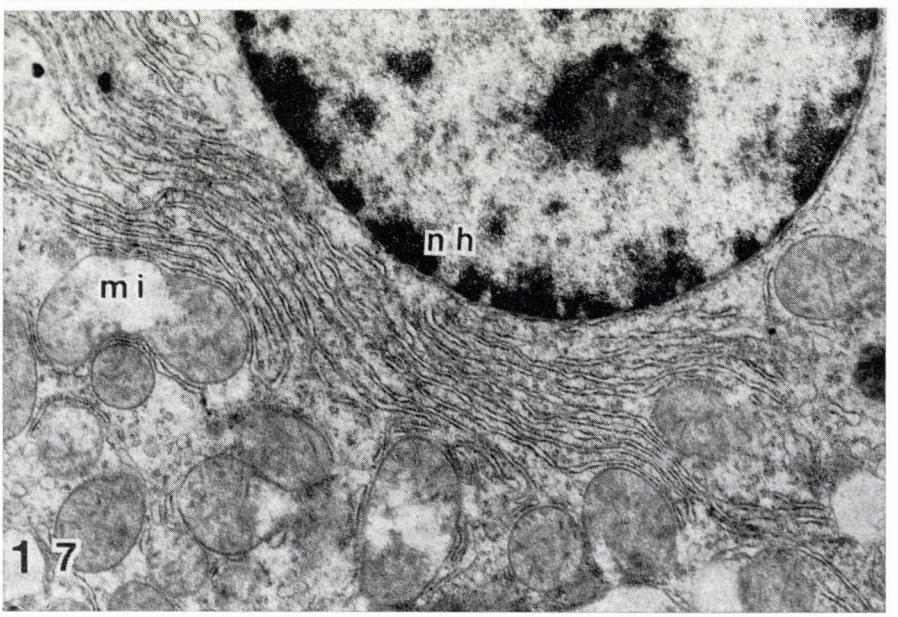

Figs 16—17. Chronic cadmium dose: Unchanged hepatocytes of centroacinous zone (×2 200). Higher magnifications of hepatocytes show microscopical changes concerning some mitochondria (mi) and nucleus heterochromatin (nh) (×17 000)

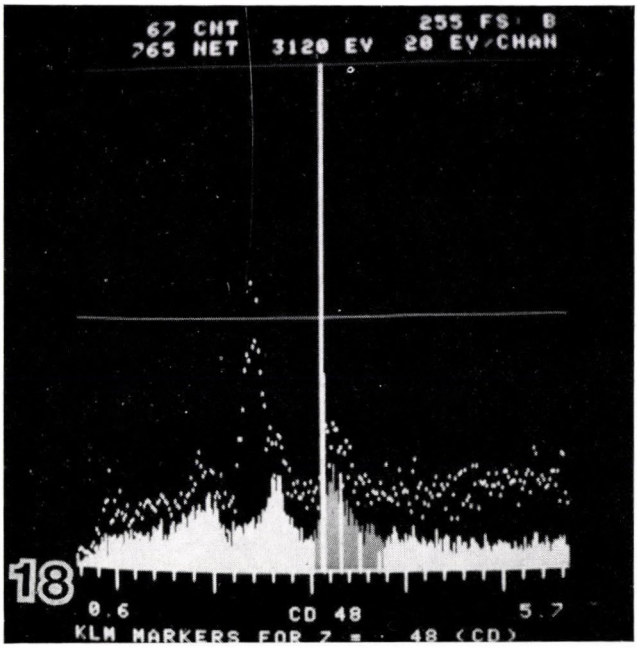

Fig. 18. Chronic cadmium dose: X-ray microanalysis EDAX system, peak showing L-lines of cadmium in mitochondria

contain more intact mitochondria and moderately dilated ER then peripheral ones.

In the majority of tests, nuclei of hepatocytes with multiplied granular component of nuclear substance were observed and in chronic tests perichromatic granules were condensed under the nuclear membrane in a higher degree. Changes of mitochondria and RER are connected with degree of cadmium retention and were verified by X-ray analysis (Fig. 19).

On a diagram (Fig. 3) it is demonstrated that after single and combined cadmium dose this metal is dispersed in liver hepatocytes, because it penetrated by diffusion through damaged spots of villi.

In acute injection test high amounts of cadmium were proved by X-ray microanalysis after half an hour first of all in nuclei of undamaged hepatocytes.

In chronic test cadmium is retained in the intestinal mucosa, especially at the base of Lieberkühn crypts as well as in the liver. X-ray analysis with an E dax system demonstrated higher cadmium amount in mitochondria (Fig. 18) than in other organellae.

Discussion

Findings on inhibition of oxygen consumption are in accordance with microscopical changes in acute tests for the liver and intestine. In the case

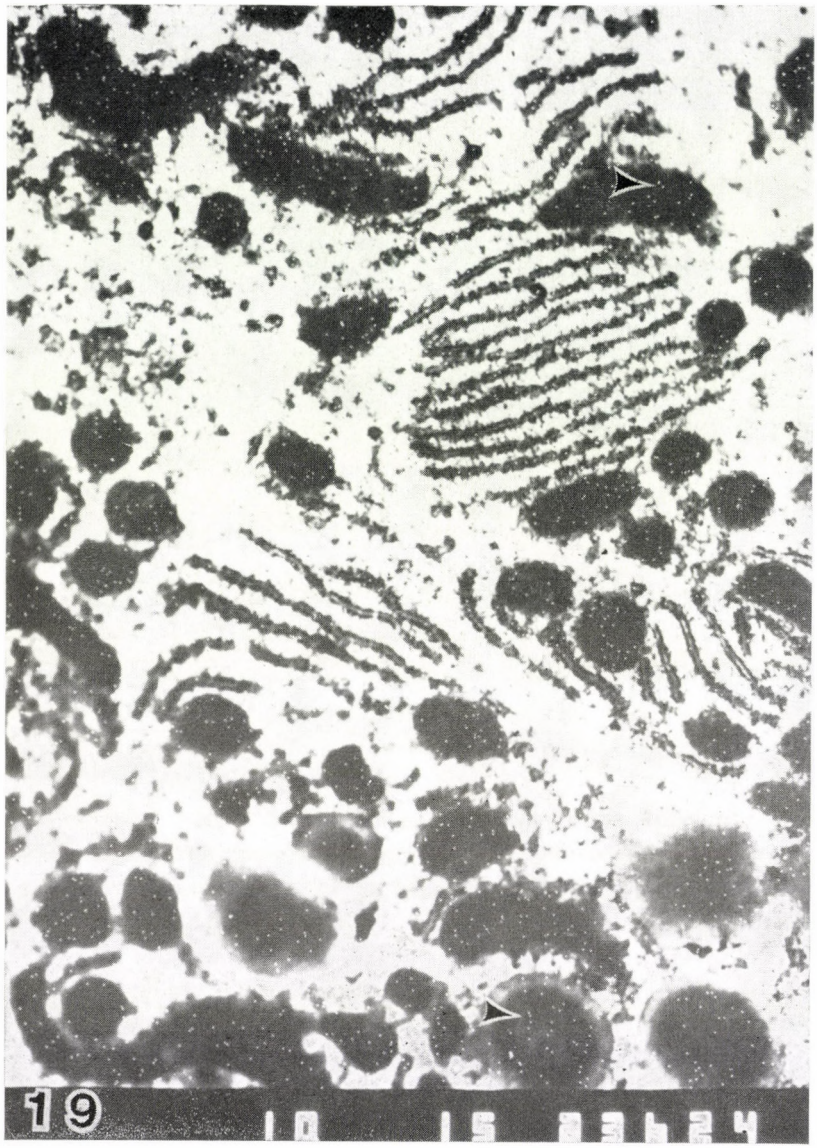

Fig. 19. Chronic cadmium dose: Point X-ray microanalysis of cadmium showing dispersive white bodies (cadmium) in the mitochondria (arrow) (×15 000)

of intestine influenced with single cadmium dose almost double inhibition was observed when compared the liver, which is supported by the finding of more microscopic damages to villi structures [8]. With acute combined cadmium dose there is increasing inhibition of respiration of hepatic slices, and injury to liver tissue is more prominent.

With prolonged exposure of tissue to cadmium with combined doses there was no inhibition of respiration in the liver, while in the intestine respiration inhibition was increasing with exposure time. In chronic tests in the intestine there are certain focal changes [8], which in the liver involve mainly mitochondria of some but not all hepatocytes. The noxious effect of cadmium in the intestine or liver depends on the extent of intracellular synthesis of cadmium binding protein — metallothioneins (MT). Higher accumulation of cadmium in the liver is probably the result of the higher binding of cadmium to liver MT [3]. Much higher MT synthesis in the liver, compared to intestine have been shown by Onosaka and Cherian [16]. Preventive effect of pretreatment with a small cadmium dose before application of a higher one on the physiological state of the liver has been shown by Morita et al. [12], assuming MT synthesis by this repeated exposure.

Major pathological changes of the liver, manifesting as damage to cell membranes with concomitant release of nuclei and cellular organelles, especially mitochondria, into sinusoidal spaces were detected by Morselt et al. [13] in a chronic test with injection exposure to $CdCl_2$. This is at variance with our findings with a similar dose but orally applied. In our experiment release of damaged mitochondria by cytoplasmic blebs into Disse spaces and to sinusoids occurs in spite of conservation of structural integrity of cells. Observation of blebs is not a specific phenomenon only after exposure to cadmium, but incubation of hepatocytes with a series of toxic noxae results in an alteration of surface morphology, manifesting as the loss of microvilli and appearance of multiple blebs on hepatocyte surface [10].

Our findings may be explained by the fact that they reflect a beginning of intoxication process of hepatic cells, which by means of cytoplasmic blebs remove their damaged cadmium containing organellae. Results of our chronic tests do not support the hypothesis of Morselt et al. [13] on the sudden disruption of liver cells. Liver fibrosis was observed only in an acute combined test after 5 days, when the larger dose caused more extensive damage to cells.

When commenting the comparative diagram of the intestine and liver (Fig. 1) with microscopic changes in acute tests and including physiological evidence, we presume rather passive cadmium transport through injured jejunal villi by means of blood transport to the hepatic tissue. By contrast, in chronic tests with relatively lower cadmium doses both methodical approaches seem to indicate the presence of intact facilitated diffusion or active transport.

Foulkes [4] arrives at a similar conclusion on the basis of his perfusion experiments with rat intestine (cadmium transport — saturable process).

Also the results of Taguchi and Suzuki [20] from in vitro tests provide evidence for a special mechanism of cadmium transport, which is unlikely to be a simple diffusion. Absorption and transport of cadmium by hepatic mitochondria was proved by X-ray microanalysis.

Together with Andersen et al. [1] we presume that presence of non-MT cadmium in the cell (even for a short time) can be harmful. This is in agreement with the statement of Hammond and Foulkes [6], that there is evidence in several systems for the distribution of cellular cadmium between more than one pool and that concentrations of non-MT cadmium and of nuclear cadmium may be determinants of cadmium toxicity.

Our results are consistent with the hypothesis of Woods and Fowler [21] that toxicity of metals in general, is of progressive character, which includes disruptive ultrastructural changes with consequent impairment of structurally and functionally associated biological processes.

Correlation between microscopic and physiological findings in acute and chronic experiments was evident for both tissues studied.

REFERENCES

1. Andersen O, Hagerstrand I, Nordberg GF: Effect of the chelating agent sodium tripolyphosphate on cadmium toxicity in mice. Environ Res 29: 54, 1982
2. Diamond EM, Kench JE: Effects of cadmium on the respiration of rat liver mitochondria. Environ Physiol Biochem 4: 280, 1974
3. Engstrom B, Nordberg GF: Dose dependance of gastrointestinal absorption and biological half-time of cadmium in mice. Toxicology 13: 215, 1979
4. Foulkes EC: Some determinants of intestinal cadmium transport in the rat. J Environ Pathol and Toxicol 3: 471, 1980
5. Friberg L, Kjellstrom T, Nordberg GF: Cadmium. In: Friberg L, Nordberg GF, Vouk VB, (eds) Handbook on the Toxicology of Metals, Elsevier, Amsterdam, New York, Oxford 1986, p. 170
6. Hammond PB, Foulkes EC: Metal ion toxicity in man and animals. In: Siegel H (ed.) Metal Ions in Biological Systems, Marcell Dekker, Inc., New York, Basel 1986, p. 177
7. Hulínská D, Vojtíšek M, Hulínský V, Novák M: X-ray microanalytical and ultrastructural study of Cd absorption and transport in the liver of rat. Acta Morphologica (in press)
8. Hulínská D, Vojtíšek M, Bittnerová D, Cikrt M, Hulínský V: Cadmium influence on the rat intestine. Acta Morphologica Hungarica (in press)
9. Jacobs EE, Jacob M, Sanadi DR, Bradley LB: Uncoupling of oxidative phosphorylation by cadmium ion. J Biol Chem 223: 147, 1956
10. Jewell SA, Bellomo G, Thor H, Orrenius S, Smith MT: Bleb formation in hepatocytes during drug metabolism is caused by disturbances in thiol and calcium homeostasis. Science 217: 1257, 1982
11. Lojda Z, Papoušek F: Základy histochemického průkazu enzymů, Skripta, Brno, 1970, str. 1
12. Morita S: Defense mechanisms against cadmium toxicity. I. A biochemical and histological study of the effects of pretreatment with cadmium on the acute oral toxicity of cadmium in mice. Japan J Pharmacol 35: 129, 1984
13. Morselt AFW, Frederiks WM, Copius Peereboom-Stegeman JHJ, Van Veen HA: Mechanism of damage to liver cells after chronic exposure to low doses of cadmium chloride. Mechanisms and Models in Toxicology. Arch Toxicol Suppl 11: 213, 1987
14. Muller L, Ohnesorge FK: Cadmium induced alteration of the energy level in isolated hepatocytes. Toxicology 31: 297, 1984
15. Nordberg GF, Kjellstrom T, Nordberg M: Exposure, dose and metabolism. In: Friberg L, Elinder CG, Kjellstrom T, Nordberg GF: (eds) Cadmium and Health. A toxicological and epidemiological appraisal, CRC Press, Boca Raton, Florida 1985, p. 160
16. Onosaka S, Cherian MG: The induced synthesis of metallothionein in various tissues of rat in response to metals. I. Effect of repeated injection of cadmium salts. Toxicology 22: 91, 1981

17. Sabbioni E, Marafante E, Amantini L, Ubertalli L, Pietra R: Cadmium toxicity studies under long-term low level exposure (LLE) conditions. The Science of Total Environ 10: 135, 1978
18. Sato N, Kamada T, Suematsu T, Shichiri M, Hayashi N, Matsumura T, Kishida Y, Abe H, Furuyama F, Ishibashi F, Cadmium toxicity and liver mitochondria J. Biochem 84: 127, 1978
19. Squibb KS, Cousins RJ, Solbon BL, Levin S: Liver and intestinal metallothionein: Function in acute cadmium toxicity. Exp Molec Pathol 25: 163, 1976
20. Taguchi T, Suzuki S: The transport mechanism of cadmium by the small intestine of rats. Jap J Hyg 34, 2: 371, 1979
21. Woods JS, Fowler BA: Alteration of mitochondrial structure and heme biosynthetic parameters in liver and kidney by Bismuth. Toxicol Appl Pharmacol 90: 274, 1987

Acta Morphologica Hungarica 37 (3—4), pp. 219—234 (1989)

ULTRASTRUCTURE OF THE ITO CELLS IN LIVER DISEASE ASSOCIATED WITH FIBROSIS

I. Bartók[1], Sz. Virágh[2], Cs. Hegedűs[1], Katalin Bartók[1]

[1]DEPARTMENT OF PATHOLOGY, PÉTERFY HOSPITAL, [2]INSTITUTE OF PATHOLOGY AND HISTOPATHOLOGY, POSTGRADUATE MEDICAL SCHOOL, BUDAPEST, HUNGARY

(Received 3 November 1988)

The ultrastructure of Ito cells was examined in percutaneous needle liver biopsies of 36 patients. In three cases the liver was normal. Four specimens showed mild or moderate fatty degeneration. In the rest of the liver samples various types of fibrosis were seen: in four cases portal, in ten centrilobular, in eight periportal fibrosis and in five cases cirrhosis. In the normal liver Ito cells occurred not only in the Disse spaces but also in the walls of the terminal hepatic venules. In livers showing portal fibrosis the ultrastructure of Ito cells was similar to that seen in the normal liver. In the fibrotic areas of liver samples showing centrilobular or periportal fibrosis or cirrhosis Ito cells localized inside the fibrotic tissue and along the border between the connective tissue and hepatocytes. These interstitial Ito cells contained few lipid, abundant rough endoplasmic reticulum with dilated tubules filled by a flocculant material, well developed Golgi complexes and often bundles of 5 nm thick filaments with densities. These cells also known as activated Ito cells were in places surrounded by immature collagen fibrils and basement membrane fragments. There was a close contact between activated Ito cells and lymphocytes. The ultrastructure of Ito cells localizing in non-fibrotic areas did not differ from that seen in normal liver lobules. These observations suggest that Ito cells are related to fibroblasts and myofibroblasts and play an important role in the pathogenesis of liver fibrosis in humans.

Keywords: Liver, liver disease, liver fibrosis, Ito cells

Introduction

Ultrastructural studies have shown that no fibroblasts are present within the liver lobules of healthy adult mammals, including humans [3, 33]. Bronfenmajer et al. [7] and Schnack et al. [31] assumed for the first time that the lipid-containing, vitamin A-storing Ito cells (ICs) probably represented resting parenchymal fibroblasts. This hypothesis was supported by evidence of Ito cell proliferation and of fine structural transitions between cells with morphological characteristics of ICs and fibroblasts in CCl_4-induced experimental liver fibrosis [11, 12, 17, 24, 34]. Recent biochemical investigations indicated collagen biosynthesis in ICs of mouse and rat liver both in culture [13, 16, 34, 36] and in situ [11, 12], and the presence of collagen was demonstrated by immunohistochemical methods in rat ICs [9, 13, 20, 36].

Send offprint requests to: I. Bartók, H-1441 Budapest, POB 76, Hungary

By the electron microscope thin bundles of 5 nm thick parallel microfilaments were detected in the cytoplasm of ICs under different conditions [4, 6, 15, 23, 35, 38], and immunohistochemical studies have demonstrated that rat ICs contain the intermediate filament protein desmin [8, 38, 41] which is characteristically found in muscle cells [19]. These observations strongly suggest that ICs may also be capable of a contractile function.

Although experimental interest in ICs has been great, relatively little is known about their role in human liver pathology. Only a few authors [10, 14, 25, 27, 29, 31] studied their morphological changes in larger groups of patients, mainly in alcohol addicts [10, 25, 27, 29].

In the present paper we report electron microscopic studies of ICs in biopsy specimens obtained from human livers affected by fibrosis of various etiology and type. The morphological characteristics of the ICs of the fibrotic liver strongly suggest that these cells are functioning as fibroblasts and myofibroblasts in human liver disease.

Patients and methods

Thirty six percutaneous needle liver biopsies taken for diagnostic purpose were examined.

For routine histological examination, liver tissue was fixed in 10 per cent buffered formalin and embedded in paraffin. Sections were stained with haematoxylin and eosin, Masson's trichrome, Gömöri's aldehyde-fuchsin, Gömöri's silver impregnation technique, Prussian blue and PAS with and without digestion with amylase.

For ultrastructural examination, tissue was fixed in 5% glutaraldehyde diluted with equal parts of Millonig buffer at pH 7.2 and distilled water, post-fixed in 1 per cent buffered osmium tetroxide solution, dehydrated and embedded in Araldite. One μm thick sections were

Table I

Types of liver fibrosis and histological diagnoses of the liver biopsy specimens

Type of fibrosis	n	Histological diagnosis (n)
1. No fibrosis	8	normal liver (3); mild steatosis (4, including 3 alcohol addicts); moderate steatosis (1 alcohol addict)
2. Portal fibrosis	5	chronic persistent hepatitis (3); portal lesion consistent with chronic alcoholic pancreatitis (2)
3. Centrilobular fibrosis	10	alcoholic hepatitis (7); pericellular fibrosis without alcoholic hepatitis in the liver of addicts (3)
4. Periportal fibrosis	8	chronic active hepatitis (5); biliary piecemeal necrosis due to lasting biliary duct obstruction (1); portal and periportal lesion consistent with chronic alcoholic pancreatitis (2)
5. Cirrhosis	4	alpha-1-antitrypsin immunoreactive and HBsAg seropositive with mild activity (1); cryptogenic with mild (2) or moderate (1) activity

stained with toluidine blue to determine the extent and localization of fibrosis. Thin sections were double-stained with uranyl acetate and lead citrate for electron microscopic examination.

The light microscopic findings are summarized in Table I. Fatty change was regarded as mild when cytoplasmic lipid vacuoles were present in up to 50 per cent of the hepatocytes, and as moderate or severe, if such vacuoles were seen in 50—75 or more than 75 per cent of them [30] respectively. The diagnosis of chronic persistent and chronic active hepatitis (5), alcoholic hepatitis (1) and biliary piecemeal necrosis (2) was based on criteria defined by an international group, periportal changes indicating chronic alcoholic pancreatitis were identified by the criteria proposed by Morgan et al [26] and cirrhosis was diagnosed by the criteria approved at the Fogarty conference [21].

The biopsy specimens were assigned to five groups (Table I), as follows: 1. non-fibrotic liver tissue; 2. portal fibrosis indicated by widening and inflammatory cell infiltration of the portal field, without destruction of the periportal limiting plate; 3. centriblobular fibrosis with or without alcoholic hepatitis, in the former case not infrequently with involvement of the intermediate zone; 4. periportal fibrosis, in which the inflammed periportal connective tissue destroyed the limiting plate and entered the periportal parenchyma; 5. liver cirrhosis. Electron microscopic examination covered the centrilobular, intermediate and periportal areas of the liver lobule in groups 1—4, and the central and peripheral regions of the nodules in group 5.

Results

1. *Non-fibrotic liver and portal fibrosis*

The specimens assigned to these groups differed from each other only with respect to the extent of portal connective tissue. Only part of the hepatocytes showed mild changes, such as the presence of lipid vacuoles and in the alcoholics, the presence of longitudinal cristae and crystalloid matrix inclusions in some mitochondria in both the centrilobular and periportal areas and in the cases of portal fibrosis an occasional occurrence of autophagic vacuoles in periportal hepatocytes. There was no change in the sinusoids and Disse spaces.

Inside the liver lobules the ICs localized in the Disse spaces (perisinusoidal ICs). Their nuclei were oval and occasionally indented. Beneath the cell membrane many superficial vesicles were seen. The cytoplasm of most ICs was heavily loaded with large pale and small dark lipid droplets (Fig. 1). The rest of the cytoplasm comprised short tubules of rough endoplasmic reticulum (RER), small Golgi complex, centriole or ciliary rootlet, and a few small mitochondria. The RER and Golgi complex were more developed and a few intermediate filaments could also be seen in ICs containing less lipid. The cytoplasm extended slender elongated processes of which only a few contained lipid droplets. At some places several mature or thin immature collagen fibrils could be seen between ICs and hepatocytes, and occasionally a discontinuous, thin, basement-membrane-like material occurred between ICs and endothelial cells.

The space between the endothelial lining cells of the terminal hepatic venule and the perivenular hepatocytes was filled by an amorphous substance and by mature collagen fibrils, between which ICs (perivenular ICs) could be

seen along with fibroblasts and myofibroblasts. The perivenular ICs contained fewer and lesser lipid droplets, better developed RER and larger Golgi complex than most perisinusoidal ICs and at the cell periphery there were thin bundles of 5 nm thick filaments with densities which were arranged parallelly with the cell membrane (Figs 2 and 3).

The perivenular myofibroblasts did not contain lipid, and the bundles of microfilaments occupied a greater part of the cytoplasm than in ICs.

2. *Centrilobular fibrosis, periportal fibrosis and cirrhosis*

a) *General characteristics*

Biopsy specimens with centrilobular pericellular fibrosis but without signs of alcoholic hepatitis showed an increase in collagen fibrils and, occasionally, the presence of an amorphous osmiophilic substance in the widened Disse space and in the intercellular space between hepatocytes. The hepatocytes themselves showed no appreciable change. In the cases of alcoholic hepatitis, large areas of the centrilobular and intermediate zones were occupied by connective tissue, which comprised bundles of collagen fibrils, fibroblasts, ICs, and at some places neutrophilic granulocytes, lymphocytes and macrophages (Figs 4 and 6). The hepatocytes contained giant mitochondria, crystalloid inclusions in the mitochondrial matrix, increase, crowding, and swelling of the mitochondria, dilatation of the RER, increase in number of autophagic vacuoles, presence of Mallory's hyaline and lytic or coagulation necrosis of single hepatocytes.

In the cases of periportal fibrosis, extensions of the portal connective tissue encircled single or several hepatocytes. Between the collagen bundles ductular cells, fibroblasts, ICs, lymphocytes, macrophages, and in part of the biopsies also neutrophilic granulocytes could be seen. In the cytoplasm of the hepatocytes trapped in or adjoining the fibrotic tissue a lamellar osmiophilic material, occasionally limited by a membrane, and many lipofuscin granules could be seen the mitochondria were swollen, the RER was dilated, and increase of the tonofilaments was also noted at some places.

The cirrhotic livers showed similar changes to periportal fibrosis along the border between the connective tissue septa and hepatocytes. Apart from the cell types observed in centrilobular and periportal fibrosis, myofibroblasts made appearance in the connective tissue septa (Fig. 16).

The fibrotic areas contained small capillary vessels at the borderline between hepatocytes and connective tissue, and also in more distant localizations. The hepatocellular surfaces facing the connective tissue were frequently bordered by continuous basement membrane (Figs 5 and 10).

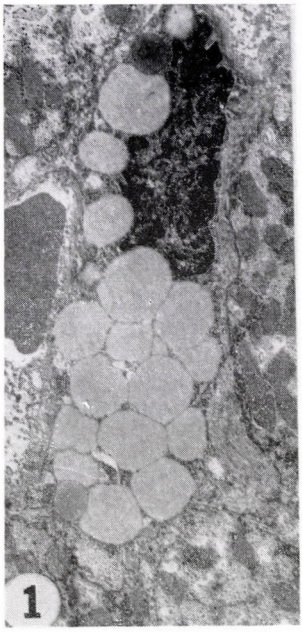

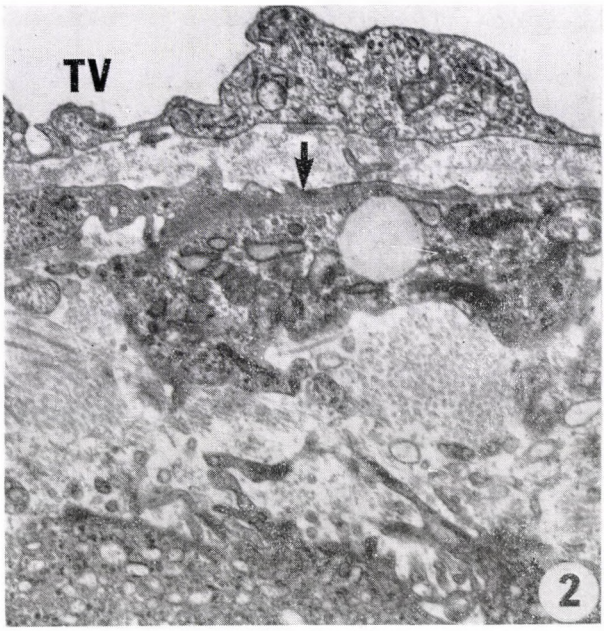

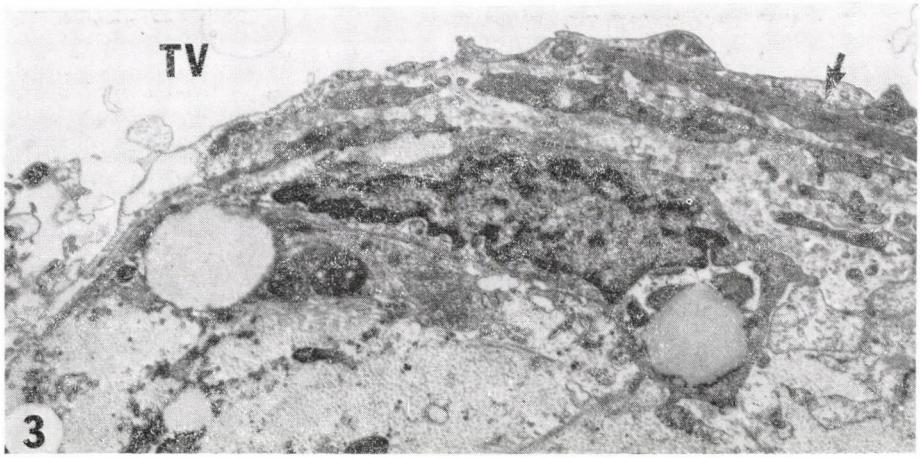

Fig. 1. Normal liver. Perisinusoidal Ito cell. The cytoplasm is occupied by lipid droplets. ×4000

Fig. 2. Wall of terminal hepatic venule (TV) in normal liver. Note the lipid-containing Ito cell process beneath the endothelial cell. Several slightly dilated RER tubules and free polyribosomes can be seen in the cytoplasm. A band of 5 nm thick filaments (arrow) extends beneath the cell membrane. ×12 000

Fig. 3. Normal liver. Note processes of a myofibroblast (arrow) and fibroblasts, and an Ito cell with dilated RER tubules and an Ito cell process beneath the endothelial lining of the terminal hepatic venule (TV). ×8000

b) *Ito cells*

In the cases of centrilobular pericellular fibrosis the ICs localized in the widened Disse spaces, which contained numerous collagen fibrils (Figs 7 and 8).

In the large fibrotic areas, in which the sinusoids were destroyed, some of the ICs localized near to hepatocytes (Fig. 9), occasionally between a capillary vessel and the hepatocyte (Fig. 10), others occurred deeper in the connective tissue between collagen fibrils and inflammatory cells (Figs 4 and 6), and around capillary vessels and bile ductules (interstitial ICs). The ICs abutting on hepatocytes had a narrow cytoplasm with long processes which

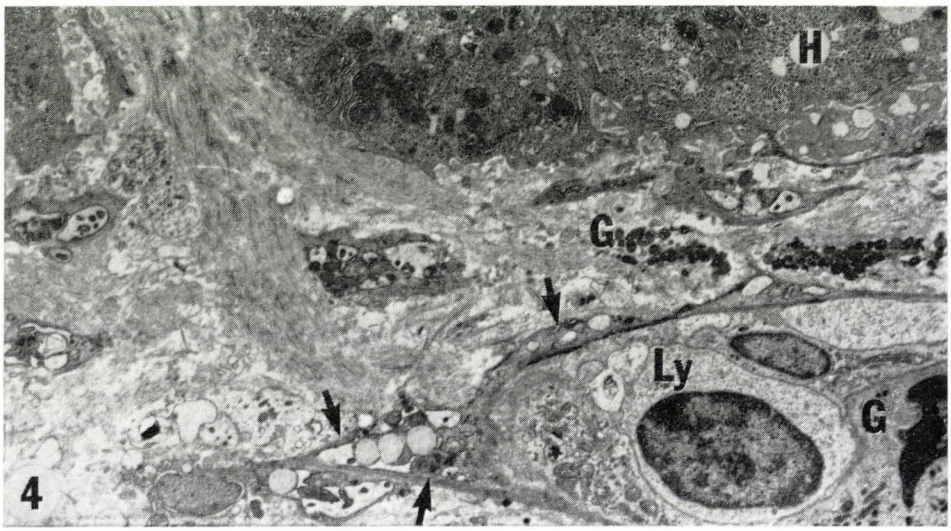

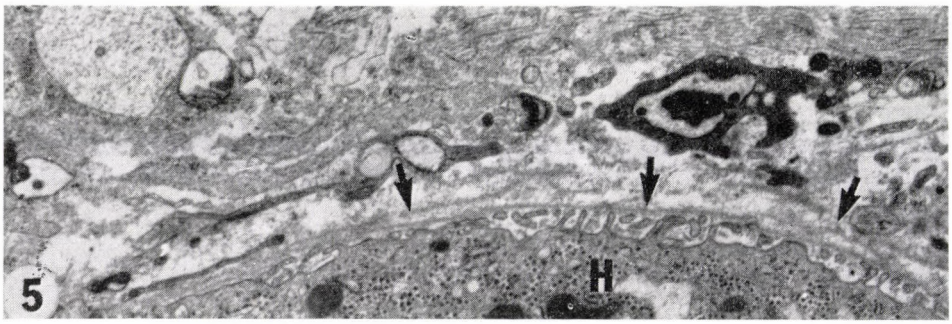

Fig. 4. Centrilobular fibrosis in alcoholic hepatitis. Collagen fibrils, a lymphocyte (Ly), neutrophilic granulocytes (G) and a long branching process of an Ito cell (arrows) with lipid droplets and dilated RER can be seen next to a hepatocyte (H). Adjoining the liver cell are long, narrow cell processes, which extend parallel to the hepatocellular border, and thick cell processes with short, dilated RER tubules. ×4000

Fig. 5. Centrilobular fibrosis in alcoholic hepatitis. The hepatocyte (H) is surrounded by continuous basement membrane (arrows), and around it cell processes similar to those shown in Fig. 4 are to be seen. ×8000

Fig. 6. Centrilobular fibrosis in alcoholic hepatitis. Lymphocytes (Ly), fibroblasts (F), Ito cells (IC), and a process of an Ito cell (arrow) can be seen between collagen fibrils. The Ito cells have undulated or indented nuclear surfaces, and dilated RER tubules are abundantly present in their cytoplasm. ×4000

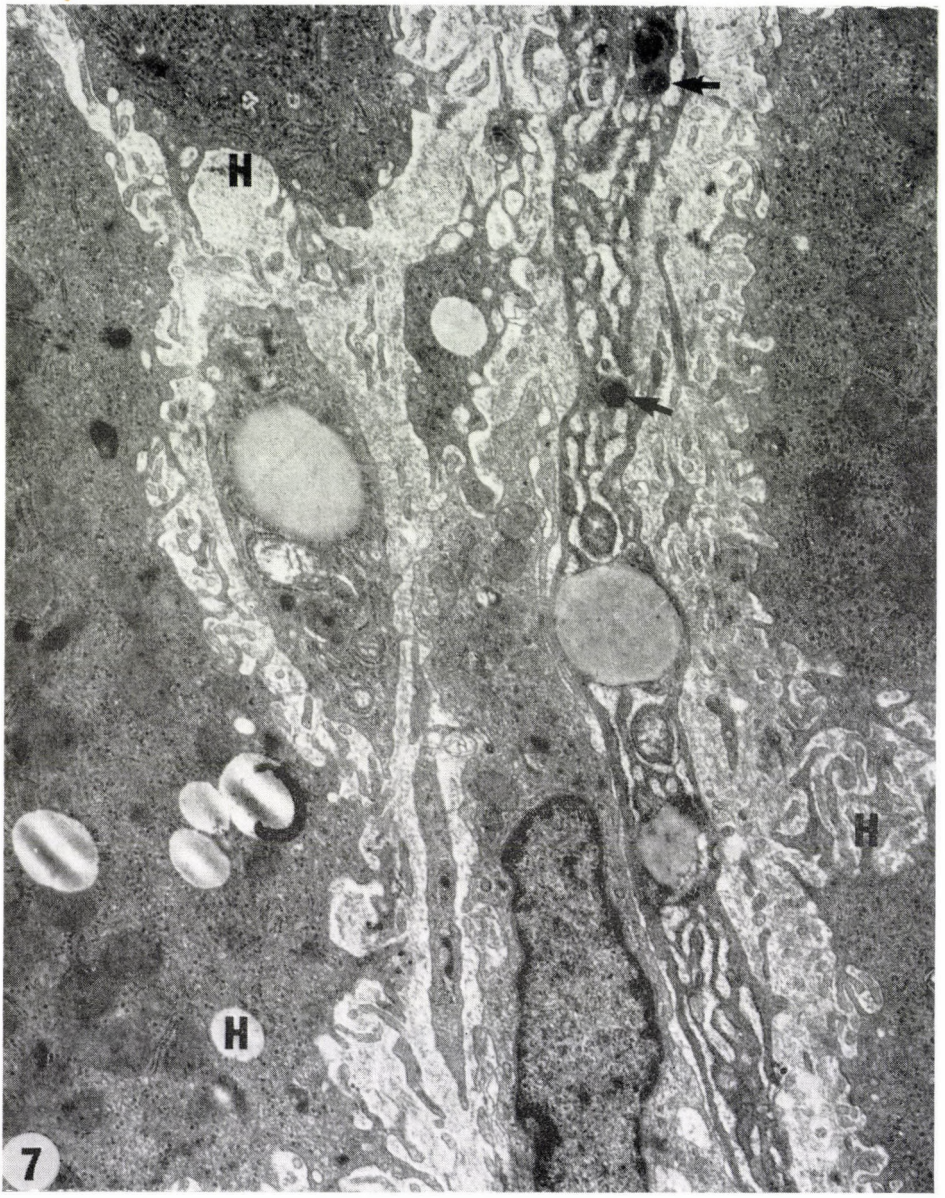

Fig. 7. Centrilobular pericellular fibrosis. In the dilated perisinusoidal recess between the hepatocytes many collagen fibrils and a long process of an Ito cell can be seen, the latter contains light and some dark (arrows) lipid droplets and abundant RER. H: hepatocyte. ×12 000

extended parallel to the hepatocellular surface. At some sites the surfaces of ICs and hepatocytes contacted each, whereas in others they were separated by collagen fibrils (Fig. 9). Long cell processes similar to those of the ICs could be frequently seen along the surface of hepatocytes (Figs 4 and 5).

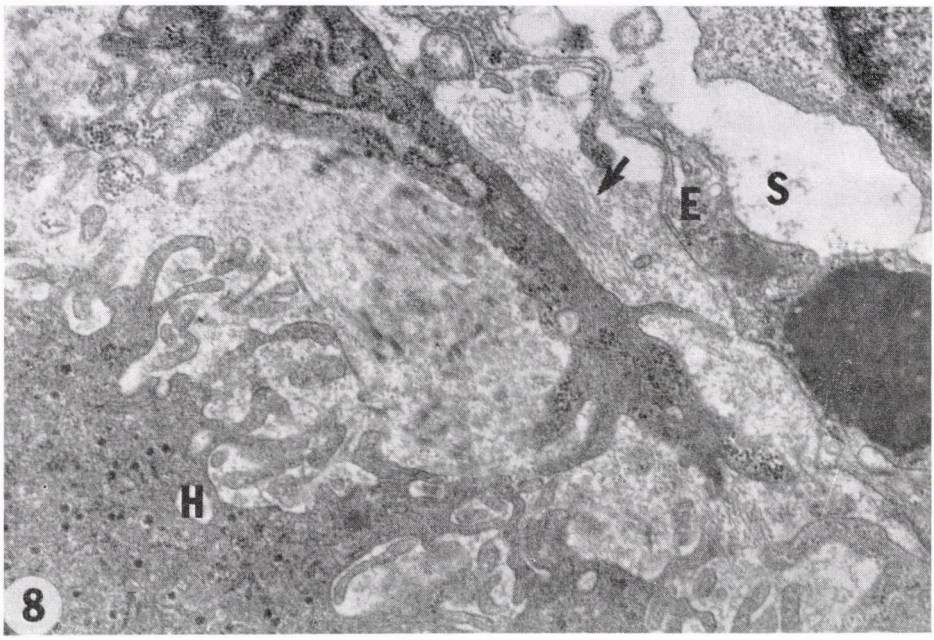

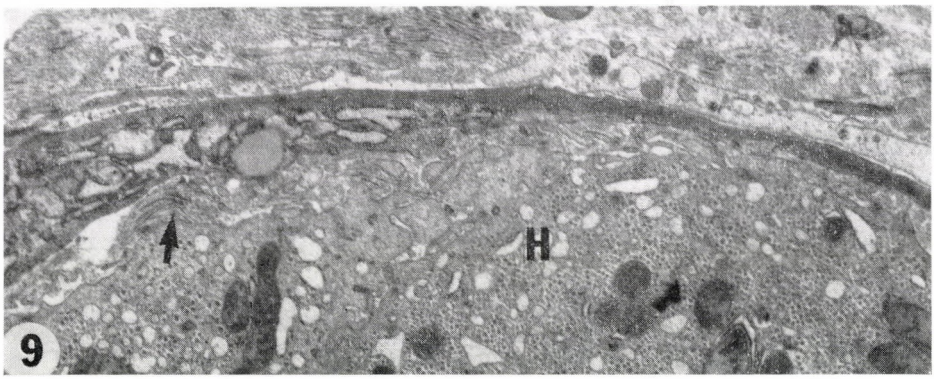

Fig. 8. Centrilobular pericellular fibrosis. In the widened Disse space an Ito cell process is visible which contains dilated RER tubules and numerous free ribosomes but no lipid. Next to the Ito cell process there are many mature and immature (arrow) collagen fibrils. S: sinusoid; E: endothelial cell; H: hepatocyte. ×20 000

Fig. 9. Periportal fibrosis in chronic active hepatitis. Borderline between hepatocytes and connective tissue. A long process of an Ito cell, which contains a lipid droplet and abundant, dilated RER, extends parallel to the hepatocellular border. The surfaces of the Ito cell process and the hepatocyte (H) are separated by collagen fibrils (arrow) at one place, and contact one another elsewhere. ×4000

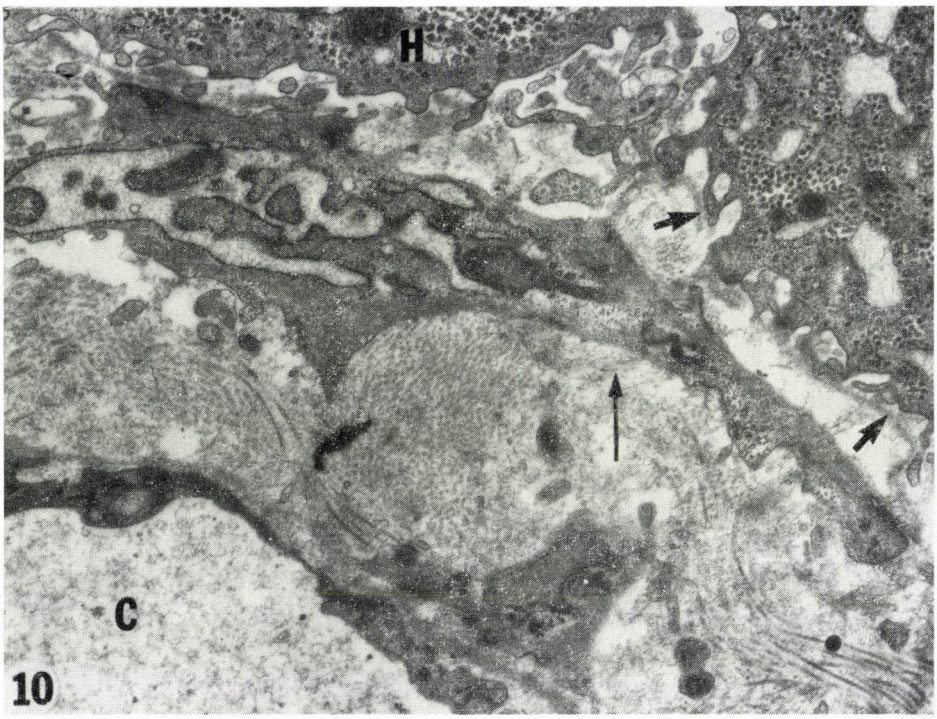
H
C
10

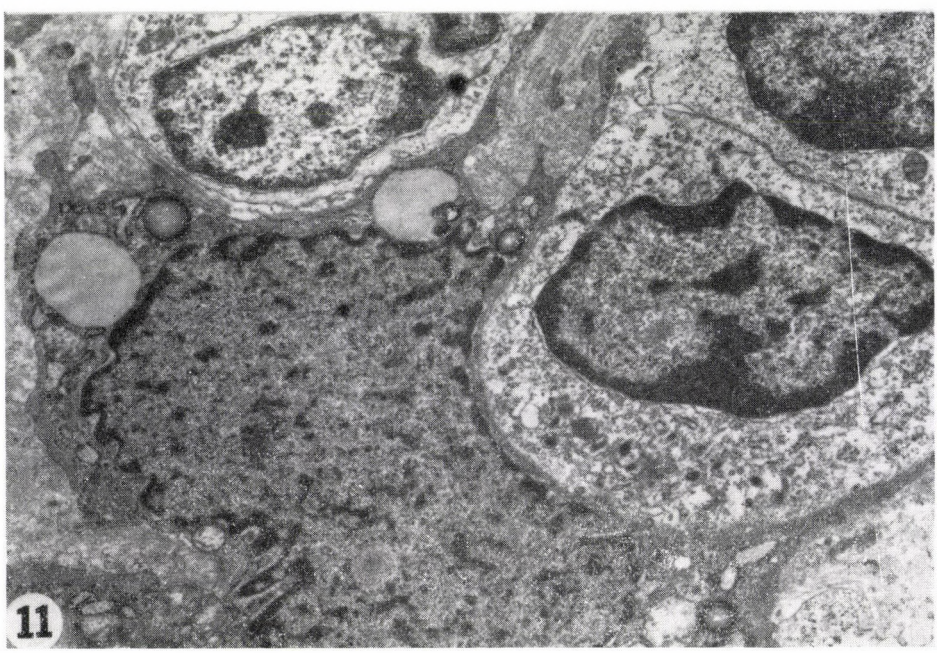
11

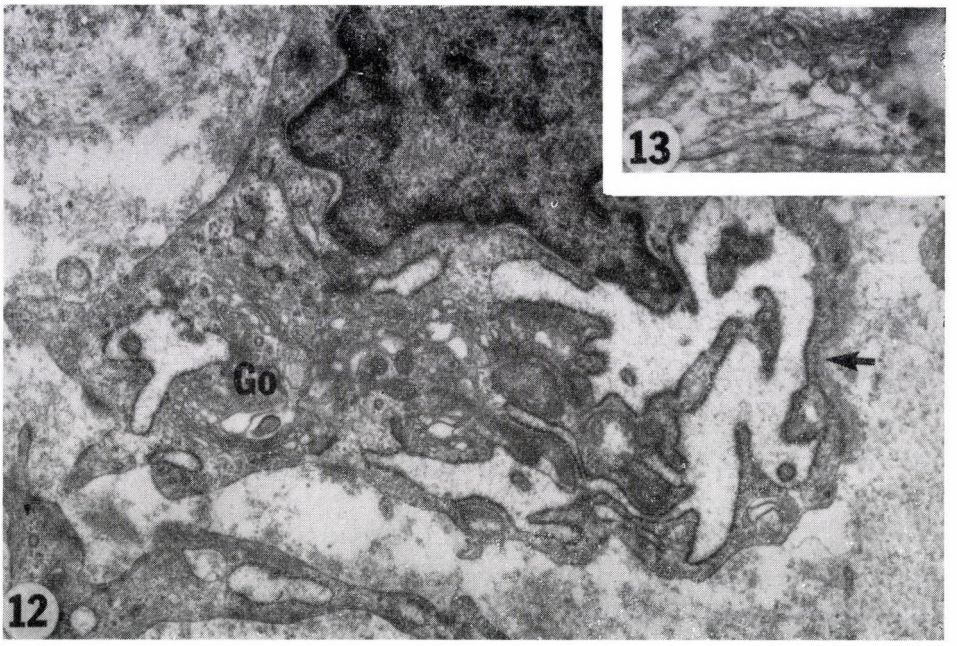

Fig. 12. Centrilobular fibrosis in alcoholic hepatitis. Detail of an Ito cell. Note abundant RER and well developed Golgi complex (Go). A few small mitochondria can also be seen. Note basement membrane (arrow) along a portion of the Ito cell membrane. ×15 000

Fig. 13. Centrilobular fibrosis. Process of an Ito cell. Many caveoles and vesicles can be seen on the cell surface, and there are a few intermediate filaments in the cytoplasm. ×28 000

Both the perisinusoidal and the interstitial ICs had an abundant elongated or star-shaped, branching cytoplasm (Figs 4, 6, 7, 8, 9, 10 and 11). Adjoining their cell membranes mature and young collagen fibrils (Figs 8, 10 and 11), and at some places thick basement membrane fragments (Figs 10, 12 and 14) were seen. Where ICs and hepatocytes were adjacent to each other, the basement membrane fragments localized between them (Fig. 10). The nuclei of the ICs had undulated or indented contours (Figs 6, 11 and 12). Some ICs had many surface vesicles and caveoles (Fig. 13). The cytoplasm contained few to many intermediate filaments (Fig. 13), and bundles of 5 nm thick parallel filaments with dense areas could be frequently seen at the cell periphery (Fig. 14). Such bundles of filaments filled — like in myofibroblasts

Fig. 10. Centrilobular fibrosis in alcoholic hepatitis. Note capillary vessel (C) in the marginal part of the fibrotic area near to hepatocytes (H). Between thick bundles of mature and immature (thin arrow) collagen fibrils and hepatocytes (H) there is an Ito cell process which contains no lipid; dilated RER tubules filled by a flocculent material and a small mitchondrium can be seen in it. Note fragments of basement membrane (thick arrows) around the hepatocytes. ×13 000

Fig. 11. Periportal fibrosis in chronic active hepatitis. Note intimate association of the Ito cell with lymphocytes. The spaces between the processes of the Ito cell are occupied by immature collagen fibrils. ×9000

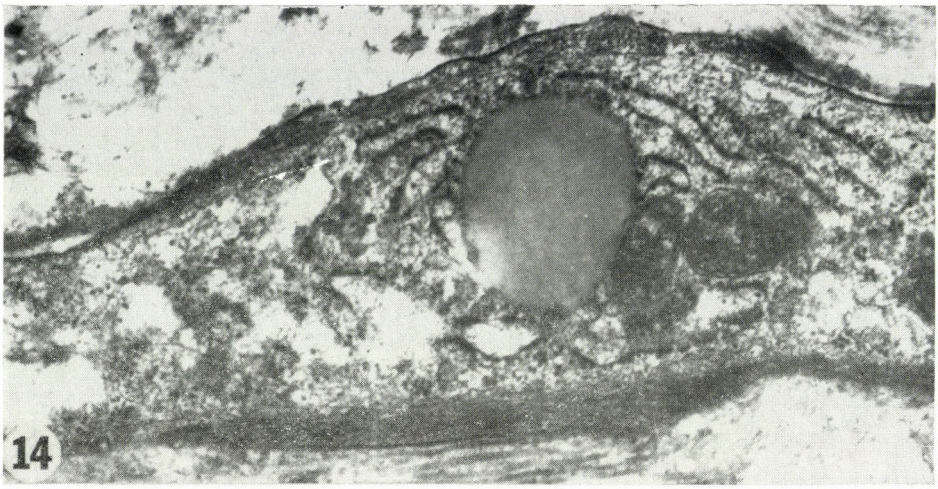
14

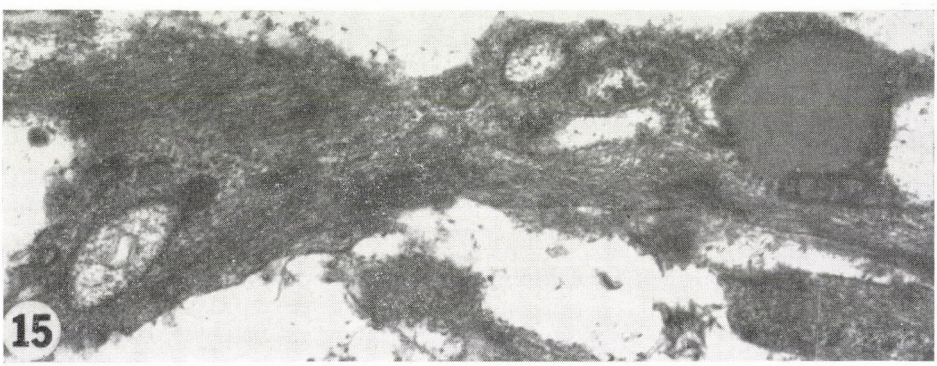
15

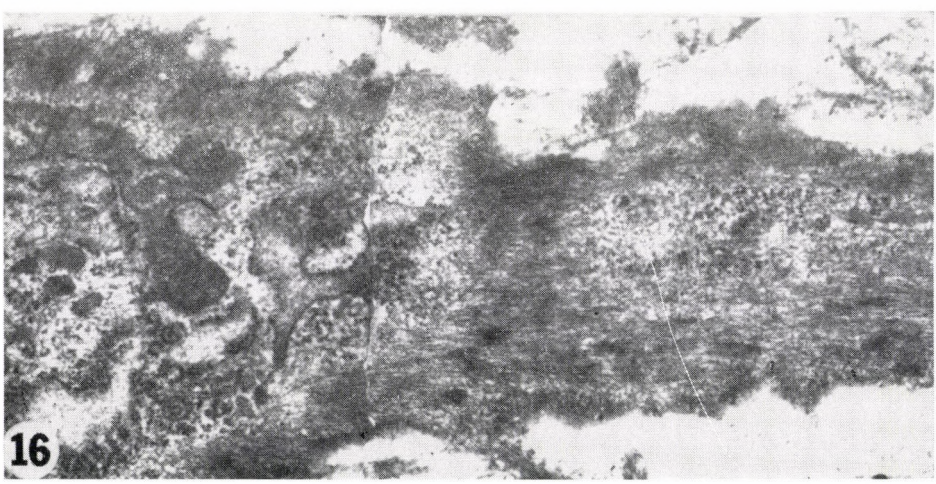
16

(Fig. 16) — the greater part of the cytoplasm of ICs which localized in the connective tissue septa of the cirrhotic liver (Fig. 15). The cell bodies and/or processes contained one or a few lipid droplets (Figs 4, 6, 7, 9, 11, 14 and 15), which occupied only a minor part of the cytoplasm. RER was abundant and its dilated tubules were filled by a flocculent material (Figs 4, 6, 7, 8, 9, 10, 12 and 14). The Golgi complex was well developed, the mitochondria were small and sparse (Figs 10, 12 and 14).

The fine structure of fibroblasts resembled that of ICs except that neither lipid droplets, nor 5 nm thick cytoplasmic filaments could be seen within them. Myofibroblasts occurred exclusively in the connective tissue septa of the cirrhotic liver (Fig. 16), and differed from the fibroblasts by the presence of numerous bands of 5 nm thick filaments with densities.

In parenchymal parts not affected by fibrosis the ICs showed ultrastructural characteristics similar to those of the normal liver lobule.

Discussion

The ICs have been synonymously termed as perisinusoidal cells referring to the fact that they localize in the Disse spaces of the intact liver lobule. Nakano et al. [27] observed in normal human liver only the presence of fibroblasts and myofibroblasts in the adventitia of the terminal hepatic venule. We detected, in addition to these ICs in the walls of terminal hepatic venules in human liver samples which were normal or showed mild or moderate fatty change. These perivenular ICs contained less lipid, more abundant RER and a more developed Golgi complex than the perisinusoidal ones, and beneath their cell membranes bands of 5 nm thick filaments with densities could be seen, similar to those seen inside the adjoining myofibroblasts. It appears that the environmental factors have an influence on the structure of ICs in the intact human liver.

Biochemical examinations have shown that cultured ICs of rat liver produced types I, III and IV collagen [13, 16, 34, 36]. The same types of collagen were demonstrated intracellularly in the ICs of rat liver [9, 13, 20, 32] and in those of healthy and alcoholic human livers as well [10]. As compared with ICs cultured from untreated rats in ICs cultured from CCl_4-treated rats

Fig. 14. Liver cirrhosis, connective tissue septum. Detail of an Ito cell with well developed RER and small mitochondria. Note fragments of thick basement membrane along portions of the cell membrane and a band of 5 nm thick cytoplasmic filaments with densities at the cell periphery. ×28 000

Fig. 15. Liver cirrhosis, connective tissue septum. The greater part of the process of an Ito cell is occupied by 5 nm thick parallel filaments with densities. ×28 000

Fig. 16. Cirrhosis, connective tissue septum. Detail of a myofibroblast. Many 5 nm thick cytoplasmic filaments with densities, well developed RER, and many free polyribosomes can be seen in the cytoplasm. ×20 000

collagen synthesis increased 4—6-fold [34]. In cultured ICs the lipid content tended to decrease, the RER became more abundant and the Golgi complex more developed with the increase of collagen synthesis [16, 34]. Enzan [11] and Enzan and Hara [12] demonstrated by electron microscopic autoradiography an incorporation of ^{3}H-proline into ICs of CCl_4-treated mice; the silver grains appeared first over the RER and Golgi complex, later over the collagen accumulated along the cell borders. The ICs of baboons fed on alcohol chronically showed increase of RER area and diminution of intracellular lipid parallel to the progression of liver fibrosis [23]. ICs in this state were termed by Kent et al. [17] as transitional cells, and by Okanoue et al. [29] as activated ICs.

In the liver samples with fibrosis examined by us, the ultrastructure of ICs localizing in non-fibrotic areas was similar to that seen in intact liver lobules, whereas the ICs localizing in the fibrotic areas contained many RER tubules filled by a flocculent material, a well developed Golgi complex, few small lipid droplets, and were at some places surrounded by immature collagen fibrils. Consequently, the ultrastructural transformation taking place in ICs of humans suffering from liver fibrosis is analogous to those shown by ICs involved in experimentally induced collagen production. Minato et al. [25] have found a significant correlation between the morphological changes of ICs, similar to those seen by us, and the rate of in vitro collagen biosynthesis in liver biopsy specimens taken from alcohol addicts. In accordance with earlier observations [4, 6, 18, 35] we detected basement membrane fragments underlying the activated ICs which is consistent with the production of type IV collagen by these cells [9, 10, 13, 20, 34, 36]. In view of this it appears that the ICs play an important role in collagen synthesis and in the pathogenesis of human liver fibrosis.

It is known that the proliferation of fibroblasts is stimulated by a macrophage-dependent factor [22] and by lymphokine produced by activated T-lymphocytes, as well [28, 39]. It is possible that similar factors are responsible for the activation of ICs. The proliferation of ICs isolated from CCl_4-treated rats was enhanced by a non-dialysable, soluble growth factor secreted by Kupffer cells of CCl_4-treated rats [34]. In the livers of patients who had died at different times after the onset of fulminant hepatitis, Tanaka and Ishikawa [37] using enzyme- and immuno-histochemical methods observed proliferation of ICs, activated macrophages, and activated T-lymphocytes together with the development of fibrosis in the necrotic areas. This accords well with our observation that macrophages frequently appeared in the surroundings of activated ICs, and the latter were intimately associated with lymphocytes in the fibrotic liver tissue.

Our earlier studies demonstrated the presence of 5 nm thick filaments, which formed thin fascicles with densities, in the surface cytoplasmic matrix

of ICs in fetal human and mouse liver [4]. Similar fascicles were found in ICs of adult humans in the present study. The 5 nm thick filaments localized inside perivenular ICs in the non-fibrotic liver, whereas in conditions of fibrosis they could be seen inside many activated ICs. These filaments were most abundant in ICs localizing inside the fibrous septa of the cirrhotic liver, i.e. in places where also myofibroblasts occurred. It appears that the fibroblast-like transformation of ICs is frequently associated with a quantitative increase of 5 nm thick filaments. Myofibroblast-like ICs were also found in human hepatocellular carcinoma [35], hepatocellular adenoma [6], perisinusoidal fibrosis associated with diabetes [18], liver fibrosis due to A-hypervitaminosis [15] and in the liver of baboons fed on alcohol [23]. Consistently with these observations, immunohistochemical methods detected the presence of desmin within ICs [8, 38]. On the other hand, the myofibroblasts which surround the terminal hepatic venule take up and store retinol after treatment with vitamin A [40]. These observations support the claim that the ICs are related to myofibroblasts.

REFERENCES

1. Baptista A, Bianchi L, De Groote J, et al: Alcoholic liver disease: morphological manifestation. Review by an international group. Lancet I: 707, 1981
2. Baptista A, Bianchi L, De Groote J, et al: Histopathology of the intrahepatic biliary tree. Review by an international group. Liver 3: 161, 1983
3. Bartók I, Tóth J, Remenár É, Virág Sz: Ultrastructure of the hepatic perisinusoidal cells in man and other mammalian species. Anat Rec 194: 571, 1979
4. Bartók I, Tóth J, Remenár É, Virágh Sz: Fine structure of perisinusoidal cells in developing human and mouse liver. Acta Morph Hung 31: 337, 1983
5. Bianchi L, De Groote J, et al: Acute and chronic hepatitis revisited. Review by an international group. Lancet II: 914, 1977
6. Bioulac-Sage P, Lamouliatte H, Saric J, Merlio JP, Balabaud C: Ultrastructure of sinusoidal cells in benign liver cell adenoma. Ultrastruct Pathol 10: 49, 1986
7. Bronfenmajer S, Schaffner F, Popper H: Fat-storing cells (lipocytes) in human liver. Arch Pathol 82: 447, 1966
8. Burt AD, Robertson JL, Heir J, Macsween R: Desmin-containing stellate cells in rat liver; distribution in normal animals and response to experimental acute liver injury. J Pathol 150: 29, 1986
9. Clement B, Emonard H, Rissel M et al: Cellular origin of collagen and fibronectin in the liver. Cell Mol Biol 30: 489, 1984
10. Clement B, Grimaud JAG, Campion JP, Deugnier Y, Guillouzo A: Cell types involved in collagen and fibronectin production in normal and fibrotic human liver. Hepatology 6: 225, 1986
11. Enzan H: Ito cells (fat-storing cells) and collagen formation in acute carbon tetrachloride liver injury. A light and electron microscopic autoradiographic study using ^{3}H-proline as a tracer. Rec Adv RES Res 24: 48, 1984
12. Enzan H, Hara H: Ito cells (fat-storing cells) and collagen formation in carbon tetrachloride-induced liver fibrosis. A light and electron microscopic autoradiographic study using ^{3}H-proline as a tracer. In: Kirm A, Knook DL, Wisse E (eds) Cells of the Hepatic Sinusoid, Vol. 1, The Kupffer Cell Foundation, Rijswijk 1986. p. 233
13. Friedman SL, Roll FJ, Bissell M: Collagen phenotype of rat hepatic lipocytes in pure primary culture. In: Kirm A, Knook DL, Wisse E (eds) Cells of the Hepatic Sinusoid, Vol 1, The Kupffer Cell Foundation, Rijswijk 1986, p. 255
14. Horváth É, Saibil FG, Kovács K, Kerényi NA, Ross RC: Fine structural changes in liver of methotrexate-treated psoriatics. Digestion 17, 489, 1978
15. Hruban Z, Russel RM, Boyler JL, Glagov S: Ultrastructural changes in livers of two patients with hypervitaminosis A. Am J Pathol 76: 451, 1974

16. Kawase T, Shiratori Y, Sugimoto T: Collagen production by rat liver fat-storing cells in primary culture. Expl Cell Biol 54: 183, 1986
17. Kent G, Gay S, Inouye T, Bahu R, Minick OT, Popper H: Vitamin A containing lipocytes and formation of type III collagen in liver injury. Proc Natl Acad Sci (USA) 73: 3719, 1976
18. Latry P, Bioulac-Sage P, Echinard E, Gin H, Boussarie L, Grimaud JA, Balabaud C: Perisinusoidal fibrosis and basement membrane-like material in the liver of diabetic patients. Hum Pathol 18: 775, 1987
19. Lazarides E: Intermediate filaments: a chemically heterogeneous developmentally regulated class of proteins. Ann Rev Biochem 51: 219, 1982
20. Leeuw de AM, McCarthy SP, Geerts A, Knook L: Purified rat liver fat-storing cells in culture divide and contain collagen. Hepatology 4: 392, 1984
21. Leevy CM, Tygstrup N: Standardisation of Nomenclature, Diagnostic Criterion and Diagnostic Methodology for Diseases of the Liver and Biliary Tract. Karger AG, Basel, 1976
22. Leibovich SJ, Ross RS: A macrophage-dependent factor that stimulates proliferation of fibroblasts in vitro. Am J Pathol 84: 501, 1976
23. Mak KM, Leo MA, Lieber CS: Alcoholic liver injury in baboon: transformation of lipocytes to transitional cells. Gastroenterology 87: 188, 1984
24. McGee JOD, Patrick S: The role of perisinusoidal cells in hepatic fibrogenesis. An electron microscopic study of acute carbon tetrachloride liver injury. Lab Invest 29: 429, 1972
25. Minato Y, Hasumura Y, Takeuchi J: The role of fat-storing cells in Disse space fibrogenesis in alcoholic liver disease. Hepatology 3, 559, 1983
26. Morgan MY, Sherlock S, Scheuer P: Portal fibrosis in the liver of alcoholic patients. Gut 19: 1015, 1978
27. Nakano M, Worner TM, Lieber CS: Perivenular fibrosis in alcoholic liver injury: ultrastructure and histologic progression. Gastroenterology 83: 777, 1982
28. Neilson EG, Phillips SM, Jimenez S: Lymphokine modulation of fibroblast proliferation. J. Immunol 128: 1484, 1982
29. Okanoue T, Burgibe EJ, French SW: The role of the Ito cells in perivenular and intralobular fibrosis in alcoholic hepatitis. Arch Pathol Lab Med 107: 459, 1983
30. Rubin E, Krus S, Popper H: Pathogenesis of postnecrotic cirrhosis in alcoholics. Arch Pathol 73: 288, 1962
31. Schnack H, Stockinger L, Wewalka F: Die Bindegewebezellen in der menschlichen Leber bei Normalfällen und pathologischen Zuständen. Wien Klin Wochenschr 78: 715, 1966
32. Senoo H, Hata R, Nagai Y, Wake K: Assembly and metabolism of collagen in the liver. In: Kirm A, Knook DL, Wisse E (eds) Cells of the Hepatic Sinusoid, Vol 1, The Kupffer Cell Foundation Rijswijk 1986, p. 227
33. Shaba JK, Patrick RS, McGee JOD: Collagen synthesis by mesenchymal cells isolated from normal and acutely damaged mouse liver. Br J Exp Path 54: 110, 1973
34. Shiratori Y, Geerts A, Ichida T, Wisse E: Collagen production and Kupffer cell-modulated proliferation of fat-storing cells in culture. In: Kirm A, Knook DL, Wisse E (eds) Cells of the Hepatic Sinusoid, Vol 1, The Kupffer Cell Foundation, Rijswijk 1986, p. 239
35. Tabarin A, Bioulac-Sage P, Boussarie L, Balabaud C, de Mascarel A, Grimaud A: Hepatocellular carcinoma developed on non-cirrhotic livers. Sinusoids in hepatocellular carcinoma. Arch Pathol Lab Med 111: 174, 1987
36. Takada A, Tsutsumi M, Takase S, Kimura T: Collagen formation by cultured fat-storing cells of rat livers. In: Kirm A, Knook DL, Wisse E (eds) Cells of the Hepatic Sinusoid, Vol 1, The Kupffer Cell Foundation, Rijswijk 1986, p. 257
37. Tanaka M, Ishikawa E: Histochemical study on the correlation between fat-storing cells, macrophages and lymphocytes in fibrotic lesion occurring after fulminant hepatitis. In: Kirm A, Knook DL, Wisse E (eds) Cells of the Hepatic Sinusoid, Vol 1, The Kupffer Cell Foundation, Rijswijk 1986, p. 259
38. Tsutsumi M, Takada A, Takase S, Yasuhara M, Matsuda Y: Characterization of isolated and cultured fat-storing cells of rat liver. In: Kirm A, Knook DL, Wisse E, (eds) Cells of the Hepatic Sinusoid, Vol 1, The Kupffer Cell Foundation, Rijswijk 1986, p. 263
39. Wahl SM, Gateli CL: Modulation of fibroblast growth by lymphokine of human T cell and continuous T cell line origin. J Immunol 130: 1226, 1983
40. Wake K, Senoo H: Morphological aspects of the differentiation of stellate cell line in the vertebrates. In: Kirm A, Knook DL, Wisse E (eds)Cells of the Hepatic Sinusoid, Vol 1, The Kupffer Cell Foundation, Rijswijk 1986, p. 215
41. Yokoi Y, Namihisa T, Kuroda H, Komatsu I, Miyazaki A, Watanabe S, Usui K: Immunocytochemical detection of desmin in fat-storing cells (Ito cells). Hepatology 4, 709, 1984

Acta Morphologica Hungarica 37 (3–4), pp. 235–243 (1989)

RENAL COMPLICATIONS IN MULTIPLE MYELOMA

B. Iványi

DEPARTMENT OF PATHOLOGY, ALBERT SZENT-GYÖRGYI UNIVERSITY OF MEDICINE, SZEGED, HUNGARY

(Received 21 November 1988)

Renal complications were studied in 81 autopsied patients suffering from multiple myeloma (47 male, 34 female, mean age 66.3 years). Kidney samples were examined for the presence of Bence Jones cast nephropathy, light chain deposition disease, amyloidosis, nephrocalcinosis, chronic urate nephropathy, acute renal failure, renal vein thrombosis, acute and chronic pyelonephritis, and tumorous infiltration of the kidney tissue. Lesions were graded under the light microscope as minimal, mild, moderate or severe. This grading and the corresponding serum creatinine levels were used to distinguish four groups: 1. morphologically and functionally intact kidney (40 cases); 2. kidney involvement with good renal function (10 cases); 3. kidney involvement with moderate chronic renal insufficiency (16 cases); 4. kidney involvement with chronic uraemia (15 cases). In patients with an impaired renal function (groups 3 and 4), Bence Jones cast nephropathy occurred most frequently (27 cases, 33%); all other complications were seen much less frequently. Among the 81 patients, two cases of kappa light chain deposition disease and three cases of amyloidosis were found. Although the semiquantitative morphology and serum creatinine levels displayed a good correlation, there were cases with marked histological changes but only a moderate impairment in renal function, suggesting that the drawing of functional conclusions from morphological changes of the kidney requires caution.

Keywords: Multiple myeloma, renal complications, Bence Jones cast nephropathy, light chain nephropathy

Introduction

A serum creatinine level above 177 μmol/l is an unfavourable prognostic sign in the clinical course of multiple myeloma [2, 12]. Bence Jones cast nephropathy, AL-amyloidosis, light chain deposition disease, pyelonephritis, etc. may occur in the background [6, 19, 29, 32, 34]. Our retrospective study analyzes the frequency of renal complications in myeloma in autopsy material, their combinations with each other and the correlation between the serum creatinine level and the degree of morphological changes.

Bence Jones cast nephropathy is a common complication of myeloma. Clinically, patients generally have light chain proteinuria and renal insufficiency. In the pathogenesis, a role is played by tubulotoxic free light chain proteins that filter in large quantities through the glomerular capillary base-

Send offprint requests to: Dr. B. Iványi, Dept. of Pathology, Albert Szent-Györgyi University of Medicine, P.O. Box 401, H-6701, Szeged, Hungary

ment membrane [13, 17, 20]. Histologically, many of the distal and collecting tubules are completely obstructed by eosinophilic, refractile casts. Around them, the tubuli are dilated, atrophic, and occasionally necrotic. The casts are usually surrounded by multinucleated giant cells of macrophage origin [33]. In the adjacent peritubular interstitium, an inflammatory infiltrate composed of lymphocytes, macrophages and some neutrophilic granulocytes is present. A variable degree of interstitial fibrosis and pronounced hyaline arteriolosclerosis accompany the lesion [6, 8, 22].

Another, less frequently encountered complication is the deposition of serum paraproteins in the form of either light chain fragments or amyloid fibrils along the renal basement membranes (paraproteinaemic kidney). In light chain nephropathy, atrophic tubules with intensely PAS-positive basement membranes, interstitial fibrosis and nodular glomerulosclerosis can be seen light microscopically [1, 15, 36]. The diagnosis is established by the detection of monotypic, usually kappa light chain fragments deposited linearly along the tubular and glomerular basement membranes [4, 6, 25]. Patients suffering from light chain nephropathy present with renal failure and non-selective proteinuria [13]. Amyloidosis occurs in 5—15 per cent of all patients with myeloma [5, 16]. Massive proteinuria with or without the nephrotic syndrome is a common finding. It is important to mention that Bence Jones cast nephropathy and paraproteinaemic kidney generally exclude each other [9, 18].

In 7—9 per cent of patients with light chain proteinuria and a normal renal function, acute renal failure may develop [30]. Infections, dehydration, hypercalcaemia, hyperuricaemia, intravenous pyelography, thrombosis of intrarenal veins, tumorous infiltration of renal parenchyma and nephrotoxic antibiotics are the main predisposing factors [10, 34].

Materials and methods

Between 1st January 1967 and 30th September 1988, 32378 autopsies were carried out in our department. Among them 81 histologically proven cases of multiple myeloma were found. The formalin-fixed and paraffin-embedded kidney blocks of these cases were recut and the slides were stained with H and E, PAS, Kossa's silver impregnation and Congo red. The latter were examined under polarized light for green birefringence. Light chain nephropathy was routinely screened from 1982 on frozen sections of kidney samples by using the direct immunofluorescence (DIF) method with FITC-conjugated antisera against antihuman IgG, IgA, IgM, kappa and lambda (Dakopatts). On the basis of the light microscopic appearance, 5 cases were found to be suspicious of light chain deposition in the period 1967—1981. These kidney sections were examined with the avidin-biotin method using anti-kappa and anti-lambda antisera (Dakopatts) as primary antibodies. The diagnosis of light chain nephropathy was established by the demonstration of the diffuse staining of tubular basement membranes for a single light chain isotype. Immunohistological positivity was controlled electron microscopically by proving the granular nature of the deposits. Light microscopically, the following lesions were graded as minimal, mild, moderate or severe in all kidneys: Bence Jones cast nephropathy, light chain nephropathy, amyloidosis, evidences of acute renal failure, nephrocalcinosis, chronic urate nephropathy, acute and chronic pyelonephritis [6], thrombosis of intrarenal veins, and tu-

morous infiltration of kidney tissue. After grading, all cases were grouped on the basis of the serum creatinine levels. If the serum creatinine level was higher than 177 μmol/l at least 3 months before death and showed progression, chronic renal insufficiency was diagnosed [7]. If uraemic symptoms were also observed in such patients, the diagnosis was chronic uraemia. On the basis of the morphological study and the corresponding clinical data, four groups were distinguished: 1) morphologically and functionally intact kidney, 2) kidney involvement with good renal function (serum creatinine level below 177 μmol/l), 3) kidney involvement with moderate chronic renal insufficiency (serum creatinine level between 177 μmol/l and 500 μmol/l), 4) kidney involvement with chronic uraemia (uraemic symptoms and serum creatinine level above 500 μmol/l).

Results

The material consisted of 81 myeloma cases (47 male, 34 female, mean age 66.3 years). Immunohistological and electron microscopic examination (Figs 1 and 4) revealed 2 cases of kappa light chain nephropathy with intense immunostaining along the tubular basement membranes. Light microscopic changes were as follows: Case 1. Severe interstitial fibrosis and tubular atrophy with foci of moderate interstitial lymphocytic infiltration. The tubular basement membranes were thickened and gave an intense PAS-reaction (Fig. 2). The glomeruli exhibited focal mesangial widening. The vasa afferentes showed moderate hyaline arteriolosclerosis. In some arterioles amyloid deposition

Table I

Kidney involvement with moderate chronic renal insufficiency

	Age and sex	Cast nephropathy	Light chain nephropathy	Amyloidosis	Evidences of acute renal failure	Nephrocalcinosis	Urate nephropathy	Acute pyelonephritis	Chronic pyelonephritis	Thrombosis of intrarenal veins	Myeloma infiltrates
1. M. J.	62, f	+++								++	+
2. P. K.	63, f	+						++			
3. Sz. P.	62, f	++									
4. Sz. H.	80, f	++				+					
5. J. N.	67, f	++									
6. Gy. K.	66, f	++	++								
7. M. B.	55, m	++			++						+
8. T. L.	54, m	++									
9. Sz. J.	56, m	+									
10. J. I.	76, m	+						++	++		
11. R. F.	72, m				++						+
12. Zs. I.	52, m	+++									
13. Sz. J.	63, m							++			
14. K. A.	73, m	++									
15. G. M.	55, m	+			++						
16. K. A.	68, m					++					

+: mild, ++: moderate, +++: severe

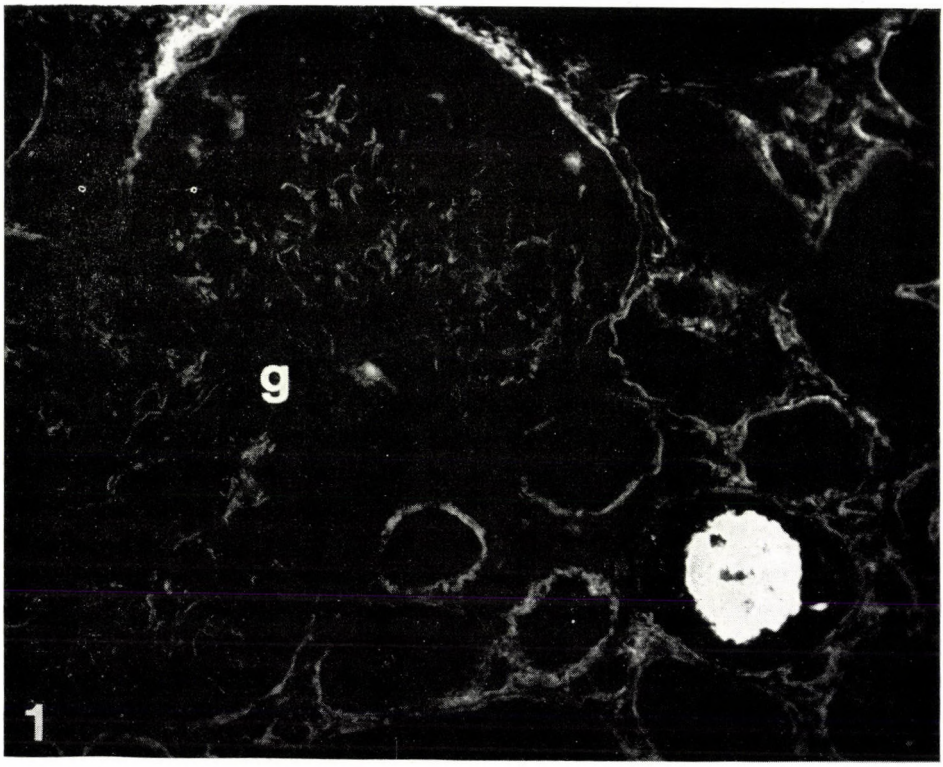

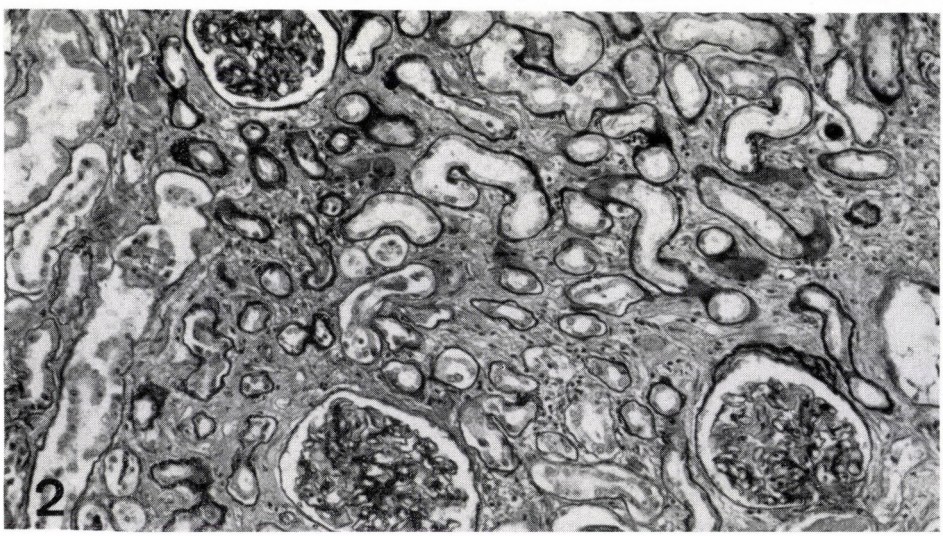

Fig. 1. Kappa light chain nephropathy. Linear staining along the tubular and glomerular (g) basement membranes and intertubular capillaries. At the lower right, a cast is to be seen in a tubule. DIF, anti-kappa, ×560

Fig. 2. Kappa light chain nephropathy. Interstitial fibrosis and focal tubular atrophy. Tubular basement membranes show an intense PAS-reaction. PAS, ×140

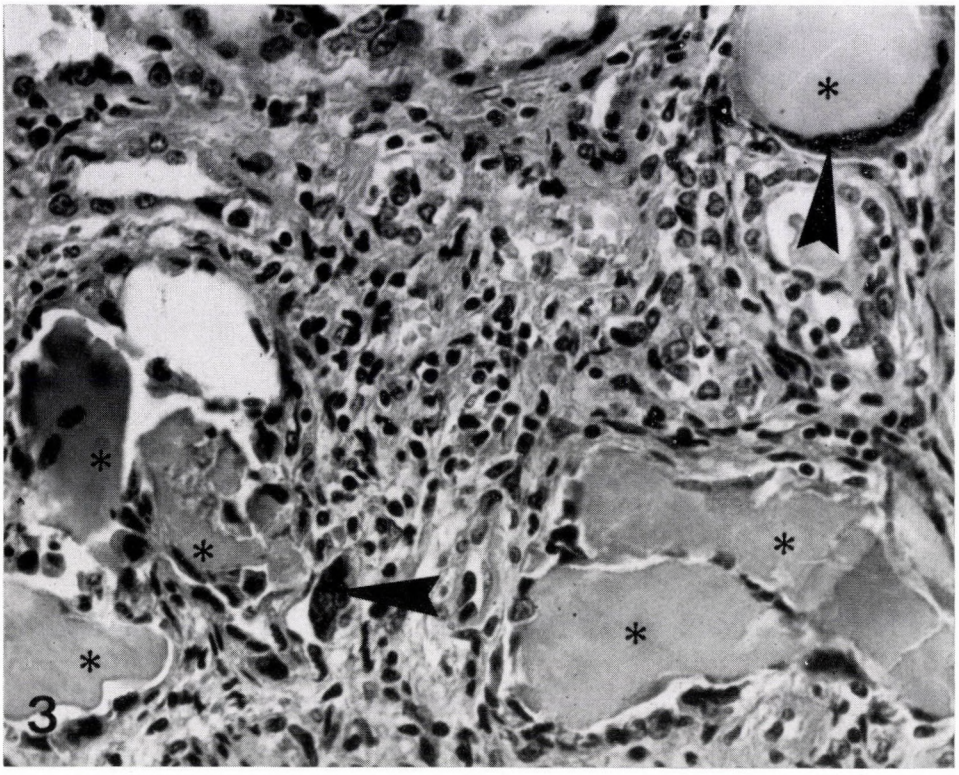

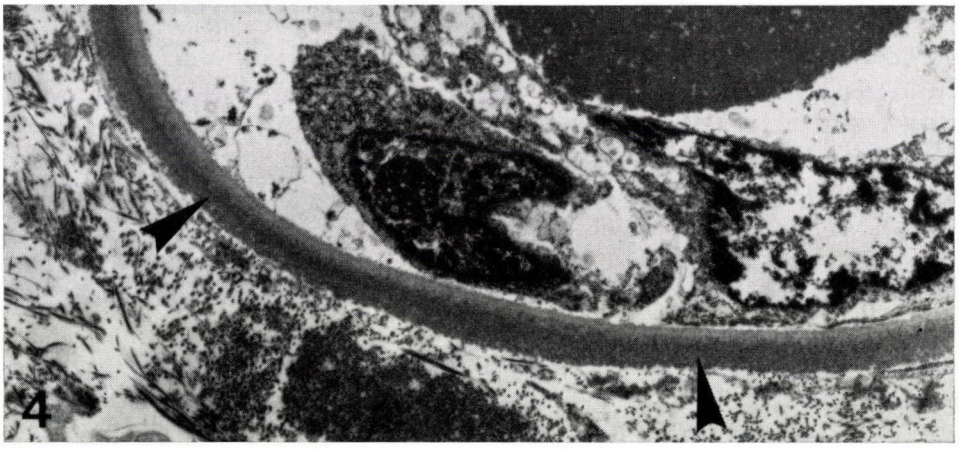

Fig. 3. Bence Jones cast nephropathy. Myeloma cylinders (asterisks) are surrounded by giant cells (arrowheads). Tubular atrophy is present. In the interstitium (at middle) lymphocytes, plasma cells and macrophages can be seen. HE, ×560

Fig. 4. Light chain nephropathy. Along the outer aspect of the tubular basement membrane, finely granular electron-dense deposit is present. Post mortem EM, ×6200

Table II

Kidney involvement with chronic uraemia

	Age and sex	Cast nephropathy	Light chain nephropathy	Amyloidosis	Evidences of acute renal failure	Nephrocalcinosis	Urate nephropathy	Acute pyelonephritis	Chronic pyelonephritis	Thrombosis of intrarenal veins	Myeloma infiltrates
1. B. M.	81, f	++						+			+
2. H. F.	68, f	+++				+					
3. B. I.	80, f		+++	+							
4. H. J.	53, f	+									
5. Sz. L.	56, f	++			+						+
6. Cs.Gy.	74, f	+++									
7. K. S.	70, f	+++				++					
8. Sz. F.	74, m	++									
9. D. J.	67, m	++						++			
10. D. M.	64, m	++									
11. Sz. P.	70, m	++									++
12. Cz. I.	64, m	+++					++				
13. D. K.	65, m	+			++	+					
14. T. S.	49, m	+									
15. P. Gy.	73, m	++									

+: mild, ++: moderate, +++: severe

could be demonstrated. Case 2. Large foci of interstitial fibrosis and tubular atrophy. The tubular lumina contained several myeloma casts surrounded by multinucleated giant cells. The adjacent peritubular interstitium was markedly infiltrated by lymphocytes and macrophages. The picture was identical to that seen in Bence Jones cast nephropathy (Fig. 3). The glomeruli were normal. A moderate hyaline arteriolosclerosis could be seen in the arterioles.

Comparison of the semiquantitative morphological and functional data revealed 40 cases the "morphologically and functionally intact kidney" group. Ten cases were classified as "kidney involvement with good renal function". In these, Bence Jones cast nephropathy, signs of acute renal failure and nephrocalcinosis of minimal or mild degree were present either alone or together. Furthermore, one case of mild and one case of moderate renal amyloidosis occurred. The latter caused the nephrotic syndrome clinically. In 16 cases, "kidney involvement with moderate chronic renal insufficiency" was diagnosed (Table I). "Kidney involvement with chronic uraemia" was identified on 15 occasions (Table II). In groups 3 and 4, Bence Jones cast nephropathy occurred on 27 occasions, kappa light chain nephropathy on 2 occasions, and amyloidosis on 1 occasion. As concerns Tables I and II, it must be emphasized that cases 1, 6 and 12 in the group "kidney involvement with moderate chronic renal insufficiency" displayed more severe morpho-

logical changes than would be expected from the functional values, whereas cases 4 and 14 in the group "kidney involvement with chronic uraemia" showed morphological changes less moderate than expected from the severity of the functional impairment.

Discussion

All known complications of myeloma were encountered in our material. For a correct morphological diagnosis, routine immunohistochemical investigation of the kidney with light chain specific antibodies is essential. In our experience, the DIF examination of frozen kidney sections is the procedure of choice because of its rapidness, simplicity, reliability and low cost [23].

The semiquantitative morphology and renal functional data generally showed a good correlation. Normal serum creatinine levels were accompanied by no or only slight pathohistological changes (groups 1 and 2, altogether 50 patients). "Kidney involvement with moderate chronic renal insufficiency" or "with chronic uraemia" (groups 3 and 4, altogether 31 patients) were coupled with moderate or severe structural alterations. However, 2 uraemic cases exhibited mild histological changes, and in 3 cases with a moderate deterioration of the renal functions severe morphological abnormalities were observed. These findings suggest that the morphologic changes of the kidney in myeloma do not always run parallel with the function: severe lesions can be accompanied by a relatively preserved renal function, and vice versa.

Chronic renal insufficiency was recorded in 31 patients (38%); it was mostly due to Bence Jones cast nephropathy (27 patients, 33%). A similar incidence was found by Schubert et al. [32]. These data suggest that roughly every third patient in unselected myeloma series will have cast nephropathy. Bohle et al. [3] have shown that the deterioration in renal function is directly correlated with the number of casts and the amount of interstitial tissue. The number of casts is of prognostic significance: survival can be prolonged in patients whose tubules are not obstructed by casts [30].

The two forms of paraproteinaemic kidney, amyloidosis and light chain nephropathy, were observed rarely in our material (3 and 2 occasions). The frequency of myeloma-associated light chain deposition disease is not yet known. Our results tentatively indicate that it is approximately the same as that of myeloma-associated amyloidosis. It is worth mentioning that one of our two light chain nephropathy cases was associated with amyloidosis. The simultaneous deposition of fibrillary (amyloid) and finely granulated (light chain fragment) forms of myeloma paraprotein in the same tissue localization has also been observed by other authors [14, 18, 19, 21, 25]. However, the pathomechanism of this phenomenon is still obscure. The other case was

associated with Bence Jones cast nephropathy. This may be of particular interest because the kidney is usually damaged either by cast formation or paraprotein deposition [9, 18]. Unfortunately chemical analysis studies were not carried out in this case; thus, data relevant to the pathogenesis of kidney damage are missing.

Other complications were also rare, probably due to the fact that chronic urate nephropathy, nephrocalcinosis, intrarenal venous thrombosis, acute renal failure and acute pyelonephritis can be controlled therapeutically. In 6 cases, we verified tumorous infiltration of the kidney tissue, mostly in mild form. As invasion of the kidney by tumorous plasma cells occurs in the terminal phase of the disease, this change has no clinico-pathologic implications.

Relatively little is known about the dynamics of development of Bence Jones cast nephropathy and paraproteinaemic kidney, or the excent to which they can be influenced therapeutically. Progress can be expected only if a renal biopsy is made in parallel with the physicochemical analysis of the light chain proteinuria and investigation of the tubular function at the very beginning of the functional decline. Although haematologists in Hungary often do not agree to kidney biopsy, there appears to be no other way to clarify the nature of the kidney damage.

REFERENCES

1. Bangerter AR, Murphy WM: Kappa light chain nephropathy. Virchows Arch A 410 : 531, 1987
2. Bartl R, Frisch B, Fateh-Moghadam A, Kettner G, Jaeger K, Sommerfeld W: Histologic classification and staging of multiple myeloma. Am J Clin Pathol 87 : 342, 1987
3. Bohle A, Gartner H-V, Laberke H-G, Kruck F: Die Niere. F. K. Schattauer Verlag, Stuttgart, 1984, p. 320
4. Bradley JR, Thiru S, Evans DB: Light chains and the kidney. J Clin Pathol 40 : 53, 1987
5. Case Records of the Massachussetts General Hospital. Case 7-1986. N Eng J Med 314 : 500, 1986
6. Churg J, Cotran RS, Sinniah R, Sakaguchi H, Sobin LH: Classification and Atlas of Tubulointerstitial diseases. Igaku Shoin Ltd., Tokyo, 1985, p. 184
7. Coe FL: Clinical and laboratory assesment of the patient with renal disease. In: Brenner BM, Rector FC (eds:), The Kidney. W.B. Saunders Co., Philadelphia, 1986, p . 703
8. Cohen AH, Border WA: Myeloma kidney. Lab Invest 42 : 248, 1980
9. Cotran RS, Rubin RH, Tolkoff-Rubin NE: Tubulointerstitial diseases. In: Brenner BM, Rector FC (eds) The Kidney. W.B. Saunders Co., Philadelphia, 1986, p. 1162
10. De Fronzo RA, Humphrey RL, Wright JR, Cooke CR: Acute renal failure in multiple myeloma. Medicine 54 : 209, 1975
11. Droz D, Noel H, Carnot F, Degos F, Ganeval D, Grünfeld JP: Liver involvement in non-amyloid light chain deposits disease. Lab Invest 50 : 683, 1984
12. Durie BGM, Salmon SE: A clinical staging system for multiple myeloma. Cancer 36 : 842, 1975
13. Fang LST: Light-chain nephropathy. Kidney Int 27 : 582, 1985
14. Ganeval D, Noel LH, Preud'homme JL, Droz D, Grünfeld JP: Light-chain deposition disease: Its relation with AL-type amyloidosis. Kidney Int 26 : 1, 1984
15. Gerlag PGG, Koene RAP, Berden JHM: Renal transplantation in light chain nephropathy: case report and review the literature. Clin Nephrol 25 : 101, 1986
16. Glassock RJ, Cohen AH, Adler ShG, Ward HJ: Secondary glomerular diseases. In: Brenner BM, Rector FC (eds) The Kidney. W.B. Saunders Co., Philadelphia, 1986, p. 1043

17. Hamblin TJ: The kidney in myeloma. Brit Med J 292 : 2, 1986
18. Hill GS, Morel-Maroger L, Méry J-Ph, Brouet JC, Mignon F: Renal lesions in multiple myeloma: their relationship to associated protein abnormalities. Am J Kidney Dis 2 : 432, 1983
19. Hofman-Guilaine C, Nochy D, Jaquot C, Tricottet V, Bariety J, Camillery JP: Association of light chain deposition disease and amyloidosis. Path Res Pract 180 : 214, 1985
20. Johns EA, Turner R, Cooper EH, MacLennan ICM: Isoelectric points of urinary light chains in myelomatosis: analysis in relation to nephrotoxicity. J Clin Pathol 39 : 833, 1986
21. Kirkpatrick CJ, Curry A, Galle J, Melzner I: Systemic kappa light chain deposition and amyloidosis in multiple myeloma; novel morphological observations. Histopath 10 : : 1065, 1986
22. Lapis K, Beregi E: A vesebetegségek klinikopathologiája. Akadémia Kiadó, Budapest, 1988, p. 149
23. Lászik Z, Iványi B, Ormos J: Immunofluorescent examination of the kidney post mortem. Histol Histopath 2 : 13, 1987
24. Maldonado JE, Velosa JA, Kyle RA, Wagoner RD, Holley KE, Salassa RM: Fanconi syndrome in adults. Am J Med 58 : 354, 1975
25. Noel LH, Droz D, Ganeval D, Grünfeld JP: Renal granular monoclonal light chain deposits: morphological aspects in 11 cases. Clin Nephrol 21 : 263, 1984
26. Palant CE, Bonitati J, Bartholomew WR, Brentjens JR, Walshe JJ, Bentzel CJ: Nodular glomerulosclerosis associated with multiple myeloma. Am J Med 80 : 98, 1986
27. Paredes JM, Mitchell BS: Multiple myeloma. Med Clin North Am 64 : 729, 1980
28. Perry MC, Kyle RA: The clinical significance of Bence Jones proteinuria. Mayo Clinic Proc 50 : 234, 1975
29. Pirani CL, Silva FG, Appel GB: Tubulo-interstitial disease in multiple myeloma and other non-renal neoplasias. In: Cotren RE (ed.) Tubulo-interstitial Nephropathies. Churchill Livingstone, New York, 1983, p. 287
30. Pozzi C, Pasquali S, Donini U, Banfi G, Casanova S, Tiraboschi G, Furci L, Porri MT Ravelli M, Lupo A, Schena FP, Brunati C, Imbasciati E, Locatelli E: Prognostic factors and effectiveness of treatment in acute renal failure due to multiple myeloma. Clin Nephrol 28 : 1, 1987
31. Randall RE, Williamson WC, Mullinax F, Tung MJ, Still WJS: Manifestations of systemic light-chain deposition. Am J Med 60 : 293, 1976
32. Schubert GE, Veigel J, Lennert K: Structure and function of the kidney in multiple myeloma. Virchows Arch A 355 : 135, 1972
33. Sedmak DD, Tubbs RR: The macrophagic origin of multinucleated giant cells in myeloma kidney: an immunohistologic study. Hum Pathol 18 : 304, 1987
34. Silva FG, Pirani CL, Mesa-Tejada R, Williams GE: The kidney in plasma cell dyscrasias: A review and a clinicopathologic study of 50 patients. In: Fenoglio CM, Wolff M (eds) Progress in Surgical Pathology, Vol. V, Masson Publishing USA, Inc., New York, 1983, p. 131
35. Smithline N, Kassirer JP, Cohen JJ: Light-chain nephropathy. Renal tubular dysfunction associated with light-chain proteinuria. N Eng J Med 294 : 71, 1976
36. Toyoda M, Kajita A, Kita Sh, Osamura Y, Shinoda T: An autopsy case of diffuse myelomatosis associated with systemic kappa light-chain deposition disease (LCDD). Acta Pathol Jap 38 : 479, 1988

Acta Morphologica Hungarica 37 (3—4), pp. 245—263 (1989)

ANTIFREEZE (ETHYLENE GLYCOL) INTOXICATIONS IN BALTIMORE. REPORT OF SIX CASES

F. INTRONA, Jr, J. E. SMIALEK

OFFICE OF THE CHIEF MEDICAL EXAMINER, DEPARTMENT OF PATHOLOGY, UNIVERSITY OF MARYLAND, USA

(Received 14 March 1989)

Records of the Office of the Chief Medical Examiner (OCME) for the State of Maryland were reviewed for all deaths related to acute ingestion of antifreeze (ethylene glycol [EG]) occurring between December 1985 and December 1987.

Six cases were identified. In three cases, the manner of death was classified as undetermined, in two suicide, and in one case the intoxication was considered to have contributed to death, but was not the main cause.

Clinically, the hospitalized subjects exhibited primary metabolic acidosis with hypocalcemia, hyperglycemia, and an elevated anion and osmolar gap.

At autopsy, the findings related to EG ingestion were typical of a non-specific drug intoxication.

Histological examinations in five cases demonstrated the presence of calcium oxalate crystals in the renal tubules; in three cases extensive renal tubular necrosis appeared related to the survival time.

The toxicological analysis in three cases revealed lethal EG levels in the blood

Introduction

Ethylene glycol (EG) is a relatively non-volatile, colourless, odorless, hygroscopic, water soluble solvent with a boiling point of 197 °C and a specific gravity of 1.12. Its structural formula is $[(CH_2)_2(OH)_2]$ and it is commercially prepared by hydration of ethylene oxide. Because of its physical proprieties, it is widely used as the principal component of many gasoline engine antifreeze solutions. In the past it has also been used in detergents, lacquers, pharmaceuticals, polishes and cosmetics, as a preservative in juices and as a substitute for glycerine in enemas. Recently, it was the coolant of the lunar module [1]. It is also used as a solvent for paints and plastics and as a component of various inks and synthetic fibers and as a softening agent for cellophane. Because of its ready availability and inexpensive cost it is a significant means of poisoning [2].

When orally ingested, EG is rapidly absorbed from the gastrointestinal tract and transported to the liver where it is metabolized by alcohol dehydro-

Send offprint requests to: Francesco Introna, Jr, Office of the Chief Medical Examiner, Dept. of Pathology, University of Maryland, USA

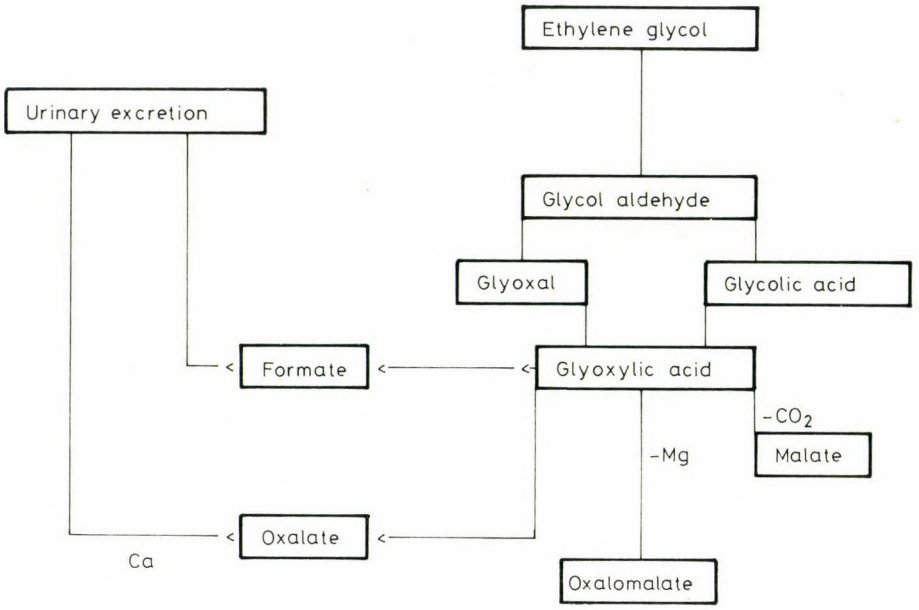

Fig. 1. Various metabolic routes. Diagram of metabolism of ethylene glycol

genase to glycolaldehyde [3]. Further metabolites are glyoxylic acid, glycoxale, glycolic and oxalic acid. The irreversible change to oxalic acid involves approximately 2.3% of the ingested dose [4]. The various metabolic routes are presented in Figure 1. Glomerular filtration and passive re-absorption are the main mechanisms involved in the renal excretion of EG and its metabolites.

Clinical pictures

The clinical course of EG intoxication may be divided into acute and subacute pictures. Berman [5] divided the acute intoxication into three stages:

The first stage has its onset from 30 min to 24 h following ingesting and is manifested primarily by central nervous system effects. The patient may appear "drunk" but without the characteristic breath odor of alcohol consumption. Nausea and vomiting commonly occur. In the early stages mild hypertension, altered ocular reflex with nystagmus and generalized depressed reflexes are often present. Crystalluria caused by calcium oxalate and hippuric acid crystals has been reported [6]. When large amounts of EG are ingested, the picture is mainly one of depression, stupor, coma, metabolic acidosis with an increased anion and osmolar gap. Proteinuria and crystalluria are also often noted. The plasma bicarbonate concentration falls to less than 10 mEq/l and concentrations less than 5 mEq/l are common. Hyperkalemia

with hypocalcemia can be frequently demonstrated [7]. The hypocalcemia is usually related to the chelation of the calcium ions by oxalate to form the relatively insoluble calcium oxalate crystals. Hypocalcemia can be so severe as to cause tetany and cardiac malfunction [1].

The corresponding microscopic pathology includes brain damage with oedema, congestion, capillary engorgement and petechial haemorrhages in the white matter, Betz cell and Purkinje cell chromatolysis, and perivascular and meningeal deposition of crystals. In the kidneys it is possible to only find the oxalate crystals in the tubular lumina without any destruction of the tubular epithelium.

After survival beyond the first 12 to 24 h the patient passes into the second stage where cardiopulmonary symptoms became prominent. Progressive tachypnea often associated with cyanosis, and metabolic acidosis with anion and osmolar gaps are also characteristic. Pulmonary oedema leading to death frequently occurs one to two days post-ingestion.

Cardiac pathology includes petechial haemorrhages and myocardial dilatation. The kidneys are grossly pale and swollen. The microscopic findings at this stage are characterized by pulmonary oedema, sometimes complicated by bronchopneumonia, with a very rare deposition of crystals in the lung tissue. Numerous large, sheaf-like, brilliant, doubly refractile, polarizable crystals of calcium oxalate can be found in the tubules of the kidneys usually without damage to the tubular epithelium.

The third stage is a rare event in fatal cases. It can be observed after the second or third day and is characterized by terminal renal failure with flank pain. The functional impairment progresses from proteinuria and oliguria, and then to anuria and uremic death.

The microscopic pathology consists of oxalate crystal deposition with either normal epithelium or slight epithelial degeneration depending on the interval from ingestion to death. Parry [1] affirmed that, after EG ingestion, microscopic renal damage is prominent within 72 h.

The subacute pattern for survival beyond the fourth day has been described by Smith [8]. The clinical features consist of a permanent lethargic state associated with continuous acidosis and uremia. Death results from terminal pulmonary oedema with respiratory failure. The microscopic findings are hydropic changes in the central portions of the hepatic lobules and hydropic and degenerative lesions of the kidneys associated with crystals in the tubules sometimes surrounded by a wall of large multi-nucleated cells. Crystals have been also observed in the leptomeningeal blood vessels, in the liver and in the spleen.

Smith [8] also observed that crystals are mainly found in the proximal convoluted tubules, but in cases with a long survival time, they can be equally distributed in the proximal, convoluted, distal and collecting tubules. If the

subject survives the acute EG intoxication, normal kidney function may be restored when tubular regeneration occurs [9, 10]. Crystals may persist in the kidneys for months [10, 11] or for years [12]; they represent relatively stable evidence of acute or chronic EG or oxalate poisoning. Conversely, Friedmann [13] did not observe any crystals 17 days after ingestion in a patient who survived and was vigorously haemo-dialyzed.

Pathophysiology

EG, itself has a low toxicity; however, its metabolites are more toxic than their precursor. Cerebral damage may be attributable to the direct toxicity of EG metabolites, especially glycolic and oxalic acid [1, 6]. The glycolaldehyde and the other aldehyde products of EG metabolism inhibit oxidative phosphorylation, glucose metabolism, protein synthesis, DNA replication and ribosomal RNA formation [14] as well as other metabolic processes, and can considered responsible for the early CNS dysfunction. However, except for small calcium oxalate crystals noted in the wall of the meningeal vessels, the anatomic alterations are not specific and may be observed in other metabolic disturbances, such as anoxia, uraemia and hypoglycemia [13]. A mild meningoencephalitis has also been reported as the direct irritant action of EG or its metabolites [1].

Even the clinical manifestation of cardiac and pulmonary involvement may be explained by a direct effect of EG and its metabolites [13].

The tubular necrosis must be also related to direct toxicity of the EG metabolites [15]. Indeed, the tubular pathology may not be associated with the presence of crystals, since there is usually good preservation of the epithelium at points of contact with the crystals. The tubular damage is more widespread than the presence of the crystals, and normally, the basement membrane is well preserved [16].

Berman [16] considers the crystals to be an interesting but incidental finding related to the production of oxalic acid. However, they can be useful in the differential diagnosis of poisoning from other substances responsible for similar clinical pictures. They have not been observed in poisoning by propylene glycol, diethylene glycol, dioxane, glycol ethers and any of the common alcohols. On the other hand, similar crystals have been noted in poisoning by oxalic acid, ethanol amine, glyoxal and glycolic acid [8].

The metabolic acidosis in the first state has been related to the accumulation of glycolic and oxalic acids [17] associated with intratubular precipitation of calcium oxalate crystals in the tubules [14] and then with renal failure and increase of lactic acid [1, 14]; indeed, the amount of EG metabolites is insufficient to account entirely for the profound metabolic acidosis with such high anion and osmolar gaps [18].

Toxicity

Acute toxicity has been described from ingestion of greater than 50 g of EG. The lethal oral dose varies considerably: 1.4 mg/kg is considered to be the lethal dose for man; this would be equivalent to ingestion of approximately 100 ml by a 70 kg man.

Baselt [19, 20] reported the average EG concentration noted in different tissues in 9 persons who died within 6 to 48 h of ingesting unknown amounts of EG as follows: blood 2.8 g/l (range 0.3—4.3 g/l); urine 5.7 g/l (range 0.6—10.8 g/l); liver 6.7 g/kg (range 0.2—15.1 g/kg); and kidney 4.6 g/kg (range 0.2—11.3 g/kg). However, larger doses have been reported. Serum EG concentrations ranging between 0.980 and 7.750 g/l have been observed 6—24 h after acute massive ingestion [6, 21, 22].

Kaye [23] considers the usual blood level in fatal cases to be 2 g/l.

Casarett [24] observed, experimentally, that oxalate crystallization in kidneys and urine did not occur following doses less than 15 ml/kg.

The half-life of EG is 4—6 h. Experimentally, acute ingestion of the poison produced a maximal blood concentration of EG in the first three hours [4]. Figure 2 demonstrates the dissipation curve after experimental ingestion of 6 mg/kg and 9 mg/kg in rates [4]. Detectable concentrations of EG have been found up to 24 h after ingestion [6, 21, 22]. The half-life time is 60 h [19]. Concentrations of oxalic acid can also be found at this time in the liver [25].

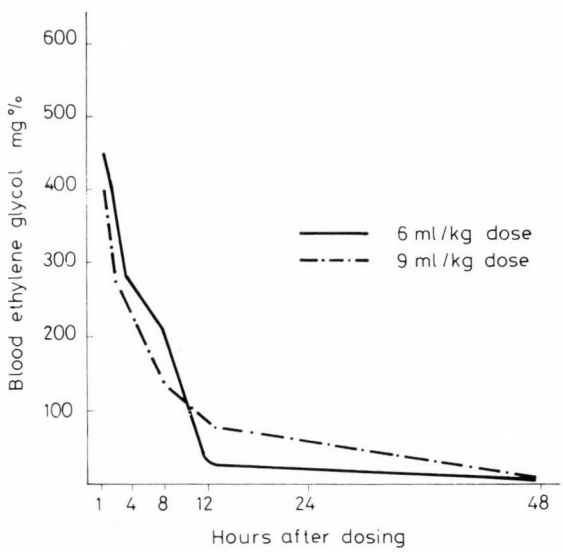

Fig. 2. Dissipation curve after experimental ingestion of 6 ml/kg and 9 ml/kg doses os EG in rates

Materials and methods

A number of techniques have been used to determine EG concentrations in biological fluids, including, calorimetric procedures after oxidation of EG to formaldehyde [26]. Routine gas chromatography for screening of volatile alcohols does not detect ethylene glycol. Light, et al [27] reported a modification of the gas chromatographic procedure that allows for detection of EG. Flame ionization can also be used to detect EG or its derivatives [28, 29]. Enzymatic spectrophotometric methods, fluorometric methods and liquid chromatography have also been described [30, 31, 32].

It is important to note that EG concentrations decline rapidly in post mortem specimens after storage in the refrigerator if the calorimetric method is used. Conversely, no decline has been observed using gas chromatography procedures [26, 33].

The records of the OCME of the State of Maryland were examined for a two-year period from December 1, 1985 through December 1, 1987. The OCME has jurisdiction over the entire State, whose current population is estimated at 4.2 million people (1980 U.S. Census). All deaths related to EG ingestion for either recreational, suicidal, accidental or undetermined purposes have been considered.

Six cases were identified and all six had complete autopsies.

Case 1

Results

A 19-year-old white male, was found semi-comatose in his room by his mother. Because of a history of insulin dependent diabetes, a diabetic coma was suspected. The subject also had a history of mental disease and depression with three previous suicide attempts. While home on leave from a psychiatric hospital, he had medications with him consisting of one container of Tegretol 200 mg, 150 tablets and one container of Norpramine 50 mg, 90 tablets.

CPR was begun at home and he was transported to a nearby hospital where he was pronounced dead two hours later.

An autopsy was performed at the OCME. External examination was negative for recent injuries. On internal examination, the brain weighed 1400 g and was grossly unremarkable. The heart weighed 350 g and was of the usual size and configuration, and the coronaries were patent. The lungs together weighed 1520 g and, on sectioning, marked congestion and oedema were noted; the liver weighed 1800 g and was grossly unremarkable; the kidneys together weighed 280 g and on sectioning a mild congestion was noted. Two hundred cc. of green granular fluid with food particles was present in the stomach.

Microscopy revealed birefringent calcium oxalate crystals (20—30 per 100x) in the proximal, distal and collecting tubules. The tubular epithelium did not show evidence of damage even at contact points with the crystals, and the basement membranes were intact. A few birefringent crystals were also observed in the thyroid. The lungs were markedly congested and oedematous and exhibited multi-focal intra-alveolar haemorrhage.

Toxicology revealed the following EG concentrations: blood 3.6 g/l, bile 4.8 g/l, urine 3.3 g/l, liver 2.0 g/kg, kidneys 1.98 g/kg and gastric content 2.8 g/l. Carbamazepine and desipramine were also found in lethal quantities [34].

Further investigation of the scene, uncovered two personal journals hidden by the decedent, clearly expressing his intention to commit suicide by ingestion of antifreeze. In these journals he documented the lethal dose of EG, the exact amount of antifreeze necessary for a fatal intoxication and the way to conceal the liquid from the attention of relatives. A green soda bottle containing approximately six ounces of antifreeze and two empty hospital prescription vials were also found hidden in his room.

The cause of death was ethylene glycol and drug intoxication and the manner of death was suicide.

Case 2

An unidentified black male was found fully dressed lying on the ground of a federal reservation in winter time.

The autopsy findings were unremarkable except for post mortem animal activity. The scalp and the calvarium were intact, the brain was slightly decomposed; on sectioning no haemorrhages were noted. The neck did not show evidence of injury. The lungs together weighed 670 g and on sectioning a reddish fluid was noted on the cut surface. The 350 g heart was unremarkable and the coronary arteries were patent. The liver weighed 1400 g and was unremarkable. The stomach was empty. The kidneys together weighed 360 g and were without note.

Microscopic examination revealed oedema and congestion with sickling of red cells in the lungs, as well as birefringent oxalate crystals in the proximal and distal tubules of the kidneys (30—50 per 100x), also with sickling of red cells. The tubular epithelium was necrotic with extensive intracellular ballooning even in the absence of crystals; the basement membrane was intact; no cellular wall was observed around the crystals. Some crystals were also observed in the cerebellum. The liver was unremarkable.

Toxicological analysis was negative for alcohol and drugs in heart blood, bile and urine. An EG assay was not performed.

Further investigation of the scene identified an empty bottle of antifreeze near the site where the body had been found.

In view of the history, terminal circumstances and the findings at autopsy, the death was attributed to hypothermia complicating sickle cell trait with contributory ingestion of antifreeze. The manner of death was classified as accident.

Case 3

Police, responding to a call of a suicide attempt, found a 29-year-old white male locked in his apartment, lying on the floor of a hall, in a pool of blood. Found near the subject was a shotgun and a half-full gallon container of antifreeze.

The subject had a history of paranoid schizophrenia. A note found on the scene indicated the subject was depressed over poor working conditions. He described in the note his ingestion of antifreeze stating it had a "sweet taste". The subject was hospitalized where he arrived awake and able to follow simple commands. A shotgun wound of entrance was observed in the upper abdomen. The blood chemical values in the ER revealed a metabolic acidosis with hypercalcemia, namely: PaO_2 77, pH 6.99, $PaCO_2$ 42, Sa/O_2 81, Base Ecc. —22, St.Bic 10, Na 141 mEq/l, K 5.6 mEq/l, CO_2 7.8 mEq/l, creatinine 6.9, Ca 30.2 mEq/l, lactate 96.4. His blood pressure fluctuated between 50 and 80 mmHg systolic. The drug screen was negative for methyl alcohol and ASA.

At laparatomy findings consisted of an intense haemoperitoneum with devitalization of the left lobe of the liver and multiple lacerations of the stomach, transverse colon and mesocolon, duodenum, small bowel, left kidneys, spleen and pancreas. Pellets and a plastic wad were recovered in the retrohepatic fossae. The subject died of exsanguination 1—1/2 h after admission.

On external examination, in addition to evidence of recent surgical therapy, a shotgun entrance wound was present in the epigastrium. The brain weighed 1300 g and was unremarkable; the heart weighed 400 g and with the exception of apical injuries due to pellets, no other lesions were noted; the coronary arteries were patent and without atherosclerotic changes. The lungs together weighed 1450 g and showed pellet injuries in both diaphragmatic surfaces; on sectioning, localized haemorrhagic areas were noted. The liver weighed 1500 g and showed recent surgical sutures in the left lobe. The kidneys together weighed 350 g and several pellet lacerations were noted in the left kidney.

Microscopic examination revealed congestion and haemorrhagic areas in the lungs. The kidneys did not show any pathologic changes and crystals were not present in the tubules.

The toxicological analysis performed on the post mortem blood revealed the presence of EG at a level of 680 mg/l. The urine was positive for EG.

The manner of death was suicide and the cause of death was a shotgun wound of the abdomen with the ingestion of antifreeze being a contributory factor.

Case 4

A 61-year-old black male said to be in fair health, was found comatose by two friends at home. He was brought to the emergency room of a hospital in severe metabolic acidosis (pH 7.07, $PaCO_2$ 11) responding only to painful stimuli. The BP was 210/110 mmHg. A subarachnoid haemorrhage was suspected. He was intubated and a CT scan of the head was performed with negative

results. He was transferred to the ICU where he remained comatose in spite of daily dialyses, assisted ventilation and rehydration therapy. Blood tests in the ER were Na 159, CO_2 8, Cl 101, lactate 15.1, anion gap 50. After the negative results of the brain scan, a possible ingestion of a toxic substance such as methyl alcohol or ASA was considered. The toxicological screening on blood and urine was negative for the common abuse substances (ethanol, methanol, isopropanol, acetone, carbontetrachloride and non-chlorinated hydrocarbons). The arterial blood gases (ABG) showed a persistent metabolic acidosis, the creatinine values increased (17 mg%) and the patient remained unresponsive. On the second hospital day he developed a seizure; his condition slowly deteriorated despite haemodialysis, and he died of cardiac arrest on the fourth hospital day.

An autopsy was performed at the hospital. The external examination was negative; the internal findings were those of pulmonary and renal insufficiency with terminal heart failure. The brain weighed 1380 g and was swollen and oedematous, with flattening of the sulci. The heart weighed 750 g and was substantially unremarkable, the coronary arteries revealed mild atherosclerosis with widely patent lumina. The lungs together weighed 2025 g and, on sectioning, oedema and congestion were noted. The liver weighed 2300 g and had a mottled tan-yellowish surface with a soft consistency. The kidneys weighed 400 g each and were considered substantially unremarkable. The provisional anatomical diagnosis was: "acute renal failure, hepatic necrosis".

Because no clear cause of death was found, the fixed brain, tissues and specimens of the hospital blood were submitted to the Office of the Chief Medical Examiner of Baltimore.

The microscopic examination revealed hypoxic-ischemic changes of the neurons of the cortex cerebri, cerebellum and brainstem, areas of myocardial fibrosis, massive centrilobular steatosis of the liver with relative sparing of the periportal areas, adenocarcinoma of the prostate and tubular necrosis with birefringent intra-tubular crystals in the kidneys (50—70 per 100x) with a peculiar accumulation in the calyces.

Blood collected on admission revealed an EG concentration of 190 mg/l. The diagnosis was EG intoxication and the manner of death was undetermined because of the unclear circumstances of ingestion.

Case 5

A 55-year-old black male was admitted to hospital after having been found unconscious, in respiratory distress, at home by his exwife. At first it was believed to be a case of alcohol ingestion because of a vague history of alcohol abuse. At the ER the BP was 120/70 mmHg, the ABG's was pH 6.99 $PaCO_2$ 7.3, PO_2 147.1, O_2S 95.6. The serum glucose was 248 mg/dl. The labora-

tory tests show Na 144 mEq/l, K 5 mEq/l, CO_2 3 mEq/l, Cl 98 mEq/l, creatinine 2.4 mg%, anion gap 43 mEq/l, osmolar gap 38, SGOT 3232 mU/ml, SGPT 671 mU/ml, LDH 4279 mU/ml, Tot. bil. 4.3 mg/dl. The patient was lethargic with Kussmaul respiration and icteric sclerae. The blood alcohol was 0.03 g/dl. The next day, the patient had seizure activity with meningeal signs and became unresponsive. Despite intensive therapy the patient developed respiratory failure and was intubated. The LDH was 8650 mU/ml and the SGOT 10 690 mU/ml. In the meanwhile, the toxicological analysis of the admission urine showed a level of EG of 5.9 mg/ml. The blood serum EG was not detectable. On day three, the patient developed renal failure and became anuric; the creatinine was 4.9 mg%. Haemodialysis was then performed but the patient continued to deteriorate. On day four, the haemodialysis had to be stopped because of hypotension (50/40), and the patient expired.

An autopsy was performed at the OCME. The external examination was normal. The brain weighed 1410 g and was grossly unremarkable; the heart weighed 300 g and some petechial haemorrhages were noted on the epicardial surface. The coronary arteries and the aorta exhibited mild atherosclerotic changes. The lungs together weighed 1980 g and on sectioning severe congestion and oedema with focal haemorrhages were noted. The liver weighed 3020 g and on sectioning the surfaces was yellow and moderately firm and greasy. The kidneys together weighed 300 g and were grossly unremarkable. The microscopic examination revealed a chronic pericarditis of the heart, focal bronchopneumonia and tubular necrosis with intra-tubular birefringent crystals in the kidneys (15—20/100x). The tubular epithelium showed intracellular ballooning and nuclear absence. The basement membrane was unremarkable, the liver showed an intense steatosis with localized areas of LFN infiltration.

The toxicological anaysis performed on the autopsy blood and bile was negative for EG.

The diagnosis was EG intoxication complicated by chronic alcoholism; the manner of death was undetermined.

Case 6

A 28-year-old black male, a known drug abuser, returned home staggering, appearing intoxicated; he fell several times and was helped to bed. He was incontinent of urine. Shortly afterward he fell from the bed and deep respirations were noted; he was brought to a hospital where he arrived combative, disoriented, conscious but responsive only to painful stimuli, agitated, moving head and extremities violently, with Kussmaul respiration.

Examination in the ER revealed the following: temperature 98 °F, blood pressure 150/85, pulse 96/m, respiration 18/m. The serum glucose was 199 mg/dl. In the urine, a few calcium oxalate crystals were seen. The labora-

tory tests showed Na 150 mEq/l, K 4.0 mEq/l, Cl 124 mEq/l, CO_2 1 mEq/l, chol 206 mg%, creatinine 1.7 mg%, Ca 10.9 mEq/l, anion gap 29 mEq/l. The ABG's revealed pH 7.04; PO_2 154, PCO_2 7.0, H_2CO_3 1.8, BE −27.3. Toxicological analysis of urine was positive for cocaine, phencyclidine (PCP) salicylates, caffeine and nicotine. A severe metabolic acidosis was noted. Ingestion of EG was suspected. A gastric lavage was performed, the patient was intubated and vigorous rehydration therapy was instituted. The ABG's then changed to 7.21/103/17/6.5/18.9. Haemodialysis was performed. The patient became more responsive and was extubated. He followed verbal commands intermittently and was able to answer questions. When asked what he took the night before he said "antifreeze". The serum lactate was 150 mg% (N.V = 2—18); the following night the patient had seizures and remained extremely agitated. He was re-intubated and an increase of serum osmolarity and lactate values were noted. The patient became progressively unresponsive and anuric. On the second day he was dialyzed but remained profoundly acidotic. He was pronounced dead that afternoon. The diagnosis at death was "multiple drug ingestion" (cocaine, PCP, ethylene glycol, ASA).

An autopsy was performed at the OCME. External examination of the body showed no evidence of recent injuries. On internal examination, the gross findings were minimal; the brain weighed 1600 g and on sectioning showed diffuse congestion and oedema. The heart weighed 400 g and was unremarkable. The lungs together weighed 1600 g; on sectioning, the parenchyma was congested and oedematous. The liver weighed 1600 g and was without note, the kidneys together weighed 260 g and were unremarkable.

The microscopic examination revealed oedema and ischemic change of neurons of the cortex. Some birefringent crystals were observed around the meningeal vessels (Fig. 3). Massive intra-tubular necrosis in the kidney weigh high concentration of birefringent crystals (30—60 X100) was also noted (Fig. 4). Small birefringent crystals were also observed in the spleen.

The toxological analysis performed on the specimen of the blood taken at the hospital admission revealed the present of EG in a concentration of 4170 mg/l.

The diagnosis was cocaine, phencyclidine and ethylene glycol intoxication and the manner of death was undetermined.

Discussion

EG was synthetized about one hundred years ago and was not considered commercially valuable until the First World War when it was used as a substitute for glycerine. To promote the non-toxicity of EG, Bachem [35] in 1917, and later Page [36] in 1927, ingested various amounts of EG without

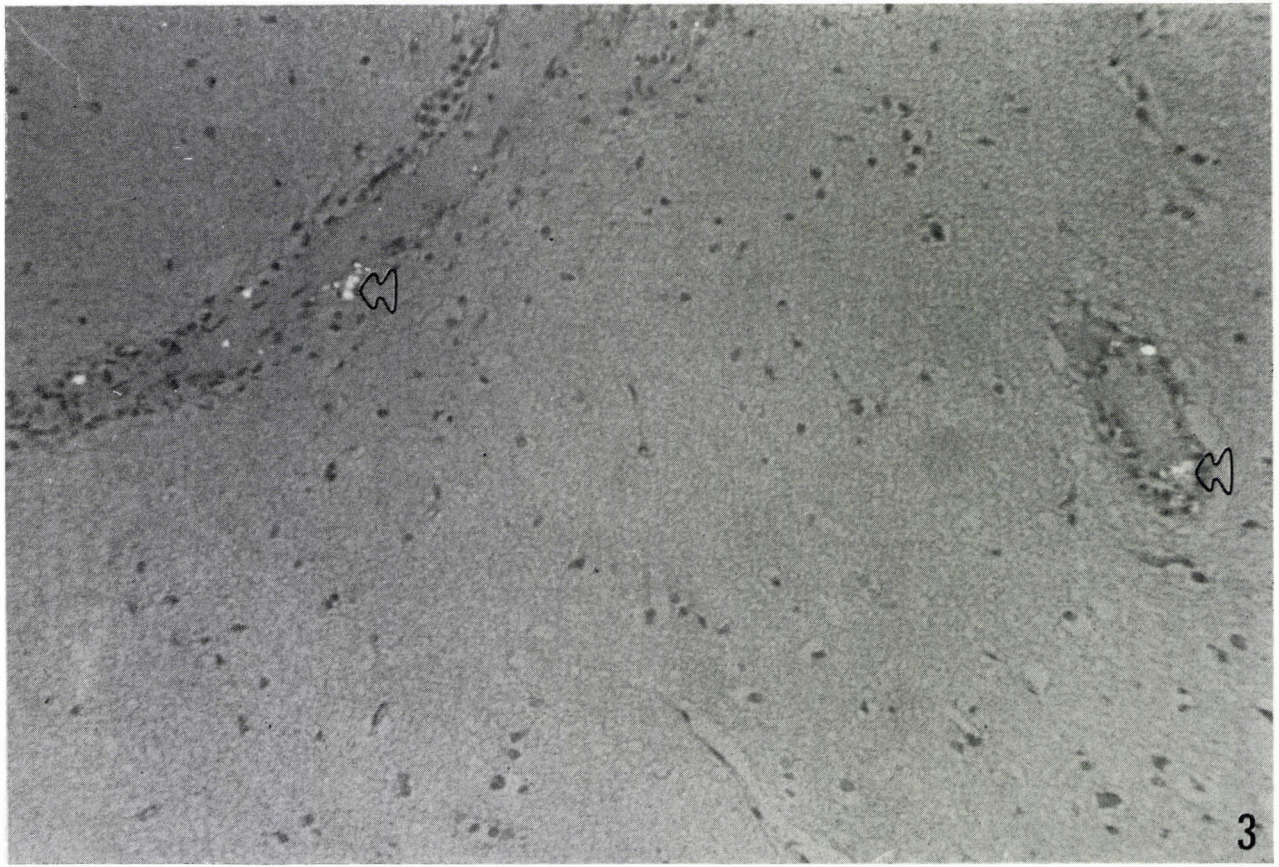

Fig. 3. Birefringent crystals around the meningeal vessels

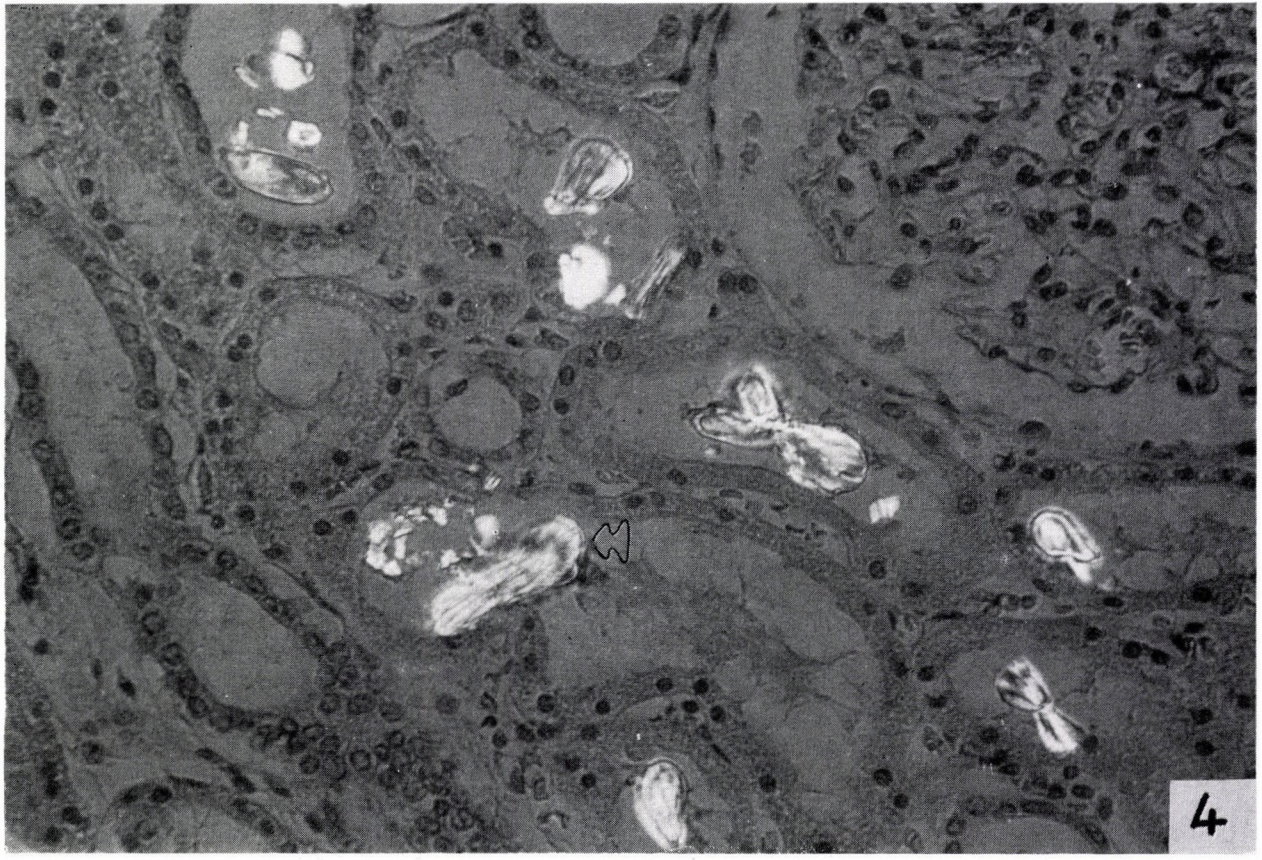

Fig. 4. Massive intra-tubular necrosis in the kidney, high concentration of birefringent crystals (30—60 ×100)

apparent effect. Based on these results, Hanzlik et al. [37] in 1931 affirmed that EG was innocuous as a solvent for medicinals apparently ignoring their own previous experimental data that suggested an intravenous minimal fatal dose of 2.2 g/kg.

In the 1930's the first two lethal cases of "Prestone" ingestion were described [38] but is was in 1937 that the "Massengill disaster" established the toxicity of the glycol compounds. Geiling and Canon [39] noted that the cause of death of at least 76 persons treated with the "Elixir of sulfanilamide Massengill" (72% diethylene glycol) was the unlabeled solvent and not, as originally suspected, the new drug sulfanilamide, which also can produce kidney damage. During and after the Second World War reports of deaths among military personnel war and prisoners were frequent. Boemke [40] described a lethal epidemic which occurred in a German military camp where EG was substituted for the coffee water.

Recently diethylene glycol has been used as an illegal additive in certain Austrian wines [41]. Actually an increase in cases of intoxication has been reported among the military personnel especially in the Middle East where it is substituted for alcohol [42, 43].

Because of its bitter-sweet taste, its exothermic effect and its physical proprieties (clear, odorless, colourless and easy miscible with water) EG could be ingested accidentally by children or by any person unfamiliar with its toxicity. As a syrup for sedative preparations it resulted in the deaths of seven children in South Africa in 1964 [44]. Jolly [45] also reported a child intoxicated by EG recently. Its use as a substitute for alcohol could be related to miserable condition in slump periods since it is relatively inexpensive and pleasant. Approximately 40—60 deaths from EG ingestion are believed to occur each year in the U.S. [2].

The six cases described above occurred in the last two years in the Metropolitan Baltimore area which could reflect an increased popularity for this substance.

From the analyses of the cases reported, summarized in Tables I and II, it is evident that certain typical features can help to establish a clinical diagnoses or initiate an investigation into a suspicious death. EG poisoning could be mistaken for an intoxication by other commonly abused substances since EG levels are not generally included as part of routine analyses of blood and urine [7]. Usually at the hospital admittance if there is no clear suspicions of EG intoxication and/or there is a previous history of ethanol abuse, the possibility of an acute ingestion of EG is not considered. For medical personnel the possibility of a massive ingestion of antifreeze should be considered clinically in the presence of an acute picture of metabolic acidosis not associated with cerebrovascular disease, ketoacidosis, lactacidosis, acute loss of alkali or primitive renal failure. The concomitant presence of a large anion and osmolar

Table I

Blood chemical study in the emergency room

Case #	1	2	3	4	5	6
Hospitalized	no	no	yes	yes	yes	yes
Survival time	—	—	1 h	5 days	4 days	36 h
Dialysis Post Ingestion	—	—	no	yes/ 24 h	yes/ 72 h	yes/ 9 h
Creatinine	—	—	6.9	4.5	2.4	1.7
Uric acid	—	—	—	—	12.3	5.8
Lactate	—	—	94.6	15.1	28	73
Anion gap	—	—	—	50	43	29
Osmolar gap	—	—	—	32	38	26
Calcium	—	—	30.2	5.4	7.4	10.9
Sodium	—	—	141	159	144	150
Potassium	—	—	5.6	13	5	4
Glucose	—	—	—	120	248	199

gaps with metabolic acidosis and secondary renal failure must be considered in the face of an acute ingestion of drugs, poisons or addictive substances as volatile alcohols, paraldehyde, cyanide, ASA and EG. Other clues pointing to the specific diagnosis of EG poisoning include: i) stupor, intoxication with the absence of alcohol on one's breath and in plasma; ii) a massive oxalate crystalluria; iii) a discrepancy between the estimated and the measured values for plasma osmolarity.

Four of the six cases examined were hospitalized and in one, the possibility of an EG poisoning was not suspected because the victim gave a history of ethyl alcohol abuse. In the other three cases the diagnosis or the suspicions of an acute EG ingestion was directly confirmed by the patients. In the three cases hospitalized where the survival time was longer than a few hours, a severe metabolic acidosis with a large anion and osmolar gaps were observed. In cases #4, #5 and #6, the classical picture of EG poisoning described by Berman [16] was noted. They were hospitalized with respiratory distress (two of them with Kussmaul respiration), with sign of CNS involvement that culminated in grand mal seizure activity. They progressed to cardiovascular collapse and renal failure from which they could not be resuscitated. The short interval between the ingestion and the neurological symptoms confirms the direct toxicity of EG and its metabolites on the CNS. Remarkable in cases #4, #5 and #6 was the constant high values of serum glucose that could be related with the altered liver metabolism. Hypocalcemia was constantly observed and it could be related with the presence of calcium oxalate crystals. Peculiarly in case #6, normal serum calcium was present at the hospital admission 9 h after the ingestion but in the second day the calci-

Table II

Principal features of six cases of ethylene glycol poisoning reported

Case #	1	2	3	4	5	6
Age	19	31	29	61	55	28
Sex	Male	Male	Male	Male	Male	Male
Race	White	Black	White	Black	Black	Black
Quantity of EG ingested (approximately)	300 cc	n/a	1500 cc	n/a	n/a	n/a
Survival time	3—5 h	n/a	3 h	120 h	96 h	44 h
Time between ingestion collection	15 h	n/a	26 h	17 h	12 h	9 h
Concentration of EG in blood mg/l	3600	n/a	680	190	not detected	4170
Concentration of EG in urine mg/l	330	n/a	positive	n/a	5.9	n/a
Concentration of crystals in kidneys ×100	20—30	30—50	Absent	50—70	10—15	30—60
Association of other drugs	Carbamazine Desipramine	Negative	Negative	Negative	Ethyl Alcohol	Cocaine PCP ASA Caffeine Nicotine
Manner of death	Suicide	Accident	Suicide	Undetermined	Undetermined	Undetermined

um dropped to 7.3 mEq/l because of the development of crystal formation-in the kidneys and urine. In the case #3 where the death occurred 3 h after the ingestion, hypercalcemia was noted and no crystals were found in the urine or in the renal tubules.

The post mortem examination did not show remarkable findings in all six cases. In one case a fatty liver related to an old history of alcohol abuse was noted.

The microscopic examination in five cases revealed birefringent, irregular crystals in the renal tubules. The crystals were noted both into the proximal then in the distal and collecting tubules. In one case they were also observed in the calyces. This finding did not seem related either to the amount of EG ingested nor the survival time. In case #1 where the subject ingested approximately 10 oz. of antifreeze and the survival time was 3—5 h the crystals were observed in the collecting tubules, otherwise in case #3 where a large amount of EG was ingested and the survival time was 3 h no crystals were observed at all in the tubules.

The concentration of the crystals in the kidneys cannot be related with the amount of EG ingested because it could be the result of multiple sublethal ingestions (crystals have been observed years after the ingestion). Only the absence of any cellular reaction around the crystals can be indicative of an acute massive ingestion of EG. In all six cases reported the ingestion of antifreeze could be considered acute, and no cellular reaction was noted around the crystals. In our cases the degeneration of the tubular epithelium did not seem related to the presence or to the concentration of the crystals. It could be related to the survival time and it seems due only to the direct effect of the EG metabolites. In case #1 where the survival time was 3—5 h, crystals were observed without any related tubular epithelium damage, while in cases #4, #5 and #6 where the survival time was longer, crystals were noted but the tubular necrosis observed was massive, widespread, not related with the presence of the crystals.

In case #6 few crystals were also observed in the wall of the meningeal arteries and in the spleen.

In just one case (#4) a centrilobular steatosis, similar to those described by Smith in the subacute poisoning after a survival of 12 days was noted; in our cases, however, the survival time was only five days and the ingestion of EG could be considered primitive stated the observed absence of any cellular reaction around the crystals in the kidney tubules. In this case (#4) where a long history of heavy alcoholism was present, the severe liver steatosis with parcellar infiltration of the periportal spaces should be related with the clinically high valves of SGPT, SGOT, LDH and bilirubin. The profile of hepatitis antibodies showed a previous hepatitis "A" without any current or recent infection and a positive immunity for hepatitis "B" virus.

The toxicological results showed high values of EG in the biological fluids in four to the six cases observed. In cases #1 and #3 the analysis was performed on the blood collected at the autopsy. In both cases the survival time was shorter than 5 h and the serum EG concentrations were consistent with death. In cases #4, #5 and #6 the analysis was performed on the hospital specimens collected in the ER. In case #4 the time between ingestion of an unknown amount of EG was 17 h. However, a high concentration of EG in the serum indicated a massive absorption of this poison. In case #5 the gap between the ingestion and the blood collection was 12 h and there was no evidence of EG. In the urine, however, a concentration of 5.9 mg/l was found. In case #6 the time between the ingestion and the collection of the blood was 9 h and the serum concentration of EG was 4170 mg/l. In case #2 the toxicological analysis for EG was not performed and the diagnosis of an acute ingestion of EG (that had a contributory rule on the cause of death) was based on the occasional finding of birefringent calcium oxalate crystals in the renal tubules not surrounded by any cellular reaction and on the scene investigation where an empty bottle of antifreeze was found.

Furthermore the toxicological analyses revealed in three cases (cases #1, #5 and #6) the association with other drug as shown in Table I.

REFERENCES

1. Parry MF, Wallach R: Ethylene glycol poisoning. Am J Med 57: 143, 1974
2. Donoghue ER, Moffett WJ: Ethylene glycol intoxication. Check sample 84.1, Forensic Pathol FP 132, 26: 1, 1984
3. Walton EW: An epidemic of antifreeze poisoning. Med Sci Law 18: 231, 1978
4. Winek CL, Shingleton DP, Shannor SP: Ethylene and diethylene glycol toxicity. Clin Toxicol 13: 297, 1978
5. Berman LB, Schreiner GE, Feys J: The nephrotoxic lesion of ethylene glycol. Ann Int Med 46: 611, 1957
6. Godolphin W, Meagher EP, Sanders HD, Frohlich J: Unusual calcium oxalate crystals in ethylene glycol poisoning. Clin Toxicol 16: 479, 1980
7. Cohen JJ, Kaisirer JP: Acido-base. Little Brown and Company, Boston, Toronto, 1982
8. Smith DE: Morphologic lesions due to acute and subacute poisoning with antifreeze (ethylene glycol) Arch Pathol 51: 423, 1951
9. Haggerty RJ: Toxic hazards: Death from permanent antifreeze ingestion. N Engl J Med 261: 1296, 1959
10. Collins JM, Hennes DM, Holzagang CR, Gourley RT, Porter GA: Recovery after prolonged oliguria due to ethylene glycol intoxication. Arch Intern Med 125: 1059, 1970
11. Klendshoj NC, Rejent TA: Tissue levels of some poisoning agents less frequently encountered. J For Sci 11: 75, 1966
12. Petri E: Pathologische Anatomie und Histologie der Vergiftungen. In: Henke F. and Lubarsch O (eds), Handbuch der speziellen pathologischen Anatomie und Histologie, Vol. 10. Berlin, Springer-Verlag 1930
13. Friedmann EA, Greenberg JB, Merrill JP, Dammin GJ: Consequences of ethylene glycol poisoning. Am J Med 32: 891, 1962
14. Levinsky NG: Case records of the Massachusetts General Hospital. N Engl J Med 301: 650, 1979
15. Bove KE: Ethylene glycol toxicity. Am J Clin Path 45: 46, 1966
16. Berman LB, Schreiner GE, Feye J: The nephrotoxic lesion of the ethylene glycol. Ann Int Med 46: 611, 1957

17. Schrier RW: Renal and electrolite disorder. Little Brown and Company. Boston—Toronto 1986
18. Moriarty RW, McDonald Jr RH: The spectrum of ethylene glycol poisoning. Clin Toxicol 7: 583, 1974
19. Baselt RC: Analytical procedures for the therapeutic drug monitoring and emergency toxicology. Biomedical Pub Davis California 1980
20. Baselt RC: Disposition of toxic drugs and chemicals in man. Biomedical Pub California 1982
21. Bowen DAL, Minty PSB, Sengupta A: Two fatal cases of ethylene glycol poisoning. Med Sci Law 18: 102, 1978
22. Cadnapaphornchai P, Taher S, Bhathena D, McDonald FD: Ethylene glycol poisoning: Diagnoses based on high osmolar and anion gaps and crystalluria. Ann Emerg Med 10: 94, 1981
23. Kaye S: Handbook of Emergency Toxicology. CC Thomas Pub Springfield, Illinois, USA 1980
24. Casarett and Doull's: Toxicology. The basic science of poisons. MacMillan Pub. Co. New York—Toronto 1980
25. Zarembsky PM, Hodgkinson A: Plasma oxalic acid and calcium levels in oxalate poisoning. J Clin Path 20: 283, 1967
26. Harger RN, Forney RB: A simple method for detecting and estimating ethylene glycol in body materials; analytical results in six fatal cases. J For Sci 4: 136, 1959
27. Light RT, Nelson KM, Eckfeldt JH: Ethylene glycol poisoning. JAMA 246: 1769, 1981
28. Brown DJ,Jain NC , Forney RB: Gas chromatographic assay of glycol-ethanol combinations in biological materials. J Forensic Sci 13: 537, 1968
29. Porter WH, Avansakul A: A gas chromatographic determination of ethylene glycol in serum. Clin Chem 28: 75, 1982
30. Gupta RN, Eng F, Gupta ML: Liquid chromatographic determination of ethylene glycol in plasma. Clin Chem 28: 32, 1982
31. Meola JM, Rossano TG, Swift TA: Florometry of ethylene glycol in serum. Clin Chem 26: 1709, 1980
32. Eckfeld JH, Light RT: Kinetic ethlene glycol assay with use of yeast alcohol dehydrogenase. Clin Chem 26: 1278, 1980
33. Winnek C: Ethylene glycol poisoning 27th Meeting AAFS, Chicago, February 19, 1975
34. Bush DM, Levine BS, Smyth DF, Caplan YH: A fatal intoxication involving carbamazepine, desipramine and ethylene glycol. J Anal Toxicol 10: 213, 1986
35. Bachem C: Pharmacologische Utersuchungen über Glykol und seine Verwendung in der Pharmazie und Medizin. Med Klin 1: 7, 1917
36. Page IH: Ethylene glycol: Pharmacological study. J Pharmacol and Exper Therap 30: 313, 1927
37. Hanzlik PJ, Seidenfeld MA, Johnson CC: General proprieties irritant and toxic actions of ethylene glycol. J Pharmacol 41: 387, 1931
38. Quaries and minor notes: Possible death from drinking ethylene glycol "Prestone". JAMA 94: 1940, 1930
39. Geiling EMK, Canon PR: Pathologic effects of elixir sulfanilamide (diethylene glycol) poisoning. A clinical and experimental correlation: Final report. JAMA 111: 919, 1938
40. Boemke F: Beitrang zur Toxikologie und Pathologie des Äthylenglykols. Virchow Arch Pathol Anat 310: 106, 1943
41. Turk J, Morrell L: Ethylene glycol intoxication. Arch Int Med 146: 1601, 1986
42. Goldsher M, Better OS: Antifreeze poisoning during the October 1973 war in the Middle East. Case Reports. Milit Med 144: 314, 1979
43. Bunuan HD: Radiator fluid poisoning in Saudi Arabia. J Trop Med Hyg 81: 151, 1978
44. Curry AS: Advances in Forensic and Clinical Toxicology. CRC Press, Cleveland Ohio, 1972
45. Jolly JB, Hualt G, Frossard C, Thieffry S, Fabiani P: Severe ethylene glycol poisoning in a child aged 6 years. Presse Med 75: 2041, 1967

Acta Morphologica Hungarica 37 (3—4), pp. 265—275 (1989)

HAEMOPHAGOCYTIC SINUS HISTIOCYTOSIS WITH MASSIVE LYMPHADENOPATHY: EARLY LESIONS, PROGRESSION AND INVOLUTION

G. Kelényi, L. Olasz

DEPARTMENT OF PATHOLOGY, STOMATOLOGICAL CLINIC, UNIVERSITY MEDICAL SCHOOL OF PÉCS, PÉCS HUNGARY

(Received 30 March 1989)

In a 26-year-old male suffering from haemophagocytic sinus histiocytosis with massive lymphadenopathy (SHML) five biopsies were performed during a period of 60 months. It seemed that the first change in SHML is the appearance of foamy histiocytes in the subcapsular sinuses at a time when accumulation of and haemophagocytosis by the histiocytes in the intermediary and medullary sinuses are not conspicuous. Progression of the lesions is indicated by the accumulation of haemophagocytic histiocytes in all sinuses and by the development of subcapsular xanthofibrous tissue areas, first focal, later confluent. Regression of the lymphadenomegaly may be due to gradual obliteration of the lymph node parenchyma by the subcapsular xanthofibrous tissue and by scarring. Even in the early phases of the disease the paracortical areas were underdeveloped. The immunophenotype of the foamy histiocytes populating the sinuses and the xanthofibrous areas is S-100$^+$, Leu-M3$^+$, VIM-13$^+$ (CD 14), MAC 387$^+$ N-PNA$^+$, OKIa$^+$, Leu-M1$^-$ (CD 15) and OKM1$^-$ (CD 11).

Keywords: Haemophagocytic sinus histiocytosis, evolution, immunohistochemistry

Introduction

Haemophagocytic sinus histiocytosis with massive lymphadenopathy (SHML), a rare, benign and usually self-limited disease, was first described as a clinicopathologic entity by Rosai and Dorfman [18, 19]. Single cases with some special features and studies dealing with several cases have been published, the largest series being that of Foucar et al. [220 cases, 8]. In most of these the diagnosis was usually made on the basis of the characteristic features of SHML as seen in one biopsy sample.

In the present study of a 26-year-old male, five biopsies were performed during a period of 60 months. On the basis of these biopsies the evolution (early lesions, progression, involution) of the disease is described. In addition, the pathomechanism of the disease is discussed in the light of an immunohistochemical analysis of the biopsies.

Send offprint requests to: G. Kelényi, Dept. of Pathology, University Medical School of Pécs, Szigeti út 12., H-7643 Pécs, Hungary

Case report

A 26-year-old male plumber was first seen in May 1983 when he had an elevated temperature, painless bilateral enlargement of the cervical lymph nodes, and a slightly enhanced red blood cell sedimentation rate (12 mm/h). Infectious mononucleosis was excluded. After the first lymph node biopsy (right submandibular, May 1983) the patient was not seen until June 1984 when he was re-admitted with greatly enlarged cervical lymph nodes. During the six weeks of hospitalization he was afebrile. Tests for toxoplasmosis were negative; We 56 mm/h, 85% granulocytosis. A second biopsy was performed (suprahyoid block dissection). Seventeen months later, the patient was re-admitted, his only complaint being greatly enlarged cervical lymph nodes. He was afebrile, We 41 to 60 mm/h. On palpation no enlarged lymph nodes were found in other regions, a chest X-ray was normal. Blood picture: slight lymphocytosis. A third biopsy was performed in December 1985. Six weeks later, in January 1986, the patient complained of laryngeal discomfort: slight dyspnoe and hoarseness due to moderate laryngeal dislocation caused by the enlarged infrahyoid lymph nodes, which were excised.

Eleven months later, in December 1986, the last remaining group of enlarged cervical lymph nodes causing some complaints to the patient when moving his head were removed. One nut-sized, relatively soft lymph node, and three bean-sized, firm lymph nodes were obtained. In the course of his disease, the patient received no corticosteroids or cytostatics.

Two months following the last biopsy, a Coombs-positive haemolytic anaemia developed, which responded well to corticosteroid therapy. At present he is symptom-free and has no enlarged lymph nodes (January, 1990).

Materials and methods

Lymph node samples were fixed in 10% neutral formalin, Bouin-solution or formalin-sublimate and embedded in Paraplast. In addition to routine procedures (HE, Giemsa, periodic acid-Schiff-reaction, reticulin), naphthol-AS-D-chloroacetate esterase reaction was performed. The binding of Ulex europaeus I and of peanut lectin (after neuraminidase, N-PNA) was demonstrated according to Fischer et al. [6]. Cryostat sections were stained by oil red O.

Immunohistochemistry

Polyclonal antibodies to immunoglobulins (IgM, IgD, IgG, IgA, IgE, kappa, lambda, Dako), J chain (Nordic), lysozyme, alpha-1-antitrypsin, alpha-1-antichymotrypsin (Dako) and S-100 (Dako and BioGenex) were applied to formalin-Paraplast sections. Following the application of rabbit antibodies, biotinylated goat antirabbit antibody was employed with alkaline phosphatase conjugated streptavidin (BioGenex). A 1 : 400—1000 dilution of the antibody MAC 387, kindly provided by Prof. Dr. D. Wright and Dr. D. B. Jones, University of Southampton, was applied after 15 min of trypsinisation also on formalin-Paraplast sections. A 1 : 100 dilution of UCHL 1, a gift from P.C.L. Beverley, Imperial Cancer Research Fund, London, was used.

The fourth and fifth biopsy samples were studied in imprints and cryostat sections. Small pieces of tissue were snap-frozen in isopentane by liquid nitrogen, and 4—8 μm-thick

sections were cut with a cryostat. The following monoclonal antibodies were used: Becton—Dickinson: Leu 1 (pan T and B-CLL cells, CD5), Leu 2a (cytotoxic-suppressor, CD8), Leu 3a (helper-inducer, CD4), Leu 7 (NK cells), Leu M1 (monocytes, myeloid cells, histiocytes, macrophages, CD 15) and Leu M3 (monocytes, macrophages). Ortho: OKT 3 (T-cells, CD3), OKT 6 (cortical thymocytes, Langerhans cells, interdigitating reticulum cells, CD 1), OKT 11 (E-rosette positive cells, CD2), OKIa (HLA-DR), OKT 9 (transferrin receptor), OKB 7 (follicular dendritic reticulum cells, OKM 1 (monocytes, myeloid cells, CD 11b). Coulter: B1 (pan B, CD 20), R 4/23 (follicular dendritic reticulum cells). The antibodies VIM-D5 (myeloid cells, lacto-N-pentaose III, CD 15), VIM 13 (monocytes, CD 14), VIM 12 (OKM 1-like, CD 11) were donated by Professor Dr. W. Knapp, Institute of Immunology, University of Vienna. Monoclonal antibodies were used in a three step immunoperoxidase (PAP) procedure or in a biotin-streptavidin-alkaline phosphatase (BioGenex) system.

Results

First biopsy (May 1983, Fig. 1)

Light microscopically, subcapsular sinuses were greatly dilated, while intermediary and medullary sinuses only moderately. The subcapsular sinuses were filled with histiocytes whose cytoplasm was broad and foamy or granular. The cells inside the other sinuses were smaller their cytoplasm showing acidophilic staining and focal Ulex europeus I positivity (predominantly sinus endothelial cells). A very few foamy histiocytes, conspicuous in sections stained for the protein S-100, were present in the intermediary and medullary sinuses. Phagocytosis of lymphocytes or granulocytes by the foam cells was minimal. Between the wall of the subcapsular sinuses and the fibrous capsule small focal accumulations of mature plasma cells were seen. There was a slight increase in number of reticulum fibres in these locations. The paracortical areas were not conspicuous. The number of plasma cells in the medullary cords as compared with those in the later biopsies was relatively small. This biopsy was not diagnostic of SHML.

Second biopsy (June 1984, Fig. 2)

The appearance of the lymph nodes was as with the first biopsy. However, there were a more or less uniform fibrous thickening of the capsule and a focal broadening of the connective tissue space between the fibrous capsule and the wall of the subcapsular sinuses (a layer of reticulin fibres was observed). In this location, near to the subcapsular sinus, there were, besides loose infiltrates of lymphocytes, some secondary follicles, groups of plasma cells and a few foamy histiocytes. In addition, there were a few round or oval sinusoidal lumina present filled with foam cells, giving the impression that small segments of the subcapsular sinus had been "pinched off" by or had "herniated" into the extrasinusoidal layer. The foam cells inside these segments of the subcapsular sinuses contained a large number of lymphocytes, in con-

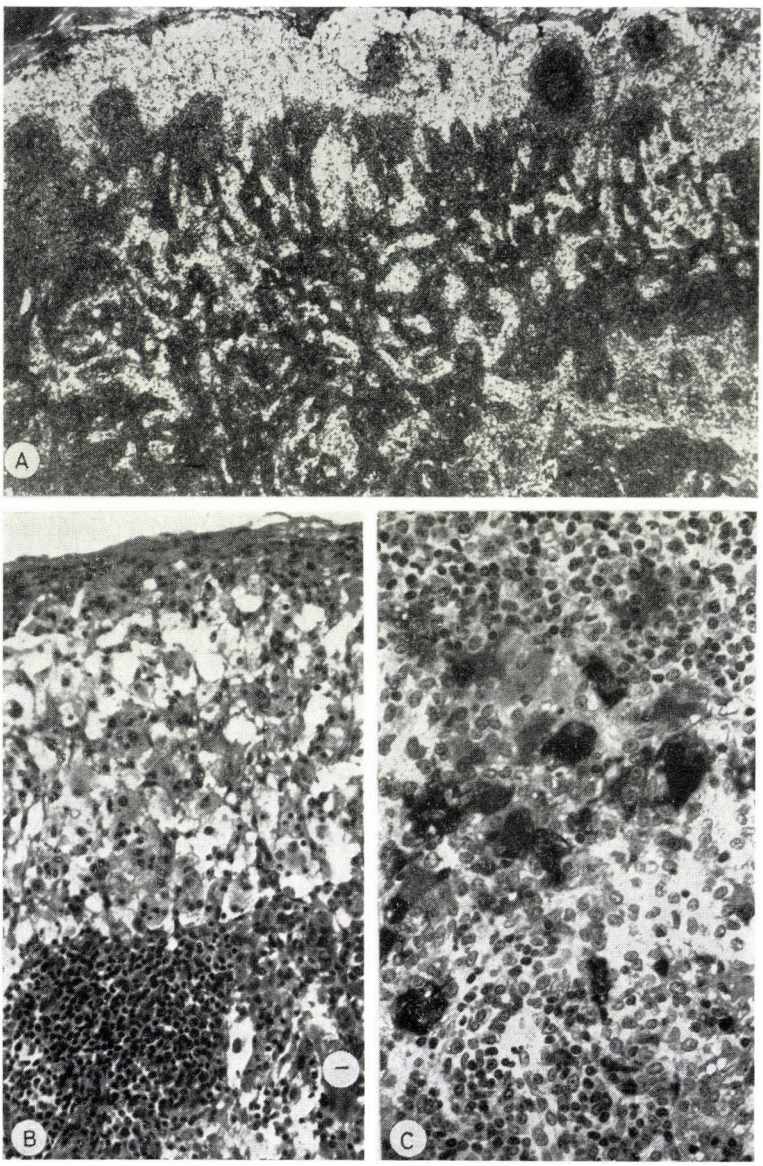

Fig. 1. (A) Lymph node, first biopsy. *(B)* Subcapsular sinuses greatly dilated, intermediary and medullary sinuses moderately dilated (HE, ×155). *(C)* A few S-100 positive histiocytes in a medullary sinus (×250)

trast to the foamy or granular histiocytes in the other sinuses, which had phagocyted only a few cells. The medullary cord plasma cells were more numerous than in the first biopsy.

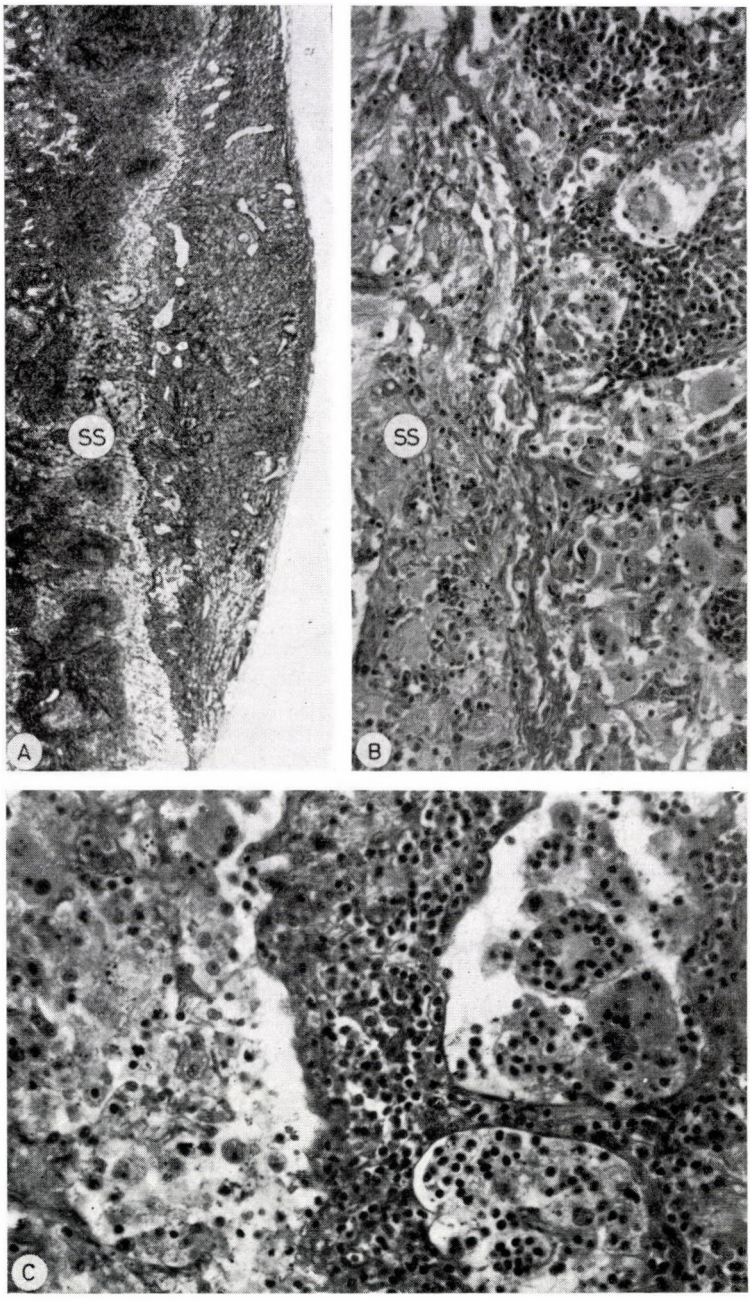

Fig. 2. Lymph node, second biopsy. *(A)* Outside the dilated subcapsular sinus (SS) and between this sinus and the fibrous capsule tissue rich in reticulum fibers in seen (reticulin, ×26). *(B)* Subcapsular sinus (SS) filled with foamy histiocytes, outside (right side) segments of "pinched off" lumina with foamy histiocytes (HE, ×155). *(C)* Foamy histiocytes in the segments of sinusoidal lumina with many phagocyted lymphocytes (detail of Fig. 2b, HE, ×250)

Third and fourth biopsies (December 1985 and January 1986, Fig. 3)

In microscopic appearance the two biopsies were identical; however, they differed from the first and second biopsies in (a) the subcapsular tissues and (b) the intermediary and medullary sinuses.

The lymphatic tissue of these lymph nodes was relatively decreased in extent due to a gradual thickening of the subcapsular (extrasinusoidal) layer, consisting of a tissue rich in reticulum and collagenous fibers. This layer, more or less focal in the 2nd biopsy, now surrounded the lymph node as a continuous layer. In some areas the subcapsular layer resembled xanthomatous or xanthofibrous tissue. Scattered inside it a few islands of lymphocytes and secondary follicles, a moderate number of plasma cells and larger segments of dilated sinuses were seen. (b) All the sinuses of the lymph node parenchyma were greatly dilated and densely populated by histiocytes with a pale or foamy cytoplasm, their vesicular nuclei sometimes being unusually large and irregular in shape. Phagocytosis by these cells of lymphocytes and granulocytes was frequently seen. In cryostat sections the histiocytes within the sinuses were weakly stained by oil red O; in the xanthofibrous area strong staining was seen. The medullary cords were densely packed with mature plasma cells. The paracortical areas were inconspicuous.

Fifth biopsy (December 1986)

The largest of the removed lymph nodes showed features similar to the third and fourth biopsies. In spite of the relatively large xanthofibrous fields, this lymph nodes was not yellow, but the three smaller nodes were.

The structure of these smaller lymph nodes was difficult to recognize. A few scattered follicles, dense groups of plasma cells and a few dilated sinuses were seen; however, most of the lymph nodes consisted of xanthofibrous tissue. In the sinuses the number of foamy histiocytes was much smaller than in the previous biopsies.

Immunohistochemistry

In all biopsies, the plasma cells were polyclonal with a predominance of IgG positive cells. Follicles were R 4/23 or OKB 7 (follicular dendritic cells) and B1 positive. In the small paracortical areas predominance of Leu 3a to. Leu 2a positive cells was seen (ratio about 10 : 1). Large histiocytes in the sinuses were lysozyme negative and showed slight alpha-1-antichymotrypsin positivity. After neuraminidase pretreatment they were strongly positive for peanut lectin and S-100 protein, the reaction of the foamy histiocytes in the xanthofibrous areas was weaker (in formalin-Paraplast sections). MAC 387

stained the foamy histiocytes (sinuses, xanthofibrous areas) weakly and the round mononuclear cells (possibly monocytes) in both locations strongly. OKT 6 did not react with the histiocytes (cryostat sections).

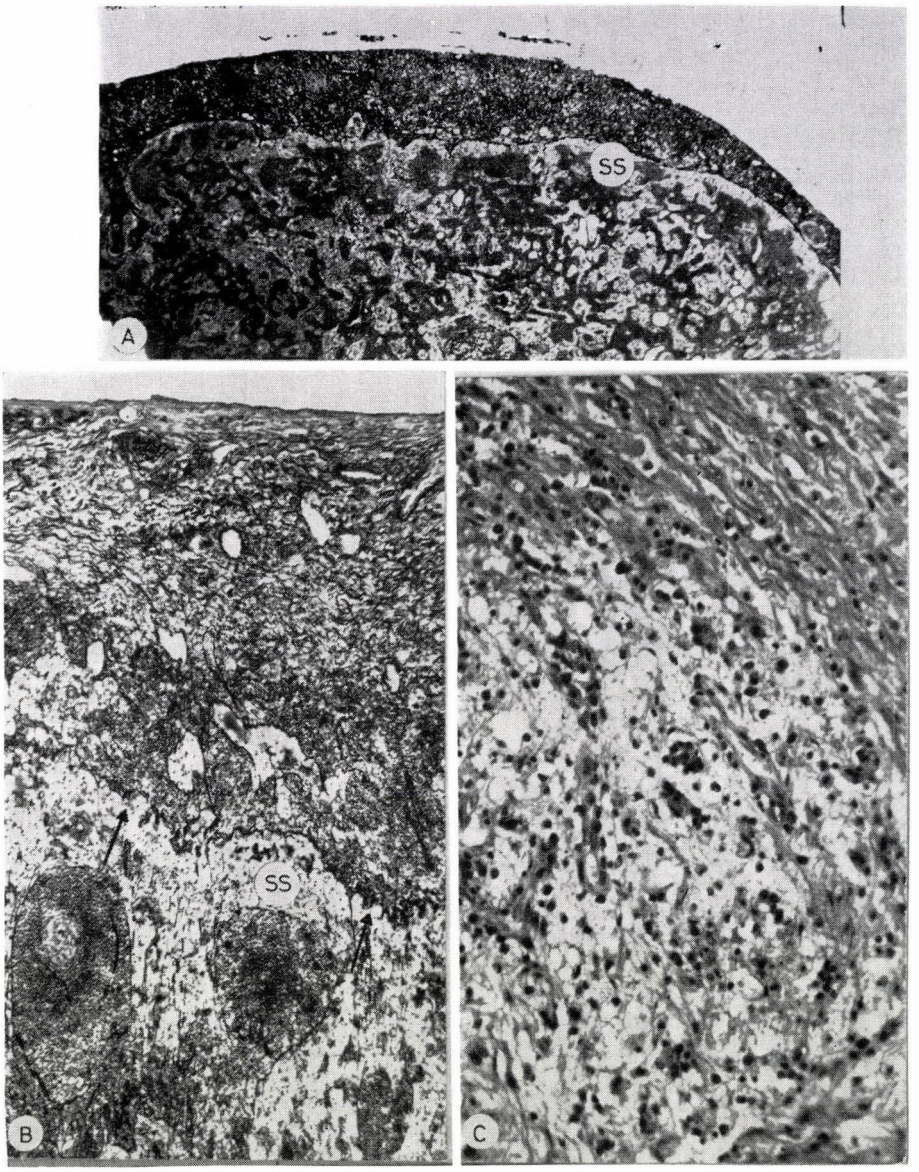

Fig. 3. Lymph node, third and fourth biopsy. *(A)* Greatly broadened layer rich in reticulum fibers between fibrous capsule and subcapsular sinus (SS) (reticulin, ×18). *(B)* Dilated subcapsular sinus (SS), distinctly separated from the subcapsular layer by thick reticulum fibers (arrows). Outside these structures, segments of dilated sinusoids and xanthofibrous tissue are seen (reticulin, ×56). *(C)* Xanthofibrous area, foam cells and lymphocytes at top capsule (HE×155)

Foamy histiocytes in the sinuses were intensively Leu M3 and VIM-13 positive, but their reaction in the subcapsular xanthofibrous tissue of the histiocytes was weaker. Histiocytes (sinusoidal, subcapsular) were negative or weakly positive with the antibody OKIa (HLA-DR) and negative with VIM-D5 and OKM 1. Only a very few were positive with Leu M1 and a weak reaction was seen with VIM-12 and Leu 3a. The small vessels of the lymph nodes were filled with cells strongly positive with VIM-D5, Leu M1, OKM 1, VIM-12 and with the naphthol-AS-D-chloroacetate esterase reaction (granulocytes).

The numerous mononuclear cells within the sinuses and in the xanthofibrous areas were OKM 1, OKIa (HLA-DR) and MAC 387 positive (VIM-D5 and Leu M1 negative). In the medullary cords of the lymph nodes such cells were infrequent. About one third of the lymphocytes phagocytes by foamy histiocytes were UCHL 1 positive (T cells).

Discussion

Haemophagocytic sinus histiocytosis with massive lymphadenopathy (SHML) is a self-limited disease, i.e. except for a few unusual cases [3, 5, 7, 8, 13, 25], it is known to regress spontaneously. Its aetiology is unknown, as is its pathomechanism, the development of the lymph node lesions and their involution. On the basis of a pathomorphological study of five consecutive lymph node biopsies during a period of 60 months in a patient with SHML the nature of the early lesions, the progression and involution of the lymph node lesions may be assessed.

The *early lymph node lesions* seem to be dilation of the subcapsular sinuses and the appearance of foamy histiocytes within them. This happens at a time when haemophagocytosis is not yet apparent and the lesions are not diagnostic of SHML. The intermediary and medullary sinuses do not contain foamy histiocytes. Even at the early stages (1st and 2nd biopsies) an accumulation of plasma cells and a slight degree of reticular fibrosis were present in the subcapsular-extrasinusoidal layer. The afferent lymphatic vessels open into the subcapsular sinuses where the initial lesions were seen. Therefore, by whatever effect the formation of foamy histiocytes is induced — it may be assumed to reach the lymph nodes through the afferent lymphatic vessels. It should be mentioned that there were no dilated lymphatics in or outside the capsule.

The *progression* of the disease is characterized by two events: (a) all the sinuses are dilated and filled with foamy histiocytes phagocyting leukocytes. This pattern is diagnostic of SHML. (b) Under a moderately thick capsule ["capsular fibrosis", 21], the subcapsular tissue is broadened with

the appearance of a xanthofibrous tissue. This develops in part from remnants of the sequestered segments of the subcapsular sinuses.

The *involution or regression of the typical lesion* occurs as a gradual increase of the subcapsular xanthofibrous and fibrous tissues and a decrease in the amount of the lymph node parenchyma. The earliest of these lesions develops at the site of accumulation of the subcapsular focal plasma cells.

A comparison of the five biopsies seems to show that after the first lesions, progression and regression may proceed simultaneously, and in different lymph nodes the pattern of the lesions varies greatly. Xanthofibrous and fibrous tissue reactions in SHML have been described before [14, 21, 25]. On the basis of extranodal lesions in a fatal multifocal form of SHML, Buchino et al. [3] distinguished a stable, a proliferative and an involutional phase of the disease.

The *origin of phagocyting histiocytes* on SHML is not clear. In most cases, as in the present one, they were found to be S-100 positive [1, 2, 4, 22], but Birbeck's granules were not seen in these cells [12, 15, 20]. In addition, we found that they were OKIa (HLA-DR) and OKT 6 (CD 1) negative. The S-100$^+$, OKT 6$^-$ phenotype has been described in interdigitating reticulum cells, Langerhans cells are said to be S-100 and usually OKT 6 positive [24]. The foamy histiocytes of the present case were intensely positive with Leu-M3, but negative with Leu-M1. Langerhans cells and sinus histiocytes on the other hand, are reported to be both Leu-M3 and Leu-M1 positive [9, 11, 17]. It is not clear whether these antibodies, which react with the cells of the mononuclear phagocyte system (MPS), define various subpopulations or rather differentiation, activation or function-related antigens. It is known of S-100 protein that it may have a role during lipolysis in adipocytes, acting as a carrier protein of free fatty acids [10]. In foamy histiocytes of SHML, which are oil red O, positive the presence of the protein S-100 may be thus function-related.

The large number of OKM 1 and MAC 387 positive round mononuclear cells inside the sinuses may represent a precursor population of foamy (phagocyting) histiocytes. This assumption is in agreement with the electron microscopic findings of Lennert et al. [12], who have seen many immigrating mononuclear cells in the sinuses in SHML. The numerous sinusoidal mononuclear cells during the progression of the disease may be considered as bloodborn cells at the site of accumulation of sustained histiocytis. Nevertheless, the immunophenotype of foamy histiocytes and that of mononuclear sinusoidal cells were found to differ, just like those of splenic cord phagocyting macrophages and sinusoidal mononuclear cells, possibly circulating monocytes [9]. In addition, mature histiocytes, which normally populate the sinuses, were found to be Leu-M1 positive [23] whereas the foamy histiocytes of the present case were negative. The strong binding by sinusoidal mononuclear cells of

OKM 1 (CD 11b) and their negative reaction with VIM-12 (CD 11) may indicate that these antibodies are bound by different epitopes [16].

On the basis of data in the literature and the present observations, the pathomechanism of SHML may be related to an undefined local abnormality in antigen processing and presentation by histiocytes resulting in their "foamy transformation" and early accumulation in the subcapsular sinus. The unusual immunophenotype of sinus histiocytes may be ascribed to their foamy transformation and/or activation. It is known that mononuclear phagocyte activation is characterized by an alteration in plasma membrane composition, e.g. increased HLA-DR expression [26]. However, the absent or weak HLA-DR expression of foamy histiocytes argues against their activated state. If foamy histiocytes are modified Langerhans cells, their migration to the paracortical areas is blocked. The atrophy or hypoplasia of the paracortex may be the result of the absence of these cells from the T-zones. The relative predominance of CD 4 positive helper T cells could be one of the reasons for the enhanced plasma cell reaction. Even in the early phase, plasma cells densely populate the lymph node pulp and are present in the vicinity of the subcapsular sinus where focal reticular fibrosis was first seen. A sustained plasma cell reaction together with the foamy histiocytes leads to the subcapsular xanthofibrous reaction and finally to the fibrous obliteration of the lymph nodes, i.e. to regression of the lesions.

REFERENCES

1. Aoyama K, Terashima K, Imai Y, Katsushima K: Sinus histiocytosis with massive lymphadenopathy. A histogenic analysis of histiocytes found in the fourth Japanese case. Acta Pathol Jap, 34: 375, 1984
2. Bonetti F, Chilosi M, Menestrina F, Scarpa A, Pelicci PG, Amorosi E, Fiore-Donati L, Kowles DM: Immunohistological analysis of Rosai-Dorfman histiocytosis. A disease of S-100 + CD 1-histiocytes. Virchows Arch (Pathol Anat), 411: 129, 1987
3. Buchino JJ, Byrd RP, Kmetz DR: Disseminated sinus histiocytosis with massive lymphadenopathy. Arch Pathol Lab Med, 106: 13, 1982
4. Chan J, Mak KL, Saw D: Sinus histiocytosis with massive lymphadenopathy. A report of 2 cases. Chinese Path 17: 609, 1985
5. Diebold J, Tixier P, Baufine X, Ducrocq H: Lymphadenopathie par histiocytose sinusale hemophagocytaire (syndrome de Destombes-Rosai-Dorfman). Étude immunologique et histopathologique d'un nouveau cas. Ann Anat Path, 21: 347, 1976
6. Fischer J, Klein PJ, Vierbuchen M, Skutta B, Uhlenbruck G, Fischer R: Characterization of glycoconjugates of human gastrointestinal mucosa by lectins. I. Histochemical distribution of lectin binding sites in normal alimentary tract as well as in benign and malignant gastric neoplasm. J Histochem Cytochem, 32: 681, 1984
7. Foucar E, Rosai J, Dorfman RF: Sinus histiocytosis with massive lymphadenopathy: a computer-assisted analysis of 211 cases with a fatal outcome. Am J Clin Path, 80: 114, 1983
8. Foucar E, Rosai J, Dorfman RF, Eyman JM: Immunologic abnormalities and their significance in sinus histiocytosis with massive lymphadenopathy. Am J Clin Path, 82: 515, 1984
9. Franklin WA, Mason DY, Pulford K, Falini B, Bliss E, Gatter KC, Stein M, Clarke LC, McGee JOD: Immunohistological analysis of human mononuclear phagocytes and dendritic cells by using monoclonal antibodies. Lab Invest, 54: 322, 1986

10. Haimoto H, Kato K, Suzuki F, Nagura H: The ultrastructural changes of S-100 protein localization during lipolysis in adipocytes. An immunoelectron microscopic study. Am J Pathol, 121: 185, 1985
11. Hsu SM, Yang K, Jaffe ES: Phenotypic expression of Hodgkin's and Reed-Sternberg cells in Hodgkin's disease. Am J Pathol, 118: 209, 1985
12. Lennert K, Niedorf HR, Blümcke S, Hardmeier Th: Lymphadenitis with massive haemophagocytic sinus histiocytosis. Virchows Arch B Zellpath, 10: 14, 1972
13. Marsh WL, McCarvick JP, Harlan DM: Sinus histiocytosis with massive lymphadenopathy. Occurrence in identical twins with retroperitoneal disease. Arch Pathol Lab Med, 112: 298, 1988
14. Mir R, Aftalion B, Kahn LB: Sinus histiocytosis with massive lymphadenopathy and unusual extranodal manifestations. Arch Pathol, 109: 867, 1985
15. Ngendahayo P, Roels H, Quatacker J, Boddaert J, Ntabomuora V, Mbonyingabo P: Sinus histiocytosis with massive lymphadenopathy in Rwanda: Report of eight cases
16. Pallesen immunohistochemical and ultrastructural studies. Histopathology, 7: 49, 1983 with G, Plesner T: The Third International Workshop and Conference on Human Leukocyte Differentiation Antigens with an up-to-date Overview of the CD Nomenclature. Leukemia, 1: 231, 1987
17. Pinkus GS, Thomas P, Said JW: Leu-M1 — a marker for Reed-Sternberg cells in Hodgkin's disease. Am J Pathol, 119: 244, 1985
18. Rosai J, Dorfman R: Sinus histiocytosis with massive lymphadenopathy. A newly recognized benign clinicopathological entity. Arch Pathol, 87: 63, 1969
19. Rosai J, Dorfman RF: Sinus histiocytosis with massive lymphadenopathy: a pseudolymphomatous benign disorder: analysis of 34 cases. Cancer, 30: 1174, 1972
20. Sanchez R, Rosai J, Dorfman RF: Sinus histiocytosis with massive lymphadenopathy: an analysis of 113 cases with special emphasis on its extranodal manifestations. Lab Invest, 36: 349, 1977
21. Walker PD, Rosai J, Dorfman RF: The osseous manifestations of sinus histiocytosis with massive lymphadenopathy. Am J Clin Pathol, 75: 131, 1981
22. Weisenburger DD, Grierson HLL, Daley DT, Linder J: Immunologic studies in sinus histiocytosis with massive lymphadenopathy. Lab Invest, 54: 68A, 1986
23. Wieczorek R, Greco MA, McCarthy K, Bonetti F, Knowles DM: Familial erythrophagocytic lymphohistiocytosis: immunohistochemical and ultrastructural demonstration of the relation to sinus histiocytes. Hum Pathol, 17: 55, 1986
24. Wood GS, Turner RR, Shiurba RA, Eng L, Warnke RA: Human dendritic cells and macrophages. In situ immunophenotypic definition of subsets that exhibit specific morphologic and microenvironment characteristics. Am J Pathol, 119: 73, 1985
25. Wright DH, Richards DB: Sinus histiocytosis with massive lymphadenopathy (Rosai-Dorfman disease): report of a case with widespread nodal and extranodal dissemination. Histopathology, 5: 697, 1981

PRINTED IN HUNGARY

Akadémiai Kiadó és Nyomda Vállalat, Budapest

INSTRUCTIONS TO AUTHORS

Form of manuscript

Contributors are requested to supply two complete copies of the manuscript including all tables and illustrations. Manuscripts should be typed double-spaced with margins of at least 4 cm. Pages should be numbered consecutively.

The *headline* should include the title of the paper, authors' names, and name and short postal address of the institute where the work was done.

An *abstract* of not more than 200 words should be supplied typed before the text. It should briefly describe the purpose of the investigations, the methods utilized, the results obtained, and the authors' principal conclusions.

Abbreviations and symbols

Abbreviations should be spelled out when first used in the text or, alternatively, a list of abbreviations might be given. The *International System of Units (SI)* should be used for all measurements. Symbols for physical quantities are to be printed in italics and should, therefore, be underlined in the manuscript. Unusual symbols should be identified on the margin.

References

References should be numbered in alphabetical order, and these numbers only should be inserted in the text (in parentheses). In the reference list each item should include the names and initials of all authors; the title of the article; the title of the journal abbreviates according to the style used in *Index Medicus* (a list of the journals indexed is printed annually in the January issue); the volume number; the first page number; and the year of publication.

Kaplan AP, Kay AB, Austen KF: A pre-albumin activator of prekallikrein. J Exp Med 135:81, 1972

Titles of books should be followed by the publisher; place of publication; and the year.

Oláh I, Röhlich P, Törő I: Ultrastructure of Lymphoid Organs. Akadémiai Kiadó, Budapest 1975

Halász B: The endocrine effects of isolation of the hypothalamus from the rest of the brain. In: Frontiers in Neuroendocrinology, eds Ganong WF, Martini L, Oxford University Press, Oxford 1969, p. 307

Tables and illustrations

Tables should be comprehensible to the reader without reference to the text. The headings should be typed above the table. Tables should be numbered with Roman and illustrations with Arabic numerals.

Figures should be identified by number and authors' name written lightly in pencil on the back. The top should be indicated on the back of prints. The letters a, b etc. should be placed in the lower left-hand corner of prints. Staining techniques and the original magnification of photomicrographs should be stated. Figure captions should be typed on a separate sheet. The approximate place of figures and tables in the text should be indicated in the manuscript on the left-hand margin.

Proofs and reprints

Reprints and proofs will be sent to the first author unless otherwise indicated. A hundred reprints of each paper will be supplied free of charge.

Periodicals of the Hungarian Academy of Sciences are obtainable at the following addresses:

AUSTRALIA
C.B.D. LIBRARY AND SUBSCRIPTION SERVICE
Box 4886, G.P.O., *Sydney N.S.W. 2001*
COSMOS BOOKSHOP, 145 Ackland Street
St. Kilda (Melbourne), Victoria 3182

AUSTRIA
GLOBUS, Höchstädtplatz 3, *1206 Wien XX*

BELGIUM
OFFICE INTERNATIONAL DES PERIODIQUES
Avenue Louise, 485, *1050 Bruxelles*
E. STORY-SCIENTIA P.V.B.A.
P. van Duyseplein 8, *9000 Gent*

BULGARIA
HEMUS, Bulvar Ruszki 6, *Sofia*

CANADA
PANNONIA BOOKS, P.O. Box 1017
Postal Station "B", *Toronto, Ont. M5T 2T8*

CHINA
CNPICOR, Periodical Department, P.O. Box 50
Peking

CZECHOSLOVAKIA
MAD'ARSKA KULTURA, Národni třida 22
115 66 Praha
PNS DOVOZ TISKU, Vinohradská 46, *Praha 2*
PNS DOVOZ TLAČE, *Bratislava 2*

DENMARK
EJNAR MUNKSGAARD, 35, Nørre Søgade
1370 Copenhagen K

FEDERAL REPUBLIC OF GERMANY
KUNST UND WISSEN ERICH BIEBER
Postfach 46, *7000 Stuttgart 1*

FINLAND
AKATEEMINEN KIRJAKAUPPA, P.O. Box 128
00101 Helsinki 10

FRANCE
DAWSON-FRANCE S.A., B.P. 40, *91121 Palaiseau*
OFFICE INTERNATIONAL DE DOCUMENTATION ET LIBRAIRIE, 48 rue Gay-Lussac
75240 Paris, Cedex 05

GERMAN DEMOCRATIC REPUBLIC
HAUS DER UNGARISCHEN KULTUR
Karl Liebknecht-Straße 9, *DDR-102 Berlin*

GREAT BRITAIN
BLACKWELL'S PERIODICALS DIVISION
Hythe Bridge Street, *Oxford OX1 2ET*
BUMPUS, HALDANE AND MAXWELL LTD.
Cowper Works, *Olney, Bucks MK46 4BN*
COLLET'S HOLDINGS LTD., Denington Estate,
Wellingborough, Northants NN8 2QT
WM DAWSON AND SONS LTD., Cannon House
Folkstone, Kent CT19 5EE
H. K. LEWIS AND CO., 136 Gower Street
London WC1E 6BS

GREECE
KOSTARAKIS BROTHERS INTERNATIONAL BOOKSELLERS, 2 Hippokratous Street, *Athens-143*

HOLLAND
FAXON EUROPE, P.O. Box 167
1000 AD Amsterdam
MARTINUS NIJHOFF B. V.
Lange Voorhout 9–11, *Den Haag*
SWETS SUBSCRIPTION SERVICE
P.O. Box 830, 2160 Sz Lisse

INDIA
ALLIED PUBLISHING PVT. LTD.
750 Mount Road, *Madras 600002*
CENTRAL NEWS AGENCY PVT. LTD.
Connaught Circus, *New Delhi 110001*
INTERNATIONAL BOOK HOUSE PVT. LTD.
Madame Cama Road, *Bombay 400039*

ITALY
D. E. A., Via Lima 28, *00198 Roma*
INTERSCIENTIA, Via Mazzé 28, *10149 Torino*
LIBRERIA COMMISSIONARIA SANSONI
Via Lamarmora 45, *50121 Firenze*
SANTO VANASIA, Via M. Macchi 58
20124 Milano

JAPAN
KINOKUNIYA COMPANY LTD.
Journal Department, P.O. Box 55
Chitose, *Tokyo 156*
MARUZEN COMPANY LTD., Book Department
P.O. Box 5050 Tokyo International, *Tokyo 100-31*
NAUKA LTD., Import Department
2-30-19 Minami Ikebukuro, Toshima-ku, *Tokyo 171*

KOREA
CHULPANMUL, *Phenjan*

NORWAY
TANUM-TIDSKRIFT-SENTRALEN A.S.
Karl Johansgata 43, *1000 Oslo*

POLAND
WĘGIERSKI INSTYTUT KULTURY
Marszalkowska 80, *00-517 Warszawa*
CKP I W, ul. Towarowa 28, *00-958 Warszawa*

ROUMANIA
D. E. P., *Bucuresti*
ILEXIM, Calea Grivitei 64–66, *Bucuresti*

SOVIET UNION
SOYUZPECHAT — IMPORT, *Moscow*
and the post offices in each town
MEZHDUNARODNAYA KNIGA, *Moscow G-200*

SPAIN
DIAZ DE SANTOS Lagasca 95, *Madrid 6*

SWEDEN
ESSELTE TIDSKRIFTSCENTRALEN
Box 62, *101 20 Stockholm*

SWITZERLAND
KARGER LIBRI AG, Petersgraben 31, *4011 Basel*

USA
EBSCO SUBSCRIPTION SERVICES
P.O. Box 1943, *Birmingham, Alabama 35201*
F. W. FAXON COMPANY, INC.
15 Southwest Park, *Westwood Mass. 02090*
MAJOR SCIENTIFIC SUBSCRIPTIONS
1851 Diplomat, P.O. Box 819074,
Pallas, Tx. 75381-9074
READ-MORE PUBLICATIONS, INC.
140 Cedar Street, *New York, N. Y. 10006*

YUGOSLAVIA
JUGOSLOVENSKA KNJIGA, Terazije 27, *Beograd*
FORUM, Vojvode Mišića 1, *21000 Novi Sad*

Index: 26.017